

https://dspace.org/

Gas-slag-metal equilibria without carbon-saturation for ferrochromium refining and stainless-steel making.

Pan, Xiaowei

1998
https://hdl.handle.net/10539/27937

Downloaded from a DSpace repository. https://dspace.org/

GAS-SLAG-METAL EQUILIBRIA WITHOUT CARBON-SATURATION FOR FERROCHROMIUM REFINING AND STAINLESS-STEEL MAKING

Xiaowei Pan

A thesis submitted to the Faculty of Engineering,
University of the Witwatersrand, Johannesburg
In fulfillment of the requirements of the degree of doctor of philosophy.
Johannesburg, 1998

DECLARATION

I declare that this thesis is my own, unaided work. It is being submitted for the Degree of Doctor of philosophy in the University of the Witwatersrand, Johannesburg. It has not been submitted before for any degree or examination in any other university.

(Signature of candidate)

The 24th day of March, 1998

ABSTRACT

In the present investigation, the multi-phase equilibria relevant to ferrochromium refining and stainless-steel making have been made in terms of gas-metal equilibria in alumina crucible and gas-slag-metal equilibria in chromium-oxide crucible and silica crucible, elucidated by 73 figures in forms of silicon distribution, sulphur partition and chromium distribution.

Gas-Metal Equilibria

The relations among carbon content, silicon content and the partial pressure of carbon monoxide in the CO/Ar gas phase annotate that carbon content increases in the alloys with the ascent of silicon content and the partial pressure of carbon monoxide. Within 0.0 to 0.15 atm of the partial pressure of carbon monoxide, the carbon content elevates up very quickly. Silicon content expedites the increase of carbon in the alloys. The carbon content of the alloys increases with the increase of silicon, when CO exists in the gas phase. On the contrary, metals can not pick up carbon if there is no carbon monoxide in the gas phase. The results are expressed in a 3-dimensional diagram and 5 figures.

Silicon Distribution in Gas-Slag-Metal Equilibria

The effects of slag's composition, metal's composition and the partial pressure of carbon monoxide on the equilibrium partition of silicon between slag and metal phases, expressed by the ratio of [Si]/(SiO_2) by mole fraction have been scrutinized. In general, as the content of chromium in the slag phase increases, the ratio of [Si]/(SiO_2) decreases. Silicon equilibrium partition increases when the partial pressure of carbon monoxide decreases.

There is a threshold for certain partial pressure of carbon monoxide. When chromium is higher than the threshold content, chromium content in the slag phase decreases very fast with a very little increase of silicon ratio, and after the threshold a substantial increase of the silicon ratio can only reduce very little chromium from slag phase to metal phase. A lower partial pressure of carbon monoxide will help to lower the threshold content of chromium with a lower ratio of silicon. The increase of alumina content in the slag phase enlarges the equilibrium distribution of silicon. With Cr-oxide crucibles, the increase of Al_2O_3 content and the partial pressure of carbon monoxide do not effect the silicon partition remarkably. The equilibrium distribution of silicon is proportional to the content of silicon in the metal phase.

The partial pressure of carbon monoxide and the crucible materials do not make the results big difference. The effects of carbon content on the distribution of silicon demonstrate that carbon content enhances the equilibrium distribution of silicon between slag and metal. A higher silicon distribution can be acquired at a lower partial pressure of carbon monoxide when the content of carbon in the metal phase excesses 0.14 mole fraction. The effect of carbon content on the ratio of $[\gamma_C]^2/[\gamma_{Si}]$ has been computed.

Sulphur Distribution in Gas-Slag-Metal Equilibria

The equilibrium distribution of sulphur between slags and metals in terms of (S)/[S] by molar fraction has been investigated at 0.034atm, 0.05atm and 0.83atm of partial pressure of carbon monoxide in Cr-oxide crucibles at 1500°C and silica crucibles at 1580°C. It is shown that sulphur transfer from metal phase to slag phase increases with lowering partial pressure of carbon monoxide, increasing MgO content, decreasing SiO_2 content, dwindling Al_2O_3 content, and declining chromium oxides in the slag phase.

It also demonstrates that sulphur transfer from metal phase to slag phase increases with enhancing carbon content of the metals; decreasing chromium content of the metal phase;

declining sulphur content in the metals; dwindling silicon content of the metal phase in the range of 0.005 to 0.02 molar fraction; and particularly lowering partial pressure of carbon monoxide in the gas phase. While the partial pressure of carbon monoxide seems no pronounced effects on the sulphur partition when carbon content in the metals is less than 0.15 of molar fraction.

The impacts of partial pressure of carbon monoxide, combined with carbon content of metal phase are influenced greatly by means of silica content in the slag phase. The relations between MgO and sulphur capacity, the effects of silicon on $[\gamma_{Si}]^{1/2}/[\gamma_S]$ and $[a_{Si}]^{1/2}/[\gamma_S]$, and the influences of silicon, carbon, chromium and sulphur on the activity coefficients of sulphur and carbon and on $[\gamma_S][\gamma_C]$ have been computed and used to interpret the experimental results.

Chromium Distribution in Gas-Slag-Metal Equilibria

By contemplating formula '$\ln L_{Cr} = x\ln\{[\%C]/P_{CO}\} + K$', which is linear with slope x and intercept K, the graphics by using the experimental data have been plotted for three series of experiments. The slopes are 1.125, 1.10 and 1.07, which represent that the ratio of $(CrO/(CrO+Cr_2O_3))$ in the slag phase is 75 per cent; 80 per cent and 86 per cent respectively. The experimental conditions for the above 3 slopes are: (1) at 1500 °C in Cr-oxide crucible under the atmosphere of carbon monoxide; (2) at 0.05atm of partial pressure of carbon monoxide in Cr-oxide crucible at 1500°C and (3) at 0.034atm of partial pressure of carbon monoxide in silica crucible at 1580°C respectively.

A higher percentage of CrO exists in the slags when a lower partial pressure of carbon monoxide is imposed. The percentage of CrO in slags higher in silica crucible, compared with that in Cr-oxide crucible. The content of chromium in the slags increases with increasing chromium in the metal phase. A lower chromium content in the slags is procured by utilizing a lower partial pressure of carbon monoxide in the gas phase. The chromium in slags decreases with increasing SiO_2.

The results achieved in Cr-crucibles at 1500°C and 0.83atm of the partial pressure of carbon monoxide, are expressed in SiO_2-(Al_2O_3+CaO+MgO)-(Cr_2O_3+Fe_2O_3) ternary diagrams by means of iso-concentration lines for carbon and chromium.

Based upon the measuring compositions of alloys in equilibrium with the slag phase, the activity coefficients and the activities for carbon and chromium in the metal phase are computed and plotted in the SiO_2-(Al_2O_3+CaO+MgO)-(Cr_2O_3+Fe_2O_3) ternary diagrams by means of iso-activity coefficient lines for carbon and chromium and iso-activity lines for carbon and chromium.

ACKNOWLEDGEMENT

The author wishes to express his appreciation and thanks to:

Professor R. H. Eric for advice, assistance and guidance throughout the course of this study.

The Council for Mineral Technology (MINTEK) for its financial support for this work and

The permission to present and publish one paper at the 7th International Ferro-Alloy Congress, 1995, Norway;

The permission to present and publish another paper at the 5th International Conference on Molten Slags, Fluxes and Salts 97, 1997, Australia.

The Ferroalloy Production Association of South Africa (FAPA) for grants which assisted both the author and the Pyrometallurgy Research Group.

LIST OF TABLES

Table 1.1. Analyses of Various Chrome Ores 3

Table 1.2. The Chemical Composition of Ferro-Chromium Alloys 10

Table 2.1. Optimised interaction energy parameters, αij(J) 66

Table 2.2. Conversion Gibbs energy of CrO and CrO1.5 in slags 67

Table 3.1. Pco Control by Ar and CO Flowrates 108

Table 3.2. Specifications of gases 110

Table 3.3. The compositions of master slags 113

Table 3.4. Composition of 1-group alloys 113

Table 3.5. Composition of 2-group alloys 114

Table 3.6. Composition of 3-group alloys 114

Table 3.7. Parameters of crucible fabrication 116

Table 3.8. Starting Composition of Metal, mass% 118

Table 4.1. Composition of the layer on the inner wall of Cr-oxide crucible by SEM-EDAX 127

Table 4.2. Composition of the layer on the inner wall of Cr-oxide crucible by chemical analysis 128

Table 4.3. Metal composition from gas-metal equilibrium at 1500 °C by mass 133

Table 4.4. Metal composition from gas-slag-metal equilibrium at 1500 °C under CO atmosphere in Cr-oxide crucible by mass 135

Table 4.5. Metal composition from gas-slag-metal equilibrium at 1500 °C at 0.05 atm of Pco in Cr-oxide crucible by mass 136

Table 4.6. Metal composition from gas-slag-metal equilibrium at 1580 °C at 0.034 atm of Pco in silica crucible by mass 137

Table 4.7. Metal composition from gas-slag-metal equilibrium for making of stainless steel at 1580 °C at 0.034 atm of Pco in silica crucible by mass.....139

Table 4.8. Slag composition from gas-slag-metal equilibrium at 1500 °C under CO atmosphere in Cr-oxide crucible by mass 141

Table 4.9. Slag composition from gas-slag-metal equilibrium at 1500 °C at 0.05 atm of Pco in Cr-oxide crucible by mass 142

Table 4.10. Slag composition from gas-slag-metal equilibrium at 1580 °C at 0.034 atm of Pco in silica crucible by mass 143

Table 4.11. Slag composition from gas-slag-metal equilibrium for making of stainless steel at 1580 °C at 0.034 atm of Pco in silica crucible by mass 144

Table 7.1. Gas-metal equilibrium data at 1500°C by mole fraction 273

Table 7.1. Gas-metal equilibrium data at 1500°C by mole fraction (continue) 274

Table 7.2. Gas-slag-metal equilibrium data at 1500°C under CO atmosphere in Cr-oxide crucibles by mole fraction 275

Table 7.3. Metal composition from the gas-slag-metal equilibrium data at 1500°C at 0.05atm of Pco in Cr-oxide crucibles by mole fraction 276

Table 7.4. Metal composition from the gas-slag-metal equilibrium data at 0.034atm of Pco and 1580°C in silica crucibles by mole fraction 277

Table 7.4. Metal composition from the gas-slag-metal equilibrium data at 0.034atm of Pco and 1580°C in silica crucibles by mole fraction(continue) 278

Table 7.5. Metal composition from gas-slag-metal equilibrium for making of stainless steel at 0.034atm of Pco and 1580°C in silica crucibles by mole fraction 279

Table 7.5. Metal composition from gas-slag-metal equilibrium data for making of stainless steel at 0.034atm of Pco and 1580°C in silica crucibles by mole fraction(continue) 280

Table 7.6. Slag composition from gas-slag-metal equilibrium data at 1500°C under CO atmosphere in Cr-oxide crucibles by mole fraction 281

Table 7.7. Slag composition from gas-slag-metal equilibrium data at 1500°C at 0.05atm of Pco in Cr-oxide crucibles by mole fraction 282

Table 7.8. Slag composition from gas-slag-metal equilibrium data at 1580°C at 0.034atm of Pco in silica-oxide crucibles by mole fraction 283

Table 7.9. Slag composition from gas-slag-metal equilibrium data at 1580°C at 0.034atm of Pco in silica-oxide crucibles for stainless-steel making by mass per cent (%) 284

Table 7.9. Slag composition from gas-slag-metal equilibrium data at 1580°C at 0.034atm of Pco in silica-oxide crucibles for stainless-steel making by mass per cent (continue) 285

Table 7.10. Relations between X_C and $[\gamma_C]$, $[\gamma_C]$, $[a_C]/[a_C]$ and (a_{CO}) with metals of C-0.45Cr-Fe-0.001S-0.005Si by mole fraction at 1550°C 286

Table 7.11. Relations between X_{Cr} and $[\gamma_{Cr}]$, $[\gamma_C]$, $[a_{Cr}]/[a_C]$ and (a_{CrO}) with metals of 0.15C-Cr-Fe-0.001S-0.005Si by mole fraction at 1550°C 287

Table 7.12. Relations between X_S and $[\gamma_{Cr}]$, $[\gamma_C]$, $[a_{Cr}]/[a_C]$ and (a_{CrO}) with metals of 0.15C-Cr-Fe-0.001S-0.005Si by mole fraction at 1550°C 288

Table 7.13. Relations between $(a_{CrO})/(a_{CrO1.5})$ and mole fraction of C, Cr, S, Si at 0.05 atm of Pco at 1550°C 289

Table 7.14. Relations between $(a_{CrO})/(a_{CrO1.5})$ and mole fraction of C, Cr, S, Si at 0.05atm of Pco at 1550°C 290

Table 7.15. Relations between $(a_{CrO})/(a_{CrO1.5})$ and mole fraction of C, Cr, S, Si under CO atmosphere at 1550°C 291

LIST OF FIGURES

Figure 1.1. Cross section of DC-plasma furnace 19

Figure 2.1. The boundary conditions for the dissolution of a chromite-ore cube in molten slag 36

Figure 2.2. Dissolution of iron oxide from the chromite-ore cube into the slag 37

Figure 2.3. Dissolution of the chromium oxide from chromite-ore cube into the slag 37

Figure 2.4. Reduction of iron oxide from chromite-ore cube in molten slag in graphite crucible 38

Figure 2.5. Reduction of chromium oxide from chromite-ore cube in molten slag in graphite crucible 38

Figure 2.6. The liquid surface for C-Cr-Fe 47

Figure 2.7. The solubility of graphite in C_{sat}-Cr-Fe system 48

Figure 2.8. Pseudo-binary sections at selected constant silicon and carbon contents in Cr-Fe-Si-C system 49

Figure 2.9. The effects of silicon and of the iron-to-chromium on the solubility of carbon in Fe-Cr-Si-C alloys at 1700°C 50

Figure 2.10. Silicon-carbon relations in Cr-Fe-Si-C alloys at 1600°C 51

Figure 2.11. Saturated carbon content in Cr-Fe-Si-C_{sat} system at 1600°C 52

Figure 2.12. Activities of CrO, $CrO_{1.5}$ and SiO_2 in the SiO_2-CrO_x quasi-binary system at 1873K in equilibrium with metallic chromium 55

Figure 2.13. Comparison of calculated iso-activity curves (solid lines) for $CrO_{1.5}$ to experimental data in CaO-SiO_2-CrO-$Cr)_{1.5}$ slags in equilibrium with Cr at 1873K 56

Figure 2.14. Comparison of activities of Cr oxides between calculation and experiments 68

Figure 2.15. The effect of the SiO_2 content of the slag phase on the Si content of the metal phase (Cr:Fe=1.3 in the metal) 76

Figure 2.16. The effect of the lime-to-alumina ratio of the slag on the Si content of the metal phase (Cr:Fe=1.3 in the metal) 77

Figure 2.17. The effect of the MgO-to-CaO ratio on the silicon distribution (25% alumina, 39.2% silica) 78

Figure 2.18. The change in silicon activity with increasing X_{Si} (1600°C) in Fe-Cr-Si-C_{sat} alloys 79

Figure 2.19. The change in silicon activity with increasing (X_{Si}+X_C) (1600°C) in Fe-Cr-Si-C_{sat} alloys 80

Figure 2.20. The influence of (X_{Si}+X_C) on the activity coefficient of Si (1600°C) in Fe-Cr-Si-C_{sat} alloys 81

Figure 2.21. The effect of basicity on the chromium content of the slags at 1500°C under CO atmosphere 82

Figure 2.22. The effect of basicity on the chromium content of the slags at 1600°C under CO atmosphere 83

Figure 2.23. The effect of (FeO) on the Cr content of the slag under CO atmosphere at 1500°C 84

Figure 2.24. The effect of (FeO) on the Cr content of the slag under CO atmosphere at 1600°C 85

Figure 2.25. The equilibrium content of silicon for various Cr-Fe-Si-C_{sat} alloys dependent on the silica activity in SiO_2-MgO-Al_2O_3 slags at 1600°C.....86

Figure 2.26. Si content of Cr-Fe(20%)-Si-C_{sat}(solid curves) and Cr-Si-C_{sat}(dashed curve) alloys at 1600°C in CO gas in equilibrium with SiO_2-MgO-Al_2O_3 slags with different M/A ratios.....87

Figure 2.27. Iso-activity lines for silica[100] and corresponding Si content in Cr-Fe(20%)-Si-C_{sat} alloys in equilibrium with SiO_2-MgO-Al_2O_3 slags at 1600°C.....88

Figure 2.28. Distribution of silicon between Cr-Fe-Si-C_{sat} alloys and SiO_2-MgO-Al_2O_3 slags at 1600°C in CO gas.....89

Figure 2.29. Contour lines of $(Cr)_{eq}$ in CaO-MgO-Al_2O_3-SiO_2 melts (1500°C).....90

Figure 2.30. Contour lines of (Cr_{eq}) in CaO-MgO-Al_2O_3-SiO_2 melts (1500°C).....91

Figure 2.31. Equilibrium concentrations of chromium in CaO-MgO-Al_2O_3-SiO_2 melts(1650°C).....92

Figure 2.32. The relation between γ_{CrO} and Molar $(CaO+Al_2O_3)/SiO_2$.....93

Figure 2.33. The effect of the replacement of (CaO) by (MgO) on $(Cr)_{eq}$ at constant ($\%Al_2O_3$)(=20) and ($\%SiO_2$).....94

Figure 2.34. Activity coefficient of silicon in liquid Fe-C-Si alloys 95

Figure 2.35. Activity of SiO_2 in SiO_2-CaO-Al_2O_3 slags at 1550°C.....96

Figure 2.36. Activity of SiO_2 in SiO_2-CaO-Al_2O_3 slags at 1600°C.....97

Figure 2.37. Activity of SiO_2 in SiO_2-CaO-MgO slags at 1600°C 98

Figure 2.38. Activity of SiO_2 in SiO_2-MgO-Al_2O_3 slags at 1600°C.....99

Figure 2.39. Activity of SiO_2 in SiO_2-CaO-MgO-Al_2O_3 slags at 1600°C, 10%, 20%, and 30% of MgO 100

Figure 3.1. A cross-section of the vertical molybdenum wound resistance furnace.....104

Figure 3.2. The entire experimental set-up 105

Figure 3.3. Flow rate of argon and carbon monoxide via tri-flat flowmeter, calibrated by Bunson Tower.....109

Figure 3.4. Temperature profile inside furnace at 1550 and 1600°C.... 112

Figure 3.5. Determination of gas-metal equilibration time at 1500°C, 0.05atm Pco with metal of 60-64%Cr, 32-34%Fe, 0.8-1.3%Si and 0.1%S 123

Figure 3.6. Determination of gas-slag-metal equilibration time at 1500°C under CO atmosphere 124

Figure 4.1. MgO-Al_2O_3-Cr_2O_3 ternary phase diagram.....130

Figure 4.2. Cr-oxide crucibles and the crucibles with Mo-wire net before and after equilibrium experiment.....131

Figure 4.3. Metal sample and slag sample diverged from Cr-oxide crucibles.....132

Figure 4.1.1. Demonstration of metal refining via blowing of oxygen/argon gas.....151

Figure 4.1.2. Relationship between carbon content and partial pressure of carbon monoxide for alloys of 61%Cr-Fe-Si-C by mass in CO/Ar gas at 1500°C 152

Figure 4.1.3. Relationship between carbon and silicon for alloys of 61%Cr-Fe-Si-C by mass in CO/Ar gas at 1500°C 153

Figure 4.1.4. Relations of carbon and silicon and partial pressure of carbon monoxide for alloys of 61%Cr-Fe-Si-C by mass in CO/Ar gas at 1500°C 154

Figure 4.1.5. Calculation of carbon content picked up from CO gas at 1500°C, alloys of 63%Cr-34%Fe-3%Si-C by mass 155

Figure 4.2.1. Effect of Cr content in slags on silicon partition with metals of 0.55Cr-Fe-C-S-0.04Si and slags of 0.01CaO-Fe_2O_3-MgO-Cr_2O_3-SiO_2-Al_2O_3, Al_2O_3/MgO=1.7.

In Cr-oxide crucibles at 1550°C 163

Figure 4.2.2. Effect of Al_2O_3 content in slags on silicon partition with metals of 0.55Cr-Fe-C-S-0.04Si and slags of 0.01CaO-Fe_2O_3-MgO-Cr_2O_3-SiO_2-Al_2O_3, Al_2O_3/MgO=1.7.

In Cr/Si-oxide crucibles at 1500°C/1580°C 164

Figure 4.2.3. Effect of Al_2O_3 content in slags on silicon partition with metals of 0.22Cr-Fe-C-S-0.04Si and slags of 0.01CaO-Fe_2O_3-MgO-Cr_2O_3-SiO_2-Al_2O_3, Al_2O_3/MgO=1.7.

In Si-oxide crucibles at 1580°C 165

Figure 4.2.4. Summary of silicon-reduction equilibrium 166

Figure 4.2.5. Effect of MgO content on silicon partition with metals of 0.55Cr-Fe-C-S-0.04Si and slags of 0.01CaO-Fe_2O_3-MgO-Cr_2O_3-SiO_2-Al_2O_3, Al_2O_3/MgO=1.7.

In Cr/Si-oxide crucibles at 1500°C/1580°C 167

Figure 4.2.6. Effect of MgO content on silicon partition with metals of 0.22Cr-Fe-C-S-0.04Si and slags of 0.01CaO-Fe_2O_3-MgO-Cr_2O_3-SiO_2-Al_2O_3, Al_2O_3/MgO=1.7, in silica crucibles

at 1580°C 168

Figure 4.2.7. Effect of SiO_2 content on silicon partition with metals of 0.55Cr-Fe-C-S-Si and slags of 0.01CaO-0.005Fe_2O_3-MgO-Cr_2O_3-SiO_2-Al_2O_3, Al_2O_3/MgO=1.7.

In Cr/Si-oxide crucibles at 1500°C/1580°C 169

Figure 4.2.8. Effect of SiO_2 content on silicon partition with metals of 0.22Cr-Fe-C-S-Si and slags of 0.01CaO-0.005Fe_2O_3-MgO-Cr_2O_3-SiO_2-Al_2O_3, Al_2O_3/MgO=1.7, in silica crucibles at 1580°C.....170

Figure 4.2.9. Effect of Cr content of metal on silicon partition with metals of Cr-Fe-C-S-0.04Si and slags of 0.01CaO-0.005Fe_2O_3-MgO-Cr_2O_3-SiO_2-Al_2O_3, Al_2O_3/MgO=1.7. In Cr/Si-oxide crucibles at 1500°C/1580°C 171

Figure 4.2.10. Effect of Cr content of metal on silicon partition with metals of Cr-Fe-C-S-0.04Si and slags of 0.01CaO-0.005Fe_2O_3-MgO-Cr_2O_3-SiO_2-Al_2O_3, Al_2O_3/MgO=1.7. In silica crucibles at 1580°C.....172

Figure 4.2.11. Effect of Si content of metal on silicon partition with metals of 0.55Cr-Fe-C-S-Si and slags of 0.01CaO-0.005Fe_2O_3-MgO-Cr_2O_3-SiO_2-Al_2O_3, Al_2O_3/MgO=1.7. In Cr/Si-oxide crucibles at 1500°C/1580°C 173

Figure 4.2.12. Effect of Si content of metal on silicon partition with metals of 0.22Cr-Fe-C-S-Si and slags of 0.01CaO-0.005Fe_2O_3-MgO-Cr_2O_3-SiO_2-Al_2O_3, Al_2O_3/MgO=1.7, in silica crucibles at 1580°C.....174

Figure 4.2.13. Effect of C content of metal on silicon partition with metals of 0.55Cr-Fe-C-S-Si and slags of 0.01CaO-0.005Fe_2O_3-MgO-Cr_2O_3-SiO_2-Al_2O_3, Al_2O_3/MgO=1.7. In Cr-oxide crucibles at 1500°C 175

Figure 4.2.14. Effect of C content of metal on silicon partition with metals of 0.22Cr-Fe-C-S-Si and slags of 0.01CaO-0.005Fe_2O_3-MgO-Cr_2O_3-SiO_2-Al_2O_3, Al_2O_3/MgO=1.7, in silica crucibles at 1580°C 176

Figure 4.2.15. Effect of carbon content on the ratio of $[\gamma_C]^2/[\gamma_{Si}]$ with base metal of Cr-Fe-C-0.001S-0.005Si at 1550°C 177

Figure 4.3.1. Effect of MgO on the distributions of sulphur with metals of 0.55Cr-C-Fe-S-Si and slags of 0.01CaO-Fe_2O_3-MgO-Cr_2O_3-SiO_2-Al_2O_3, Al_2O_3/MgO=1.7, 0.03-0.05/0.02-0.1 Si in Cr/Si oxide crucibles at 1500°C/1580°C 194

Figure 4.3.2. Effect of MgO on the distributions of sulphur with metals of 0.22Cr-C-Fe-S-Si and slags of 0.01CaO-Fe_2O_3-MgO-Cr_2O_3-SiO_2-Al_2O_3, Al_2O_3/MgO=1.7, 0.02-0.1 Si in Si oxide crucibles at 1580°C 195

Figure 4.3.3. Relationships between MgO and sulphide capacity Cs at 1500°C, ... 196

Figure 4.3.4. Effect of Cr of slags on the distributions of sulphur with metals of 0.55Cr-C-Fe-S-Si and slags of 0.01CaO-Fe_2O_3-MgO-Cr_2O_3-SiO_2-Al_2O_3, Al_2O_3/MgO=1.7, 0.03-0.05/0.02-0.1 Si in Cr/Si oxide crucibles at 1500°C/1580°C.....197

Figure 4.3.5. Effect of Cr of slags on the distributions of sulphur with metals of 0.22Cr-C-Fe-S-Si and slags of 0.01CaO-Fe_2O_3-MgO-Cr_2O_3-SiO_2-Al_2O_3, Al_2O_3/MgO=1.7, 0.02-0.1 Si in Si-oxide crucibles at 1580°C.....198

Figure 4.3.6. Effect of Al_2O_3 on partition of sulphur with metals of 0.55Cr-Fe-C-S-Si and slags of 0.01CaO-Fe_2O_3-MgO-Cr_2O_3-SiO_2-Al_2O_3 Al_2O_3/MgO=1.7, 0.03-0.05/0.02-0.1 Si in Cr/Si oxide crucibles at 1500°C/1580°C.....199

Figure 4.3.7. Effect of Al_2O_3 on partition of sulphur with metals of 0.22Cr-Fe-C-S-Si and slags of 0.01CaO-Fe_2O_3-MgO-Cr_2O_3-SiO_2-Al_2O_3, Al_2O_3/MgO=1.7, 0.02-0.1 Si in Si-oxide crucibles at 1580°C.....200

Figure 4.3.8. Effect of SiO_2 on the distribution of sulphur with metals of 0.55Cr-Fe-C-S-Si and slags of 0.01CaO-Fe_2O_3-MgO-Cr_2O_3-SiO_2-Al_2O_3, Al_2O_3/MgO=1.7, 0.03-0.05/0.02-0.1 Si in Cr/Si oxide crucibles at 1500°C/1580°C.....201

Figure 4.3.9. Effect of SiO_2 on the distribution of sulphur with metals of 0.22Cr-Fe-C-S-Si and slags of 0.01CaO-Fe_2O_3-MgO-Cr_2O_3-SiO_2-Al_2O_3, Al_2O_3/MgO=1.7, 0.02-0.1 Si in Si-oxide crucibles at 1580°C.....202

Figure 4.3.10. Effect of [C] on the distribution of sulphur with metals of 0.55Cr-Fe-C-S-Si and slags of 0.01CaO-Fe_2O_3-MgO-Cr_2O_3-SiO_2-Al_2O_3, Al_2O_3/MgO=1.7, 0.03-0.05/0.02-0.1 Si in Cr/Si oxide crucibles.....203

Figure 4.3.11. Effect of [Cr] on the distribution of sulphur with metals of 0.55Cr-Fe-C-S-Si and slags of 0.01CaO-Fe_2O_3-MgO-Cr_2O_3-SiO_2-Al_2O_3, Al_2O_3/MgO=1.7, 0.03-0.05/0.02-0.1 Si in Cr/Si oxide crucibles at 1500°C/1580°C.....204

Figure 4.3.12. Effect of [Si] on the distribution of sulphur with metal of 0.55Cr-Fe-C-S-Si and slags of 0.01CaO-0.007Fe_2O_3-MgO-Cr_2O_3-SiO_2-Al_2O_3, Al_2O_3/MgO=1.7.....205

Figure 4.3.13. Effect of [C] on the distribution of sulphur with metals of 0.22Cr-Fe-C-S-Si and slags of 0.01CaO-Fe_2O_3-MgO-Cr_2O_3-SiO_2-Al_2O_3, Al_2O_3/MgO=1.7, 0.02-0.1 Si in Si-oxide crucibles at 1580°C.....206

Figure 4.3.14. Effect of [Si] on the distribution of sulphur with metals of 0.22Cr-Fe-C-S-Si and slags of 0.01CaO-0.007Fe_2O_3-MgO-Cr_2O_3-SiO_2-Al_2O_3, Al_2O_3/MgO=1.7, in Si-oxide crucibles at 1580°C 207

Figure 4.3.15. Relations of activity coefficients of si[illegible] and sulphur with silicon content in the alloys of 0.15C-0.45Cr-0.001S-Si-Fe by mole fraction at 1550°C 208

Figure 4.3.16. Effects of silicon content on $[\gamma_{Si}]^{1/2}/[\gamma_S]$ and $[a_{Si}]^{1/2}/[\gamma_S]$ at 1550°C, with metals containing 0.15C-0.45Cr-0.001S-Si-Fe by mole fraction 209

Figure 4.3.17. Effect of silicon, carbon, chromium and sulphur on the activity coefficient of sulphur ($[\gamma_S]$) at 1550°C with base alloys of 0.15C-0.45Cr-0.001S-0.01Si-Fe 210

Figure 4.3.18. Effect of silicon, carbon, chromium and sulphur on the activity coefficient of carbon ($[\gamma_c]$) at 1550°C with base alloys of 0.15C-0.45Cr-0.001S-0.01Si-Fe 211

Figure 4.3.19. Effect of silicon, carbon, chromium and sulphur on the term of($[\gamma_s][\gamma_c]$) at 1550°C with base alloys of 0.15C-0.45Cr-0.001S-0.01Si-Fe 212

Figure 4.4.1. Variation in the ln partition ratio of chromium with the ln partition ratio of carbon to 0.83atm Pco at 1500°C in Cr-oxide crucible.....221

Figure 4.4.2. Variation in the ln partition ratio of chromium with the ln partition ratio of carbon to 0.05atm Pco at 1500°C in Cr-oxide crucible.....222

Figure 4.4.3. Variation in the ln partition ratio of chromium with the ln partition ratio of carbon to 0.034atm Pco at 1580°C in silica crucible.....223

Figure 4.4.4. Formalisation of chromium in slags with partial pressure of carbon monoxide. Case 1 at 0.034atm Pco in silica crucible at 1580°C; case 2 at 0.83 and 0.05atm of Pco in Cr-oxide crucible at 1500°C.....224

Figure 4.4.5. Influence of C, Cr and Si on the ratio of CrO to $CrO_{1.5}$ with base metals of 0.15C-0.55Cr-0.001S-0.005Si-Fe by mole fraction at 0.83atm Pco and 1500°C.....225

Figure 4.4.6. Influence of C, Cr and Si on the ratio of CrO to $CrO_{1.5}$ with base metals of 0.15C-0.55Cr-0.001S-0.005Si-Fe by mole fraction at 0.05atm Pco and 1500°C.....226

Figure 4.4.7. Influence of C, Cr and Si on the ratio of CrO to $CrO_{1.5}$ with base metals of 0.15C-0.45Cr-0.001S-0.005Si-Fe by mole fraction at 0.034atm Pco and 1550°C 227

Figure 4.4.8. Effect of [Cr] on chromium of slags with metals of Cr-Fe-C-S-Si and slags of 0.01CaO-0.007Fe_2O_3-MgO-Cr_2O_3-SiO_2-Al_2O_3 Al_2O_3/MgO=1.7, [Cr]>0.20, 0.03-0.05/0.02-0.1 Si in Cr/Si oxide crucibles 237

Figure 4.4.9. Effect of [Cr] on chromium of slags with metals of less Cr-Fe-C-S-Si and slags of 0.01CaO-0.007Fe_2O_3-MgO-Cr_2O_3-SiO_2-Al_2O_3, Al_2O_3/MgO=1.7, [Cr]<0.22, 0.02-0.1 Si in Si-oxide crucibles at 1550°C 238

Figure 4.4.10. Effect of [C] on chromium of slags with metals of 0.55Cr-Fe-C-S-Si and slags of 0.01CaO-Fe_2O_3-MgO-Cr_2O_3-SiO_2-Al_2O_3 Al_2O_3/MgO=1.7, 0.03-0.05/0.02-0.1 Si in Cr/Si oxide crucibles 239

Figure 4.4.11. Effect of [C] on chromium of slags with metals of 0.22Cr-Fe-C-S-Si and slags of 0.01CaO-Fe_2O_3-MgO-Cr_2O_3-SiO_2-Al_2O_3 Al_2O_3/MgO=1.7, 0.02-0.1 Si in Si-oxide crucibles at 1550°C 240

Figure 4.4.12. Relations between carbon and $[\gamma_C]$,$[\gamma_{Cr}]$ and $[a_{Cr}]/[a_C]$ with base metals of C-0.45Cr-0.001S-0.005Si-Fe by mole fraction at 1500°C 241

Figure 4.4.13. Relations between chromium and $[\gamma_C]$,$[\gamma_{Cr}]$ and $[a_{Cr}]/[a_C]$ with base metals of C-0.45Cr-0.001S-0.005Si-Fe by mole fraction at 1500°C.....242

Figure 4.4.14. Effect of MgO on chromium of slags with metals of 0.55Cr-Fe-C-S-Si and slags of 0.01CaO-Fe_2O_3-MgO-Cr_2O_3-SiO_2-Al_2O_3 Al_2O_3/MgO=1.7, 0.03-0.05/0.02-0.1 Si in Cr/Si oxide crucibles.....243

Figure 4.4.15. Effect of MgO on chromium of slags with metals of 0.22Cr-Fe-C-S-Si and slags of 0.01CaO-Fe_2O_3-MgO-Cr_2O_3-SiO_2-Al_2O_3 Al_2O_3/MgO=1.7, 0.02-0.1 Si in Si-oxide crucibles at 1580°C.....244

Figure 4.4.16. Effect of Al_2O_3 on chromium of slags with metals of 0.55Cr-Fe-C-S-Si and slags of 0.01CaO-Fe_2O_3-MgO-Cr_2O_3-SiO_2-Al_2O_3 Al_2O_3/MgO=1.7, 0.03-0.05/0.02-0.1 Si in Cr/Si oxide crucibles.....245

Figure 4.4.17. Effect of Al_2O_3 on chromium of slags with metals of 0.22Cr-Fe-C-S-Si and slags of 0.01CaO-Fe_2O_3-MgO-Cr_2O_3-SiO_2-Al_2O_3 Al_2O_3/MgO=1.7, 0.02-0.1 Si in Si-oxide crucibles at 1580°C.....246

Figure 4.4.18. Effect of SiO_2 on chromium of slags with metals of 0.55Cr-Fe-C-S-Si and slags of 0.01CaO-Fe_2O_3-MgO-Cr_2O_3-SiO_2-Al_2O_3 Al_2O_3/MgO=1.7, 0.03-0.05/0.02-0.1 Si in Cr/Si oxide crucibles.....247

Figure 4.4.19. Effect of SiO_2 on chromium of slags with metals of 0.22Cr-Fe-C-S-Si and slags of 0.01CaO-Fe_2O_3-MgO-Cr_2O_3-SiO_2-Al_2O_3 Al_2O_3/MgO=1.7, 0.02-0.1 Si in Si-oxide crucibles at 1580°C.....248

Figure 4.4.20. Relations between silicon and $[a_{Cr}]/[a_C]$ with base metals of C-0.45Cr-0.001S-0.005Si-Fe by mole fraction at 1500°C.....249

Figure 4.4.21. Effect of Si on chromium of slags with metals of 0.55Cr-Fe-C-S-Si and slags of 0.01CaO-Fe_2O_3-MgO-Cr_2O_3-SiO_2-Al_2O_3 Al_2O_3/MgO=1.7, 0.03-0.05/0.02-0.1 Si in Cr/Si oxide crucibles.....250

Figure 4.4.22. Relations between silicon and activity of CrO (a_{CrO}) with base metals of C-0.45Cr-0.001S-0.005Si-Fe by mole fraction at 1500°C.....251

Figure 4.4.23. Effect of [Si] on chromium of slags with metals of 0.22Cr-Fe-C-S-Si and slags of 0.01CaO-0.007Fe_2O_3-MgO-Cr_2O_3-SiO_2-Al_2O_3, Al_2O_3/MgO=1.7, in Si-oxide crucibles at 1550°C 252

Figure 4.4.24. Carbon iso-concentration line of metals containing Cr-Fe-C-0.25%Si-(0.03-0.4)%S at 1500°C under CO atmosphere 253

Figure 4.4.25. Chromium iso-concentration line of metals containing Cr-Fe-C-0.25%Si-(0.03-0.4)%S at 1500°C under CO atmosphere 254

Figure 4.4.26. Iso-activity coefficient line for carbon in SiO_2-(Al_2O_3+CaO+MgO)-(Cr_2O_3+Fe_2O_3) ternary diagram with metals containing Cr-Fe-C-0.25%Si-(0.03-0.4)%S at 1500°C under CO atmosphere 255

Figure 4.4.27. Iso-activity coefficient line for chromium in SiO_2-(Al_2O_3+CaO+MgO)-(Cr_2O_3+Fe_2O_3) ternary diagram with metals containing Cr-Fe-C-0.25%Si-(0.03-0.4)%S at 1500°C under CO atmosphere 256

Figure 4.4.28. Iso-activity line for carbon in SiO_2-(Al_2O_3+CaO+MgO)-(Cr_2O_3+Fe_2O_3) ternary diagram with metals containing Cr-Fe-C-0.25%Si-(0.03-0.4)%S at 1500°C under CO atmosphere 257

Figure 4.4.29. Iso-activity line for chromium in SiO_2-(Al_2O_3+CaO+MgO)-(Cr_2O_3+Fe_2O_3) ternary diagram with metals containing Cr-Fe-C-0.25%Si-(0.03-0.4)%S at 1500°C

under CO atmosphere 258

CONTENTS

DECLARATION I-1

ABSTRACT. I-3

ACKNOWLEDGEMENT. I-7

LIST OF TABLES. I-8

LIST OF FIGURES. I-14

1. INTRODUCTION 1

1.1. CHROMIUM RESERVES 1

1.1.1. Chromite and Its Properties 1

1.1.2. Chromite Ore Reserves of the World 2

1.2. USAGE OF CHROMIUM ORES 6

1.3. BENEFICIATION OF CHROMITE ORES 8

1.4. PRODUCTION OF FERROCHROMIUM ALLOYS 9

1.4.1. Conventional Methods of Production 9

1.4.2. The Production Patterns of ferrochromium Alloys in the World 12

1.5. TECHNOLOGICAL TRENDS IN CHROMIUM ALLOY PRODUCTION AND SUPPLY 15

1.5.1. Features of Submerged-Arc-Furnace Technology 16

1.5.2. DC Arc or DC Plasma Technology 17

1.5.3. Preheating Technology 21

1.5.4. Pre-Reduction Technology 21

1.5.5. Direct Stainless Steel 24

1.6. MOTIVATION OF THE INVESTIGATION 26

2. LITERATURE SURVEY 29

2.1. GENERAL CONSIDERATIONS AND KINETIC STUDIES 29

2.2. KINETIC STUDIES 34

2.3. EQUILIBRIUM STUDIES 43

2.3.1. Metal Phase 43

2.3.2. Slag Phase 53

2.3.3. Slag Models 59

2.3.4. Slag-Metal Equilibrium 69

3. EXPERIMENTAL PROCEDURE 101

3.1. EXPERIMENTAL SET-UP 101

3.1.1. Furnace Assembly 101

3.1.2. Control of Partial Pressure of Carbon Monoxide 106

3.1.3. Temperature Control and Temperature Profile..... 110

3.1.4. Preparation of synthetic Al_2O_3-CaO-Cr_2O_3-Fe_2O_3-MgO-SiO_2-S Slags 111

3.1.5. Preparation of Cr-Fe-C-Si-S Alloys.....113

3.2. PREPARATION OF CHROMITE AND Cr-OXIDE CRUCIBLES.....

.....115

3.3. EXPERIMENTAL PROCEDURE.....117

3.3.1. Gas-Metal Equilibrium in Alumina Crucible 117

3.3.2. Gas-Slag-Metal Equilibrium in Cr-oxide and Alumina crucibles.....119

3.3.3. Determination of Equilibration Time.....120

3.3.4. Chemical Analyses 122

4. RESULTS AND DISCUSSIONS 125

4.1. EQUILIBRIUM RELATIONSHIPS OF CARBON, SILICON AND Pco BETWEEN GAS PHASE AND METAL PHASE.....146

4.1.1. Equilibria in Oxygen-Blowing Processes 146

4.1.2. Equilibrium Relationships of Carbon, Silicon and Pco 147

4.2. SILICON DISTRIBUTION BETWEEN SLAG AND METAL AT DIFFERENT PARTIAL PRESSURE OF CARBON

MONOXIDE 156

4.2.1. Influ... of Slag Composition on the Silicon Partition 158

4.2.2. Effects of Metal Composition on the Silicon Partition 161

4.3. EQUILIBRIUM PARTITION OF SULPHUR BETWEEN SLAG AND METAL AT DIFFERENT PARTIAL PRESSURE OF CARBON MONOXIDE 178

4.3.1. Influence of Slag Composition on Equilibrium Distribution of Sulphur 179

4.3.2. Influence of Metal Composition on Equilibrium Partition of Sulphur 186

4.3.3. Influence of Partial Pressure of Carbon monoxide 190

4.4. CHROMIUM DISTRIBUTION BETWEEN SLAG AND METAL AT DIFFERENT PARTIAL PRESSURE OF CARBON MONOXIDE 213

4.4.1. Formalisation of chromium oxides in slag phase 214

4.4.2. Variation of Chromium Content in slags 228

4.4.3. Representation of Iso-C and Iso-Cr Contents in Ternary Slag Diagrams 234

5. CONCLUSIONS 259

5.1. GAS-METAL EQUILIBRIA 260

5.2. Silicon Distribution in Gas-Slag-Metal Equilibria 260

5.3. Sulphur Distribution in Gas-Slag-Metal Equilibria 261

5.4. Chromium Distribution in Gas-Slag-Metal Equilibria 262

6. REFERENCE 264

7. APPENDICES 273

1. INTRODUCTION

1.1. CHROMIUM RESERVES

1.1.1. Chromite and Its Properties

The mineral chromite has the theoretical composition $FeO.Cr_2O_3$ with a theoretical content of 68 per cent Cr_2O_3 and 32 per cent FeO by weight. It is one of a group of isomorphous cubic minerals known as spinels which can be represented by the general formula $XO.Y_2O_3$ where X is a divalent metal ion usually iron, calcium, magnesium or manganese and Y is a trivalent metal ion usually iron, chromium or aluminium. The spinels have a wide range of mutual solid solubility. In natural chromite the replacement of chromium and iron by other elements always occurs to some extent. The chromium is replaced mainly by aluminum and the iron by magnesium, which are the main reasons why the commercial chrome ores rarely contain more than 50 to 55 per cent Cr_2O_3 and some contain up to 20 per cent of both Al_2O_3 and MgO. Analyses of typical chromite ores from various deposits are given in table 1.1[1,2].

Chromite varies in colour from dark brown to jet black and usually occurs in a m. ve form with a granular structure, although individual crystals are octahedral. The interstitial material usually consists of magnesium silicates. Compared with most other minerals it is fairly soft, its hardness being 5.5 on Moh's scale. Its density ranges from 4.6 for high grade ores to 4.0 for low grade ores. Its melting point varies with its composition in the range 1545 to 1730 °C. It has a lustre approaching to that of metals and it is almost insoluble in acids[3].

1.1.2. Chromite Ore Reserves of the World

Lead chromite ($PbCrO_4$), an orange-red mineral found in the Beresof Mine on the eastern slopes of the Ural Mountains in 1766, was the first known and mined source of chromium. Sixty years later, a deposit of the black mineral chromite was found in Maryland in U.S.A. in 1827, and this deposit was the only available source of chromite ore in the world for about twenty years. In 1848 high-grade chromite deposits were discovered in Turkey, and these constituted the main source of supply until the discovery of chromite ore in India and Rhodesia in about 1906[2]. Chromite ore is obtained from major sources in ten different countries, but about 98 per cent of world's chromite reserves are found in the Republic of South Africa (68%) and Zimbabwe (30%)[4].

South Africa

Of the world's total reserves of chromite ore, which amount to 3330 Mt, 68 per cent or 2270 Mt are in the Republic of South Africa and 30 per cent or 1000 Mt in Zimbabwe. The vast reserves of chromite in South Africa are all situated in the Transvaal and form a mammoth geological intrusion termed the Bushveld Igneous Complex, said to be the largest igneous rock complex in the world. This geological phenomenon enables South Africa to lay claim to the world's largest known reserves of andalusite, vanadium, platinum, platinum-group metals and chromite. To facilitate a true appreciation of the magnitude of South Africa's chromite resources, an interesting analogy may be drawn. If chromite were to be represented by crude oil, then, on the percentage basis, the country's contribution to world reserves would be slightly more than the combined reserves of Canada, the United States, Western Europe, Eastern Europe and the entire Middle East[4].

Table 1.1. Analyses of Various Chrome Ores[1]

country	type or use	Cr_2O_3	FeO	Al_2O_3	MgO	CaO	SiO_2	Cr/Fe
South Africa	Standard Friable	44.50	24.71	15.03	10.05	0.31	3.86	1.58
South Africa	Hard lump	42.41	24.80	15.95	8.35	0.36	6.27	1.50
South Africa	High grade	48.40	22.87	13.94	10.72	0.20	2.55	1.86
Zimbabwe	Selukwe	49.70	14.37	13.10	13.06	0.46	6.77	3.05
Zimbabwe	Selukwe	47.00	11.93	12.65	15.46	1.77	5.71	3.47
Zimbabwe	Selukwe Refractory	42.63	15.65	13.80	15.77	0.32	8.59	2.40
Zimbabwe	Great dyke	50.73	16.38	13.01	13.23	0.75	4.33	2.73
Zimbabwe	Great dyke	47.00	16.00	10.00	18.00	0.50	8.50	2.70
Cuba	Camagtey	30.84	13.18	20.03	18.92	0.91	5.33	2.08
Cuba	Moa Bay	36.00	14.51	27.50	16.53	0.45	3.85	2.19
Philippines	Masinloc	32.21	12.27	30.20	18.06	0.44	5.00	2.21
Philippines	Acoje Concentrate	49.32	18.80	11.37	15.85	---	3.50	2.30
Turkey	Metallurgical	48.26	14.11	13.03	16.85	0.96	5.08	3.02
Turkey	Kefdag	42.44	12.50	16.75	17.92	0.25	6.21	2.97
Turkey	Refractory	37.10	13.94	24.35	17.74	0.22	4.34	2.36
New Caledonia	Metallurgical	51.10	14.15	11.16	16.96	0.10	5.75	3.20
Russia	Metallurgical	53.87	12.56	9.63	13.27	1.06	5.822	3.77
Russia	Refractory	39.08	13.98	17.35	16.07	0.65	9.38	2.46
Yugoslavia	Metallurgical	49.73	15.16	10.40	15.90	0.422	5.98	2.90
India	Orissa	49.90	13.85	10.85	15.26	0.17	6.25	3.17
India	Mysore,Refractory	41.53	22.41	13.40	12.34	0.06	6.91	1.63
Greece	Tsagli No.1	45.18	15.16	17.08	15.82	0.35	3.80	2.60
Greece	Domnikos	35.80	16.30	22.12	14.50	0.54	5.96	1.92
United States	Stillwater	38.30	23.20	15.45	13.43	----	6.00	1.47
Pakistan	Baluchistan	48.40	15.20	10.80	16.37	0.30	4.98	2.82
Sierra Leone	Kambui Hills	42.00	14.08	21.23	16.16	0.05	4.81	2.53

The Bushveld Igneous Complex in South Africa, an enormous saucer-like intrusive igneous mass, extends for about 400 km from east to west, and roughly the same distance from north to south, and is located in the central and slightly western portion of the Transvaal. The Complex is highly mineralized, comprising deposits of fluorspar and tin in the acidic phase, platinum group metals and chromite (which are associated with nickel, copper, and cobalt sulphide), and magnetites, which occur together with vanadium and titanium in discrete layers. The major reserves of platinum group metals occur in the UG-2 Reef and Merensky Reef, which constitute the largest known deposits of chromium, vanadium, and platinum in the world. The four major areas in which chromite ore is mined are the eastern chromite belt, the western chromite belt, the Zeerust district, and the area south of Potgietersrus.

The deposits in the Zeerust and Potgietersrus areas, where the resources are limited, have the highest Cr_2O_3 content (52 to 57 per cent) and the highest chromium-to-iron ratios (2.0 to 2.9). The major deposits are in the western and eastern Bushveld, where the resources are vast but are of lower grade (45 per cent Cr_2O_3) and have chromium-to-iron ratios of 1.5 to 1.6. Other deposits have slightly lower Cr_2O_3 contents and lower chromium-to-iron ratios(about 1.4). In all, 21 mines have been established in these areas. Chromite ores from Zimbabwe and Turkey have a higher chromium-to-iron ratio of 3.0 and 3.5 respectively.

The chromite ores mined fall basically into two categories -- the hard lumpy variety and the friable type. In the vast chromite reserves of South Africa, 70 per cent is classed as lower grade chromite ores and only 30 per cent can be high grade chromite (chromium-rich, high chromium-to-iron ratio, hard and lumpy). These are both derived from underground mining operations as the nature of the deposits precludes the use of open-cast mining. Most of these ores then undergo an up-grading operation in beneficiation plants, which characteristically use simple screening and hand-sorting operations. In some cases, complex heavy-medium, magnetic, gravity separation techniques may be necessary. Intermediate and more widely used operations comprise crushing, washing-screening, hand-sorting or crushing, and washing-grinding-gravity separation. For gravity separation, mainly spiral concentrators are used although shaking tables are used in a few instances. The up-graded

ores, which generally have chromium-to-iron ratios of 1.3 to 2.4, are then either railed for export or sent to smelting plants for conversion into ferro-chromium[4].

Zimbabwe[4,5]

Zimbabwe is the largest known source in the world of the high-chromium ores with officially published figures giving reserves of 560 Mt or about 86 per cent of the total world's reserves of the high-chromium ores and a similar additional amount as potential further reserves. Reserves of high-chromium ores for the remainder of the world, including South Africa and Eastern Europe, have been estimated at approximately 90 Mt (about 14 per cent of the total world's reserves). With a potential of a further 87 Mt, Southern Africa sub-continent holds 98 per cent of the presently identified reserves of chromite ores in the world.

The chromite ores of Zimbabwe can be classified into two main types: the seam deposits occurring in the Great Dyke and the alpine or podiform deposits. The Great Dyke deposits comprise the major part of the known reserves of Zimbabwe chromium ores. In the alpine deposits chromium occurs as isolated occurrences in ultrabasic intrusions, not associated with the Great Dyke.

For many years, the ores from the podiform deposits in Zimbabwe, which are hard and lumpy and have a chromium-to-iron ratio of 3.0 and higher, were the principal raw material used by the ferro-chromium industry of the Western World. The depletion of these resources led to the exploitation of the chromite ores from the Great Dyke, which currently contains the entire reserves of chromite ore in Zimbabwe. The chemical compositions of the both ores have been listed in table 1.1. The ore from the Lower Group seams of the Great Dyke is of high grade, 43 to 54 per cent of Cr_2O_3 with chromium-to-iron ratios of 2.6 to 3.5, but is much more friable than the ore from podiform deposits, and is not readily amenable to mechanised mining. The chemical variations between the different podiform ores are complex and they cannot be characterised as simply as the seams on the Great Dyke. The range in Cr_2O_3 content of podiform's ores is very similar to that of the Great Dyke ores, the mean of 44% Cr_2O_3 is slightly less than the mean of 47% Cr_2O_3 for the

Great Dyke ores. The mean chromium-to-iron ratio is somewhat greater than 2.9 (ranging from 1.9 to 4.1), compared with 2.7(ranging from 2.0 to 3.5) for the Great Dyke ores. This is due to the generally lower content of approximately 12% FeO in the podiform ores, compared with approximately 16% FeO in the Great Dyke.

The Former U.S.S.R. and the Eastern Bloc

The reserves of chromite ores in the former USSR appear to be fairly substantial and are located almost entirely in the Ural Mountains, where the first chromium-containing mineral was discovered. An early Roskill report estimated the reserves at only 43 Mt. However, carefully sifting of the available evidence from German and U.S.A. sources indicates that the reserves may be much larger, amounting to over 200 Mt of proven reserves and 180 Mt of potential reserves, i.e. about one-sixth of those in South Africa. On average, the proven resources appear to contain about 50 per cent Cr_2O_3 and to have a chromium-to-iron ratio between 2.8 and 3.0.

Albania emerged comparatively recently in the production of chromite ore. The deposits, which are located in the Dinaric Alps, have estimated reserves of 22 Mt of massive hard ore with an average Cr_2O_3 content of 43 per cent and a chromium-to-iron ratio of 3.0. Most of the ore is suitable for metallurgical and refractory usage, but a substantial proportion of the run-of-mine ore appears to be subjected to beneficiation processes, probably to produce concentrates for the production of chemicals.

1.2. USAGE OF CHROMIUM ORES

The three main areas for the first-use consumption of chromium ores are the metallurgical industry (ferro-chromium alloys and chromium metal), the refractories industry (refractories and foundry sands), and the chemical industry.

The metallurgical use results from the addition of chromium to improve the strength, corrosion and oxidation resistance of iron, nickel and other metals. For addition to ferrous alloys, chromium is usually produced as a ferro-chromium alloy containing approximately 70 per cent chromium.

In order to be suitable for the production of ferro-chromium, chrome ore should contain a minimum of 48 per cent of Cr_2O_3 with sulphur and phosphorus contents each less than 0.1 per cent and the ratio of chromium to iron preferably not less than 2.8. Silica is an undesirable constituent and the combined content of alumina and magnesia is preferably below 25 per cent. The minimum value of 48 per cent Cr_2O_3 is commonly taken as a basis for price evaluation.

Chromite ores are used extensively for refractory purposes. It differs from most other refractories in common use in that it is chemically almost neutral and consequently it resists attack by both acids and bases at high temperatures. Although pure chromite has a high melting point, the ore consists of chromite embedded in a matrix of magnesium silicates which have a lower softening temperature. For the best quality chromite refractories, therefore, it is desirable to have an ore with as low a silicate content as possible and it is desirable to keep this as low as 5 per cent if possible. The refractoriness also decreases with increasing iron content. For refractory purposes, therefore, an ore is required to have high contents of Cr_2O_3, Al_2O_3 and with low silicate and iron oxide contents. The combined content of Cr_2O_3 and Al_2O_3 is usually 57 to 63 per cent.

The chemical use of chromite is almost entirely for the primary production of sodium dichromate. For this purpose the chromite should contain a minimum of around 45 per cent Cr_2O_3. The iron content can be much higher than for metallurgical or refractory use and a common chromium-to-iron ratio is 1.6. Silica should be less than 8 per cent and sulphur must be at a low level. The large chemical use of chromite is for tanning and for the production of pigments. The tanning industry employs chrome alum and dichromates while the chrome pigments are usually produced from lead chromate. Chrome oxide green is 97-99 per cent chromic oxide, Guignet's green is a hydrated chromic oxide, while chrome yellow and zinc chrome are lead and zinc chromates.

Another important chemical use of chromite is for surface treatment of metals in which a sodium dichromate dip is used for cleansing and pickling prior to galvanizing steel and for brightening the surface of brass. Chromium electroplating for wear resistance and for decorative finishing is also an example of chemical use of chrome ores since it is carried out in a chromic acid bath, the chromic acid being prepared from sodium dichromate. Finally, chromite and other chromium compounds are used extensively as colouring agents in ceramic glazes and in glass making.

1.3. BENEFICIATION OF CHROMITE ORES

The stable structure of chromite ores implies their beneficiation is limited to those capable of removing the physically associated gangue minerals, gravity-concentration processes normally being applicable. Some degree of beneficiation treatment is applied to the ore from most of the deposits in the world. The milling cost in Zimbabwe are possibly the lowest in the world because of the nature of the ore, but the mining and freight costs are relatively high. South Africa chromite ores all undergo at least rudimentary beneficiation. Several methods are employed, the choice depending to a considerable degree on the type of product desired. Simple screening and hand-sorting operations may be adequate in some cases, but complex heavy medium, magnetic, and gravity separation may be necessary in others. Intermediate and more widely used operations comprise crushing, washing screening, hand sorting or crushing, and washing-grinding-gravity separation. For gravity separation, mainly spiral concentrators are used; although shaking tables are used in a few instances

Recoveries are usually within 80 to 85 per cent but, with the limitation of the beneficiation process, The Cr_2O_3 grade can be increased by only 1 to 4 per cent. The operating cost for beneficiation are relatively low, probably in the range R3.50 to R12 per ton of feed, of which the labour component accounts for 40 to 50 per cent. Precise data are not available for the tonnages of ore treated by the various beneficiation processes employed. Only about

30 per cent of the chromite ore mined in South Africa can be classified as 'lump ore' (a production of just under 1 Mt/a), most of which is used for the production of ferro-chromium in submerged-arc-furnaces. At an 85 per cent recovery of the chromium in the ore into the ferro-alloy, 2t of ore are needed to produce 1t of ferro-alloy, and about 2 Mt of ore containing 44 per cent Cr_2O_3 are needed to produce 900 kt of alloy. Therefore, ferro-chromium producers absorb a substantial proportion of the beneficiated ore and leave about 1 Mt of beneficiated ore for other purposes. A large proportion of the beneficiated ore is too fine to be fed direct to submerged-arc-furnaces, and requires some form of agglomeration before it can be used. Some of the concentrates from the grinding and beneficiation processes constitute the starting materials for the production of chemicals, refractories, and foundry sands.

1.4. PRODUCTION OF FERRO-CHROMIUM ALLOYS

1.4.1. Conventional Methods of Production

The largest use of chromium in metallurgical production is for the manufacture of chromium steels. For this purpose, chromium may be used as an iron-chromium addition alloy, which can be produced directly from the mineral chromite without the necessity for any preliminary treatment to separate iron and chromium in the ore. Commercial ferro-chromium contains 45 to 75 per cent chromium and is produced by the direct reduction of chrome ore. The theoretical composition $Cr_2O_3.FeO$ contains 68 per cent Cr_2O_3 and 32 per cent of FeO by weight, which corresponds to a chromium:iron percentage proportion of 65:35. In practice, as noted before, due to contamination by oxides of aluminium, magnesium and silicon the content of chromic oxide in the ore rarely exceeds 50 to 55 per cent and is often less. For the production of metallurgical ferro-alloys, chrome ore is selected with a minimum chromic oxide content of 48 per cent and with a chromium to iron ratio as high as possible. Four types of ferro-chromium are commercially produced:

1. High carbon ferro-chromium (including charge chrome)
2. Medium carbon ferro-chromium
3. Low carbon ferro-chromium
4. Low carbon, high chromium

Each type of ferro-chromium is divided into two groups by phosphorous content, namely normal P content with maximum P content of 0.05 per cent in the alloys, and low P content with maximum P of 0.03 per cent. The compositions of the alloys are listed in table 1.2.

Table 1.2. The Chemical Composition of Ferro-Chromium Alloys

Type	Cr%	C%	Si%	S%
H-Carbon	45--75	4.0--10	Up to 6	Up to 0.05
M-Carbon	45--75	0.5--4	Up to 1.5	Up to0.05
L-Carbon	45--75	Up to 0.5	Up to 1.5	Up to0.03
L-C,H-Cr	75--95	Up to 0.5	Up to 1.5	Up to0.03

Note: maximum nitrogen content is 0.15% for the low-carbon alloy; and for the low-carbon and high-chromium alloy, maximum N is 0.20% and maximum Ni 0.15%, maximum Co 0.02%.

High Carbon Ferro-Chromium

The commercial production of high carbon ferro-chromium dated back to the first industrial use of low chromium alloy steels in about 1760 to 1870. Small quantities had, however, been produced at a much earlier date, usually by the rather simple method of heating the oxides of iron and chromium mixed with powdered charcoal in a crucible, a method first proposed by P.Berthier in 1821[6]. This method continued to [illegible] it was supplanted by the direct reduction of chromite and chrome-ferrous iron ore with coke or coal in a blast furnace, an innovation due to E. Fremy[7]. At first this method was used to produce ferro-chromium with quite low chromium content, usually not more than 7 or 8 per cent. The ferro-chromium went by the name of 'Tasmanian Pig Iron' derived from the fact it could be

produced by the direct reduction of the chrome-ferrous iron ore of Tasmania. To produce higher chromium content required higher blast temperatures and the use of large quantities of coke and it was not until 1870 to 1880 that ferro-chromium containing as much as 30 to 40 per cent chromium was in regular commercial production. The first ferro-chromium, as it is known today, containing 70 per cent chromium, was produced in Sweden and its production was first described by E. G. Odelstjerna [8] in 1886.

The major improvement in the production of ferro-chromium came with the introduction of the electric arc furnace instead of the blast furnace. To obtain even chromium content of 30 to 40 per cent in the blast furnace involved very high fuel costs. Since the furnace ran at a relatively low temperature the carbon content, which was often as high as 10 to 12 per cent, was much higher than that produced in the modern electric arc furnace process. Sulphur and phosphorus also were present in much larger amount than in the modern product. Attempts were made to produce higher chromium content by increasing the temperature in the blast furnace by means of an oxygen enriched blast but this process was much too expensive to compete with the electric arc furnace process. The development of the electric arc furnace and its application to the reduction of chromite ore is due to H. Moissan[9] and has led to the modern commercial production on a very considerable scale of high carbon ferro-chromium containing 67 to 71 per cent chromium and about 4 to 6 per cent carbon.

The electric furnace most commonly used for its production is the open top submerged arc furnace, in which the arc occurs between electrodes submerged in the charge. The steel furnace shell is lined with chromite or some other suitable refractory and the metal can be taped as necessary during the reduction. The chromite used is of a selected grade containing a minimum of 48 per cent Cr_2O_3 and a ratio of chromium to iron approximating to 3.0. The content of silica in the chromite is as low as possible. Coke is usually employed as the reductant. The charge is fed into the top of the furnace where it is continually rubbed to prevent the accumulation of dangerous gas pockets, containing carbon monoxide which is evolved as a consequence of the reduction reaction. The high carbon ferro-chromium collects at the bottom of the furnace and is tapped into ladles and cast into chill moulds. When it is cool, it is broken up and sorted to remove adhering slag. It is graded according to its carbon content and is sold in various grades.

Low Carbon Ferro-Chromium

The changes in the production of stainless steel affected the consumption pattern of chromium alloys in the past decades because about 79 per cent of the world's chrome products are used for the production of steel and other special alloys. Low carbon ferro-chromium was used to a large extent in the past, but high carbon ferro-chromium became dominant as the conventional processes for stainless-steel production utilizing electric arc furnace were replaced by oxygen-blowing processes, such as AOD, and VOD. Due to the problems coming from the use of high carbon chromium and coming from the limitation of steelmaking itself, certain amount of low carbon ferro-chromium, about 6 per cent of the total ferro-chromium, has to be used to produce steels and other special alloys [10]. For the production of a low carbon alloy, the chromium oxides must be reduced by a non-carbonaceous reducing agent like the silicon component of ferro-silicon or ferro-chromium-silicon. The most common method employed for the production of low carbon ferro-chromium involves the very vigorous mixing of a molten lime-chromite slag with ferro-silicon or ferro-chromium-silicon. The iron and the chromium are both reduced from the spinel, and the chromium-to-iron ratio in the ore prevails in the ferro-chromium alloy. This fact has a pronounced bearing on the economic aspects of ferrochromium production, since the price of the product is determined by the contained units of chromium present. Former specifications usually called for a chromium content of not less than 60 per cent, but this was waived as a result of the large tonnage of charge chrome sold by South Africa.

1.4.2. The Production Patterns of Ferrochromium Alloys in the World

In South Africa

Major attention has been given to South Africa, which is currently the largest producer of ferro-chromium alloys in the world. It can be seen that the production of ferro-chromium alloys by South Africa in the 1990s represented about one-third of the total production in the world. Up to thirty years ago, the chromite ores mined in South Africa were considered

to be suitable mainly for use in the chemical industries since the high iron content is beneficial in the production of sodium dichromate. Smaller quantities of ores with a higher alumina content were used for the production of foundry sands. Almost all the chromite mined up to 1960 was exported, although small quantities were used locally for the production of sodium dichromate. The South Africa ores were not seriously considered for smelting to produce ferro-chromium, mainly because of their low ratios of chromium to iron (about 1.5). World ferro-chromium producers preferred to use the ores from Zimbabwe and the former USSR, since those ores were hard and lumpy and had chromium-to-iron ratios of 2.5 to 3. In addition, low carbon ferro-chromium was essential for the manufacture of stainless steel.

After solving some problems, the low-grade ores mined in South Africa were used to produce an alloy containing 50 to 52 per cent of chromium, 6 to 7 per cent of silicon and 6 to 8 per cent of carbon. This product was described as 'CHARGE CHROME'. After some aggressive marketing campaigns, this alloy was accepted by stainless-steel producers world wide, which gave a great impetus to South African ferro-chromium industry. The production of ferro-chromium in South Africa really began to escalate in the 1970s, rising from 200 kt in 1973 to 1900 kt in 1995 (being equivalent to about 35 per cent of the world's total).

In the U.S.A.

In the decade 1950 to 1960, U.S. imports of chromite ore reached a maximum of just over 1.5 Mt/a or 65 per cent of the world exports of this commodity. In the decade 1970 to 1980, the imports of chromite ore were 1.06 Mt/a or only 23 per cent of world exports. South Africa was still the main supplier of chromite ore to the United States, accounting on average for 44 per cent of all the U.S. imports of this commodity from 1977 to 1980.

The apparent consumption of ferro-chromium in the U.S.A. rose from 190 kt in 1970 to 293 kt in 1981. During that period, the imports of ferro-chromium as a percentage of the apparent consumption rose from 12 to 76 per cent.

A recent calculation by the U.S. Bureau of Mines indicated that the weighted average cost per pound of contained chromium in high carbon ferro-chromium smelted in South Africa from local chromite ore is $0.32 f.o.b. Durban, whereas that for the same ore smelted in the U.S.A. would be $0.43 f.o.b. Pittsburg. As transportation costs to the U.S.A. could range from $0.04 to $0.12 per pound, the difference is not considered to represent a major competitive advantage for producers in South Africa. However, the depreciation in the recent exchange rate of the Rand versus the US dollar has undoubtedly contributed materially to increased exports of ferro-chromium from South Africa.

In Japan

In Japan, which uses some of the most up-to-date and efficient metallurgical processes in the world, the same change in the ferro-chromium production is becoming evident. Japan's imports of chromite ore ranged from 962 kt in 1979 to 645 kt in 1983, with those from South Africa remaining fairly constant at 42 to 47 per cent of the total. The respective production of ferro-chromium in Japan in 1977 and 1983 fell from 380.2 to 297.77 kt, whereas the imports rose from 104.1 to 297 kt. The local production was equivalent to 90 per cent of the consumption in 1977, but fell to 56 per cent in 1983. Except for the low figures for 1982, the production of stainless steel in Japan in this period was fairly constant, being within the range 1.75 to 1.84 Mt/a.

There appears to be little doubt that the production of ferro-chromium in Japan will continue to fall, since three plants were closed down in 1983/1984. Increased costs of fuel for the generation of electrical energy, possibly aggravated by the imposition of stringent regulations for the control of atmospheric pollution, have resulted in an average production cost in Japan of at least $0.45(U.S.) per pound of contained chromium, compared with a c.i.f. cost of around $0.40(U.S.) per pound of imported alloy.

In the former USSR and the Eastern Bloc

In addition to the dominant position of South Africa among world producers of ferro-chromium, the increasing influence of the former U.S.S.R. and the countries in the Eastern Bloc has to be highlighted. The production of ferro-chromium in those countries was less severely affected by the world recession in the steel industry than it was in the Western World, and that those countries accounted for about one-third of the total world production in the very early 1980s. China is an unusual country: it appears to have produced up to 90 kt of ferrochromium but has only minute known reserves of chromite ores. Until 1978 most of the ore required by China was obtained from Albania, but, after a breakdown in relations between the two countries, China has to obtain ore from various alternative suppliers, one of which is reported to be Zimbabwe, which also supplies China with ferro-chromium.

1.5. TECHNOLOGICAL TRENDS IN CHROMIUM ALLOY PRODUCTION AND SUPPLY

The production of ferro-chromium alloys is dominated by the submerged-arc-furnace. Submerged-arc smelting of ferro-chromium, according to D. Slatter[11], is now a mature technology where improvements to decrease costs are becoming increasingly difficult. As a result, some ferro-chromium producers are introducing new technologies to be more cost effective and to produce better products. These developments included are D.C. plasma smelting, pre-heating and pre-reduction processes, and processing units such as the rotary kiln, rotary hearth furnace and fluid-bed reactor. Finally, the question of 'direct stainless steel' is discussed with its implications for the future's supply of ferro-chromium.

1.5.1. Features of Submerged-Arc-Furnace Technology

Strengths

The major advantage of the submerged-arc-furnace for smelting chromite may be described as:

1. Relatively easy to control provided the charge is well classified to maintain a permeable overburden and allow escape of reduction gases, and provided also that the charge composition is well calculated and remains constant to maintain steady state of electrical conditions and target slag composition;

2. Self regulating, with power input determining rate of consumption of overburden;

3. Some preheating and pre-reduction of the overburden by the hot, ascending reaction gases.

Weaknesses

The shortcomings of the submerged-arc-smelting technology for ferro-chromium production can be noted as:

1. Requires lump ore or agglomerated ore fines for maximum operating efficiency and maximum chromium recovery. This is an important factor, for example, in South Africa where approximately 70 per cent of the chromite mined is produced as fines. Agglomeration by pelletising or briquetting is costly and may not be entirely effective in furnace operations.

2. High cost coke is required as a reductant mainly to achieve correct electrical resistivity in the burden. Coal can be used in part to adjust resistivity but there may be problems with evolution and combustion of volatiles above the burden, with consequent overheating of the furnace superstructure;

3. Furnace operation and metallurgical control is dictated by the quality and physical form of the charge, and by the slag composition;

4. Slow and diluted response to deliberate changes in charge composition;

5. Chromium recoveries range from poor (65%) with high fines usage, to moderate (80%);

6. Waste-gas utilisation not practical unless the furnace is closed.

There have, however, been some recent developments to improve the efficiency of submerged-arc-furnace. These include:

1. Computerised control to optimise power inputs;
2. Closed top operations with utilisation of off-gas energy;
3. Pelletised and pre-oxidised fines feed;
4. Optimising slag compositions for maximum chromium recovery.

For example, minimising MgO:CaO ratio in the slag improves chromium spinel dissolution thus enabling more complete chromium reduction and improved chromium recovery. Similarly, changing from basic to acid slag practice also increases spinel dissolution and chromium recovery but there are penalties in the control of silicon and sulphur in the alloy, and in decreased taphole refractory life.

1.5.2. DC Arc or DC Plasma Technology

Various organisations have carried out developmental work in the use of D.C. arc or D.C. plasma technology for smelting chromite to ferro-chromium. In U.K., for example, non-consumable electrode was used [12]. In Sweden SKF with their non-transferred arc heaters

was incorporated in their Plasmamelt Process which became a commercial operation in Malmo but unfortunately only operated for a short time before being closed down as a result of the recent decline in the ferro-chromium market[13]. The transferred arc with hollow graphite electrodes was developed by the South Carolina Research Authority, SCRA, a joint development with Macalloy in the United States[14]. The most successful development in this field has been the collaborative programme between Mintek and the Former Middleburg Steel and Alloys (MS&A)[11,15]. This commenced in the late 1970s, accelerated rapidly in the early 1980s and resulted in the world's first commercial D.C. arc furnace in 1984[16]. The furnace was rated at 16 MVA and operated until 1988 when it was reconstructed and uprated to 40 MVA. It is still the only D.C. arc furnace in world producing ferrochromium alloys. The furnace's main features are shown in figure 1.1. These include: single central hollow graphite electrode; DC transferred arc from the graphite electrode (cathode) to the copper bus tube (anode) at the base plate of the furnace via a conducting refractory hearth; fine materials feed though the hollow electrode; open-bath smelting operation; closed furnace with single gas off-take.

Many of the weaknesses of the submerged arc furnace are the strengths of the D.C. arc furnace, such as:

- operation with ore fines without prior agglomeration;
- use of cheaper reductant such as anthracite or coal, which allows a wider choice of reductant so that sulphur and phosphorus inputs can be minimised;
- achievement of higher chromium recoveries (>85%);
- changes in charge composition are reflected rapidly in slag and/or metal composition;
- great freedom in metallurgical control; for example, because slag resistivity is no longer a limitation, high CaO slags, with conductivities too high for submerged-arc-furnace operation, can be used for production of extra low sulphur alloys;
- closed top operation is simplified with single electrode only, and collection and utilization of waste-gas energy becomes a better proposition;
- better control of, and greater range in, product composition; for example, alloys with ultra low contents of S and P (by reductant choice and slag-composition control) and silicon levels from less than 1% to 3-4% can be produced on request.

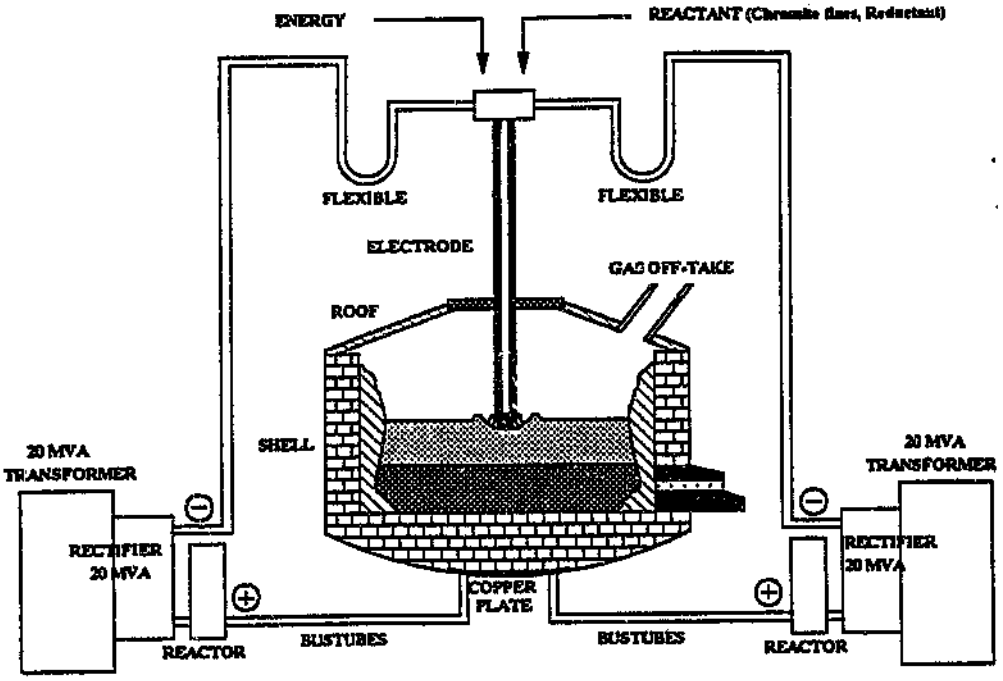


Figure 1.1. Cross section of DC-plasma furnace [15]

The D.C. arc furnace also has the ability to produce chromium-bearing alloys other than high-carbon ferro-chromium or charge chrome. For example, selective reduction of low Cr:Fe chromite ores can be carried out to produce a low chromium high iron (but high sulphur) alloy and a slag with an increased Cr:Fe ratio. This slag may be subsequently processed to high carbon ferrochromium with a greater chromium content that was impossible with the original ore. The production of medium-carbon ferro-chromium (0.5-4.0% C) can be made by reacting charge chrome fines with chromite ore fines, the ore being reduced by the silicon and carbon contained in the charge chrome. The by-product is a low-grade chromium slag with a high Cr:Fe ratio for processing to high chromium alloys.

There are, however, some important control factors to be considered and some disadvantages in D.C. arc operation:

1. Strict operation control is necessary requiring reliable and comprehensive instrumentation, data logging and process control systems. For example, the feed:power balance is critical; excess power(or insufficient feed) leads to superheating of the bath with grave implications for refractory and furnace integrity, while insufficient power(or excess feed) causes freezing of the bath, electrode blockages and tapping problems;

2. Stray arcing can be a problem;

3. Taphole maintenance is more critical than in a submerged-arc-furnace;

4. Lower thermal efficiency than a submerged-arc-furnace due to greater radiation loss from the open-bath operation and higher-temperature gases leaving the system.

The most important area for development work on the D.C. arc furnace is to improve its thermal efficiency by using the energy in the furnace off-gases. This has to lead to the next technological improvement, which is discussed in the following section.

1.5.3. Preheating Technology

Some preheating is inherent in submerged arc furnace operation with the hot furnace gases ascending through the overburden. In addition, Outokumpu have incorporated a degree of preheating by directing the hot off-gases through overhead bins containing the charge and by using the furnace gases to preheat a pelletised chromite feed. The most effective application of pre-heating is, however, likely to be linked to the D.C. arc furnace[11].

Because the charge to the D.C. arc furnace consists of fine materials, it appears logical to use a fluidised-bed system as the pre-heater. Experimental test-work was carried out by MS&A with Mintek and the development has been conducted by Samancor. In 1994, a large pilot operation was successfully completed and the process is ready for commercial application. It is estimated that preheating of the charge to the D.C. arc furnace in this manner will decrease the electrical energy requirement by approximately 1 Mwh/t alloy and increase furnace throughput by approximately 30 per cent. The effective use of off-gas energy in preheating the charge is a step towards decreasing the use of electric energy, a high cost component in the production of ferro-chromium in many countries. A further step in decreasing the electrical energy component is to pre-reduce the chromite using cheaper sources of energy prior to final electric smelting.

1.5.4. Pre-Reduction Technology

Significant developments in pre-reduction have already been made and others are in progress or will undoubtedly be made in the future, as this is an area in which substantial cost savings may be realised. The following is a brief survey of existing or potential pre-reduction processes[11].

SDK/CMI Process

Developed and used originally by Showa Denko (SDK) in Japan and subsequently installed

by Consolidated Metallurgical Industries in South Africa in the mid-1970s. This was the first commercial pre-reduction process for chromite. In the process, chromite ore fines are milled finer, pelletised with coke as reductant, and fired in a rotary kiln to approximately 1400 °C. The kiln is heated by pulverised coal burner. The pellets achieve approximately 60 per cent total metallisation of chromium and iron, and are discharged into a submerged arc furnace for final smelting.

The major advantages of the process include:

- decrease electrical energy requirement (approximately 2.2 Mwh/t alloy versus 3.8 Mwh/t alloy for submerged arc smelting);
- use of low cost coal-based energy;
- greater flexibility in furnace slag composition with respect to electrical conductivity due to the decreased proportion of reductant in the charge, thus the CaO content of slag can be higher for desulphurisation of the metal;
- higher chromium recoveries than in submerged arc furnace smelting; and the utilization of ore fines.

The major disadvantages, meanwhile, of the process are: costs incurred in milling and pelletising the ore fines; requirement for coke in the pellets; only moderate levels of metallisation, mainly the iron component which is more easily reduced; relatively high carbon content in the final alloy; accretion formation in the kiln.

CDR Process

To address some of the apparent weaknesses of SDK Process, Krupp commenced development of a rotary kiln pre-reduction process in 1984, based partly upon their earlier experience of the Krupp CODIR Process for DRI production. MS&A and Samancor were jointly involved in batch trial and pilot trial on the process. A commercial plant was installed at the Middleburg Ferro-chrome plant in 1990 and named CDR for Chrome Direct Reduction.

Amongst the advantages anticipated for this process over, for example, the SDK Process, are: direct use of un-agglomerated chromite fines; self agglomeration of the fines in the high temperature zone (approximately 1500°C) where the charge becomes pasty; use of low cost coal for both the energy source and the reductant; high degree of metallisation (80% to >90%); further decreases in the electrical energy required for final smelting to approximately 1.6 Mwh/t alloy for cold charging and 1.2 Mwh/t for hot charging.

Difficulties associated with the operation and which are receiving attention include: accretion formation and its prevention or elimination; determining the most suitable refractories, particularly in relation to accretion forming tendency; effective temperature measurement within the kiln along the reaction zone maintaining a constant degree of pre-reduction and agglomeration.

The commercial plant has had some developmental difficulties but these are being progressively resolved and already many of the perceived advantages have been realised. With the high levels of metallisation, which are attained, the final furnace treatment becomes mainly a melting rather than a smelting operation. A dedicated furnace for treating the kiln product may be either a submerged arc furnace operating as a slag resistance furnace or a D.C. arc furnace.

Rotary Hearth Furnace

The rotary hearth furnace is potentially capable of pre-reducing chromite and pilot tests have been conducted to investigate it for this application. The chromite fines are pelletised with coal as reductant, charged as a stationary monolayer onto the moving rotary hearth and discharged after one revolution. Potential advantages include: low cost pellets due to low pellet strength requirement; use of coal in the pellets for the same reason; rapid metallisation (15 to 20 minutes) to high levels (80%) at temperature of 1450°C; low maintenance cost compared with rotary kilns; no accretion formation. The pilot tests, however, demonstrated that there is a strong tendency for the pellets to re-oxidise rapidly due to difficulties in maintaining a sufficiently low P_{O_2} in the pellet monolayer. Further development work is necessary.

Fluidised-Bed Technology

If the fluidised bed can be used as a pre-heater for chromite why not a pre-reducer as well? The reason is that pre-reduction of chromite requires temperatures of at least 1300°C, preferably 1350-1400°C. At those temperatures, with carbonaceous reductant and, therefore, ash components present, incipient fusion and clinkering occurs, resulting in breakdown of the fluidised-bed operation. If the pre-reduction temperature of chromite could be lowered significantly, the fluidised bed may become an effective unit for this purpose. In this respect, work which may be of great significance has been carried out by Kawasaki[17] and by MS&A and Samancor into the use of hydrocarbons as reductant. Kawasaki tested methane. MS&A/Samancor have investigated other hydrocarbon-bearing Gases, and more significantly, coal volatile as a hydrocarbon source. These tests have shown that hydrocarbons have a remarkable effect upon lowering the reduction temperature of chromite, particularly if the chromite has been pre-oxidised. For example, at 1100°C a total metallisation of 52 per cent (71% Fe met. and 40% Cr met.) has been achieved with liquid petroleum gas (LPG) whereas with coke as reductant but under otherwise similar conditions, only 5 per cent total metallisation is achieved (6.5% Fe met. and 1.0 Cr met.). The Mechanism by which this low-temperature reduction takes place is not fully understood and requires deeper investigation. However, if this reaction can be engineered on a large scale using coal volatile, the implications for chromite pre-reduction processes could be far reaching.

1.5.5. Direct Stainless Steel

It is undoubted that the changes in the technique of stainless steel production will affect the consumption pattern of chromium alloys, as it happened in the past decades, because about 79 per cent of the world's chromite products are absorbed mainly for the production of the steel. An alternative approach for the stainless-steel producers is to consider the supply of chromium units by some other means, which may be more cost effective. This leads us into

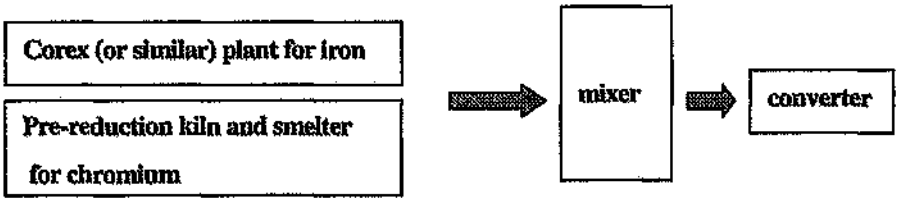
the realm of the so-called **'direct stainless steel'**

What is direct stainless steel? The terminology is, based upon D. D. Slatter's opinion [11], subject to widely differing interpretations. It ranges from simple hot transfer of molten ferro-chromium to the steel smelt-shop, to direct smelting of chromite and oxide nickel ores to produce a molten stainless steel ***'pig'***, with various other options between these two extremes. One of the definition of a direct stainless steel process is: " a process for producing liquid iron, chromium (and nickel) units directly from their ores and converting these to stainless steel with no production of intermediate solid forms". It should be noted that the term 'direct stainless steel' and the definition given, make no statement about how it is to be made. It is rather a statement of a differed approach or philosophy to chromium (and nickel) units supply and may use existing or anticipated smelting and pre-reduction units. The critical feature, whatever process operation is used, is that it must by definition take place at the stainless steel plant itself. In this sense the concept is a threat to all ferro-chromium producers and those not associated with a steel plant. A wide variety of processes, or combinations of processes, may be suitable for 'direct stainless steel' and stainless steel producers who embark upon this route, are likely to each have their own preference best suited to individual conditions or requirements. Other than the direct transfer of liquid ferrochromium to the smelt-shop, various possibilities arise:

1. The chromium and iron (and nickel) units must be combined as the ores from the start in the correct proportions for the stainless steel grade, and co-smelted by various alternative process operations. For example,



2. The ores may be reduced and smelted separately, and then combined at the converter, such as



3. Pre-reduced chromite (via CDR or SDK-type processes) may be added directly to the iron melt where the carbon and silicon will reduce the most of the balance of the unreduced chromium. Supplemental energy for final reduction and melting will be required. Such a process has been carried out by Kawasaki Steel where the pelletised pre-reduced chromite from a rotary kiln is charged to molten iron in a converter. The supplemental heat is supplied by injection and combustion of coke with oxygen.

4. Direct addition of chromite ore to the iron melt allowing silicon and carbon to reduce the chromite. This has been investigated by various producers including NKK, Kobe Steel and Krupp. Potential disadvantages of the processes such as these include extra slag volumes from the chromite gangue and a probable poor chromium recovery from the chromite due to the preferential reduction of iron in the chromite.

It has been reported[11] that Kawasaki Steel will start to produce stainless steel using a direct chromium ore smelting and reduction process in which chromium ore and ferro-chromium are fed directly to a converter containing liquid iron.

1.6. Motivation of the Investigation

The changes in the technique of stainless steel production considerably affected the consumption pattern of chromium alloys in the past decade because about 79 per cent of the world's chrome products are used for the production of the steel and other special alloys. Low-carbon ferrochromium was used to a large extent in the past, but high-carbon ferrochromium becomes dominant as the conventional stainless-steel making processes utilizing electric arc furnace are replaced by oxygen-blowing processes, such as AOD and VOD.

The problems, however due to the use of high-carbon ferrochromium, such as long refining time, high slag volumes, high refractory consumption, and high consumption of oxygen in

steelmaking processes, may result in a tendency to increase the use of medium-carbon ferrochromium refined from high-carbon ferrochromium.

The demand for refining of high-carbon ferrochromium may also increase in the future because high-grade chromite (chromium-rich, high-ratio, hard and lumpy) reserves are declining fast [16]. There are about 2270 Mt of chromite ores (about 68 per cent of the world' reserves) in South Africa but only 30 per cent of the reserves can be classed as high-grade chromite ores.

Upgrading techniques and agglomeration techniques, consequently, have to be employed for the conventional production of ferrochromium in submerged arc furnaces, which will make the alloy several percentage points higher in carbon and silicon than that produced from hard, lumpy, high-grade chromites[19,20].

The alloy produced from low-grade chromites, called "charge chrome", usually contains above 6 per cent of carbon and above 2 per cent of silicon with chromium content below 58 per cent. Low-grade chromites can not be converted to low-carbon(C<0.5%) or medium-carbon(C 0.5%-4%) ferrochromium via the conventional silicothermic ore/lime reduction under economically feasible conditions[4].

Decarbonization of charge chrome by oxygen-blowing processes may suggest a production path to a lower-carbon, lower-silicon, high-quality ferrochromium, which could be utilised more efficiently by steelmakers.

Oxygen-blowing processes by top-blowing, bottom-blowing and by the combination of the both have been used on an industrial scale [2,26-36]. A new attempt to increase decarbonization of the metal by adding nickel was investigated recently by W.Dresler[21,22].

The knowledge of the gas-slag-metal equilibrium without carbon saturation is of fundamental importance to understand the pyro-metallurgical processes of ferro-chromium refining and stainless-steel production. Furthermore, it is also very essential to handle with

the problems, which occur in the processes during the decarbonization of liquid alloy, such as losses of Cr and Fe from alloy to slag, Si transfer from slag to alloy, elimination of S and P from alloy to slag.

A lot of efforts, up to now, has been made on the slag-metal equilibrium and the distributions of some elements. Investigations, particularly in the system of Cr-Fe-Si-Ca-Mg-Al-C-O conducted under the condition of carbon saturation[23-33], has displayed great significance to the production of high carbon ferro-chromium alloy. The inadequate knowledge of the gas-slag-metal equilibrium without carbon saturation in the concerned system, the utilisation of the vast reserves of lower-grade chromite in South Africa, and the practical demand from ferrochromium refining and stainless-steel production **stimulated the project.**

Domains of the Investigation

The project has been conducted towards the following three aspects:

1. Complete 3-phase-gas-slag-metal equilibrium in Cr-Fe-Si-C-S alloys, Al_2O_3-CaO-CrOy-FeOx-MgO-SiO_2-S slags, and CO/Ar gas. The carbon content in metal phase could vary from zero to about 8 per cent pertinent to the requirement of ferro-chromium refining. The partial pressure of CO in CO/Ar gas phase could change in the levels of 0.83atm, 0.05atm, and 0.034atm related to the conditions of AOD and VOD.

2. Equilibrium distributions of Cr, Si, and S between slag and metal phase in Cr-oxide crucible and silica crucible under different partial pressures of carbon monoxide, which are relevant to the conditions of the production processes.

3. Systematic design of all experiments and systematic treatment of all experimental data, in order to achieve systematic and complete results, which would help to understand better the production processes and would be easily utilised by the industry.

2. LITERATURE SURVEY

2.1. GENERAL CONSIDERATION

Pyro-metallurgical processes are complex heterogeneous reactions commonly involving the coexistence of a number of crystalline and liquid phases, both metallic and oxidic, at elevated temperatures. Furthermore these condensed phases (crystalline or liquid) have important interactions with gaseous species, particularly with oxygen.

Reactions involved between slag and metal are redox exchange reactions which are accompanied by an exchange of electrons between the reacting species as they are transferred to and from non-polar metallic phase and ionic molten slag. These reactions are, in principle, identical to gas-slag reactions with regard to the exchange of electrons. In most cases the transfer of a reactant from metal to slag is an oxidation process, such as:

$$\underline{Fe} + \underline{O} = (Fe^{2+}) + (O^{2-}) \qquad (2.1)$$

$$\underline{Cr} + \underline{O} = (Cr^{2+}) + (O^{2-}) \qquad (2.2)$$

Slags are capable of dissolving small amounts of neutral metal atoms, presumably lodged in the holes in the slag structure. They can also dissolve water in some form, probably dissociated; and can pass either oxygen or hydrogen or both from a furnace atmosphere through to a melt below[34]. The transmission of oxygen is very easy in the case of a slag containing iron oxide, or the oxide of any other metal which can display more than one valency.

Although the reactions as formulated above are accepted, their equilibrium constants cannot

be evaluated because the thermodynamic activity or activity-coefficient of an individual ion cannot be determined experimentally, for the same reasons which precluded the determination of activities of ions in concentrated aqueous solutions [35]. Although the derivation of reaction-equilibrium relations from an ionic structural model is of theoretical interest, their application to slag-metal reaction equilibria in multi-component systems has not been particularly rewarding when compared with the much simpler conventional methods of representing the slag-metal equilibria in terms of the measured thermodynamic quantities.

When a slag is involved in chemical reactions, the knowledge of the activities of its constituents would always be useful. Values of these activities have been difficult to obtain, because their determination requires difficult high-temperature experimentation and very accurate chemical analyses. The range of interest lies often between the Raoult's law and Henry's law ranges, and suitable standard states are not always easy to specify in such "strong" solutions. Because of lack of activity data for multi-component slags, the slag-metal equilibrium relations are often represented in terms of concentrations of reactants and products by invoking the mass-action law. The isothermal equilibrium constant K thus expressed varies with the slag composition, when the activity-coefficients of oxide reactants and products in the expression of the equilibrium constant are omitted.

The determination of phase-relations in quaternary systems, and the representation and interpretation of quaternary phase diagrams, is usually more complicated than for binary and ternary systems. The complications arise not because the application of the phase rule to four component systems is more difficult than in cases with less components, but because the relations are more difficult to represent geometrically with the introduction of one more component. One additional composition variable must be accounted for, and four composition axes are necessary in order to represent the equilibria adequately. The geometrical figure commonly used to represent four component systems is a regular tetrahedron, with one component at each apex. Thus all three dimensions of space are expended in expressing composition variables, and there is no axis in these quaternary diagrams along which temperature is shown explicitly. Instead, temperatures are illustrated

by indirect methods. It is much easier, however to analyze these systems by making systematic sub-divisions of the tetrahedron into smaller units in order to obtain meaningful data and to present them in a clear manner. One of these methods is to choose planes representing compositions of mixtures having a constant content of one of the components. Such planes are parallel to one of the faces of tetrahedron used to represent the quaternary system. The state of equilibrium in metallurgical reactions involving three or more phases cannot be evaluated accurately without giving due consideration to interrelations among different reactions occurring simultaneously. Also, the formation of volatile reaction products may impede the ultimate approach to equilibrium, because of continuous loss of material from the system. This should be kept in mind when evaluating the data.

For a better understanding of how reaction took place and how equilibrium was achieved, a number of kinetic studied were analyzed. In such studies, in order to determine the rate of slag-metal reactions, the change in concentration of a particular element either in slag or metal phase has to be determined with time either directly or indirectly. The results can be examined in terms of the various rate equations for chemical reaction control mechanisms or mass transport control, in order to establish a unique rate controlling process for the particular experimental conditions. In most of these kinetic studies the slowest reactions taking place in particular systems and their rates are studied, which provides useful information for determining the equilibration time for the present system.

Chromium in slags, like any of the transition metal ions, can respond to such changes in the oxidation conditions by changing its valency. It may also change its structure role, for example by acting as a network modifier under reducing conditions, but as a network former when the slag is oxidised. The nature and behaviour of chromium in SiO_2-CaO-Al_2O_3-FeO-CrO_x in equilibrium with Fe-Cr-Si alloys was determined by Rankin and Biswas[36] by means of thermodynamic analysis of the equilibrium data. The experiments were conducted at 1600°C in alumina and silica crucibles. The data were analyzed in terms of the equilibria:

$$(CrO_x) + x\underline{Fe} = \underline{Cr} + x(FeO) \qquad (2.3)$$

$$K_{2.3} = (a^{x}_{(FeO)}\, a_{\underline{Cr}})/(a_{(CrO_x)}\, a^{x}_{\underline{Fe}}) \qquad (2.4)$$

and

$$2(CrO_x) + x\underline{Si} = 2\underline{Cr} + x(SiO_2) \qquad (2.5)$$

$$K_{2.5} = (a^{2}_{\underline{Cr}}\, a^{x}_{(SiO_2)})/(a^{x}_{\underline{Si}}\, a^{2}_{(CrO_x)}) \qquad (2.6)$$

These constants were defined as

$$K'_{2.3} = ((\%Fe)^{x}\, \%\underline{Cr})/((\%Cr)(\%\underline{Fe})^{x}) \qquad (2.7)$$

$$K'_{2.5} = (\%\underline{Cr})^{2}/((\%Cr)^{2}(a\underline{Si})^{x}) \qquad (2.8)$$

In $K'_{2.5}$ the silica term was omitted, since it was approximately constant for each group of runs (silica saturation).

These expressions may be rewritten in terms of activity coefficient multiplied by concentration for each activity. Finally, by taking logarithms and rearranging, the following equations were obtained:

$$\log[(\%Cr)/(\%\underline{Cr})] = x\log[(\%Fe)/(\%\underline{Fe})] + \log[(\gamma_{(FeO)}\, \gamma_{\underline{Cr}}\, C_1)/(\gamma_{\underline{Fe}}\, \gamma_{(CrO)} K'_{2.5})] \qquad (2.9)$$

$$\log[(\%Cr)/(\%\underline{Cr})] = -(x/2)\log(a_{\underline{Si}}) + \log[(\gamma_{(FeO)}\, \gamma_{\underline{Cr}}\, C_2)/(\gamma_{\underline{Fe}}\, \gamma_{(CrO)} K'_{2.3})] \qquad (2.10)$$

where C_1 and C_2 are the constants representing all constants for converting mole fractions

to mass percentages. For the first series of experiments in alumina crucibles in the study, Rankin and Biswas found the average value of the x to be 1.07. This meant that 86 per cent of chromium present in the slag was in the form of Cr^{2+} ions and the balance was Cr^{3+}. For the second series of experiments under silica saturation (silica crucibles), the average value of x for all groups was found to be 1.04. This corresponds to a value of 92 per cent of Cr^{2+} ion in the slag, the balance being Cr^{3+}. The apparent equilibrium constants of reaction 2.3 and 2.5 at 1600°C for the slag-metal system were constant at each $CaO:SiO_2:Al_2O_3$ ratio. $K_{2.3}$' increased markedly with an increase in $CaO:SiO_2$ ratio at constant Al_2O_3 content, and increased slightly with an increase in Al_2O_3 content at constant $CaO:SiO_2$ ratio.

Spectroscopic analysis can provide data about the electronic and physical configuration, and hence can supply the structural role of transition metal ions in slags. Such studies can also provide information about the slag matrix. An investigation of Cr(II), Cr(III), and Cr(VI) in silicate slags has been made recently by H. Marston and B. B. Argent[37]. They used spectroscopic and chemical analyses to investigate the behaviour of chromium in four vitreous lime-silicate slags produced under reducing and oxidising conditions. The slag composition is in the range of CaO 30% to 37%, MgO 0% to 7%, Al_2O_3 0% to 16%, SiO_2 40% to 60%, Cr_2O_3 0.05% to 3% by mass at temperature between 1550 °C to 1600 °C. In the slags equilibrated at $P_{O_2} = 1.6*10^{-9}$ bar, 71 per cent of chromium is present as Cr(II), reducing to an average figure of 14 per cent at $P_{O_2} = 1.1*10^{-5}$ bar. At $P_{O_2} = 0.1$ bar, 14 per cent is Cr(VI). In each case, the balance is Cr(III). Spectroscopy provided evidence of Cr(III) in all slags. The varying quantities of Cr(II) and Cr(VI) were detected, but not simultaneously in the same samples. Within the compositional range studied, no consistent effect of the chromium level, the slag basicity or the presence of MgO or Al_2O_3 on either the chromium distribution or the molar absorptivity could be discerned.

2.2. KINETIC STUDIES

A number of papers on the mechanism of chromium reduction have been published in recent years [38-49]. There are two main viewpoints on the reduction mechanism. One is based on liquid-solid phase reaction. It is considered that the ore may melt and reduction may take place in the slag. The other is based on most reduction occurring in the solid state. The first mechanism suggests that appropriate additions of flux and the quick formation of slag may assist smelting. The second, however, advocates that pre-reduction of chromite ore is an essential way to improve production.

The kinetics of the reduction of iron and chromium from high-carbon ferro-chromium slags was studied by Boronenkov et al[38] by using thermogravimetric analysis (TGA). Graphite or alumina crucible was used with carbon-saturated ferrochromium. At high chromic-oxide content of the slag (more than 6 per cent), the reduction of chromium from slag is controlled by the process of carbon oxidation and desorption of the carbon monoxide from the system. Whereas at lower concentration of chromic oxide in the slag (less than 2 per cent), the reaction is retarded by the diffusion of chromium ions in the slag.

R. C. Urquhart[39] investigated the reduction of Transvaal chromite ores in high-carbon ferro-chromium by using the technique of stationary charge in controlled environment (SCICE). It shows that at temperatures up to 1500 °C, reduction of the chromite ore is controlled by the diffusion of iron and chromium ions in the chromite spinel. At 1500 °C, the reduction rate of chromium from the chromite spinel is increased by the fluxing reaction. In the presence of slag, at temperatures higher than 1500 °C, the reduction of chromite ore by carbon is quite rapid. The reduction of iron from the chromite ore satisfies an expression that described a topochemical reaction starting simultaneously on the surface of the cubic crystals. However the reduction of chromium from the ore does not follow a unique mechanism over the temperature range investigated. Examination of the dissolution of chromite ore in the slag as part of the reduction process was done. The results showed that the dissolution of iron and chromium ions from the chromite ore into the slag is controlled

by the diffusion of iron and chromium ions, away from the interface into the bulk of the slag. The rate of reduction of iron and chromium from the slag is greater than the rate of dissolution of the oxides into the slag. That means that the mechanism of dissolution may change from a first-order process to one of higher order owing to the stirring motion caused by gas evolution during the reduction of the oxides. For the condition of the dissolution, Bird et al[40] expressed the diffusion equation as:

$$(\partial C^{\xi}/\partial t) = D^{\xi}/S(\partial^2 C^{\xi}/\partial x^2 + \partial^2 C^{\xi}/\partial y^2 + \partial^2 C^{\xi}/\partial z^2) \quad (2.11)$$

where C^{ξ} represents the concentration of iron or chromium ions in the slag in ($g\ cm^{-3}$);

D^{ξ}/S represents the diffusion coefficient for iron or chromium ions in the slag in ($cm^2\ s^{-1}$);

t represents time in (s).

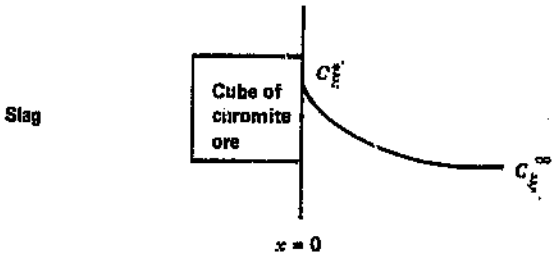
Since Fe^{2+}, Fe^{3+}, Cr^{2+}, and Cr^{3+} can all be present in the slag, the iron ions will be designated Fe^{n+} and the chromium ions Cr^{n+}. The equation (2.11) is commonly known as Ficks second law and valid for diffusion-mass transfer exclusively. The boundary conditions in these experiments (figure 2.1.) are such that the equation can be rewritten as:

$$(\partial C^{\xi}/\partial t) = 6D^{\xi}/S(\partial^2 C^{\xi}/\partial x^2) \quad (2.12)$$

$$\xi = C^{\xi^*} A(D^{\xi}/S^* t/\pi)^{1/2} \quad (2.13)$$

where ξ refers to Fe or Cr ions expressed in grams and A is the surface area of the cube under consideration in cm^2.

The data [39] obtained by simultaneous dissolution of a chromite ore into slag and reduction of the dissolved iron and chromium oxides with carbon are shown in figure 2.2, 2.3, 2.4, 2.5. It is evident that the rate of reduction of iron and chromium from the slag is greater than the rate of dissolution of the iron and chromium oxides into the slag.



Consider diffusion from one face of the cube in the positive x-direction

1. $t < 0$, $C_\xi = C_\xi^\infty = 0$ for all x

2. $t = 0$, $C_\xi = C_\xi^*$ at $x = 0$

   $C_\xi = C_\xi^\infty$ for $x > 0$

3. $t \to \infty$, $C_\xi \to C_\xi^*$ for finite x

Boundary condition 2 assumes that ξ immediately ... es saturation in the slag (C_ξ^*) at the face of the chromite cube.

Figure 2.1. The boundary conditions for the dissolution of a chromite-ore cube in molten slag[39]

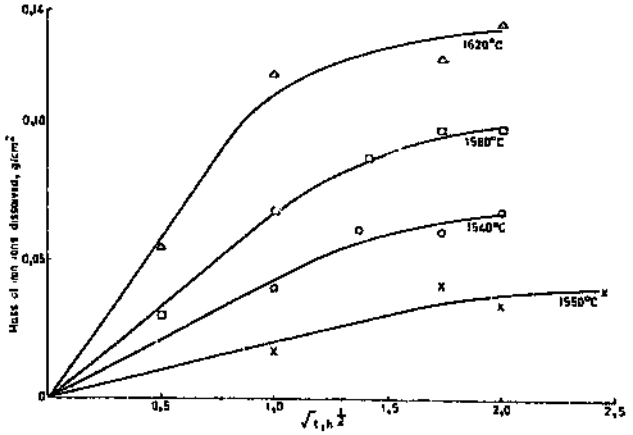


Figure 2.2. Dissolution of iron oxide from the chromite-ore cube into the slag [39]

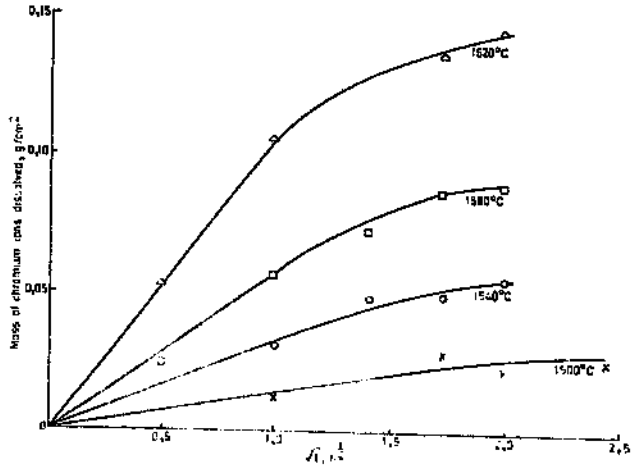


Figure 2.3. Dissolution of the chromium oxide from chromite-ore cube into the slag[39]

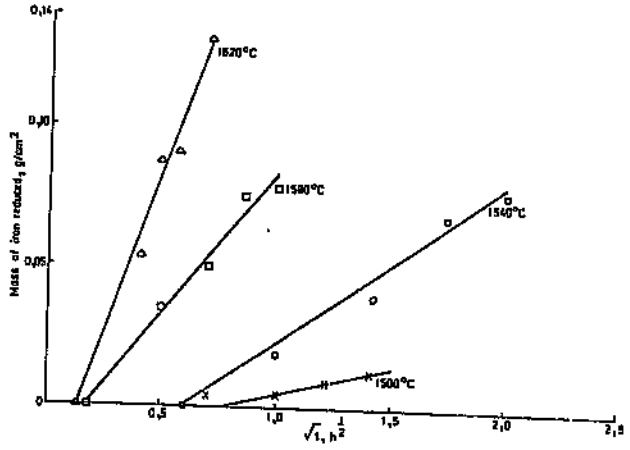


Figure 2.4. Reduction of iron oxide from chromite-ore cube in molten slag in graphite crucible[39]

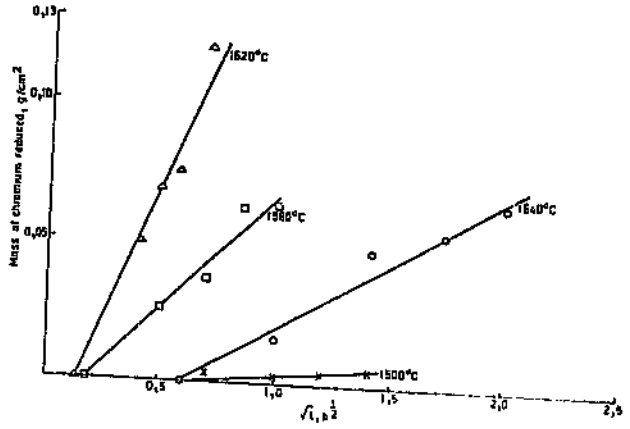


Figure 2.5. Reduction of chromium oxide from chromite-ore cube in molten slag in graphite crucible [39]

The kinetics of chromite dissolution in liquid slags has been studied by O.Demir and R. H. Eric[41]. In their study rotating cylinder technique was used, where chromite cylinders were immersed in the slag phase, to study the dissolution behaviour of chromite in SiO_2-Al_2O_3-MgO-CaO slags in the temperature range of 1535°C and 1700°C in graphite crucibles. The data for the rate of dissolution is obtained by sampling the slags at predetermined intervals, designed by a statistical procedure. The experimental work conducted hitherto illustrates that the dissolution of chromite in liquid slags contained in graphite crucibles takes place parallel with the reduction of iron oxide and chromium oxide at the crucible walls. The complete dissolution takes place comparatively fast. When the chromite cylinder dissolves the chromium and iron contents of the slag together with other contents, which form the chromite phase, increase to a maximum, then a certain amount of iron and chromium removal occurs via the reduction of FeO and Cr_2O_3 by carbon supplied by the graphite crucible. The reduction of the oxide phase taking place at the crucible walls indicates the transport of oxide phase through the liquid slag phase to the reaction site.

The kinetics of reduction of iron oxide and chromium oxide from slags by carbon or/and silicon dissolved in liquid iron have been studied by many investigators because of their prime importance in steelmaking. Chromium transfer between carbon-saturated Fe-Cr alloy and CaO-silica-alumina slags was studied by McCoy and Pilbrook[42] in the temperature ranged from 1500 to 1600 °C and in the slag-basicity range from 0.6 to 2.5 in terms of lime:silica ratio. The reduction of chromium oxide from these slags was found to be first order with respect to chromium. The reaction rate was $1x10^{-3}$ g Cr $min^{-1}cm^{-2}$(pct Cr^{-1}), and was substantially independent of temperature and basicity in the range studied. They could not obtain a constant slag:metal distribution ratio for chromium due to simultaneous reduction of silica from the slag. This was explained by the slowness of the reduction of silica from slag to metal, which was about 20 to 60 times slower than chromium reduction under the conditions studied.

The reduction behaviour of chromium oxide from a basic steelmaking slag (45% CaO, 35% silica, 10% MgO, 10% alumina) by silicon dissolved in liquid iron was studied by Robinson and Pehlke as cited by H. Cengizler[43]. The experiments were carried out under Ar

atmosphere, with the slag and metal phase held in zirconia crucibles. In the study, the reduction of chromium oxides from the slag was analyzed in two distinct processes: an initial period where trivalent chromium was rapidly reduced according to the reaction:

$$(Cr_2O_3) + \underline{Si} = (SiO_2) + (CrO) + \underline{Cr} \qquad (2.14)$$

and a following period when the divalent chromium was reduced to chromium in the metal phase according to the reaction:

$$(CrO) + 1/2\underline{Si} = 1/2(SiO_2) + \underline{Cr} \qquad (2.15)$$

Both reaction were rapid, equilibrium being attained with two hours at 1575°C. From the effects of changes in composition, stirring rate, and temperature, the rate limiting step was found to be the transport of trivalent chromium from the bulk slag to the slag-metal interface.The reduction of divalent chromium was not sensitive to variations in stirring rate or silicon content of the metal, but the effect of change of temperature was large. The rate of divalent chromium reduction was found to be determined by an interfacial chemical reaction which was first-order with respect to divalent chromium in the slag.

The effect of flux addition on the kinetics of chromite-ore reduction with carbon was investigated thermo-gravimetrically by Healy et al [44] Neuschutz et al[45] with the addition of graphite powder and different fluxes composed of silica, CaO, alumina, MgO, and CaF_2. The reduction is always accelerated by the addition of fluxes. Furthermore, samples containing a flux shows two stages of acceleration with temperature, the first one starting at 1020 to 1120 °C, the second one at 1200 to 1320 °C, while fluxless samples only exhibited the first stage which did not start before 1200 °C. The first acceleration effect is therefore attributed to the solid-state formation of ternary oxides, which apparently leads to surface roughening and to more frequent micro-cracking of the chromite grains, thus facilitating metal phase nucleation. The second effect is attributed to the formation of liquid slags. They enhance the reduction by dissolving part of the $MgO.Al_2O_3$ surrounding the unreduced chromite and by accelerating the transport of Cr ions to the reductant. By the addition of

fluxes the temperature for 90% reduction of Lebowa chromite fines was lowered by up to 150 °C.

The solid-state reduction beha viour of Bushveld Complex chromites by carbon in the presence of silica flux was investigated by P. Weber[46]. Their results shows that the addition of silica together with a graphite reductant did not promote the reduction of chromite at temperatures below 1400 °C. At temperature above 1400 °C the addition of silica with graphite, or using char as the reductant, results in a considerable enhancement of the reduction rates.

The kinetic measurements on the reduction of chromite ore from a lime-silicate slag by carbon dissolved in a high-carbon ferro-chromium bath were conducted by Fujita, Tsomondo et al[47] and Dai[48] at temperatures between 1500 and 1650°C. The results show that for chromium-oxide saturated slags, the rate of oxidation of carbon is independent of the oxide content. Carbon diffusion from the bulk alloy to the alloy/slag interface is envisaged to be rate controlling in the initial instance. Later, the reaction appears to exhibit mixed control kinetics.

The mass transfer rate of chromium oxide in molten slag phase has been studied by Shin-ya Kitamura et al[49] by the analysis of Cr-ore reduction rate in combined blowing converter. Using a 600 kg scale experiment and a 100t scale industrial furnace (LD-OB), the influences of temperature (T), stirring energy (Es), [%Cr], diameter of furnace(L), amount of carbon for reduction(Wc) and characteristics of Cr source on the reduction behaviour were clarified. Assuming the transfer of Cr oxide in molten slag phase to the carbon-slag and metal-slag interfaces was the rate-controlling step, the reduction rate can be expressed by the following equation:

$$-d(\text{Cr oxide})/dt = \{4.78(10.0203[\%Cr])(S/Ws)+0.45(Wc/Ws)\}* (Es/Es_0)^{1/2}\{\exp(-Q/RT)/\exp(-Q/RT_0)\}(L/L_0)^{2/3} \quad (2.16)$$

where,

- S -- the geometric surface area of molten iron,
- Ws -- the weight of the slag,
- Q -- the activation energy,
- Subscript "o" -- the standard state of the experiment,
- Es – the stirring energy,
- L – the diameter of furnace,
- Wc -- the amount of carbon as reductant.

From the studies mentioned above, the kinetics is fundamentally important to understand the mechanism of the reactions relevant to the ferro-chromium production and refining.

The knowledge of the reaction mechanism, the reaction rate and the all factors which are pertinent to the chromite reduction, is essential for the thermodynamic investigation. It can be very useful in the following aspects:

- Selection of the reaction system, including slag, metal, gas and crucible,
- Experimental design,
- Determination of the equilibrium time,
- Analysis of the experimental results.

The knowledge of the kinetics mentioned above is utilised with the thermodynamics available so far to help conduct this research project.

2.3. EQUILIBRIUM STUDIES

A number of investigations on phase equilibria, thermodynamic activities, and on slag-metal equilibrium distribution of some elements pertinent to some parts of the present system have been done in the past. The equilibrium between slag and metal phases at a given temperature is mainly controlled by the compositions of gas, metal and slag phases individually.

2.3.1. Metal Phase

Griffing et al[50], investigated phase equilibria for C-Cr-Fe alloy compositions in which the chromium content ranged from 0 to 94 per cent and the carbon content from 1.4 to 11.7 per cent at temperatures of up to 1800°C. The derived ternary liquidus surface is shown in figure 2.6, where solid lines represent the liquidus isotherms. The broken lines and the binary edges are the liquidus field boundaries of the primary crystals. The solubility of carbon in C-Fe, C-Cr and C-Cr-Fe alloys is shown as a function of chromium content in figure 2.7. It can be seen that as the chromium content of the alloy increases the carbon solubility increases.

The phase equilibria in the Fe-Cr-Si-C system were investigated by J.C.M. Wethmar[51,52]. In this study the composition of the alloys were so selected that the quaternary system could be divided into five pseudo-ternary sections at carbon levels of 4, 5, 6, 7 and 8 per cent. Alloys representative of three levels of silicon concentration, viz. 0, 5 and 10 per cent and four specified Cr:Fe ratios were selected at each carbon level. Molten samples were kept in alumina crucibles under a protective atmosphere of purified argon. After the alloys had been homogenized by holding them at temperatures above the estimated liquidus temperatures, the alloy samples were quenched down to room temperature and analyzed both chemically and metallographically. The results, illustrated in figure 2.8,

show that the liquidus temperatures of the alloys increase with an increase both in carbon content and in ratio of chromium to iron. The primary phase is $(Cr,Fe)_7C_3$ for the entire range of alloys investigated. The temperature interval over which this primary phase crystallized increases with an increase in carbon content and the chromium to iron ratio and with a decrease in silicon content.

Studies on the solubility of carbon in Fe-Cr-Si alloys were of great help in determining the initial alloy compositions and in analysing the results of the present system. Lucas and Wentrup[53] studied the solubility of carbon in synthetic Fe-Cr-Si alloys under laboratory conditions, ensuring fairly reliable saturation of the alloy with respect to carbon, and determined the carbon content. An increase in chromium content causes an increase in the solubility of carbon , but this effect can be neutralised by a simultaneous increase in the silicon content. A number of studies on the Fe-Cr-Si-C quaternary system have been done by Petrushevskii and Gel'd[54,55,56] at 1700 °C in the range of 0 to 35 per cent silicon, 0 to 100 iron, 0 to 93 chromium. Their results are summarised in figure 2.9 in the form of parametric graphs plotted for various values of the Fe-to-Cr ratio. The solubility of carbon in these alloys decreases steadily with increasing silicon and iron contents. The effect of silicon, as can be seen from the figure 2.9, is particularly strong.

Most recently, Kossyrev and Olsen[57] investigated carbon solubilities for Cr-Si-C and Cr-Fe-Si-C alloys (Cr/Fe=4, 1.5, 0.25) in a resistance furnace at 1600°C in Ar atmosphere with graphite crucibles. The metal samples were analyzed for carbon and silicon and some samples and crucible/metal interfaces were investigated by electron microprobe analysis. The silicon carbon relation measured in Cr-Fe-Si-C alloys with different Cr/Fe ratios are presented in Figure 2.10. For chromium rich alloys, the carbon content increases initially with increasing silicon content in the metal. Study of the metal and the crucible/metal interface in the electron microprobe shows that the solubility curve representing iron free Cr-Si-C alloy shows two breaks, dividing the system into three areas. In the first area, carbon increases with increasing silicon content. After silicon reaches a critical value, carbon content decreases with increasing silicon content. The critical silicon value decreases when Cr-to-Fe ratio reduces. The critical-silicon value disappears when the

ratio of Cr to Fe is less than 1.5. In the first area, the primary crystals in the metal are Cr_7C_3; in the next area the primary crystals are Cr_3C_2; and in the third area only SiC.

With increasing silicon content the stable carbide phases are Cr_7C_3, Cr_3C_2 and SiC. For alloys with Cr/Fe=4 there seems to be a fourth area between 10 and 15.5% Si. Metallographic observations indicates absence of any additional carbide phase between the graphite crucible and the metal in this area which means that graphite is a stable phase between the M_3C_2 (M=Cr+Fe) SiC stability areas. Further, there is no area of M_7C_3 stability in alloys with Cr/Fe=1.5 and there is no area of M_3C_2 stability with Cr/Fe ratio less than approximately 1.2. The resulting phase diagram of the Cr-Fe-Si-C_{sat} system and lines of iso-carbon concentrations at 1600 °C are sketched in figure 2.11, projected from the carbon corner to the Cr-Fe-Si triangle. The symbol C_{sat} is used for all carbon saturated melts, regardless of whether the coexisting phase is graphite or some carbide.

Activities in the liquid Cr-Fe-C system above 1600°C was studied by G. W. Healy[58]. In this study $\ln\gamma_C$ was obtained by Gibbs-Schuhmann integration of an analytical expression of $\ln\gamma_C$ which was calculated using data from the literature. Maps of activities of carbon and chromium at 1600, 1800, and 2000°C are presented. Dresler[59] investigated the activities of silicon and carbon in liquid iron-silicon-carbon alloys. Activity functions for silicon and carbon were determined based upon dilute solution data for silicon and carbon and saturation data for carbon in the presence of silicon, applying the Gibbs-Schuhmann integration. Carbon and silicon activities were described with mathematical relationships in the ternary system iron-silicon-carbon higher than 1.5 in the metal between 0 and 26 per cent silicon and carbon saturation. The effect of carbon content on the partial molar enthalpy of mixing for silicon was shown to be fairly small.

Another work of thermodynamic model, applicable to computer modelling, developed by W. Dresler[60] is capable of predicting carbon content for the liquid system Fe-Cr-Ni-C-Si with the temperature range of 1500 to 1800°C. The model was successfully applied to experimental results of FeCr alloys, FeCrNi master alloys, and stainless steel.

Futhermore, the kinematic viscosity and the electrical resistance of iron-chromium alloys over the range 0-80% Cr at 1400-1850°C was undertaken by Pavars et al[61]. The kinematic viscosity of iron-chromium melts varies with composition, reaching a maximum at $N_{Cr} = N_{Fe}$. The isotherms for activation energy, free energy, and entropy of activation of viscous flow are similar in shape. The non-monotonic variation with composition in the fundamental characteristics of internal friction is explained by the energetic non-equivalence of the inter-particle interactions and also by the greater rigidity of the bonds between like atoms.

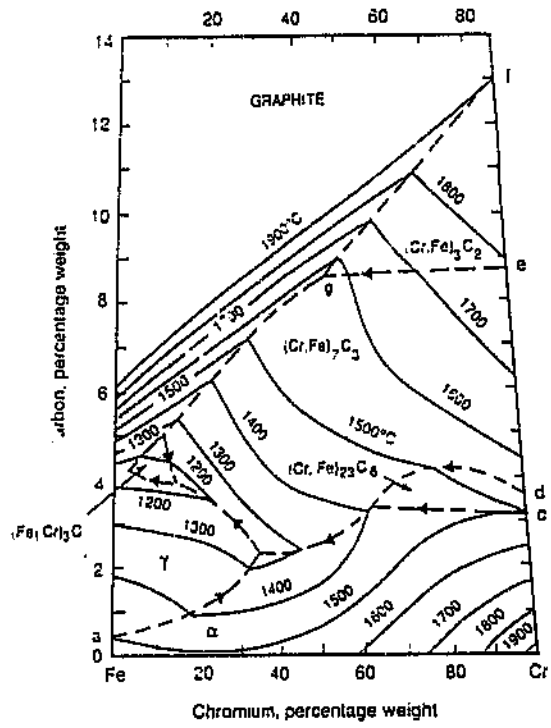


Figure 2.6. The liquid surface for C-Cr-Fe. After Griffing et, al [60]

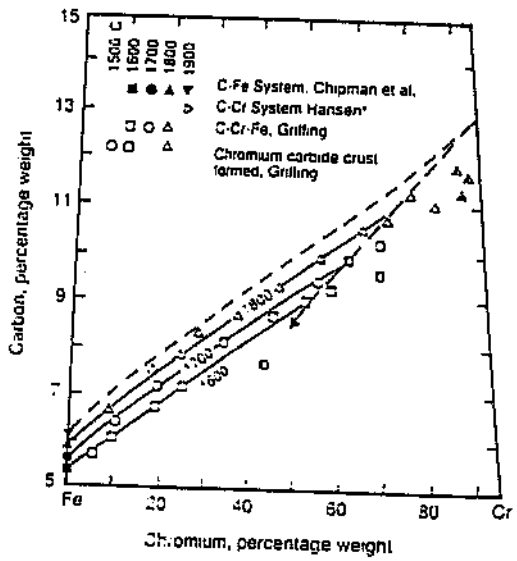


Figure 2.7. The solubility of graphite in C_{sat}-Cr-Fe system. After Griffing et, al[80]

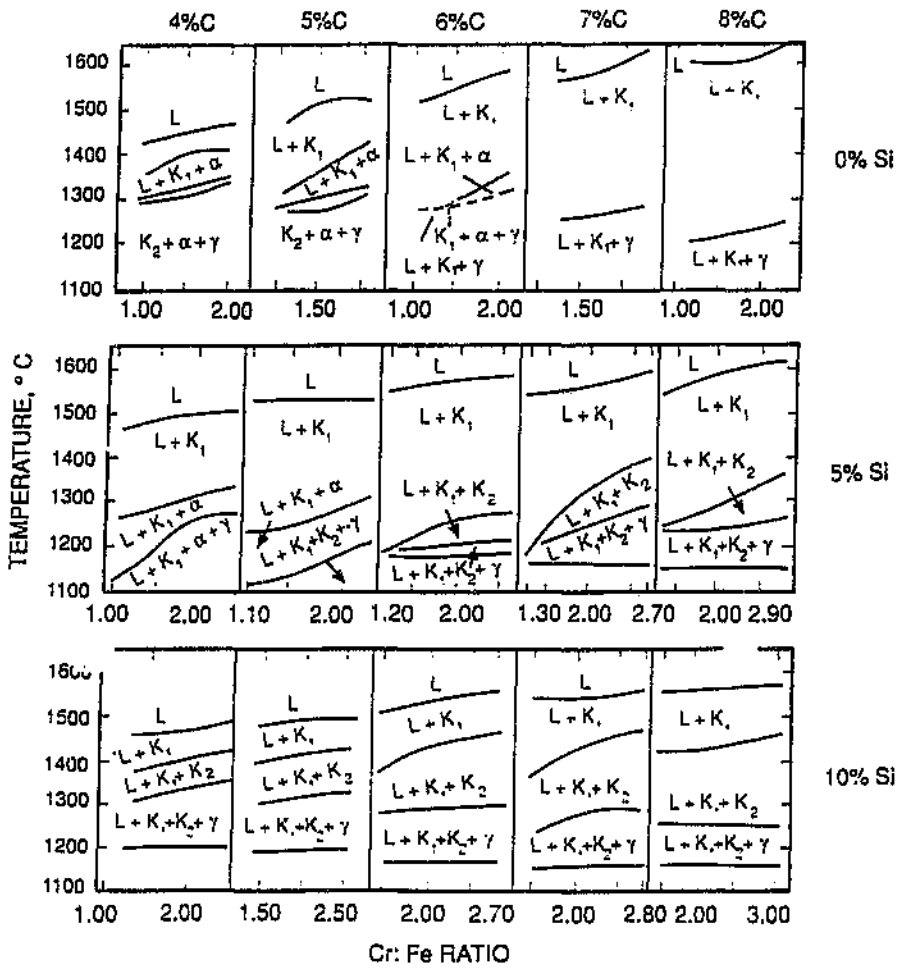


Figure 2.8. Pseudo-binary sections at selected constant silicon and carbon contents in Cr-Fe-Si-C system. After Wethmar et. al [81,82].

Key: L = liquid, K_1= $(Cr,Fe)_7C_3$, K_2= $(Cr,Fe)_{23}C_6$, α = α-Fe-Cr solid solution.

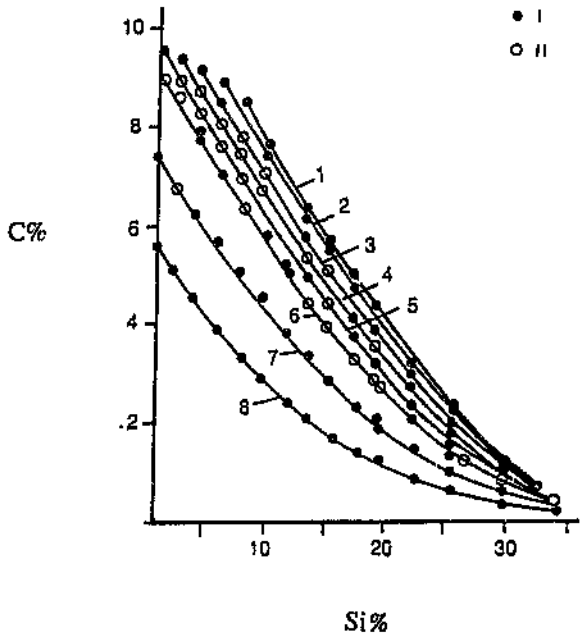


Figure 2.9. The effects of silicon and of the iron-to-chromium on the solubility of carbon in Fe-Cr-Si-C alloys at 1700°C. After Petrushevski and Gel'd[51].

Key: A--carbon content (% by mass); B--silicon content(% by mass);

materials: I--pure; II—technical;

Fe:Cr ratio: 1-0.0, 2-0.11, 3-0.25, 4-0.43, 5-0.67, 6-1.0, 7-3.0, 8-Cr=0

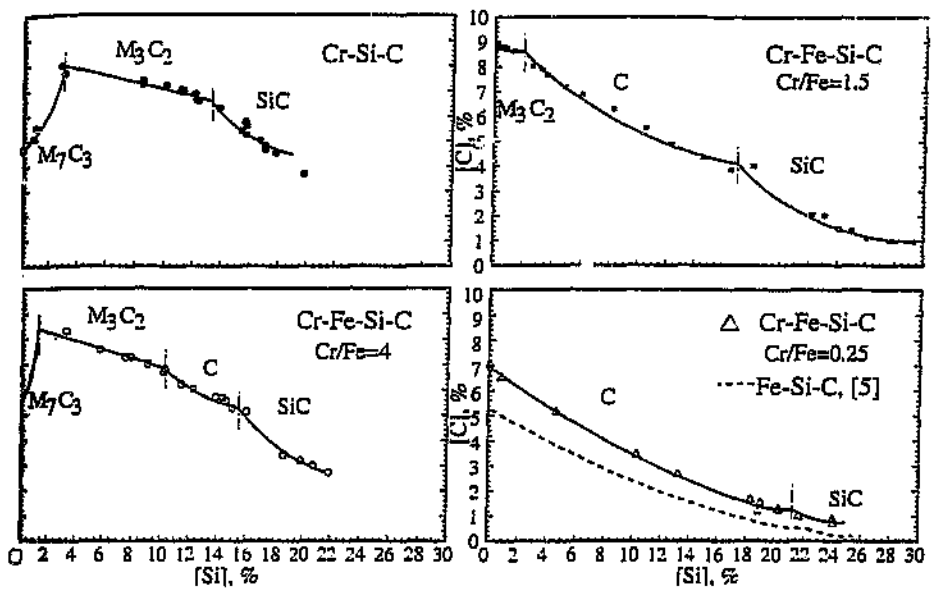


Figure 2.10. Silicon-carbon relations in Cr-Fe-Si-C alloys at 1600°C. After Kossyrev and Olsen [57]

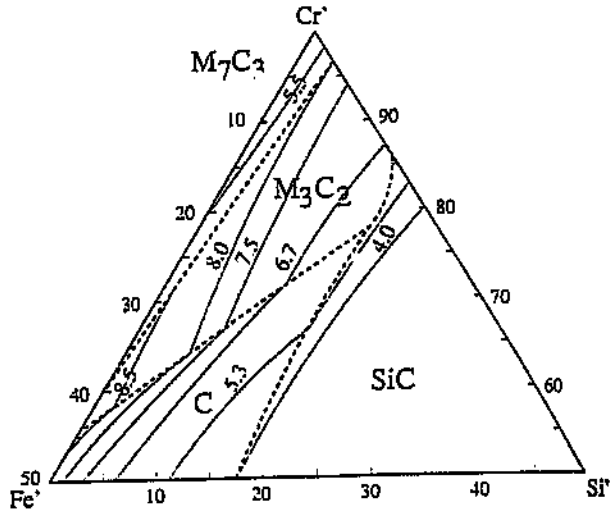


Figure 2.11. Saturated carbon content in Cr-Fe-Si-C_{sat} system at 1600°C. After Kossyrev and Olsen[57]

Legend:

Cr'=100[Cr]/(100-[C],

Fe'=100[Fe]/(100-[C]),

Si'=100[Si]/(100-[C])

2.3.2. Slag Phase

From the thermodynamic standpoint, the reactions in certain atmosphere between slag and metal control the chromium recovery in the processes of ferrochromium production. In order to evaluate the equilibrium distribution, to optimize the process for a higher recovery of chromium from the minerals, and further to evaluate slag modelling, the solubility of chromium oxides in slags, the thermodynamic activities of chromium oxides (and generally SiO_2 as well) are generally required.

Activities of chromium oxides in several multi-component slag systems and in the quasi-binary system SiO_2-CrO_x were recently studied by Y. Xiao and L. Holappa[62,63]. A $LaCrO_3$ resistance furnace, oxygen probe, and Cr-Ag alloy were used for the measurement of activities in chromium oxide-silica slag[63]. The isostatically-pressed zirconia solid electrolyte crucibles were supplied by Nippon Kagaku Togyo Co. The solid electrolyte oxygen probe, $Mo/Cr+Cr_2O_3/ZrO_2(MgO)$, consisted of a 9 mol% MgO stabilized zirconia crucible as an oxygen conductive electrolyte, and a mixture of 4 parts Cr and 1 part Cr_2O_3 by weight as a reference electrode. The probe was sealed with Al_2O_3 cement. A molybdenum wire of 0.5 mm in diameter was used as an electrical lead. Electrical contact to the outer surface of the zirconia probe was accomplished by a Cr-Ag alloy equilibrated with the slag, and a ZrO_2-Mo cement rod welded to a Mo wire in order to reduce the reaction between the electrical lead and the slag/alloy melt. In analogy with iron oxide containing slags, the chromium oxide slags have the same problem of varying oxidation state of chromium or non-stoichiometry of CrO_x in slags depending on temperature, slag basicity and even total chromium oxides content in the system equilibrated with metallic chromium. When $CrO_{1.5}$ is mixed with other slag-forming oxide components at high temperatures in contact with metallic chromium, the following equilibrium of chromium oxides can be expected in the slag-metal reaction system under the experimental conditions:

$$2(CrO_{1.5}) + \underline{Cr} = 3(CrO) \qquad (2.17)$$

$$_{\Delta}G^{\circ} = 25690 - 13.36T \text{ (cal/mole)} \qquad (2.18)$$

Chromium is therefore distributed in the slag as both divalent and trivalent states in different fractions, depending on the experimental conditions. In their studies[62,65] by using chromium crucible, the activity of metallic chromium is unity, the activities of chromium oxides have the relation of $a_{CrO} = 0.94(a_{CrO1.5})^{2/3}$. The experimental results of the activities of CrO and $CrO_{1.5}$ and the oxidation state of chromium in the SiO_2-CrO_x slag system are shown in figure 2.12. The activity of SiO_2 were calculated by the Gibbs Duhem equation. The activities of CrO and $CrO_{1.5}$ increase with increasing concentration of total chromium oxides, but the divalent chromium fraction decreases slightly. The explanation could be that the higher chromium oxide content will raise the system's oxygen partial pressure and may also slightly increase the slag basicity. The higher the slag basicity, the lower the divalent chromium fraction, and the higher the activities of chromium oxides. Based upon other activity data and the regular solution model, the iso-activity lines of CrO and $CrO_{1.5}$ in the CaO-SiO_2-CrO_x quasi-ternary system at equilibrium with pure metallic chromium were calculated and shown in figure 2.13.

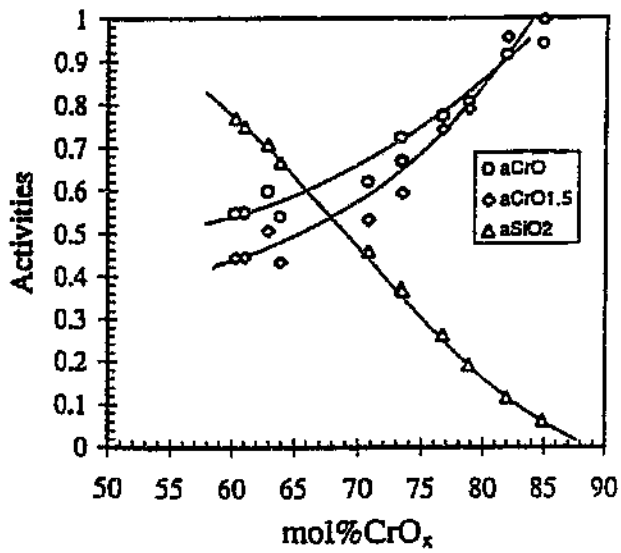


Figure 2.12. Activities of CrO, $CrO_{1.5}$ and SiO_2 in the SiO_2-CrO, quasi-binary system at 1873K in equilibrium with metallic chromium.

Standard state--pure solid $CrO_{1.5}$ and pure liquid CrO. After Xiao and Holappa[63]

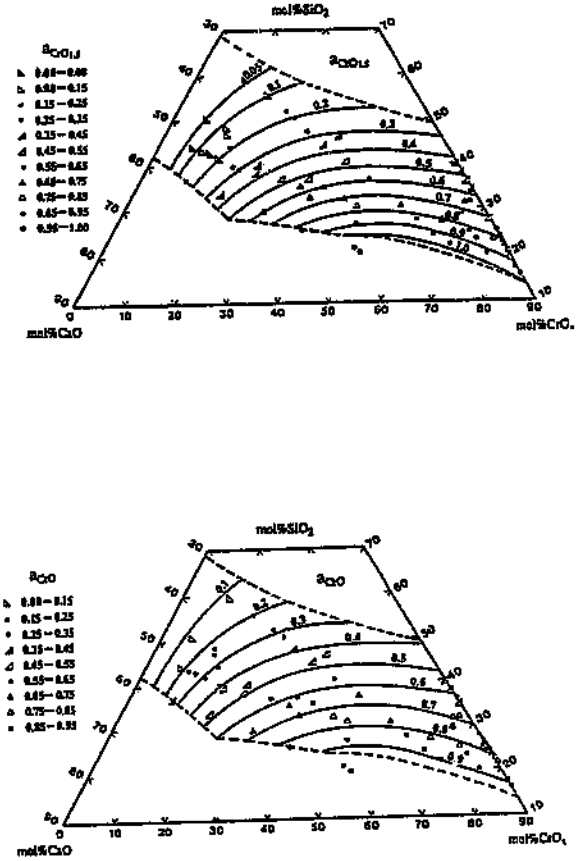


Figure 2.13. Comparison of calculated iso-activity curves (solid lines) for $CrO_{1.5}$ to experimental data in $CaO\text{-}SiO_2\text{-}CrO\text{-}CrO_{1.5}$ slags in equilibrium with Cr at 1873K. After Xiao and Holappa [63]

The solubility of chromium oxide in slags is also a very interesting field of study as it is one of the most important aspects of smelting reduction of chromium ore in order to increase the chromium yield by decreasing the undissolved chromite particles in the slags. Morita and Sano[64] investigated the solubility of $MgO.Cr_2O_3$ in $MgO-Al_2O_3-SiO_2-CaO$ melts at 1600°C. In air the solubility of $MgO.Cr_2O_3$ was found to be 1.1 to 4.5 per cent of Cr_2O_3 for $MgO-SiO_2$ melts. When Al_2O_3 was added to the melts, the solubility decreased to less 1 per cent of Cr_2O_3, and Cr in the coexisting $MgO.Cr_2O_3$ was replaced by Al in proportion to Al_2O_3 content in the slags. For MgO-CaO melts the solubility substantially rose to as much as 40 to 55 per cent of CrO_x, although more than 50 per cent of chromium was Cr^{6+} in the air. For $MgO-Al_2O_3-SiO_2-CaO$ melts, which are typical for smelting reduction of chromium ore, the solubility decreased with increasing MgO and Al_2O_3 contents. The effect of CaO/SiO_2 ratio on the solubility in the melts was found to be unexpectedly small as long as CaO was present. When 22.1 per cent BaO was added to $20\%MgO-20\%Al_2O_3-30\%SiO_2-30\%CaO$ melts, an increase in the solubility from 1.1 per cent to 4.4 per cent Cr_2O_3 was observed in air.

Under reducing conditions, for $MgO-SiO_2$ melts saturated with SiO_2 however, the CaO addition had no effect on the solubility of $MgO.Cr_2O_3$ at $Po_2 = 2.37x10^{-11}$ atm. For $20\%MgO-Al_2O_3-SiO_2-CaO$ ($CaO/SiO_2 = 1$) melts, the solubility decreased with increasing Al_2O_3 content at $Po_2 = 2.73x10^{-10}$ atm. This trend is consistent with that in air, though the solubility was twice as much as that in air. They thought in the conclusion that careful adjustment of slag composition, mainly by lowering MgO and Al_2O_3 contents, is recommended to enhance the dissolution of $MgO.Cr_2O_3$ for promotion of the reduction of chromium ore, and that the strongly reducing condition on smelting reduction also functions favourably for the dissolution of chromium ore into molten slags through the appearance of CrO.

The physicochemical properties, viscosity, electrical conductivity, of slags in the system $MgO-Al_2O_3-SiO_2$ and their application to the technology of ferro-alloy smelting were studied by Johnston, Johchens and Howat [65]. At constant SiO_2 concentration, the viscosity increases with a decrease in the ratio of MgO to Al_2O_3. The order of change is

approximately the same for the various levels of SiO_2 concentration. At constant MgO to Al_2O_3 ratios, the viscosity values increase with increase in the concentration of SiO_2. Increases in the silica content bring about a very marked increase in the viscosity of all slags. The same effect was observed at all temperature levels and at all MgO to Al_2O_3 ratios. The character of the change of viscosity with composition does not vary much from one temperature to another, indicating a regular disruption of the anionic lattice. The specific electrical conductivities (in S m^{-1}) of slags increase with increasing MgO-to-Al_2O_3 ratio at constant SiO_2 composition and increase with decreasing SiO_2 composition at constant MgO to Al_2O_3 ratio. In all instances, the values of specific conductivity are sufficiently high to permit the assumption that the mechanism of conduction is ionic.

2.3.3. Slag Models

It is very well known that slags have a very important role in most pyro-metallurgical operations. In spite of this major role, precise information about their properties and behaviours is incomplete. Furthermore, when the experimental difficulties are concerned in determining their thermodynamic properties, the estimations obtained by using slag models are rather considered as reliable information. The most successful estimations such as the ones developed by Flood-Grjotheim's[66] model, are limited to highly basic steelmaking slags. Elliot and his co-workers[67] revised this application due to an error in the use of free energy. Grjotheim and Brun[68] applied this model to the experimental results investigating phosphorus and manganese distribution between slag and molten metal.

The most fundamental structural-based slag models have been developed by Toop and Samis[69] and Masson[70,71,72]. Toop and Samis developed a theoretical treatment which allowed the most probable number of anions in any acid or basic silicate slag to be calculated in terms of an equilibrium constant for the equilibrium between singly bonded oxygen--O^-, doubly bonded oxygen--O^0, and free oxygen--O^{2-}, ions in the slags as described by:

$$O^0 + O^{2-} = 2O^- \qquad (2.19)$$

In this approach, for binary silicate systems, the equilibrium constant was assumed to be characteristic of the cation.

Masson expressed the distribution of anions in terms of ionic fraction rather than concentration of reactive groupings. Although this allows more specific conclusions to be reached regarding the concentration of polyionic species, the treatment is limited to melts of $X_{SiO_2} < 0.5$. In Masson's approach, two cases were considered: one in which the SiO_4^{4-} ion is considered to be a bifunctional mer unit and the other in which the SiO_4^{4-} ion is

considered to be a tetra functional mer unit.

In the former case, only two of the Si-O$^-$ groups on any SiO_4^{4+} ion can react to form poly-silicate ions. Therefore, only linear chain ion formation is possible. In the latter case four of the Si-O$^-$ groups on a SiO_4^{4+} ion may react, thus permitting the formation of branching chain ions. By making use of the vast experience in the studies of polymerization processes, Masson made some assumption in his model:

ion fractions are related to thermodynamic activities by the Temkin equation:

$$a_{MO} = N_{M^{2+}} * N_{O^{2-}} \qquad (2.20)$$

The first assumption implies that the silicate ions consist exclusively of linear and branched chains of general formula $Si_xO_{3x+1}^{2x+2-}$. The distribution of anions in such a system is considered in terms of the equilibrium constant for the reaction between the SiO_4^{4+} and any species of chain length x to yield the next higher number and free oxygen ion. Thus the depolymerization reaction can be written as:

$$SiO_4^{4-} + Si_xO_{3x+1}^{2(x+1)-} = Si_{x+1}O_{3x+4}^{2(x+2)-} + O^{2-} \qquad (2.21)$$

When the constitution of binary silicate melts is considered in terms of linear chains alone, the equilibrium ratio, $K_{(x)}$, for the reaction (2.21) is assumed to be independent of x. The chain growth by addition of monomer can occur at only two sides, namely, the ends of the chain, in linear chains. Similarly, depolymerization of monomer from the chain can also occur at two locations. Therefore the equilibrium constant for the reaction (2.21) is independent of chain length. Denoting the equilibrium constant for the reaction to be K, the sum of the ion fractions of silicate anions is obtained as:

$$\sum N_{silicate} = N_{Si_2O_7} + N_{Si_3O_{10}} + N_{Si_4O_{13}} \qquad (2.22)$$

Substituting for the individual ion fractions, the summation reduces to

$$\Sigma N_{silicate} = N_{SiO4}/(1-KN_{SiO4}/No^{2-}) \qquad (2.23)$$

If silicate and oxygen are considered to be the sole ionic species in the melt,

$$\Sigma N_{silicate} = 1 - No^{2-} \qquad (2.24)$$

Substitution of which into equation (2.23) will give

$$N_{SiO4} = (1-No^{2-})/[1-K+K/(No^{2-})] \qquad (2.25)$$

The mole fraction of silica in the binary melt was expressed in term of N_{SiO4} and N_{o2-} and using equation (2.19) and the Temkin's equation:

$$a_{MO} = N_{M2+}*N_{O2-} \qquad (2.26)$$

Masson derived the following expression:

$$1/N_{SiO4} = (3-K+a_{MO})/(1-a_{MO}) + K(K-1)/[a_{MO}/(1-a_{MO})+K] \qquad (2.27)$$

The size distribution of silicate poly-ions was given by:

$$N_x = \{1/[1+a_{MO}/(K(1-a_{MO})]\}^{x-1}\{1/[(K/a_{MO})+1/(1-a_{MO})]\} \qquad (2.28)$$

The value of K for various binary system was obtained by curve fitting of experimentally-determined activity-composition relationships.

Whiteway, Smith and Masson[73] derived the following theoretical equations for the size distribution of the poly-ions:

$$N_x = (3x!)(2a/3)^{(x-1)}(1-2a/3)^{(2x+1)}(1-No^{2-})/[(2x+1)!x!] \qquad (2.29)$$

N_x is the ion fraction of x-mer, a is the fraction of Si-O$^-$ groups present in the completely depolymerized state which have reacted to form doubly-bonded oxygen and free oxygen ions, and $N_{o^{2-}}$ is the ion fraction of free oxygen. From this distribution function and the Temkin equation, the activity of basic oxide expressed by a_{MO} was expressed in terms of mole fraction of SiO_2 and $K_{1,1}$ the equilibrium ratio for x=1, as:

$$1/N_{SiO2} = \{1-1/[1/3+a_{MO}/[K_{1,1}(1-a_{MO})]]\}/(1-a_{MO}) + 2 \qquad (2.30)$$

and the size distributions were obtained by

$$N_x = (3x)!\{1/[1+3a_{MO}/[K_{1,1}(1-a_{MO})]^{(x-1)}\{1/[1+K_{1,1}(1-a_{MO})/(3a_{MO})]\}^{(2x+1)}(1-a_{MO})/[(2x+1)!x!] \qquad (2.31)$$

The distributions closely resemble those calculated previously using linear chain model. Masson, Sommerville and Sosinsky[74] also extended the polymer theory to ternary silicate melts. They calculated the optical basicities of mixtures in the two ternary system which are FeO-CaO-SiO_2 and FeO-MnO-SiO_2 and the values of $K_{1,1}$ by interpolation. Another approach using oxygen and cation sub-lattices was introduced by Yokokawa and Niwa[75]. A similar model to this was developed by Kapoor and Frohberg[76]. According to this model, the properties of multi-component systems are represented by using binary parameters.

Gaskell[77] has reviewed all these models and outlined the basics of the approaches used. In Gaskell's review, additional to the models already mentioned above, another structural slag model also outlined was of Lin and Pelton's[78]. According to this study, a structural model is given for binary silicate systems having MO-SiO_2 type where MO is a basic

oxide and silicate tetrahedra and oxygen bonds are considered as structural units. The model considers the dependence of the enthalpy of the bonds on composition. One major advantage of this model is that it permits to calculate the numbers of ions of any configuration as it is not restricted to consideration of chain silicate ions.

A statistical model has been developed for complex slag systems by Gaye and Welfringe and studies related to the same model have been carried out by Gaye and other investigators[79-82]. It was extended from the model of Kapoor and Frohberg[76] to represent the properties of multi-component systems. The model is based on the description of the liquid slag in terms of cells composed of an oxygen anion surrounded by two cations, and makes use of only binary parameters (2 to 3 per binary system). the assumptions made in this model were as follows:

- An anionic sub-lattice without vacancies filled with oxygen ions and a cationic sub-lattice;

- The cationic sub-lattice is filled with the cations in the decreasing order of their charge;

- The structure is described in terms of symmetric (i-O-i) and asymmetric (i-O-j) cells (i and j being two different atoms),in numbers R_{ij}, ..$2R_{ij}$.., and the energy parameters consist of parameters for asymmetric cell formation, and parameters of interaction between cells.

R_{ij} refers to the fraction of i-O-j cells for a random distribution of cations on their sub-lattice. Although it is an oversimplification of the actual polymeric structure of the melt, in the $CaO-SiO_2$ system, a Si-O-Si cell represents a doubly bonded oxygen (O°), a Si-O-Ca cell represents a singly bonded oxygen (O^-) and a Ca-O-Ca cell represents a free oxygen ion (O^{2-}). Thus, the computed numbers R_{Si-Si} and $2R_{Si-Ca}$, of Si-O-Si and Si-O-Ca cells reflects the degree of polymerization of the melt. The very complex equations developed permit the calculation of the thermodynamic activities of the all oxide components and the

phase diagrams. In addition, experimental runs were done for systems containing up to six components chosen among MnO-CaO-MgO-SiO_2-Al_2O_3-Fe_2O_3-FeO. A very satisfactory agreement between the experimental data and calculated values was found in the studies on thermodynamic activities of MnO in manganese slags and slag-metal equilibria by H. Cengizler[43].

Regular Solution Model, originally proposed in 1961 by Lumsden[80], has been applied to the systems involving the following components: Al_2O_3, CaO, CoO, Cu_2O, FeO, Fe_2O_3, MgO, MnO, NiO, P_2O_5, PbO, SiO_2, TiO_2 and ZnO for thirty years by many researchers[81-91]. Xiao and Holappa[63] most recently assessed the thermodynamic data on slags containing CaO, SiO_2, MgO, Al_2O_3, CrO and Cr_2O_3 components by using the regular solution model to mathematically describe the activities of chromium oxides in different chromium containing slags. A group of middle parameters were obtained. The calculated activities of chromium oxides were quite comparable to those experimentally measured. In the melts with regular solution behaviour, the molecular/ionic species such as SiO_2 or SiO_4^{4-} were taken as "dissociated" ionic species consisting of Si^{4+} cations and O^{2-} anions. It was assumed that the cations are almost randomly distributed among a three dimensional matrix of oxygen anions (O^{2-}). The mixing energy of the system can be expressed in terms of the binary interaction energies between cations and the mole fractions of the cations. Due to the fact that there is not any restriction for choosing the standard state of the activity, in order to calculate the activities of species, the hypothetical pure liquid oxides with regular nature was taken as the standard states of chromium oxides. The conversion energy from this hypothetical regular solution standard state (R.S.) to the conventional standard states(pure solid or liquid) is necessary[87]. The general relations expressing the excess Gibbs energy of the multi-component solutions based on regular model are listed as follows:

$$RT\ln(g_i)_{(R.S.)} = Sa_{ij}X_j^2 + SS(a_{ij}+a_{ik}-a_{jk})X_jX_k \qquad (2.32)$$

$$RT\ln(g_i)_{(s/l)} = RT\ln(g_i)_{(R.S.)} + \Delta G_{conv} \qquad (2.33)$$

here, $a_{ij} = a_{ji}$, $a_{ij} = a_{jk} = a_{ik} = 0$, and ΔG_{conv} is the conversion factor associated with the change in the standard states. These parameters can be assessed by the experimental data. The distribution of divalent and trivalent chromium in the slags equilibrated with metallic chromium is very important in order to clarify the activities of chromium oxides in slags. The quantitative relation between the oxidation state of chromium and their activity coefficient can be derived from the thermodynamic relationship. The distributions of divalent chromium and trivalent chromium can be obtained as follows:

$$CrO_{1.5}(s) = CrO(liq.) + 1/4O_2 \qquad (2.34)$$

$$\Delta G^{\circ} = -RT\ln(a_{CrO}Po_2^{1/4}/a_{CrO1.5})$$
$$= 52785 - 14.31T \quad (cal/mole) \qquad (2.35)$$

The divalent to trivalent chromium ratio, a constraint in the assessment, can be expressed as:

$$\ln(X_{CrO1.5}/X_{CrO}) = \ln(\gamma_{CrO}/\gamma_{CrO1.5}) + (1/4)\ln P_{O2}$$
$$+ 26565/T - 7.199 \qquad (2.36)$$

In their present assessment work[62], multiple linear regression analysis has been used as a quick and conventional method for determining the model parameters. The assessment was processed from binary $CaO\text{-}SiO_2$ system to multi-component systems step by step. The experimental data in $CaO\text{-}SiO_2$ system were taken from the literature. The activity data for chromium oxides were based on the experimental data obtained in both of their present and previous work[62,63] over $CrO\text{-}CrO_{1.5}\text{-}SiO_2$, $CrO\text{-}CrO_{1.5}\text{-}CaO\text{-}SiO_2$, $CrO\text{-}CrO_{1.5}\text{-}CaO\text{-}SiO_2\text{-}MgO$, $CrO\text{-}CrO_{1.5}\text{-}CaO\text{-}SiO_2\text{-}AlO_{1.5}$, $CrO\text{-}CrO_{1.5}\text{-}CaO\text{-}SiO_2\text{-}MgO\text{-}AlO_{1.5}$ systems. A group of interaction energy parameters were optimized mathematically, and are given in table 2.1. Due to lack of thermodynamic data of chromium oxide complexes, the physical significance of model parameters can not be discussed in the present stage.

Table 2.1. Optimised interaction energy parameters, a_{ij}(J), between cations in CrO-$CrO_{1.5}$-CaO-SiO_2-MgO-$AlO_{1.5}$ slags[63].

i/j	Cr^{2+}	Cr^{3+}	Ca^{2+}	Si^{4+}	Mg^{2+}	Al^{3+}
Cr^{2+}	.....	32710	-6140	-60540	5520	-30285
Cr^{3+}	32710	.....	44235	-48975	28085	-46210
Ca^{2+}	-6140	44235	.....	-139100	-100420	-154810
Si^{4+}	-6054[illegible]	-48975	-139100	.....	-66940	-127610
Mg^{2+}	5520	28085	-100420	-66940	.....	-71130
Al^{3+}	-30285	-46210	-154810	-127610	-71130	.....

Because the chromium containing slags are not strictly regular solutions, the conversion energies for changing the standard state of activity coefficients from the hypothetical regular solution to the traditional pure solid or pure liquid were also optimized simultaneously by the experimental data. The obtained conversion Gibbs energies for CrO and $CrO_{1.5}$ are recorded in table 2.2.

Based on the activity data by Sharma and Richardson et al[92-96], The activities of SiO_2 in CaO-SiO_2 binary system have been evaluated by the quadratic mathematical formula based on the regular solution model. The interaction energy parameters for CaO and SiO_2 were approximately derived, and the conversion Gibbs energy of silica from pure solid to hypothetical liquid with regular nature was also obtained as: 51346-13.88T(J).

The calculated results based on the regular solution model and the experimental results are shown in figure 2.13. The comparison between calculated activities and those

experimentally measured in SiO_2-CrO-$CrO_{1.5}$, CaO-SiO_2-CrO-$CrO_{1.5}$, CaO-SiO_2-CrO-$CrO_{1.5}$-MgO, CaO-SiO_2-CrO-$CrO_{1.5}$-$AlO_{1.5}$, CaO-SiO_2-CrO-$CrO_{1.5}$-MgO-$AlO_{1.5}$ systems are shown in figure 2.14. This figure expresses the assessed activities of chromium oxides in all the related slag systems. The system containing Al_2O_3 had a larger deviation from the regular solution behaviour.

Table 2.2. Conversion Gibbs energy of CrO and $CrO_{1.5}$ in slags from the hypothetical pure liquid with the regular solution nature to the traditional pure solid or liquid standard state[63].

Reactions	Gibbs energy change (J)
CrO(liq) = CrO(R.S.)	77150-33.5T
$CrO_{1.5}$(s) = $CrO_{1.5}$(R.S.)	74967-37.5T
$CrO_{1.5}$(liq) = $CrO_{1.5}$(R.S.)	10152-12.6T
$CrO_{1.5}$(s) = $CrO_{1.5}$(liq)	64815-24.9T

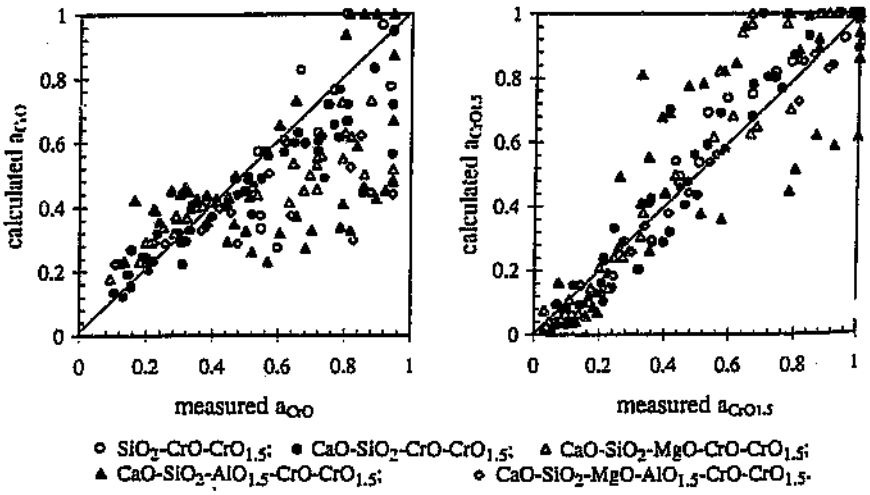


Figure 2.14. Comparation of activities of Cr oxides between calculation and experiments, after Xiao and Holappa[63]

2.3.4. Slag-Metal Equilibrium

A number of investigations on slag-metal equilibrium distribution of some elements pertinent to some parts of the present system have been done in the past. The equilibrium between slag and metal phases at a given temperature is mainly controlled by the compositions of the gas, metal and slag phases individually.

The equilibrium between the carbon saturated Fe-Cr-Si-C alloys and SiO_2-CaO-MgO-Al_2O_3-CrO_x-FeO_y slags was studied under argon atmosphere and carbon monoxide at temperatures of 1500 °C and 1600°C by M. Akyuzlu and R. H. Eric[33]. The investigation deals with a complex slag-metal equilibrium involving eight components distributed between the Fe-Cr-C-Si metal phase and the SiO_2-CaO-MgO-Al_2O_3-CrO_x-FeO_y slag phase. The metal and slag compositions and temperatures studied are relevant to actual ferrochromium smelting operations. Samples of selected metal and slag in equal masses were placed in graphite crucibles and heated in a vertical molybdenum-wound resistance furnace. At the end of the equilibration, the crucibles were quenched by dropping into water. The equilibration time was determined after a series of metal-slag equilibria runs, which were carried out at 1500°C at times varying from 3 to 14 hours but at the same initial compositions. The approach to equilibrium was established by analysis of the silicon content of the metal since the silica reduction is the slowest reaction in the system.

It was found by preliminary experiments that a minimum of 10 hours was necessary for equilibration at 1500°C. Both the reduction and oxidation of silicon were investigated; reduction took 10 hours and oxidation being much quicker. The actual runs in their studies, however, were conducted for 12 hours. After equilibration and quenching, the distinct slag metal phases were separated, cleaned [illegible] sary, and sent for analysis.

The carbon content of the metal was analyzed by a Leco analyzer and the other constituents of the metal by the ICP method. The Al_2O_3, SiO_2, CaO and MgO constituents of the slag were analyzed by X-ray fluorescence, and its iron and chromium content by

the o-phenanthroline colorimetric and fdiphenylcarbazide colorimetric methods respectively. In addition, some X-ray diffraction analyses and metallographic examinations were conducted on metal samples in order to detect the carbides. Over 150 experiments were conducted, from which 115 successful ones were selected for analysis. The results were expressed in terms of silicon distribution and chromium distribution.

Distribution of Silicon

The silicon content of the metal phase was directly proportional to the silicon content of the slag with which it was in equilibrium. This is illustrated in figure 2.15. The increase of silicon content in the metal with increasing silica in the slag was more pronounced at 1600°C. This was explained by the increase in the value of the equilibrium constant of reaction 2.37 as the temperature increases, shifting the reaction toward the right.

$$(SiO_2) + 2\underline{C} = \underline{Si} + 2CO(g) \qquad (2.37)$$

For example, for a chromium to iron ratio of 1.7 in the metal phase (not illustrated in figure 2.15), as the silicon content of the slag increased from about 30 to 40 mass per cent, the silicon content in the metal increased dramatically from 1.5 to 8.0 mass per cent. The effect of the CaO-to-Al_2O_3 ratio on the silica reduction is illustrated in figure 2.16. In general, as the ratio increases, the silicon content of the metal decreases. This indicates that as lime replaces alumina in the slag, the activity of silica in the slag decreases, in accordance with the network modification power of CaO. The higher the content of CaO in the slag, the more will it break the silica network, releasing free oxygen ions and resulting in an increase in metal oxide activities and a decrease in silica activity. As Al_2O_3 was replaced by lime in slags of low silica content, the equilibrium silicon content in the metal increased. In the case of high-silica slags,(containing more than 20 per cent of silica), the opposite effect was observed, which is in agreement with the study made by Rein and Chipman[95].

The effect of the MgO-to-CaO ratio on the partition ratio of silicon (% Si in slag / % Si in metal) is shown in figure 2.17. It was observed that, as the ratio of MgO to CaO increased, the partition ratio decreased. This is an indication of the fact that, as MgO replaces CaO in the slag, the activity of silica in the slag increases, resulting in an increase in the silicon in the metal. By using the activities of silica from Rein and Chipman's study[95], and by using the equilibrium constant for the reaction (2.37), K = 0.2184, activity of carbon is unity, Pco=1.0 atm at 1600°C, the activity of silicon (with pure liquid silicon as the standard state) was calculated in some of the carbon saturated Fe-Cr-Si-C alloys. The results, shown in figure 2.18 within the dilute range studied, have considerable negative de- -ion. The figure 2.19 illustrates the change in activity of silicon with increasing silicon and carbon contents by molar fraction. The influence of molar fraction of silicon and carbon on the activity coefficient of silicon in the Fe-Cr-Si-C_{sat} alloys at 1600°C is indicated in figure 2.20.

Distribution of Chromium

In the study by Akyuzlu and Eric[33], the chromium and iron contents of the slag were very low. The slags usually contained less than 0.5 per cent of Cr_2O_3 and 0.3 per cent of Fe_2O_3 by mass. Even when those two oxides were initially added up to 10 per cent to the charge in a number of the experiments, they were reduced to their equilibrium values indicated above. This was mainly due to the highly reducing conditions prevailing in the experiments. The effect of basicity on the chromium content of the slags is shown in figure 2.21 and 2.22. At low basicities, the chromium content (calculated as Cr) of the slag decreased rapidly as the basicity increased from 0.4 to 0.8 at 1500°C for both argon and carbon monoxide atmosphere and from 0.7 to 1.0 at 1600°C for carbon monoxide atmosphere. Thereafter, once the threshold value had been passed, the basicity did not dramatically affect the chromium solubility in the slag, which tended to a constant value around 0.15 per cent by mass. This behaviour proves that operation with high basic slags

just below the threshold value is one of the means of to lower chemical chromium losses to the slags. The effect of FeO in the slag on its chromium content is illustrated in figure 2.23 and 2.24. Those typical diagrams are for the experiments done at 1500 and 1600°C. There is direct proportionality between the chromium and iron contents in the slag. Such behaviour can be explained by the phenomenon of oxygen transfer from the slag phase to metal phase by means of FeO; that is, FeO in the slag oxidizes chromium in the metal phase at the slag-metal interface. Thus, the more FeO the slag contains, the more will be its chromium content.

Kossyrev and Olsen[97] studied the distribution of silicon between slag and metal in the SiO_2-MgO-Al_2O_3 and Cr-Fe-Si-C_{sat} system in graphite crucibles at 1600°C in CO atmosphere. The silicon content of each alloy depended on the silica activity in the slag and on the iron content of the metal at given conditions. The equilibrium content of silicon for various Cr-Fe-Si-C_{sat} alloys dependent on the silica activity in SiO_2-MgO-Al_2O_3 slags is illustrated in figure 2.25. Figure 2.26 shows the equilibrium silicon content in Cr-Fe(20%)-Si-C_{sat} (solid curves) and Cr-Si-C_{sat} (dashed curve) alloys equilibrated with SiO_2-MgO-Al_2O_3 with different MgO/Al_2O_3 ratios at CO atmosphere. It is possible to calculate the distribution of silicon between the slag system and the various Cr-Fe-Si-C_{sat} alloys as well as between Cr-Fe-Si-C_{sat} alloys and other slag systems where the silica activities are well known. Based upon the activities of SiO_2 by Richard and Chipman[98], the activity and activity coefficient of silicon can be calculated. The calculated results indicate that the relation between $\log\gamma_{Si}$ and N_{Si} shows a linear character in the investigated alloys of N_{Si} 0.22 to 0.32 (5%Cr or 25%Cr, and 20 %Fe), as described by the following correlation equation:

$$\log\gamma_{Si} = 0.444N_{Si} - 0.706 \qquad (2.38)$$

The calculated silicon distribution between the alloys of Fe-Si-C_{sat}, Fe-Cr(5%)-Si-C_{sat}, Fe-Cr(25%)-Si-C_{sat}, Cr-Fe(20%)-Si-C_{sat}, and Cr-Si-C_{sat} with SiO_2-MgO-Al_2O_3 slags in CO atmosphere are shown in figure 2.27 and figure 2.28.

Morita, Maeda and Sano[51,97] made a study of the thermodynamics of chromium oxide in molten $CaO-MgO-Al_2O_3-SiO_2$ slags coexisting with solid carbon. In this study chromium in the slag was found to exist as CrO in equilibrium with (solid) Cr_3C_2, solid carbon and one atmosphere of CO. The equilibrium concentration of chromium in the slags were determined at 1500 and 1600 °C, as illustrated in figures 2.29, 2.30 and 2.31. The activity coefficients of CrO were calculated from the determined concentrations and is shown in figure 2.32. In the $CaO-Al_2O_3-SiO_2$ melts, Al_2O_3 was observed to increase the activity coefficient of chromium in the region where chromium oxide behaved as a base. Therefore the equilibrium concentration of chromium in slag phase decreases with increasing Al_2O_3 at constant ratio of $CaO:SiO_2$. The results shown in figure 2.33, illustrate that when alumina=20% and (CaO+MgO)=30%, 40%, 50% in the slags, chromium in the slag increases with the replacement of CaO by MgO in the range of MgO less than 20 per cent by mass.

When studying metal-slag equilibrium, activity of silica in the slags is widely used to calculate the activity of silicon in the metal phase. The most popular results were from the study done by Rein and Chipman[95]. In their study, the activity of SiO_2 in the entire liquid system $SiO_2-CaO-MgO-Al_2O_3$ at 1600°C was calculated from the distribution of silicon between those slags and Fe-Si-C alloys saturated with either graphite or silicon carbide, the activity coefficient of silicon in those alloys, and the requisite thermodynamic data. The activities of other components in the ternary systems $SiO_2-CaO-Al_2O_3$, $SiO_2-MgO-CaO$, $SiO_2-MgO-Al_2O_3$ were computed from these data by the Gibbs-Duhem equation with the aid of known free energies of several of the inter-oxide compounds and the accepted phase diagrams. In the distribution experiments, silica reduction proceeded to equilibrium according to either of the following reactions, the second being applicable when the silicon content of the metal exceeded 22.0 or 22.4 per cent by weight at 1550 or 1600°C.

$$SiO_2 \text{ (in slag)} + 2C \text{ (graphite)} = \underline{Si} \text{ (in Fe-Si-C alloy)} + 2CO(g, 1atm) \qquad (2.39)$$

$$\Delta G^\circ = 170{,}300 - 87.9T \quad \text{(cal/mole)} \qquad (2.40)$$

$$SiO_2 \text{ (in slag)} + 2SiC(b) = 3\underline{Si} \text{ (in Fe-Si-C alloy)} + 2CO \text{ (g, 1atm)} \quad (2.41)$$

$$\Delta G^\circ = 225,100 - 105.7T \quad \text{(cal/mole)} \quad (2.42)$$

The activity of SiO_2 in the slag is readily obtained from the equilibrium composition when the standard free-energy change in the reaction and the activity coefficient in the metal are known. In their calculation, the pure solid phase which is stable at the experimental temperature is selected as the standard state for each component, specifically cristobalite for silica. The uncertainty of reaction (2.39) is established to be ±0.5 Kcal. For reaction (2.41), it may be larger since this depends on SiC as well as on SiO_2 and C. However, since the free energy of SiC was determined by means of these reactions, its application to the problem of SiO_2 activities was unlikely to entail large errors. The activity of silicon in the alloy is $\gamma_{Si}N_{Si}$ and the values of γ_{Si} was taken from the work of Chipman and Baschwitz[98]. A slight modification of the curves of Chipman and Baschwitzz is required in order to avoid activities of silica greater than unit in the saturated solution. A downward adjustment amounting to 0.04 in $\log\gamma_{Si}$ at $N_{Si} = 0.42$ was applied without changing the curve below 0.38. The resultant curves shown in figure 2.34 are less severely curved in the region of $N_{Si} = 0.5$ to 0.7. The over-all uncertainty in $\log\gamma_{Si}$ would appear to be less than ±0.1. Activities of SiO_2 in SiO_2-CaO-Al_2O_3 slags at 1550 and 1600°C, in SiO_2-CaO-MgO slags at 1600°C, in SiO_2-MgO-Al_2O_3 slags at 1600°C, and in SiO_2-CaO-MgO-Al_2O_3 slags with 10% MgO, 20% MgO and 30% MgO are illustrated in figures 2.35, 2.36, 2.37, 2.38, and 2.39.

Although it appears that a substantial amount of information has been available on chromium-containing systems of both slag phase and metal phase, the majority of these are related to the conditions of high carbon ferro-chromium production. The conditions are the saturation of carbon in the metal phase, and atmosphere of carbon monoxide in the gas phase. There are very few studies on the thermodynamics and gas-slag-metal equilibria under the condition of either un-saturation of carbon in the metal phase or lower partial pressure of carbon monoxide in the gas phase, which are pertinent to the refining of ferro-chromium alloys and the making of stainless steel by means of oxygen-blowing methods combined with argon blowing or/and vacuum treatments, such as VOD and AOD used widely in industries. This investigation, therefore is directed to fill in some of these gaps.

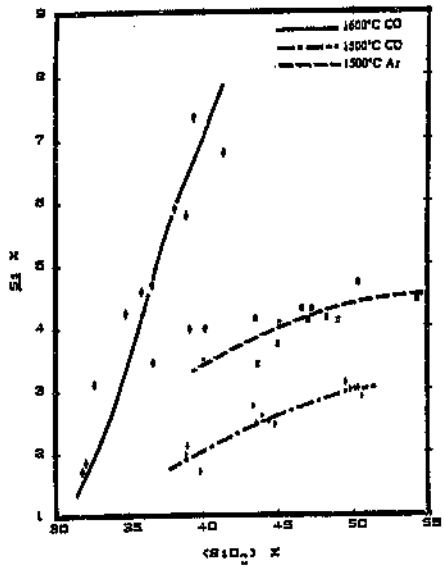


Figure 2.15. The effect of the SiO_2 content of the slag phase on the Si content of the metal phase (Cr:Fe=1.3 in the metal). After M. Akyuzlu and R.H. Eric[33]

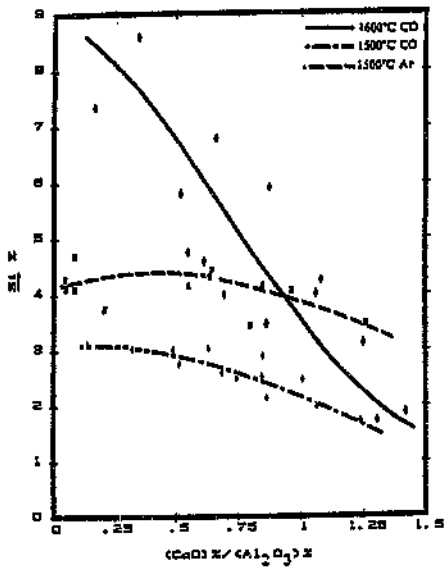


Figure 2.16. The effect of the lime-to-alumina ratio of the slag on the Si content of the metal phase (Cr:Fe=1 3 in the metal). After M. Akyuzlu and R.H. Eric[43]

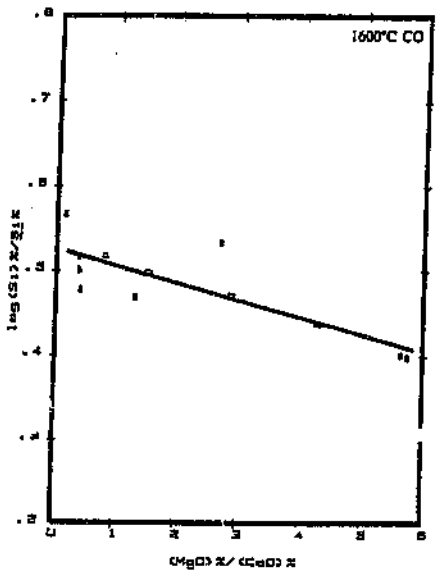


Figure 2.17. The effect of the MgO-to-CaO ratio on the silicon distribution (25% alumina, 39.2% silica). After M. Akyuzlu and R.H. Eric [39]

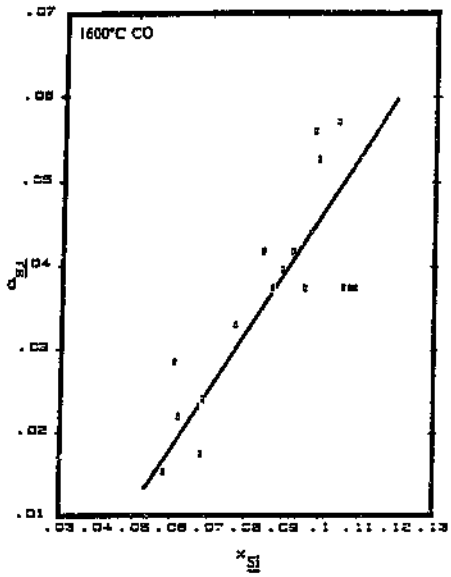


Figure 2.18. The change in silicon activity with increasing X_{Si} (1600°C) in Fe-Cr-Si-C_{sat} alloys. After M. Akyuzlu and R.H. Eric[33]

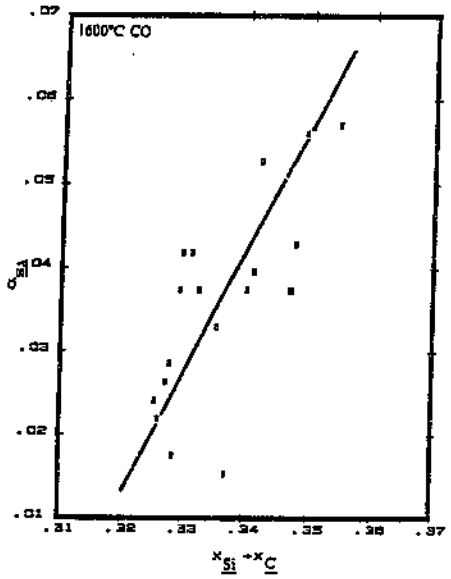


Figure 2.19. The change in silicon activity with increasing ($X_{Si}+X_C$) (1600°C) in Fe-Cr-Si-C_{sat} alloys. After M. Akyuzlu and R.H. Eric[33]

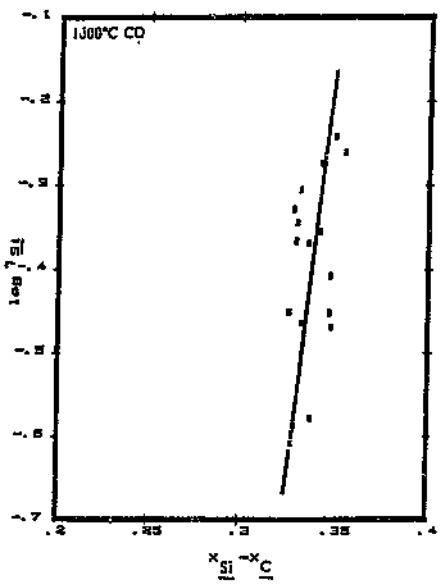


Figure 2.20. The influence of $(X_{Si}+X_C)$ on the activity coefficient of Si (1600°C) in Fe-Cr-Si-C_{sat} alloys. After M. Akyuzlu and R.H. Eric[33]

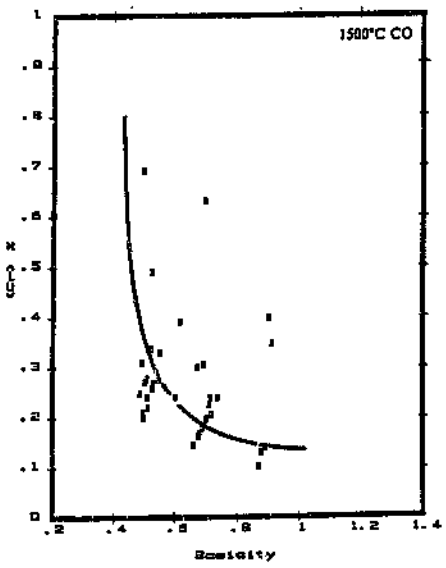


Figure 2.21. The effect of basicity on the chromium content of the slags at 1500°C under CO atmosphere. After M. Akyuzlu and R.H. Eric[33]

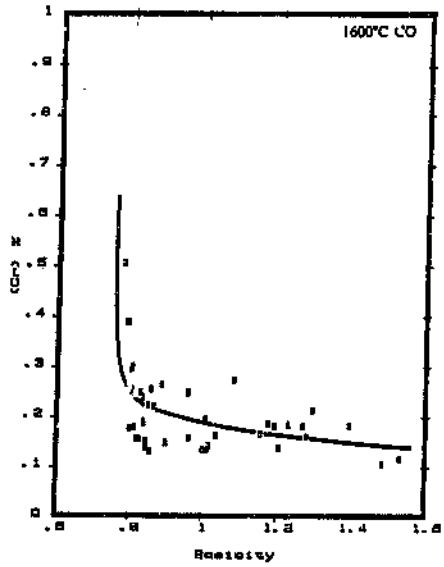


Figure 2.22. The effect of basicity on the chromium content of the slags at 1600°C under CO atmosphere. After M. Akyuzlu and R.H. Eric[33]

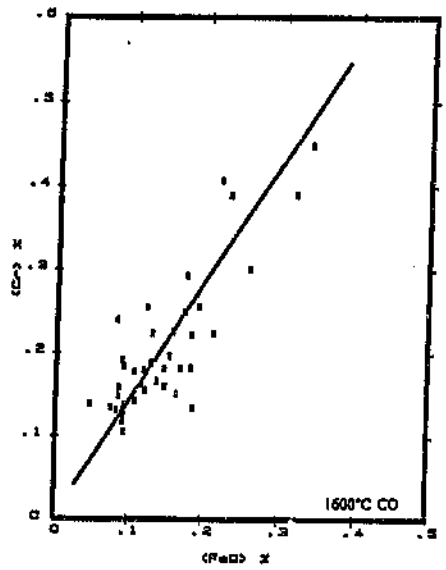


Figure 2.23. The effect of (FeO) on the Cr content of the slag under CO atmosphere at 1500°C. After M. Akyuzlu and R.H. Eric [33]

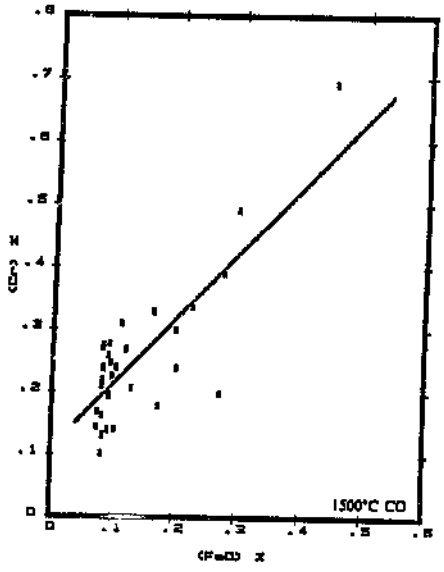


Figure 2.24. The effect of (FeO) on the Cr content of the slag under CO atmosphere at 1600°C. After M. Akyuzlu and R.H. Eric[33]

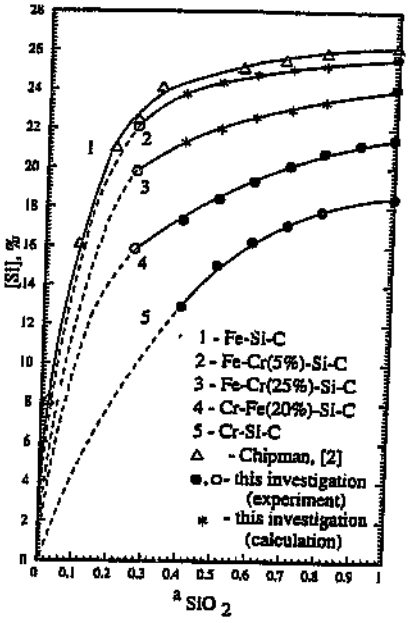


Figure 2.25. The equilibrium content of silicon for various Cr-Fe-Si-C_{sat} alloys dependent on the silica activity in SiO_2-MgO-Al_2O_3 slags at 1600°C. After Kossyrev and Olsen[57]

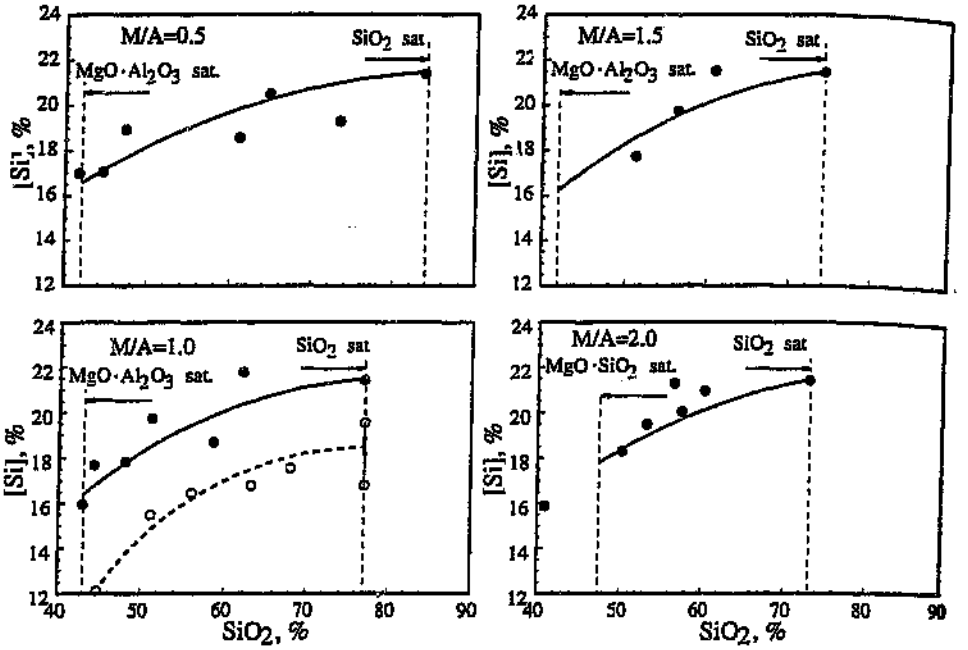


Figure 2.26. Si content of Cr-Fe(20%)-Si-C_{sat}(solid curves) and Cr-Si-C_{sat}(dashed curve) alloys at 1600°C in CO gas in equilibrium with SiO_2-MgO-Al_2O_3 slags with different M/A ratios. After Kossyrev and Olsen[57]

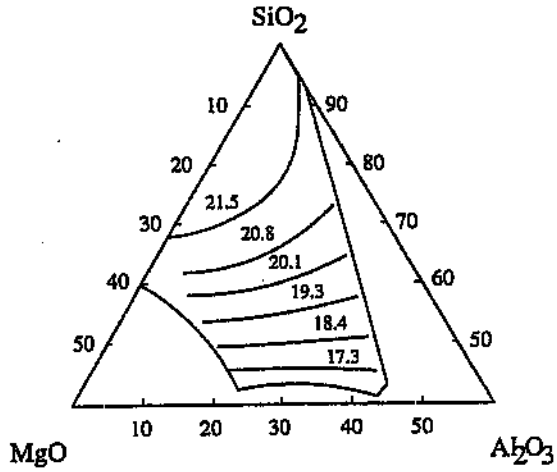


Figure 2.27. Iso-activity lines for silica[180] and corresponding Si content in Cr-Fe(20%)-Si-C_{sat} alloys in equilibrium with SiO_2-MgO-Al_2O_3 slags at 1600°C . After Kossyrev and Olsen[57]

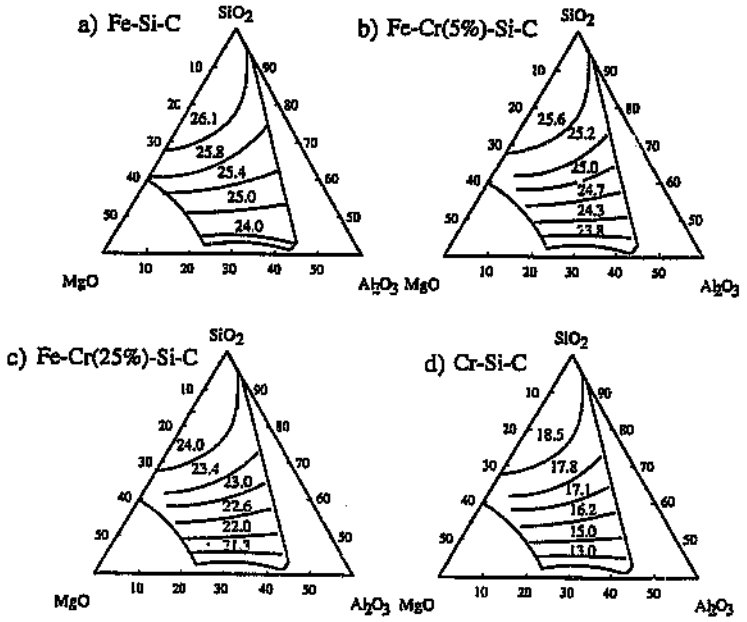


Figure 2.28. Distribution of silicon between Cr-Fe-Si-C_{sat} alloys and SiO_2-MgO-Al_2O_3 slags at 1600°C in CO gas. After Kossyrev and Olsen[57]

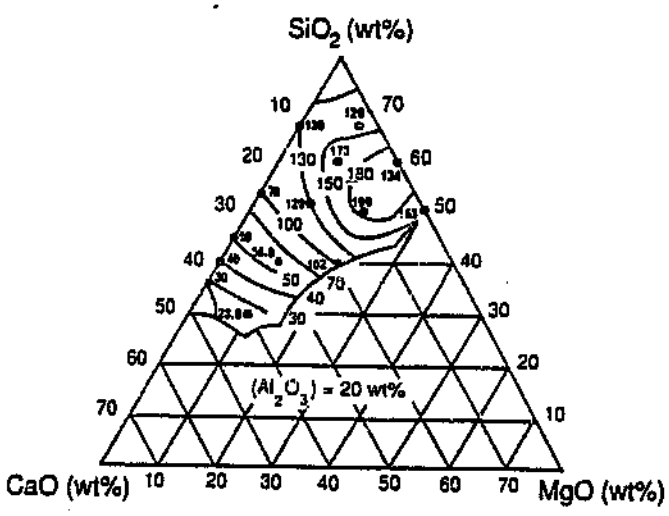


Figure 2.29. Contour lines of $(Cr)_{eq}$ in $CaO-MgO-Al_2O_3-SiO_2$ melts (1500°C). After Maeda and Sano [64]

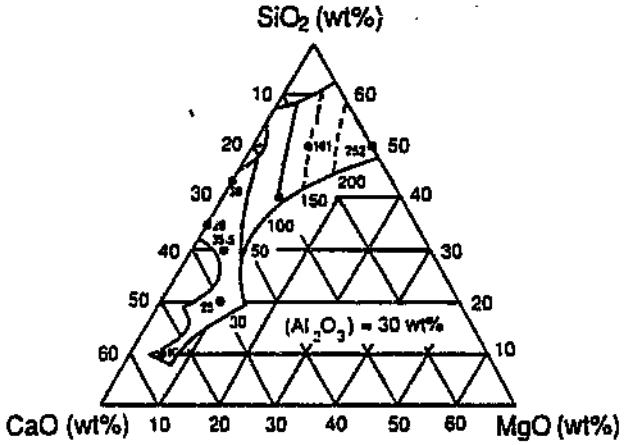


Figure 2.30. Contour lines of (Cr_{eq}) in CaO-MgO-Al_2O_3-SiO_2 melts (1500°C). After Maeda and Sano [64]

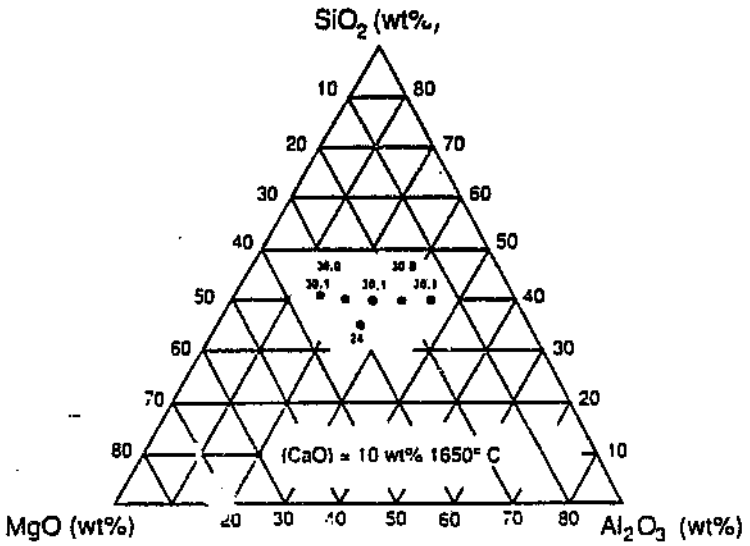


Figure 2.31. Equilibrium concentrations of chromium in CaO-MgO-Al_2O_3-SiO_2 melts (1650°C). After Maeda and Sano [64]

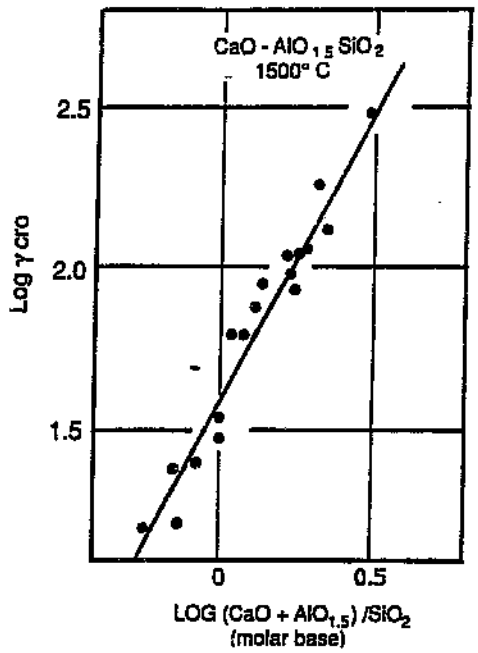


Figure 2.32. The relation between γ_{CrO} and Molar $(CaO+Al_2O_3)/SiO_2$. After Maeda and Sano[61]

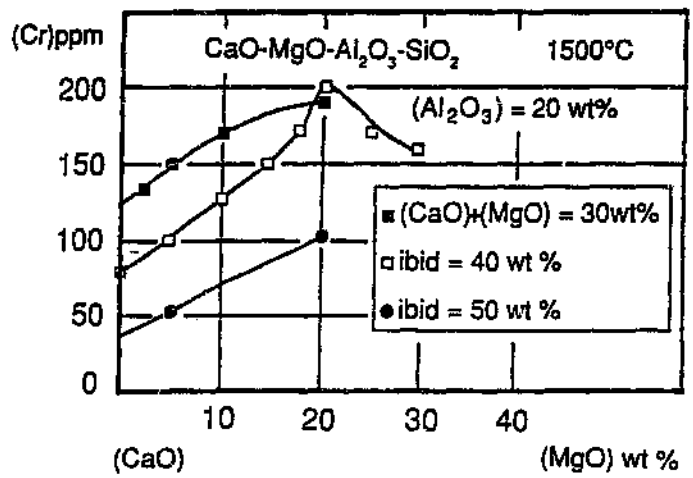


Figure 2.33. The effect of the replacement of (CaO) by (MgO) on $(Cr)_{eq}$ at constant ($\%Al_2O_3$)(=20) and (SiO_2). After Maeda and Sano [64]

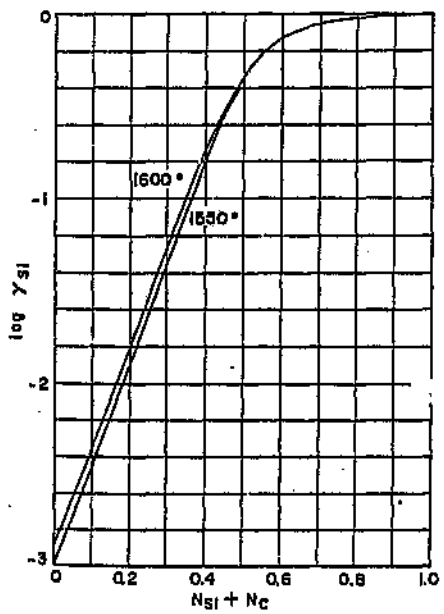


Figure 2.34. Activity coefficient of silicon in liquid Fe-C-S. [illegible] Chipman and Baschwitz [98]

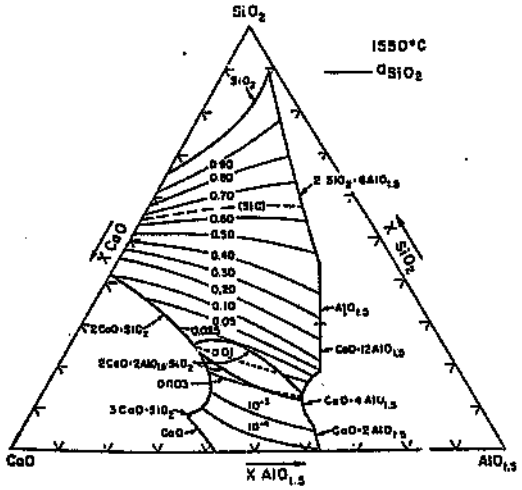


Figure 2.35. Activity of SiO_2 in SiO_2-CaO-Al_2O_3 slags at 1550°C. After Rein and Chipman [95]

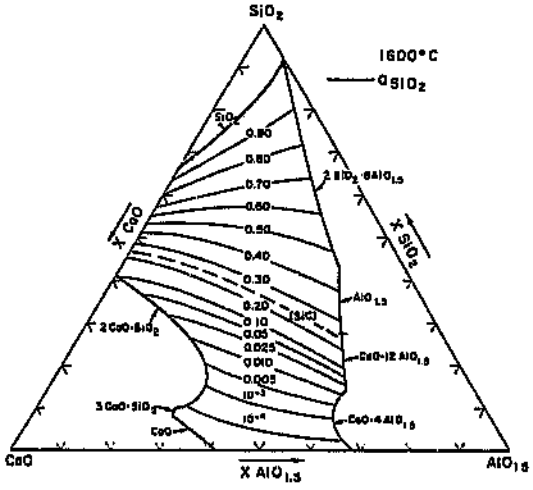


Figure 2.36. Activity of SiO_2 in SiO_2-CaO-Al_2O_3 slags at 1600°C. After Rein and Chipman [95]

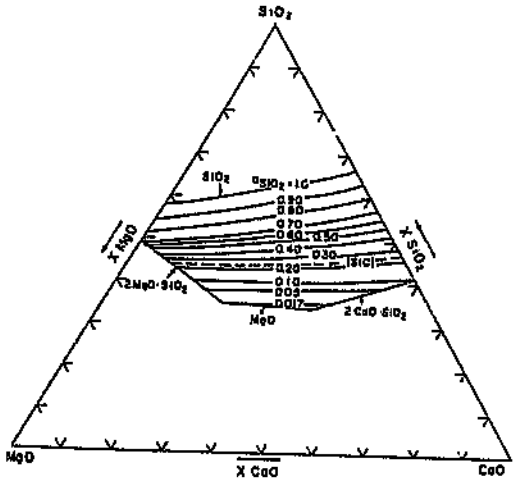


Figure 2.37. Activity of SiO_2 in SiO_2-CaO-MgO slags at 1600°C. After Rein and Chipman [95]

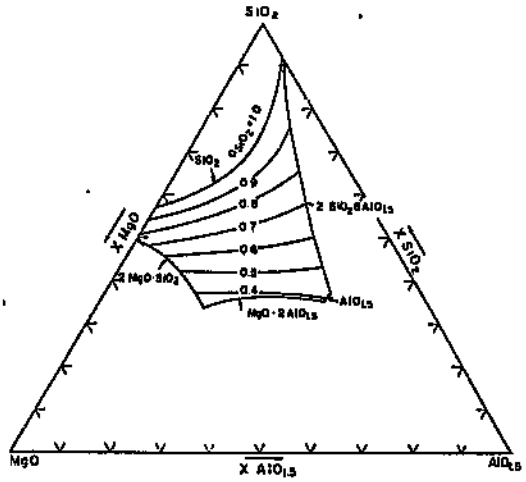


Figure 2.38. Activity of SiO_2 in SiO_2-MgO-Al_2O_3 slags at 1600°C. After Rein and Chipman [95]

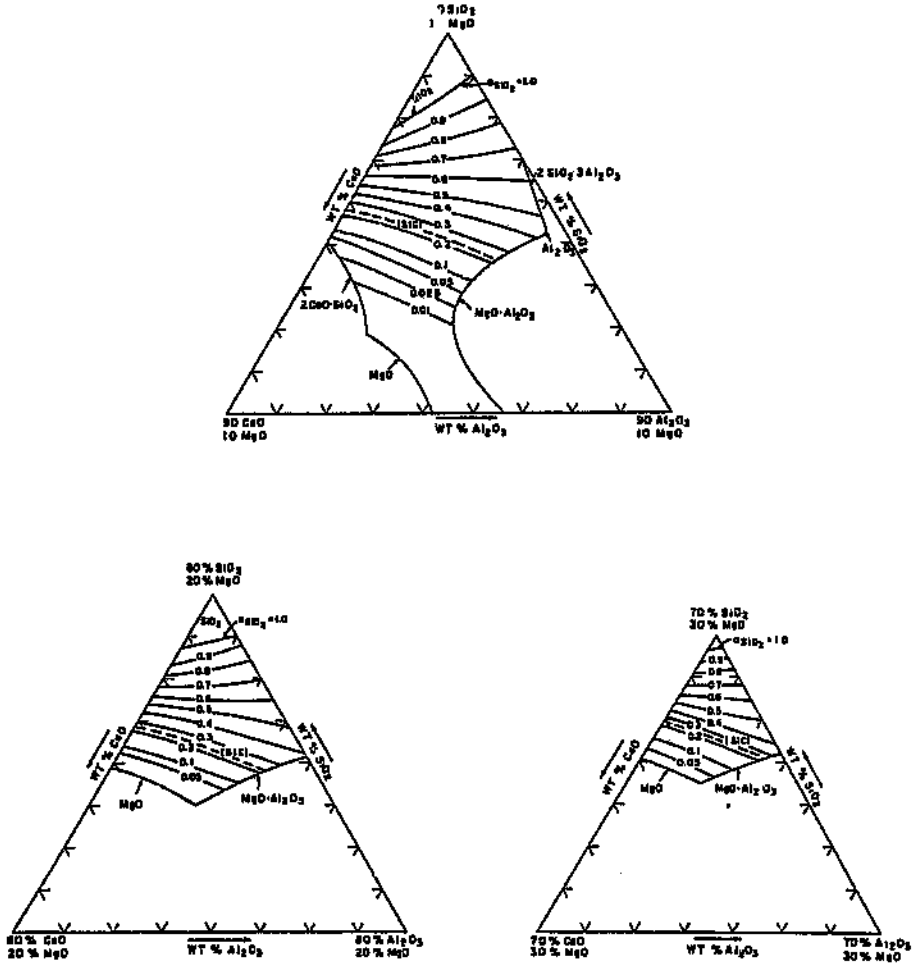


Figure 2.39. Activity of SiO_2 in SiO_2-CaO-MgO-Al_2O_3 slags at 1600°C, 10%, 20%, and 30% of MgO. After Rein and Chipman [96]

3. EXPERIMENTAL PROCEDURE

3.1. EXPERIMENTAL SET-UP

All experiments were conducted in a molybdenum wound resistance furnace. The molybdenum heating element was protected by cracked ammonia gas. The ancillary equipment included facilities for temperature measurement and control, gas purification and partial-pressure control.

3.1.1. Furnace Assembly

A gas-tight vertical molybdenum wound resistance furnace heated electrically was assembled and employed for the equilibrium experiments. Figure 3.1. and 3.2. show the reaction furnace and the complete set-up used for the experimentation. Although the figures are self-explanatory, it is worth commenting further on the construction and operating characteristics of the experimental system.

The steel-made furnace shell of 460mm in both length and diameter is water-cooled at the top and bottom. A re-crystallized alumina tube with 50mm inner diameter, 60mm outside diameter and 1000mm length was used as the work (reaction) tube. The work tube was water-cooled at both ends with brass plates and tubing. Bostik silicon seal was used as a sealant for the body of the furnace. The work tube was fitted to the steel shell at the top and bottom with two compressed O-rings, which ensured gas-tight conditions. The top edge of the furnace was also additionally water-cooled with tubing in order to prevent the burning of silicon sealant due to the high temperature involved. An

extension bellow was connected at the top of the furnace which allowed to release the stress produced by the thermal expansion of the work tube.

Another alumina (heating) tube of 500mm in length, 80mm in inner diameter was assembled around the work tube within the shell of the furnace. The molybdenum wire was wound onto the heating tube and was protected from oxidation by a reducing atmosphere provided by anhydrous ammonia which decompose into hydrogen and nitrogen at temperature above 700°C. The decomposition of anhydrous ammonia at higher temperatures (1500-1600°C) yields enough hydrogen to keep the oxygen potential below the equilibrium level needed for MoO formation.

The anhydrous ammonia gas was introduced from the bottom end of the furnace though the ammonia inlet and, after passing through the furnace shell, was vented to the fume hood through the ammonia outlet at the top of the furnace shell. Similarly, the gas or gas mixture with which the work tube was continuously purged during operation was introduced from the bottom end of the work tube through the gas inlet which is on the bottom brass plate and, after passing through the reaction tube, was vented to the fume hood through the gas outlet which is on the top brass plate. For this reason and also to avoid thermal shocks, the furnace was kept at 900°C and above when not in use.

The molybdenum wire was covered by alumina cement for protection and embedded in a pool of spherical alumina bubbles (diameters in the range of 1mm to 3mm) which served as thermal insulators. All this assembly, including the alumina bubbles was placed in a tabular alumina tube of 230mm inner diameter. The space between the steel shell and the tabular alumina tube was filled with insulating wool. Two electrically insulated gas-tight terminals connected the windings to the electrical power cables at the bottom of furnace shell.

A special winding technique was used to obtain the desired temperature, and temperature profile, which provided a 20mm hot zone inside the work tube with ±1°C at

1600°C. Approximately 16 meters of molybdenum resistance wire, 0.9mm in diameter, were used for the winding. The overall resistance was 0.65 to 0.7 ohm at room temperature. The normal current in the circuit was about 17 amperes when the furnace was operating at 1500°C. The same winding technique was used for the experiments at 1580°C. When the molybdenum wire is longer(the resistance higher than 0.9 ohm at room temperature), the temperature in the hot zone could not reach 1500°C even with a maximum current of the furnace.

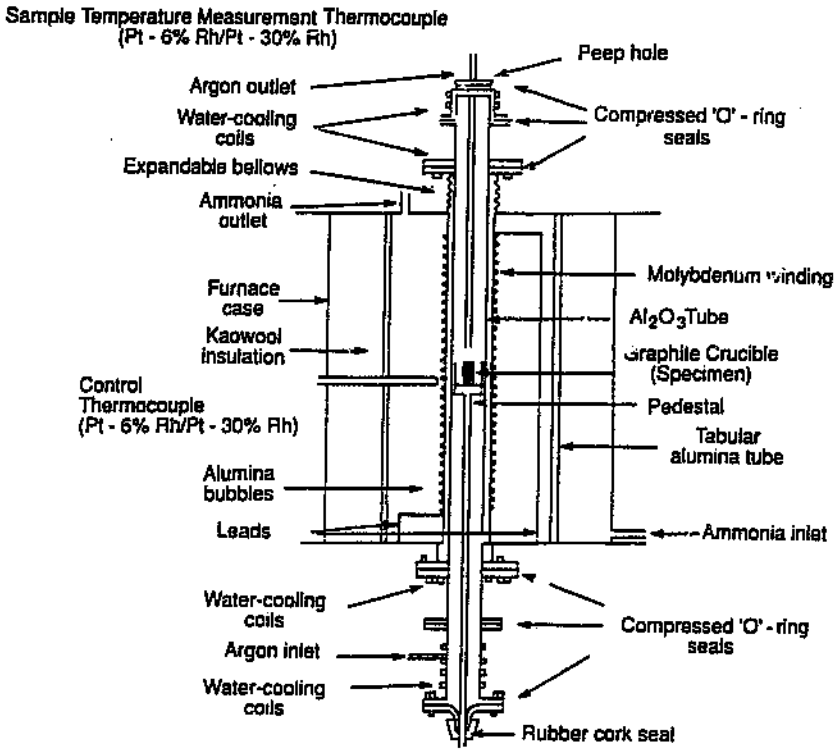


Figure 3.1. A cross-section of the vertical molybdenum wound resistance furnace.

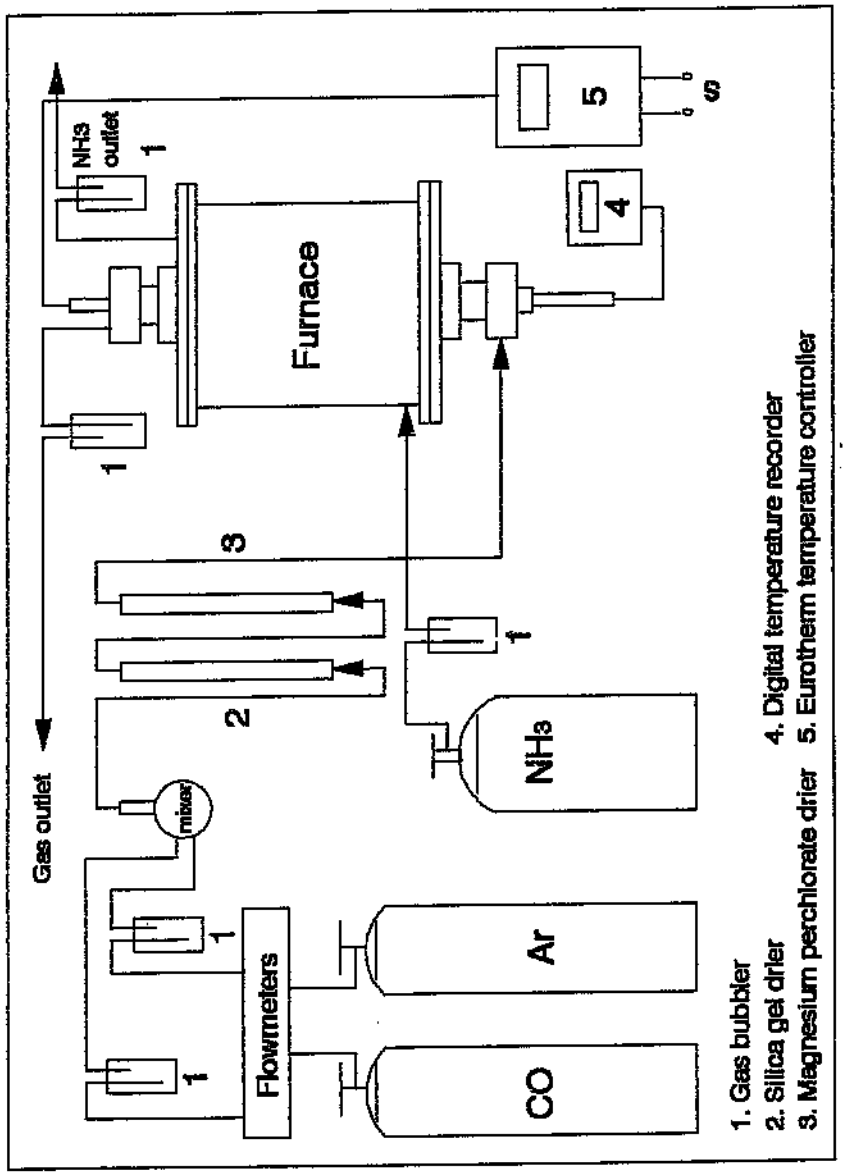


Figure 3.2. The entire experimental set-up.

3.1.2. Control of Partial Pressure of Carbon Monoxide

The ancillary equipment for control of partial pressure of carbon monoxide gas involved gas purification, measurement of gas flow rates, and mixing of Ar and CO gases.

All gases, before mixing, passed over drying columns of silica gel, anhydrous magnesium perchlorate and ascarid. For all experiments, the total pressure in the system was equal to the ambient pressure, which is 0.83atm in Johannesburg. Two tri-flat flow meters were used to measure the flow rates of argon and carbon monoxide. The tri-flat flow meter consists of a tapered glass tube with axis vertical and smaller end at the bottom. Inside the tube is a spherical float of a diameter such that it fits the diameter of the tube at the bottom, but it free to move vertically. At any flow rate within the range of the meter, gas entering the bottom of the tube raises the float, increasing the area between the float and tube until the upward hydraulic forces are balanced by the weight of the buoyed float.

Flowrate, therefore, is indicated by the position of the float on the graduated scale etched in the glass tube. The scales can be supplied by factory, calibrated to read directly in terms of flowrate for a given fluid under stated operating conditions. Under common circumstances, however, the scales on the tube do not indicate flowrate directly, but readings can be converted to flowrate for a variety of fluids, such as CO and Ar gases, by methods of conversion equations. With a given size of meter and float material, the calibration is calculated using the following practical equations:

$$N = A[(P_f - P_{opt})P_{opt}]^{1/2}(V_{opt})^{-1} \qquad (3.1)$$

$$W = CB[(P_f - P_{opt})P_{opt}]^{1/2} \qquad (3.2)$$

where:

N, viscous influence number;

A, size factor (from Table 7)[99];

P_f, float density, g/cc;

P_{opt}, gas density at Operating Temperature, g/cc;

V_{opt}, fluid viscosity at Operating Temperature, centipoise;

W, flowrate at OPT, g/min;

C, flow coefficient;

B, size factor (from Table 7)[99];

Using these equations with the appropriate Float Characteristic Curve, the flowrate via the Tri-flat meter for the given gas at the operating temperature (OPT), and the operating pressure (OPP), can be calculated.

Although the flow rates of the Ar and CO gases can be calculated, they are not accurate enough because of several reasons, such as the inaccurate data, reading from the figures in the handbook[99] at low flowrate, the contamination of the meters, and the wear inside the meters, etc. It is necessary to make sure what are the actual flow rates of Ar and CO via the meters. A 50ml Bunson Tower was used to calibrate the two flowmeters. The results can be seen in figure 3.

Partial pressure of carbon monoxide in (CO + Ar) gases at total pressure of 0.83 atm (the ambient atmosphere in Johannesburg), can be calculated:

$$Pco/0.83 = \text{Flowrate(CO)}/[\text{flowrate(CO + Ar)}] \qquad (3.3)$$

When CO flowrate takes 5, 6, 3, 2, 1 and Ar flowrate takes 0, 3.38, 5.04, 4.78, 5.18 respectively (cc/min), the Pco is 0.83, 0.498, 0.121, 0.059, 0.046 atm. respectively. When Pco is very low, such as, 0.02 and 0.01 atm, the CO flowrate must be maintained at the level as low as possible. The results can seen in table 3.1.

It is essential to calibrate the flowrates of both CO and Ar gasses at the certain scale readings frequently, to have accurate control of Pco.

Table 3.1. Pco Control by Ar and CO Flowrates

CO Scale Readings	CO Flowrate cc/s	Ar S[illegible] Rea[illegible]s	Ar Flowrate cc/s	Pco atm.
5.0	0.4145	0.00	0.0000	0.830
6.0	0.6471	3.38	0.4359	0.498
3.0	0.1478	5.04	0.8667	0.121
3.0	0.1478	5.18	0.9336	0.113
2.0	0.0649	4.78	0.8501	0.059
2.0	0.0649	5.00	0.8665	0.058
1.0	0.0543	5.18	0.9336	0.046
1.0	0.0543	5.53	1.0684	0.040
1.0	0.0543	6.00	1.2241	0.035
1.0	0.0543	7.00	1.6392	0.032
1.0	0.0543	9.00	2.5742	0.017
1.0	0.0543	10.00	3.0408	0.015
1.0	0.0543	11.00	3.5630	0.012
1.0	0.0543	13.00	4.6512	0.010

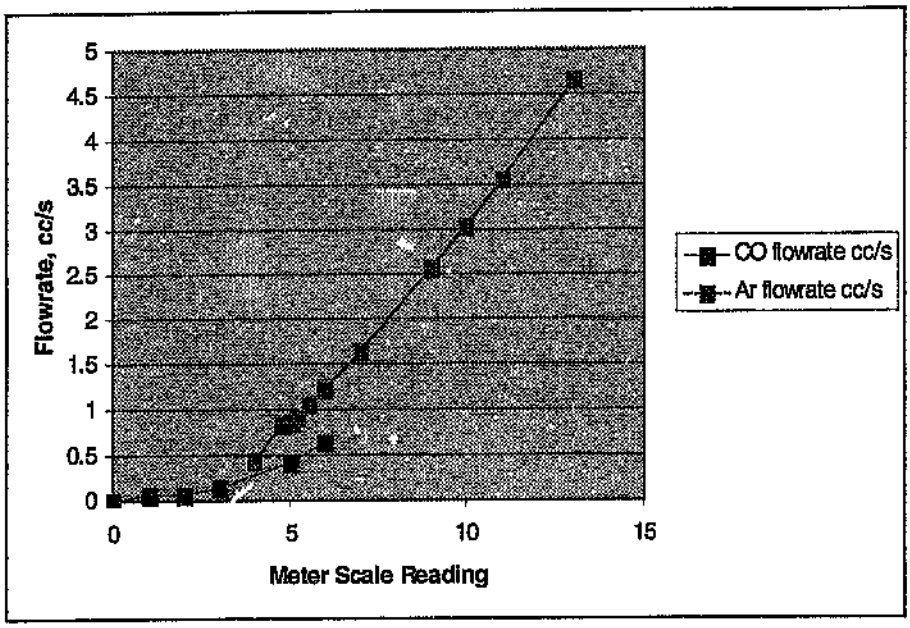


Figure 3.3. Flow rate of argon and carbon monoxide via tri-flat flowmeter, calibrated by Bunson Tower.

The specifications of all gases used in the experiments, namely carbon monoxide, argon, nitrogen, are listed in table 3.2.

Table 3.2. Specifications of gases

Gas	Grade	Impurities	Suppler
CO	Chemically pure CO > 99.959%	O_2 < 10 ppm H_2O < 5 ppm N_2 < 70 ppm CO_2 < 20 ppm CH_4 < 100 ppm H_2 <300 ppm Ar < 3 ppm	AFROX
Ar	HP Ar > 99.998%	H_2O < 3 ppm O_2 < 3 ppm H_2 <15 ppm total <20 ppm	AFROX
N_2	N_2 > 99.995%	H_2O < 3 ppm O_2 < 3 ppm hydrocarbons <1ppm	AFROX

3.1.3. Temperature Control and Temperature Profile

Actual hot zone temperature in the furnace was measured with a Pt-6%Rh/Pt-30%Rh(B-type) thermocouple, which was calibrated against a standard thermocouple of the same type. The standard thermocouple was calibrated according to the melting point of silver and gold. The temperature of the system was checked every run by lowering the thermocouple from the 1200°C zone to the hot zone. This was done because the thermocouple held at 1500/1580°C for prolonged period, failed due to excessive temperature. The power unit of the furnace was a type 0703 25 A, 220 V, Eurotherm

thyristor power pack which was connected to the furnace with a B-type thermocouple placed adjacent to the middle of the external surface of the heating winding. The unit was set according to the actual temperature readings registered by the previously mentioned thermocouple.

The temperature profiles at 1550 °C and 1600 °C can be seen in figure 3.4. At 1600 °C, there is a 2 cm space inside the furnace with the temperature change of ±1 °C, which can be used as constant temperature area, as called Hot Zone. All metal and slag inside a crucible must be put precisely within the hot zone, in order to maintain experimental temperature accurately. When the temperature in the hot zone is less than 1600 °C, the length of hot zone increases. It is worth noting that the temperature distribution inside the furnace must be re-measured every time when the furnace has to be adjusted, such as change of the heating element, and replace of the alumina-working tube, etc.

3.1.4. Preparation of synthetic Al_2O_3-CaO-Cr_2O_3-Fe_2O_3-MgO-SiO_2-S Slags

The slag samples for experiments were prepared as a homogeneous mixture made from pre-melted master slags. All oxides, namely Al_2O_3, CaO, Cr_2O_3, Fe_2O_3, MgO, SiO_2, and S are chemically pure, supplied by SAARCHEM. Individual oxides, kept in a vacuum desiccator, were added to master slags according to the different needs of experiments. Four master slags were pre-melted in graphite crucibles and crashed in an agate mortar after cooling. The compositions of the master slags are listed in table 3.3. The oxides used in the preparation of master slags, namely, Al_2O_3, CaO, MgO and SiO_2 were also chemically pure grades.

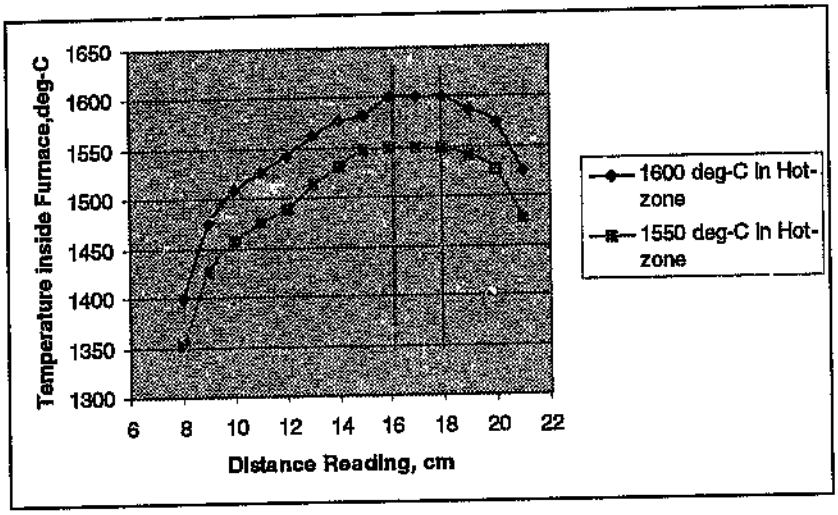


Figure 3.4. Temperature profile inside furnace at 1550°C and 1600°C.

Table 3.3. The compositions of master slags by mass%

Number	Al_2O_3	CaO	MgO	SiO_2
MS1	37.00	2.00	27.00	34.00
MS2	20.00	2.00	36.00	42.00
MS3	25.00	5.00	18.00	52.00
MS4	15.00	5.00	15.00	65.00

3.1.5. Preparation of Cr-Fe-C-Si-S Alloys

The metal charges were prepared by using chemically pure powder of chromium, silicon, sulphur and extra pure iron. Nineteen alloys in three groups were used in different experiments. Their compositions are shown in table 3.4, 3.5, and 3.6. The former two groups of metals were used for the investigation pertinent to ferro-chromium refining. The third group of alloys were used for the study related to stainless-steel making.

Table 3.4. Composition of group-1 alloys by mass%

No.	Cr	C	Si	S	Fe
M1-1	65.00	15.00	5.00	0.50	14.50
M1-2	65.00	10.00	3.00	0.50	21.50
M1-3	65.00	12.00	3.00	0.50	19.50
M1-4	65.00	8.00	2.00	0.50	24.50
M1-5	65.00	5.00	2.00	0.50	27.50
M1-6	65.00	3.00	2.00	0.50	29.50

Table 3.5. Composition of group-2 alloys by mass%

No.	Cr	C	Si	S	Fe
M2-1	65.00	15.00	1.00	0.20	18.80
M2-2	65.00	10.00	1.00	0.20	23.80
M2-3	65.00	12.00	1.00	0.20	21.80
M2-4	65.00	8.00	1.00	0.20	25.80
M2-5	65.00	5.00	1.00	0.20	28.80
M2-6	65.00	3.00	1.00	0.20	30.80

Table 3.6. Composition of group-3 alloys by mass%

No.	Cr	C	Si	S	Fe
M3-1	20.00	2.50	0.00	0.10	77.40
M3-2	20.00	2.00	0.00	0.10	77.90
M3-3	20.00	1.50	0.00	0.10	78.40
M3-4	20.00	1.00	0.00	0.10	78.90
M3-5	20.00	0.50	0.00	0.10	79.40
M3-6	20.00	0.20	0.00	0.10	79.70
M3-7	20.00	0.10	0.00	0.10	79.80

3.2. PREPARATION OF CHROMITE AND CHROMIUM OXIDE CRUCIBLES

According to the technique and procedure used by T.R. Curr[100] and O. Demir[41], chromite crucibles and chromium oxide(Cr_2O_3) crucibles were manufactured, considering the factors like binder, sintering-temperature, sintering-time, sintering-atmosphere, and even the heating-temperature after sintering and drilling. The procedure is listed as the following:

1. Making chromite cylinders and Cr-oxide cylinders by pressing chromite powder and Cr oxide powder respectively, mixed with 3% of 25%-sodium silicate solution or 3% of water with a 2-ton hydraulic press using a special tool steel mold;

2. Sintering/heating in air, N_2 or CO gas at 1200-1520°C;

3. Drilling a hole into cylinder, finished with a bottom of 5 mm thickness.

The details of crucible fabrication are highlighted in table 3.7. Chromite used was from the Bushveld LG-6, and Cr-oxide was chemically pure Cr_2O_3 powder supplied by SAARCHEM. Cr-oxide crucibles were proved to be strong enough to hold slag and metal for the studies of gas-slag-metal equilibrium. Sintering atmosphere does not make apparently different to make hard and strong cylinders. Sintering temperature plays a great role to make cylinders hard. It is better to heat cylinder to 1200°C first to get the cylinder easily drilled and then reheat to 1420°C or 1520°C to make the crucibles drilled from the cylinder harder and stronger.

Table 3.7. Fabrication parameters of chromite and chromium oxide crucibles

No.	Binder 3% by mass	Sintering Temp °C	sintering time, h	Sintering-atmosph-ere	Sinter-temp °C after drilling
001	25%NaSi	1200	15	air	
002	water	1200	15	air	
003	water	1420	6	air	
004	water	1520	15	CO	
005	water	1520	24	air	
006	25%NaSi	1200	6	air	1520
007	water	1200	6	N_2	1520

3.3 EXPERIMENTAL PROCEDURE

Four groups of experiments have been conducted to investigate the gas-slag-metal equilibria related to the refining of ferro-chromium and the making of stainless steel. The four groups are:

1. gas-metal equilibrium in alumina crucible;
2. gas-slag-metal equilibrium in Cr-oxide crucible under CO atmosphere;
3. gas-slag-metal equilibrium in silica crucible;
4. gas-slag-metal equilibrium in silica crucible for stainless-steel making.

Group 1 to group 3 are relevant to ferro-chromium refining and group 4 pertinent to stainless-steel making.

3.3.1 Gas-Metal Equilibrium in Alumina Crucible

All materials used in the experiments were of chemically pure grade. The metals used were in powder form. The experiments started with the alloys containing 65%Cr, 0-5%Si, 0.01 and 0.1%S and Fe as the balance, as listed in table 3.8. Alumina crucible of 40 mm in height; 25 mm in inner diameter and 28 mm in outer diameter was charged with metal powder and was located in the 20 mm hot zone of the molybdenum wound resistance furnace at 1500 °C. Equilibration was conducted at different partial pressures of carbon monoxide, which made the alloys pick up carbon by reaction with the gas phase. The crushed alloys were sent to MINTEK for chemical analysis. The equilibration time was determined experimentally as 20 hours (see Section of equilibration for the details).

TABLE 3.8. Starting Composition of Metal by mass%

No.	Cr	Si	S	Fe
M1	65.00	0.00	0.10	34.90
M2	65.00	0.50	0.10	34.40
M3	65.00	1.00	0.10	33.90
M4	65.00	2.00	0.10	32.90
M5	65.00	5.00	0.10	29.90
M6	65.00	0.00	0.01	34.99
M7	65.00	0.50	0.01	34.49
M8	65.00	1.00	0.01	33.99
M9	65.00	2.00	0.01	32.99
M10	65.00	5.00	0.01	29.99

3.3.2. Gas-Slag-Metal Equilibrium in Cr-oxide/Alumina crucibles

Experiments started with 2-3g of metal, 3-5g of slag in pure Cr_2O_3 crucibles of 18mm in height; 25mm in inner diameter; and 30mm in outer diameter. Different amount of Cr_2O_3 was added into master slags. Three master slags and group-1 and group-2 of metals were used for the experiments in Cr-oxide crucibles.

About 50 per cent of experiments failed due to the cracking of the crucibles. In order to prevent the crucibles from cracking by thermal shock, very slow speed of locating the crucible from temperatures below 200°C to the hot zone, taking 20 minutes, 30 minutes, even 60 minutes was employed. But it did not release the cracking problem.

Alumina cement was dressed thickly outside a Cr-oxide crucible to form a strong cement crucible outside in order to increase the strength of the Cr-oxide crucible. An alumina crucible, or a zirconia crucible, or a molybdenum crucible were placed outside a Cr-oxide crucible, filling the space between two crucibles with Cr_2O_3 powder. The cracking still frequently happened because the space between Cr-oxide crucible and the outside crucible increased during the experiments, which seems that Cr-oxide crucible increases volume fairly little at the elevated temperature.

Molybdenum wire of 0.7mm in diameter was used to make a net fitted outside a Cr-oxide crucible as tight as possible (the net will break the crucible if fitted too tight). Since the molybdenum net was used to support the Cr-oxide crucible, the cracking was finally under control. Silica crucibles of the same size as Cr-oxide crucible were used to conduct experiments at lower partial pressure of carbon monoxide in ferro-chromium system and in stainless-steel system.

The charged crucible with metal and slag was located to the hot zone slowly, and then was quenched by being dropped into water after being held for the period of 13 hours

determined experimentally as the equilibration time. The distinctive metal phase and slag phase were separated very carefully, cleaned when necessary, crushed, and sent to MINTEK for chemical analysis.

3.3.3 Determination of Equilibration Time

The term of equilibrium refers to a state, in which all reactions reach to an end and no change will take place at all. In the studies on gas-slag-metal system, the term means multi-phase chemical equilibrium, in which all chemical reactions remain constant in the system, including (CO/Ar)gas phase, slag phase, metal phase and crucible phase. No change in compositions of all phases will occur and system becomes independent of time. As far as the experimental work is concerned, the equilibration time, which is the minimum time used to acquire the equilibrium for the system is very important. It is, unfortunately, not as clear as its definition. It is actually varied dependent on different investigators from few hours to more than 20 hours, according to the size of crucible, amount of slag/metal, temperature, etc.

Equilibration time was determined by two series of experiments for gas-metal equilibrium in alumina crucibles and for gas-slag-metal equilibrium in Cr-oxide crucibles.

In gas-metal equilibrium, experimental runs started with 3g metal of same composition at 1500°C at 0.05atm of partial pressure of carbon monoxide. After certain period of time, samples cooled by quenching into water and prepared for chemical analysis. Only carbon content of the alloys was analyzed because the carbon content only can come from gas phase which is a mixture of argon and carbon monoxide. The experimental time ranged from 2 hours to 72 hour. Figure 3.5 shows that carbon content of the metal phase increases very quickly until 8 to 10 hours and after 20 hours the carbon content hardly changes with experimental time, up to 72 hours. Therefore, 20 hours was determined for

the equilibration time for the gas-metal studies. The same size of crucibles and same amount of metals were used for the subsequent experiments. Under the circumstances of those experiments with partial pressure of carbon monoxide higher than 0.05atm, the equilibration time of 20 hours was still used even though a shorter time could be used for those experiments, due to the easiness and quickness of picking carbon from the gas phase with higher carbon potential.

In gas-slag-metal equilibrium, experiments were run with 3g of metal and 4g of slag in Cr-oxide crucibles at 1500°C under carbon monoxide atmosphere. The sample was cooled by being quenched into water, after being kept for certain experimental time, ranging from 2 hours to 15 hours. The equilibration time was determined in terms of the changes of all components of slag, namely Al_2O_3, CaO, Cr_2O_3, Fe_2O_3, MgO, S, and SiO_2. The results are shown in figure 3.6, and it was established that a minimum of 13 hours was necessary.

Related experimental measurements were conducted by Fulton and Chipman[106] in their study on the reduction of silicon from blast furnace-type slags by carbon saturated iron-carbon alloys at temperatures of 1425 to 1700°C, for slags containing up to 20% Al_2O_3. The experiments were carried out under CO atmosphere. At 1600°C under the conditions of rapid stirring, the approach to equilibrium required more than eight hours.

In a study similar to present equilibrium system by Akyuzlu and Eric[38], The equilibration time was determined by a series of metal-slag equilibria experiments in graphite crucible charged with about 4 grams of metal and 4 grams of slag, which were carried out by varying the time from 3 to 14 hours while keeping initial compositions the same. The approach to equilibrium was established by analysing the silicon dissolved in the metal as a parameter. Both the reduction and the oxidation of the silicon was investigated, even though it was stated that silicon oxidation is four times faster than silica reduction at 1525°C. The oxidation behaviour was studied at low silica contents of slags. It was found that a minimum of 10 hours was necessary.

3.3.4. Chemical Analyses

The analytical work was done at MINTEK's analytical laboratories. The carbon of the metal was analyzed by means of a Leco analyzer, the other constituents of the metal by the I.C.P. method. The basic constituents of the slag were analyzed by means of the X-ray fusion method, its Fe and Cr contents by means of the O-phenanthroline colorimetric and F-diphenylcarbazide colorimetric methods respectively.

In addition, some X-ray diffraction analyses and metallographic examination of the slag samples and crucible samples were carried out, in order to detect metal in slag and detect the interface of slag and crucible. No metal particles were found inside the quenched slag phase. The study on the interaction between slag phase and Cr-oxide crucible is conducted and can be found in the following part.

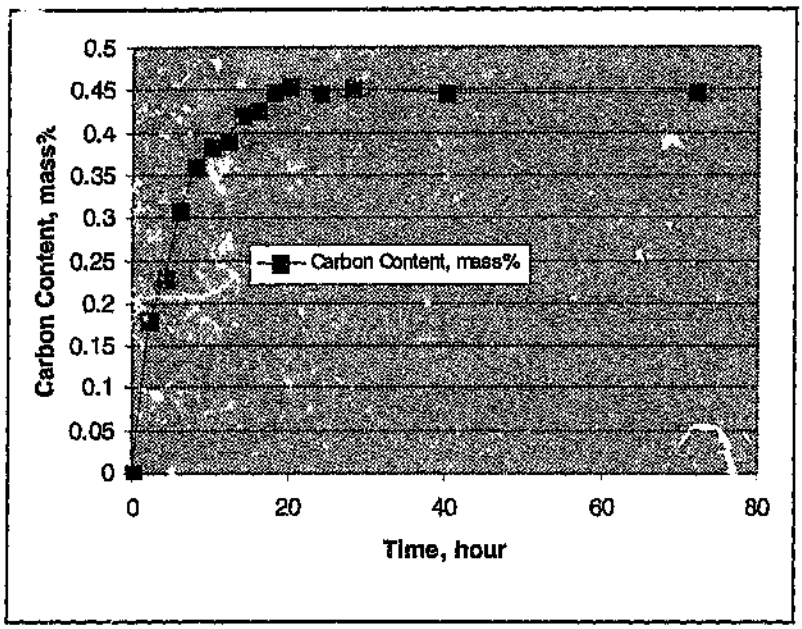


Figure 3.5. Determination of gas-metal equilibration time at 1500°C, 0.05atm Pco with metal of 60-64%Cr, 32-34%Fe, 0.8-1.3%Si and 0.1%S.

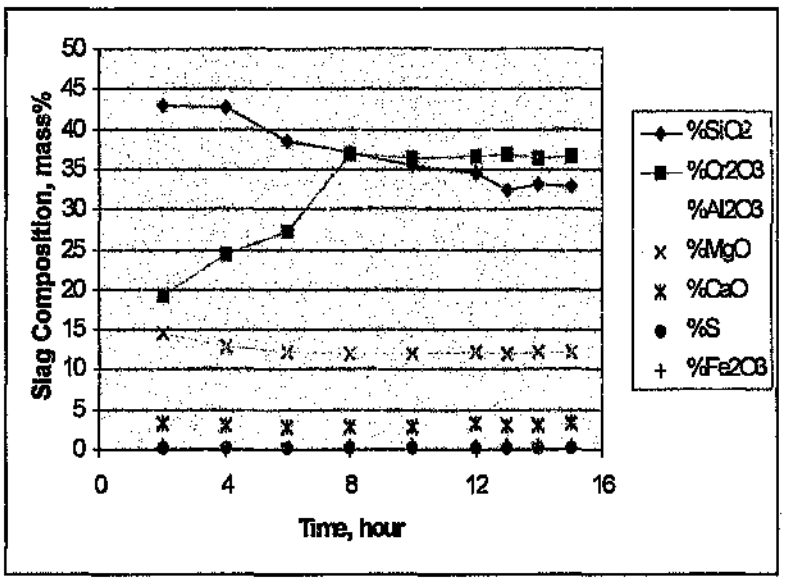


Figure 3.6. Determination of gas-slag-metal equilibration time at 1500°C under CO atmosphere.

4. RESULTS AND DISCUSSIONS

Results of the experimental work with relevant discussions are gathered in four subsections of this chapter:

1. Equilibrium relationships between C, Si and Pco in the gas-metal system;
2. Equilibrium distribution of silicon in the slag-metal system;
3. Equilibrium distribution of sulphur in the slag-metal system;
4. Equilibrium distribution of chromium in the slag-metal system;

Each section contains the results related to both ferrochromium alloys and stainless steel (which contains about 15 to 25 per cent of chromium by mass). Samples from 168 experiments were chemically analyzed at MINTEK. Among them, 51 metal samples were from gas-metal equilibrium experiments and 234 samples of slag and metal were from 117 successful gas-slag-metal experiments in which about 50 experiments were from those conducted in Cr-oxide crucibles.

It is worth mentioning some of the problems and difficulties occurred in the experimental work. The major problems come from the choice of crucible materials and the highly frequent breakdown of experimental furnace. The cracking of the Cr-oxide crucibles was the biggest difficulty in the experiments. In addition, the behaviour of the Cr-oxide crucibles is necessary to explain the major reasons that these crucibles can be employed for the investigation.

Problems and Difficulties

The crucible material is the first major problem to be handled in the present investigation. The crucible materials must be very stable so that no reaction takes place with the slag phase and metal phase or the reactions with the crucible materials must be much slower than the reactions between slag and metal so that the reactions with crucible can be ignored. On the laboratory scale, very little work has been done in the domains of gas-slag-metal equilibrium without carbon saturation in the metal phase, primarily because of the problems confronted in attempting to contain liquid slags and metals in laboratory crucibles at the experimental temperatures. Since graphite is an ideal crucible material for the slag-metal experimental studies, most investigations have been carried out under carbon saturation. For studies where CaO-SiO_2-MgO-Al_2O_3-FeO_x-CrO_y slags are used, CaO crucibles, silica crucibles, MgO crucibles and alumina crucibles can be used on slag-metal equilibrium by saturation of the slag phase with the corresponding oxide of the crucible. In the present investigation, chromium oxide (Cr_2O_3) is used to manufacture crucibles and they have been utilised for the gas-slag-metal equilibrium studies pertinent to ferrochromium refining and stainless-steel making. However, they were prior to cracking.

In order to prevent the crucibles from cracking by thermal shock, very slow speed of locating the crucible from temperatures below 200°C to the hot zone, taking up to 60 minutes, was used. Furthermore, the crucibles were pre-heated to 1400°C in a electrically heated muffle furnace before they were very slowly put into the Mo-resistance experimental furnace, which improved no difference. Alumina cement was dressed thickly outside a Cr-oxide crucible to form a strong cement crucible outside in order to increase the strength of the Cr-oxide crucible. An alumina crucible, or a zirconia crucible, or a molybdenum crucible was placed outside a Cr-oxide crucible,

filling the space between two crucibles with Cr_2O_3 powder, pre-heated to 1400°C in the muffle furnace for the same purpose. The cracking still frequently happened until molybdenum wire of 0.7mm in diameter was used to make a net fitted outside a Cr-oxide crucible.

The behaviour of Cr-oxide crucibles in the gas-slag-metal system

The behaviour of the Cr-oxide crucibles can be used to explain the major reasons that the molten slags and liquid metals can be held in the Cr-oxide crucibles for the period of time long enough for the equilibrium experiments. In the investigation of the behaviour of the Cr-oxide crucibles, chemical analysis, microscope, scanning-electro-microscope (SEM) with EDAX and X-ray diffraction are utilised.

A layer is found on the inner wall of the crucibles, which appears brighter and denser than the matrix of the crucibles. By the use of scanning-electro-microscope with EDAX, the composition in the middle and on the internal and external sides of the layer is measured and illustrated in table 4.1.

Table 4.1. Composition of the layer on the inner wall of Cr-oxide crucible by SEM-EDAX by mass percentage

Position	Cr_2O_3	Fe_2O_3	Al_2O_3	CaO	MgO	SiO_2
inside	92.96	1.05	2.62	0.15	2.43	0.79
middle	93.26	1.17	2.38	0.19	2.40	0.60
outside	93.18	0.95	2.29	0.26	2.62	0.70

A very high homogeneity of the composition is displayed inside the layer. X-ray diffraction analysis was taken on the layer and on the inner wall of the crucible above slag phase. The major oxide inside the layer and inside the wall is Cr_2O_3. Very little o. $MgAlCrO_4$, $MgCa_{1.5}Cr_{0.5}O_4$, and $(Cr,Fe)_2O_3$ exists in the layer. Chemical analysis has also been made and the chemical composition is listed in table 4.2. The contents of SiO_2, CaO and Fe_2O_3 are very low, not more than 1 per cent by mass. The major constituents of the layer are Al_2O_3, MgO and Cr oxides analysed in terms of Cr_2O_3. They are 5.87, 7.61 and 84.57 per cent respectively.

Table 4.2. Composition of the layer on the inner wall of Cr-oxide crucible by chemical analysis by mass percentage.

Cr_2O_3	Fe_2O_3	Al_2O_3	CaO	MgO	SiO_2
84.57	0.82	5.87	0.37	7.61	0.76

The composition obtained by chemical analysis and scanning-electro-microscope(SEM) with EDAX is quite consistent, besides the fact that the results from SEM-EDAX elucidates a higher content of chromium in the layer of the Cr-oxide crucibles. The reason may be the Cr contamination (from the bulk of the crucible) of the surface of the layer during grinding and polishing of the specimen. By analysis of the Cr_2O_3-MgO-Al_2O_3 ternary diagram, seen in figure 4.1, the liquidus temperature of the layer increases from about 2047°C of the melting temperature of the pure Cr_2O_3 to about 2070 °C with increase of MgO from 0 to 7.61 and Al_2O_3 from 0 to 5.87 with a ratio of MgO to Al_2O_3 7.61/5.87, as illustrated by the straight line in figure 4.1.

The layer, formed by the reactions between Cr-oxide crucible and slag, may play an important role in holding the slag and metal stable for the experimental investigation of the gas-slag-metal equilibrium. The Cr-oxide crucibles and the crucibles with the Mo-wire net are pictured and can be seen in figure 4.2. Figure 4.3 shows the metal and the slag diverged from the Cr-oxide crucibles after the equilibrium experiments.

About 200 experiments have been conducted. 170 successful ones were selected for chemical analysis at MINTEK. The failure of the unsuccessful experiments was mainly due to the cracking of Cr-oxide crucibles. In a few occasions, it was due to the inadequate amount of slag remained in the crucible for analysis. The analysis results are shown in Tables 4.3 to 4.11.

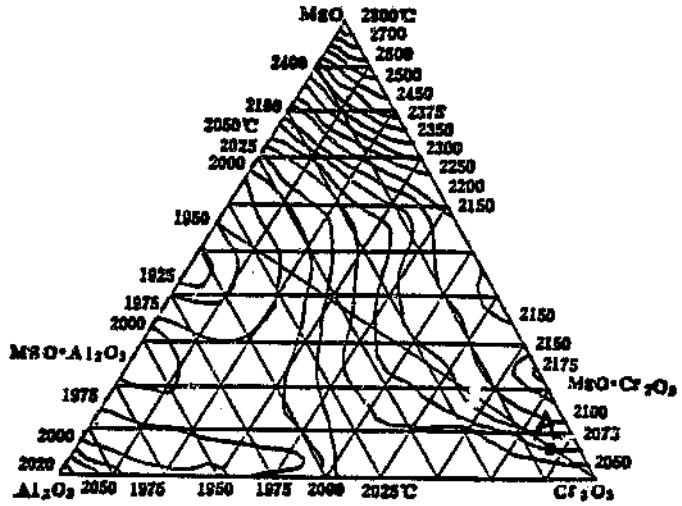


Figure 4.1. MgO-Al_2O_3-Cr_2O_3 ternary phase diagram with liquidus temperature

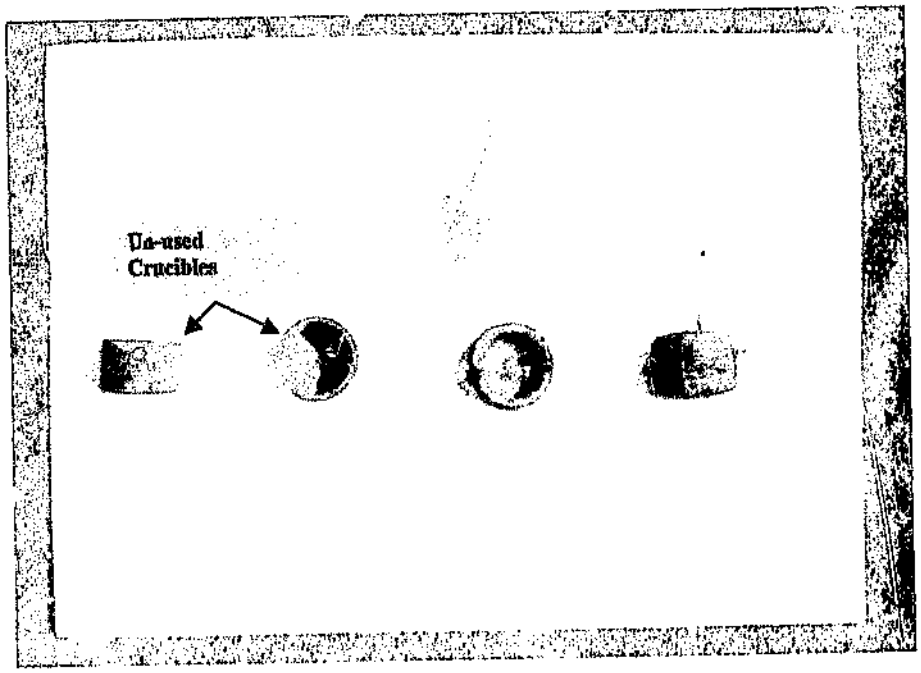


Figure 4.2. Cr-oxide crucibles and the crucibles with Mo-wire net before and after equilibrium experiment. Two crucibles on the lift side of the photograph are unused.

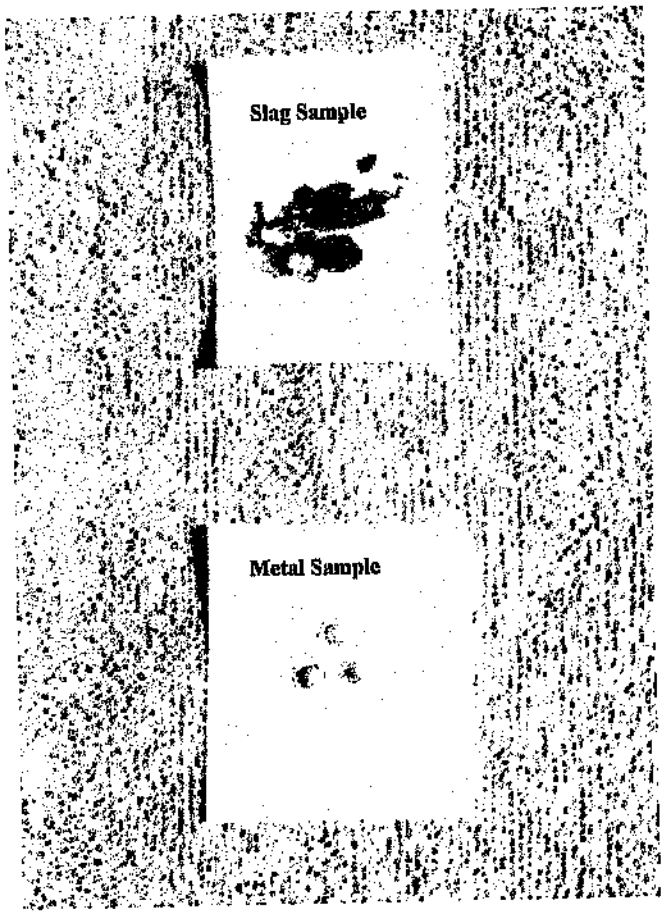


Figure 4.3. Metal sample and slag sample diverged from Cr-oxide crucibles.

Table 4.3. Composition of metal phase from Gas-metal equilibrium at 1500°C in mass%.

No.	%Cr	%Fe	%Si	%S	%C	Pco atm
39-1	58.27	38.80	0.23	0.10	2.60	0.83
39-2	58.80	39.00	0.52	0.10	1.58	0.50
39-3	62.22	35.40	0.73	0.10	1.55	0.10
39-4	61.45	36.40	0.68	0.10	1.37	0.10
39-5	63.76	34.00	0.81	0.10	1.33	0.05
39-6	51.43	38.60	1.07	0.10	0.80	0.01
39-7	60.58	37.60	0.97	0.10	0.75	0.01
39-8	65.56	32.80	0.87	0.10	0.67	0.01
39-9	65.00	33.90	1.00	0.10	0.00	0.00
42-1	65.40	35.20	1.06	0.10	0.64	0.01
42-2	62.60	32.70	0.93	0.01	0.45	0.01
42-3	64.60	32.90	0.98	0.01	0.44	0.01
42-4	66.10	30.70	0.90	0.01	0.36	0.01
42-5	58.50	34.50	0.85	0.01	0.36	0.01
42-6	59.00	34.80	0.82	0.01	0.29	0.01
42-7	53.20	44.90	0.09	0.01	0.10	0.01
42-8	70.20	25.50	0.79	0.01	0.36	0.01
42-9	94.00	2.72	1.31	0.01	0.21	0.01
42-10	40.60	57.20	0.4	0.01	0.13	0.01
42-11	40.40	56.30	0.39	0.01	0.84	0.01
42-12	62.50	35.60	0.29	0.01	1.17	0.83
42-13	60.90	34.80	0.38	0.01	2.39	0.10
42-14	62.20	35.30	0.30	0.01	1.31	0.01
42-15	67.60	31.90	0.30	0.01	0.78	0.05

Table 4.3. Composition of metal phase from Gas-metal equilibrium at 1500°C in mass% (continue).

No.	%Cr	%Fe	%Si	%S	%C	Pco atm
42-16	64.60	34.50	0.38	0.01	0.93	0.05
42-17	64.20	34.70	0.39	0.01	0.96	0.10
42-18	67.30	31.90	0.36	0.01	0.21	0.10
42-19	61.10	33.40	0.44	0.01	3.55	0.83
42-20	80.40	13.60	3.00	0.01	7.10	0.83
42-21	80.40	6.20	3.18	0.01	7.07	0.50
42-22	79.50	6.30	3.20	0.01	5.23	0.50
42-23	88.90	7.20	3.14	0.01	2.82	0.02
42-24	93.20	5.00	2.69	0.01	2.07	0.01
43-1	59.40	35.80	0.50	0.01	3.43	0.83
43-2	58.80	37.20	0.91	0.01	1.22	0.10
43-3	59.10	37.40	0.89	0.01	1.20	0.10
43-4	29.70	68.20	0.67	0.01	0.61	0.10
43-5	76.90	14.10	0.76	0.01	4.08	0.10
43-6	74.00	15.80	0.78	0.01	4.63	0.10
43-7	64.00	28.80	0.87	0.01	2.48	0.10
43-10	63.30	34.60	0.78	0.01	0.76	0.10
43-12	63.80	34.10	0.78	0.01	0.72	0.83
43-13	61.80	33.10	0.87	0.01	0.91	0.83
43-14	60.00	34.50	1.12	0.01	1.12	0.01
43-15	57.80	29.20	3.13	0.01	0.80	0.01
43-16	61.20	29.40	4.16	0.01	1.22	0.01
43-17	60.80	28.90	4.00	0.01	1.00	0.01
43-18	43.50	53.20	0.38	0.01	1.03	0.50
43-19	43.50	50.20	0.83	0.01	1.04	0.50

Table 4.4. Metal composition from gas-slag-metal equilibrium at 1500°C under CO atmosphere in Cr-oxide crucibles in mass%.

Number	%Cr	%Fe	%Si	%S	%C
48-1	52.80	41.80	0.33	0.03	3.17
48-2	52.70	41.90	0.31	0.03	3.18
48-3	49.40	48.40	0.51	0.18	2.12
48-4	41.90	58.10	0.37	0.11	1.68
48-5	27.50	70.30	0.27	0.10	0.68
48-11	58.90	37.40	0.34	0.11	3.78
48-12	23.30	74.60	1.01	0.11	3.77
48-13	45.20	51.83	0.37	0.11	2.50
49-1	44.20	53.30	0.32	0.13	2.12
49-2	46.90	47.70	0.24	0.14	1.92
49-3	55.30	37.60	0.20	0.10	2.11
49-4	19.70	76.80	0.20	0.23	0.42
49-5	42.30	48.50	0.26	0.14	0.32
49-6	55.40	37.90	0.20	0.07	2.09
49-11	64.10	28.00	0.22	0.29	3.93
49-12	56.00	32.80	0.20	0.28	1.15
49-13	56.70	36.00	0.20	0.24	0.79
49-14	40.10	58.00	0.26	0.30	1.83
49-15	57.90	30.50	0.60	0.16	3.99
49-16	49.15	33.00	0.20	0.23	0.42
49-17	56.70	42.45	0.20	0.23	0.42

Table 4.5. Metal composition from gas-slag-metal equilibrium at 1500°C under 0.05atm of Pco in Cr-oxide crucibles in mass%.

Number	%Cr	%Fe	%Si	%S	%C
52-1	50.90	34.40	0.37	0.04	3.84
52-2	66.90	26.60	0.45	0.05	2.57
52-3	60.20	28.10	0.67	0.11	2.19
52-4	57.20	35.20	0.26	0.01	5.22
52-5	50.10	44.20	0.28	0.13	3.21
52-6	51.50	40.20	0.53	0.13	5.15
52-9	54.20	36.80	0.20	0.04	3.81
52-11	50.50	38.70	0.21	0.06	4.62
52-12	23.56	75.42	1.02	0.10	5.82
52-13	49.10	46.40	0.28	0.04	3.27
52-14	32.27	61.62	0.29	0.04	5.78
52-15	48.40	46.50	0.27	0.04	3.29
52-17	42.30	52.82	0.27	0.04	4.57

Table 4.6. Metal composition from gas-slag-metal equilibrium under 0.034atm of Pco at 1580°C in silica crucibles in mass%.

Number	%Cr	%Fe	%Si	%S	%C
53-8	48.40	46.50	0.27	0.04	3.29
57-1	57.60	36.40	4.73	0.14	0.06
57-2	61.10	33.30	4.05	0.34	1.61
57-3	66.10	25.70	1.07	0.01	6.54
57-4	66.10	25.60	1.83	0.01	6.03
57-5	63.00	28.50	2.46	0.01	5.42
57-6	58.20	34.80	5.21	0.29	0.97
57-11	63.80	28.00	1.59	0.01	6.54
57-12	65.20	27.40	3.27	0.28	3.85
57-13	56.90	35.50	5.57	0.35	0.50
57-14	63.20	28.90	1.86	0.19	5.37
57-15	62.50	29.50	4.37	0.26	2.46
57-16	61.30	31.40	3.45	0.25	2.89
57-17	61.20	31.50	5.06	0.26	1.70
57-18	60.90	31.40	5.14	0.32	1.34

Table 4.6. Metal composition from gas-slag-metal equilibrium under 0.034atm of Pco at 1580°C in silica crucibles in mass% (continue).

Number	%Cr	%Fe	%Si	%S	%C
57-21	59.30	27.90	2.27	0.13	6.03
57-22	61.70	29.70	1.57	0.23	5.67
57-23	59.50	32.90	1.73	0.21	3.39
57-24	56.30	37.20	4.32	0.30	1.21
57-25	55.70	38.90	4.54	0.27	0.17
57-26	64.00	29.00	1.37	0.20	5.22
57-31	61.30	29.40	1.61	0.30	4.30
57-32	54.50	37.60	3.19	0.34	1.74
57-33	59.50	30.70	1.29	0.16	5.96
57-34	59.80	32.10	1.23	0.17	4.01
57-35	53.80	38.50	2.48	0.15	2.09

Table 4.7. Metal composition from gas-slag-metal equilibrium pertinent to stainless-steel making under 0.034atm of Pco at 1580°C in silica crucibles in mass%.

Number	%Cr	%Fe	%Si	%S	%C
48-2	8.51	93.90	0.38	0.12	0.03
48-6	2.50	95.30	0.27	0.24	0.17
53-1	14.80	80.60	1.56	0.03	3.42
53-2	11.90	83.30	1.73	0.08	2.85
53-3	10.70	86.00	0.64	0.08	2.50
53-4	12.10	85.30	0.42	0.20	2.52
53-5	11.00	89.70	0.43	0.21	1.57
53-6	10.90	88.30	0.37	0.34	1.29
53-7	8.08	90.40	0.23	0.35	0.18
53-11	13.10	81.90	0.59	0.25	1.52
53-12	12.20	85.50	0.35	0.23	1.49
53-13	8.67	88.90	0.20	0.30	0.56
53-14	5.14	92.80	0.20	0.41	0.61
53-15	12.30	85.90	0.20	0.41	0.28
53-16	8.90	89.20	0.20	0.30	0.44
53-17	8.82	89.60	0.20	0.27	0.74
53-19	4.20	95.00	0.20	0.36	0.44
53-21	6.02	93.10	0.20	0.28	1.23

Table 4.7. Metal composition from gas-slag-metal equilibrium pertinent to stainless-steel making under 0.034atm of Pco at 1580°C in silica crucibles in mass% (continue).

Number	%Cr	%Fe	%Si	%S	%C
56-1	16.20	79.80	1.42	0.21	1.73
56-2	15.50	80.60	1.45	0.14	1.50
56-3	18.40	77.80	1.51	0.43	0.43
56-4	16.60	80.10	1.19	0.39	1.27
56-5	7.82	90.50	0.45	0.34	0.49
56-6	16.00	80.10	1.58	0.19	1.82
56-13	16.80	81.80	0.33	0.01	0.21
56-14	16.60	83.10	0.81	0.08	0.30
56-15	16.90	81.80	0.41	0.07	0.36
56-16	17.30	76.50	1.74	0.10	2.11
56-21	14.90	85.20	0.20	0.12	0.34
56-22	16000	81.10	1.39	0.27	1.17
56-23	18.30	77.10	1.73	0.04	2.96
56-24	19.30	78.20	1.15	0.28	0.73
56-25	16.90	80.70	1.11	0.40	1.63
56-26	20.30	76.30	0.54	0.45	2.14
56-27	3.73	94.80	0.20	0.50	0.92
56-28	20.20	77.10	0.66	0.35	1.61
56-29	21.40	74.90	0.52	0.44	1.68

Table 4.8. Slag composition from gas-slag-metal equilibrium at 1500°C, under CO atmosphere in Cr-oxide crucibles in mass%.

Number	Al_2O_3	CaO	MgO	SiO_2	Cr	Fe	S
48-1	19.20	1.54	12.30	44.10	14.64	0.30	0.01
48-2	19.50	1.51	12.60	43.80	22.28	0.28	0.03
48-3	20.60	1.52	14.20	43.20	13.30	0.60	0.05
48-4	19.10	1.45	11.70	42.40	17.00	0.48	0.03
48-5	18.30	1.26	11.10	38.80	18.80	0.59	0.02
48-11	19.20	1.43	11.50	52.50	9.40	0.25	0.18
48-12	16.50	1.37	11.30	62.10	4.90	0.81	0.01
48-13	17.03	1.17	11.03	33.32	23.76	1.21	0.08
49-1	17.70	1.27	10.30	42.70	18.12	0.62	0.04
49-2	12.60	0.75	7.04	42.40	24.43	0.49	0.09
49-3	11.70	0.74	7.35	46.60	21.48	0.43	0.08
49-4	10.90	0.64	6.21	54.90	16.97	0.71	0.06
49-5	6.41	0.32	3.67	46.60	26.96	1.42	0.09
49-6	11.70	0.74	7.31	46.10	21.42	0.44	0.08
49-11	44.40	0.68	6.76	24.10	13.03	0.78	0.03
49-12	26.80	0.30	2.34	10.50	34.96	1.90	0.02
49-13	28.20	0.34	3.36	21.80	28.39	0.80	0.04
49-14	22.30	0.33	2.64	25.90	33.73	0.74	0.12
49-15	10.80	0.86	7.77	58.40	14.23	2.67	0.09
49-16	13.70	0.70	7.74	29.40	26.50	0.41	0.03
49-17	10.90	0.64	6.21	54.10	16.97	0.71	0.06

Table 4.9. Slag composition from gas-slag-metal equilibrium at 1500°C, at 0.05atm of Pco in Cr-oxide crucibles in mass%.

Number	Al_2O_3	CaO	MgO	SiO_2	Cr	Fe	S
52-1	20.10	1.49	13.10	45.00	13.27	0.26	0.02
52-2	20.10	1.46	13.20	42.80	14.37	0.28	0.02
52-3	17.70	1.18	11.50	33.80	22.99	0.51	0.03
52-4	21.60	1.77	15.10	47.60	8.42	0.50	0.01
52-5	18.90	1.63	11.10	47.00	14.03	0.33	0.04
52-6	22.20	1.72	14.70	45.90	9.37	0.30	0.04
52-9	15.40	1.43	10.30	59.80	5.75	1.55	0.02
52-11	13.60	1.05	9.48	61.50	7.46	0.52	0.03
52-12	16.57	1.38	11.35	62.35	4.91	0.79	0.01
52-13	17.03	1.17	11.03	33.32	23.76	1.21	0.08
52-14	19.86	1.78	19.76	35.41	6.22	0.82	0.08
52-15	19.00	1.80	11.70	47.40	10.54	0.97	0.01
52-16	19.78	1.37	17.20	38.22	9.86	0.87	0.04

Table 4.10. Slag composition from gas-slag-metal equilibrium at 1580°C, at 0.034atm of Pco in silica-oxide crucibles in mass%.

Number	Al_2O_3	CaO	MgO	SiO_2	Cr	Fe	S
53-8	14.40	0.89	6.06	49.90	14.78	2.54	0.06
57-1	15.60	0.88	5.82	55.60	13.55	0.48	0.06
57-2	15.70	0.85	5.53	58.70	11.84	0.38	0.03
57-3	18.30	1.10	8.98	59.00	6.98	0.45	0.01
57-4	17.80	1.19	9.57	55.40	9.17	0.48	0.03
57-5	18.10	1.15	9.16	55.50	9.24	0.39	0.03
57-6	17.90	0.60	5.71	57.30	10.63	0.68	0.05
57-11	22.50	0.94	10.80	55.20	5.43	0.36	0.02
57-12	17.20	1.02	7.69	58.30	8.83	0.41	0.04
57-13	18.90	0.93	7.65	55.40	10.61	0.32	0.04
57-14	21.10	0.87	10.00	54.20	8.21	0.29	0.05
57-15	21.30	0.81	10.20	52.10	9.85	0.34	0.03
57-16	20.40	0.79	8.99	53.60	9.65	0.32	0.02
57-17	19.20	0.72	7.56	57.20	9.24	0.42	0.02
57-18	19.50	0.77	7.90	55.80	9.92	0.34	0.04
57-21	15.70	0.75	11.10	58.60	8.01	0.45	0.05
57-22	15.60	0.77	11.90	56.00	9.78	0.39	0.06
57-23	14.90	0.73	10.00	57.80	10.61	0.44	0.04
57-24	14.50	0.61	7.05	60.80	11.49	0.39	0.05
57-25	14.00	0.59	8.05	55.10	14.79	0.37	0.04
57-26	12.20	10.40	10.40	59.40	11.91	0.45	0.06
57-31	12.10	10.90	10.90	55.10	14.03	0.47	0.07
57-32	11.60	9.83	9.83	53.90	16.08	0.61	0.06
57-33	14.90	10.60	10.60	59.00	9.17	0.49	0.06
57-34	11.90	10.50	10.50	55.30	14.71	0.52	0.06
57-35	11.90	9.40	9.40	54.40	15.33	0.51	0.03

Table 4.11. Slag composition from gas-slag-metal equilibrium at 1580°C, at 0.034atm of Pco in silica-oxide crucibles pertinent to stainless-steel making in mass%.

Number	Al_2O_3	CaO	MgO	SiO_2	Cr	Fe	S
53-1	21.80	1.47	13.50	55.90	1.32	0.29	0.02
53-2	20.40	1.27	11.20	59.30	1.51	0.47	0.02
53-3	20.30	1.37	11.70	56.40	3.76	0.71	0.03
53-4	19.40	1.24	11.00	55.70	5.25	0.85	0.02
53-5	18.00	1.12	9.28	55.00	7.32	1.22	0.02
53-6	17.10	1.02	8.35	52.80	9.72	1.72	0.03
53-7	16.00	0.97	7.31	52.70	11.56	1.77	0.04
53-11	15.00	0.98	8.55	61.40	6.51	1.74	0.03
53-12	15.20	0.97	8.53	61.50	6.19	1.13	0.02
53-13	13.50	0.86	7.42	57.70	11.84	2.02	0.03
53-14	12.40	0.65	4.63	57.40	12.86	3.33	0.04
53-15	11.20	0.73	6.22	46.50	19.77	4.67	0.06
53-16	12.70	0.83	7.53	52.10	15.39	2.57	0.04
53-17	14.30	0.87	7.33	61.60	8.28	1.75	0.02
53-19	21.80	0.66	10.40	56.30	4.73	1.92	0.02
53-21	23.50	0.71	10.70	56.50	3.36	1.43	0.02
56-1	21.70	0.75	9.57	55.80	5.316	0.63	0.01
56-2	23.00	0.81	11.00	54.50	4.12	0.78	0.01
56-3	21.90	0.88	11.20	49.50	8.21	0.71	0.02
56-4	21.20	0.75	9.46	54.90	6.01	0.57	0.02
56-5	19.60	0.68	8.34	54.90	7.94	1.71	0.02

Table 4.11. Slag composition from gas-slag-metal equilibrium at 1580^{O}C, at 0.034atm of Pco in silica-oxide crucibles pertinent to stainless-steel making in mass% (continue).

Number	Al_2O_3	CaO	MgO	SiO_2	Cr	Fe	S
56-6	23.60	0.89	12.10	53.40	2.22	0.54	0.02
56-13	12.10	0.24	0.54	56.30	16.23	1.54	0.02
56-14	12.40	.022	0.10	61.80	13.34	1.49	0.02
56-15	12.30	0.23	0.10	62.00	13.27	1.51	0.02
56-16	12.10	0.22	0.10	57.00	17.11	1.51	0.03
56-21	21.60	0.76	9.19	57.10	4.63	0.51	0.02
56-22	23.60	0.88	11.00	53.90	4.00	1.09	0.01
56-23	24.70	0.90	12.30	55.00	1.92	0.38	0.03
56-24	23.70	0.89	12.30	51.50	4.89	0.53	0.02
56-25	21.00	0.73	8.68	57.30	5.60	0.59	0.02
56-26	22.30	0.87	11.20	50.00	7.94	0.57	0.01
56-27	21.30	0.79	9.33	53.60	5.11	3.64	0.03
56-28	21.80	0.91	10.50	49.60	8.76	0.74	0.02
56-29	21.70	0.91	12.10	40.50	13.89	0.59	0.02

4.1. EQUILIBRIUM RELATIONSHIPS BETWEEN CARBON, SILICON AND PARTIAL PRESSURE OF CARBON MONOXIDE

This part of the results was presented at the International Ferro Alloy Congress 1995 (INFACON 7) and published in the proceeding, June, 1995[10], with some of the results from the gas-slag-metal equilibrium in Cr-oxide crucibles, which will be discussed late in the section 4.4.

4.1.1. Equilibria in Oxygen-Blowing Processes

There are two types of equilibria in the oxygen-blowing processes, namely metal-gas equilibrium and gas-slag-metal equilibrium. When oxygen or oxygen and argon gas is introduced into metal bath, the oxidation reactions take place at the interfaces of metal and gas bubbles. The metal-gas equilibrium will be valid until the bubbles come up to the interfaces of metal/slag on the top of the bath. Thereafter, metal-slag-gas equilibrium takes over at the interfaces of metal and slag, involving CO or (CO+Ar) gas, as shown in figure 4.1.1. The metal-gas equilibrium plays an important role in monitoring the carbon content of the alloy. Meanwhile, the removal of sulphur, the loss of chromium and the control of silicon would be more closely correlated to the gas-slag-metal equilibrium.

4.1.2. Equilibrium Between Carbon, Silicon and Pco

Relationship Between Carbon and Partial Pressure of Carbon Monoxide

The result shown in figure 4.1.2. illustrates that carbon content in the alloy which has no Si increases from 0.0 per cent to about 2.6 per cent by mass when Pco rises from 0 to 0.83 atm. Carbon in the alloy containing 3 per cent of silicon ascends from 0.0 per cent to about 7.2 per cent with the increase of the partial pressure of carbon monoxide from 0 to 0.83 atm. When Pco increases to 0.15 atm, the carbon picked up from the gas is fast. Silicon in the alloy promotes the increase of carbon in the alloys.

The result shown in figure 4.1.3 also demonstrates that carbon content of the alloys increases with the increase of Si in the alloy, when CO exists in the gas phase. On the contrary, metals can not pick up carbon if there is no carbon monoxide in the gas phase.

The above results are expressed in a 3-dimensional drawing in figure 4.1.4, which manifests the carbon pick-up of the alloys with the increase of Si content and the partial pressure of carbon monoxide.

The carbon picked up in the alloys increases slowly with the increase of the partial pressure of carbon monoxide when silicon content is comparatively low in the alloys. The carbon pick-up is promoted by more silicon of the alloy phase, while the carbon content increases with the increase of the partial pressure of carbon monoxide, even when no silicon exists in the alloy phase.

It is also found in the current experiments that sulphur in the alloy does not change with silicon content and the partial pressure of carbon monoxide.

The way carbon is picked up from carbon-monoxide gas may be discussed by the following reactions:

$$[Si] + 2CO = 2[C] + SiO_2 \qquad (4.1.1)$$

$$2[Cr] + 3CO = 3[C] + Cr_2O_3 \qquad (4.1.2)$$

$$[Cr] + CO = [C] + CrO \qquad (4.1.3)$$

$$[Fe] + CO = [C] + FeO \qquad (4.1.4)$$

$$2[Cr] + [Fe] + 4CO = 4[C] + FeOCr_2O_3 \qquad (4.1.5)$$

Here [ ] refers to species in metal phase. There may be more reactions like reaction (4.1.5), forming complex components. It is shown in figure 4.1.5 that reaction (4.1.1), (4.1.2), (4.1.5), and (4.1.3) are the dominant ones causing the alloy to pick up carbon from the gas phase. The calculation in figure 4.1.5 is based on the free-energy changes of the reactions at 1500 °C for the alloy of 63%Cr, 3%Si, 34%Fe by mass, assuming that pure oxides are formed.

The results from the current study are in good agreement with the work done by Kossyrev and Olsen recently[57],which shows that carbon solubility increases with an increase of silicon content with 0 to 3 per cent of silicon.

They investigated carbon solubilities for Cr-Si-C and Cr-Fe-Si-C alloys (Cr/Fe=4, 1.5, 0.25) in a resistance furnace at 1600°C in Ar atmosphere with graphite crucibles. Figure 2.10 presented the results. For chromium rich alloys, the carbon content increases initially with increasing silicon content in the metal. Study of the metal and the crucible/metal interface in the electron microprobe shows that the solubility curve

representing iron free Cr-Si-C alloy shows two breaks, dividing the system into three areas. In the first area, carbon is increasing with increasing silicon content. After silicon reaching a critical value, carbon content decreases with increasing silicon content. The critical silicon value decreases when Cr-to-Fe ratio reduces. The critical silicon value disappears when the ratio of Cr to Fe is less than 1.5 in the metal phase. In the first area, the primary crystals in the metal are Cr_7C_3; in the next area the primary crystals are Cr_3C_2; and in the third area only SiC. With increasing silicon content the stable carbide phases are Cr_7C_3, Cr_3C_2 and SiC. For alloys with Cr/Fe=4 there seems to be a fourth area between 10 and 15.5 per cent of silicon by mass. Metallographic observations indicates absence of any additional carbide phase between the graphite crucible and the metal in this area which means that graphite is a stable phase between the M_3C_2 (M=Cr+Fe) SiC stable areas. Further, there is no area of M_7C_3 stability in alloys with Cr/Fe=1.5 and there is no area of M_3C_2 stability with Cr/Fe ratio less than approximately 1.2. In our study, the ratio of Cr to Fe is over 2 and the results at CO atmosphere are in good agreement with their results.

Lucas and Wentrup[53] studied the solubility of carbon in synthetic Fe-Cr-Si alloys under laboratory conditions, ensuring fairly reliable saturation of the alloy with respect to carbon, and determined the carbon content. An increase in chromium content causes an increase in the solubility of carbon, but this effect can be neutralised by a simultaneous increase in the silicon content. A number of studies on the Fe-Cr-Si-C quaternary system have been done by Petrushevskii and Geld[54,55,56] at 1700 °C in the range of 0 to 35 per cent silicon, 0 to 100 per cent iron, 0 to 93 per cent chromium.

The relationships of carbon, silicon and the partial pressure of carbon monoxide are essential to determine the O_2/Ar ratio for the decarbonization processes via O_2/Ar blowing. The reason is because that the contents of silicon and carbon in the alloys correlated with the partial pressure of carbon monoxide in the bubbles of CO/Ar gas, which comes from the reactions of decarbonization. In another word, any one parameter among carbon content, silicon content and partial pressure of carbon monoxide, will be determined by the other two. For example, when silicon content and the partial pressure

of carbon monoxide are fixed, the minimum carbon content, reduced by O_2/Ar blowing, can be predicted. On the other hand, when the contents of silicon and carbon in the alloy are decided, the maximum ratio of O_2/Ar, which can be converted from the maximum partial pressure of carbon monoxide, should be used in the processes.

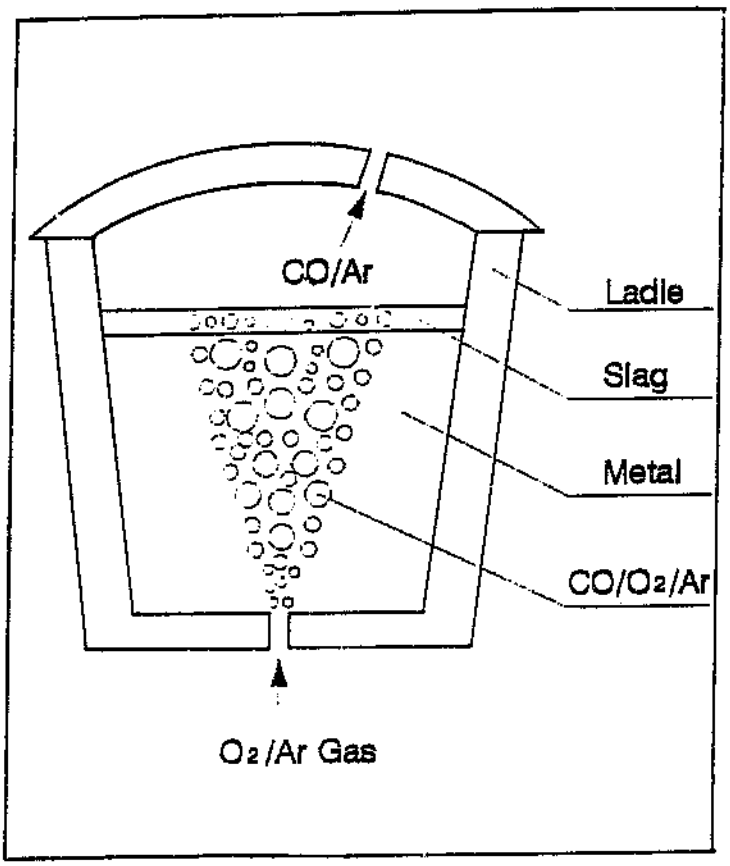


Figure 4.1.1. Demonstration of metal refining via blowing of oxygen/argon gas.

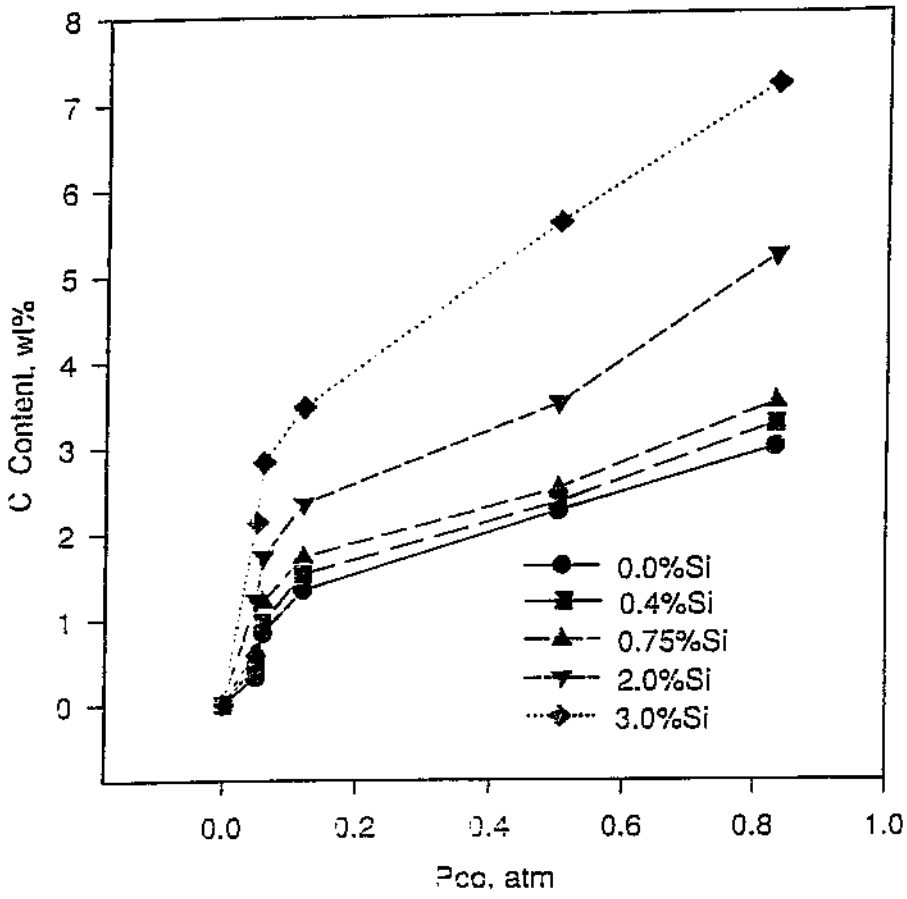


Figure 4.1.2. Relationship between carbon content and partial pressure of carbon monoxide for alloys of 61%Cr-Fe-Si-C by mass in CO/Ar gas at 1500°C.

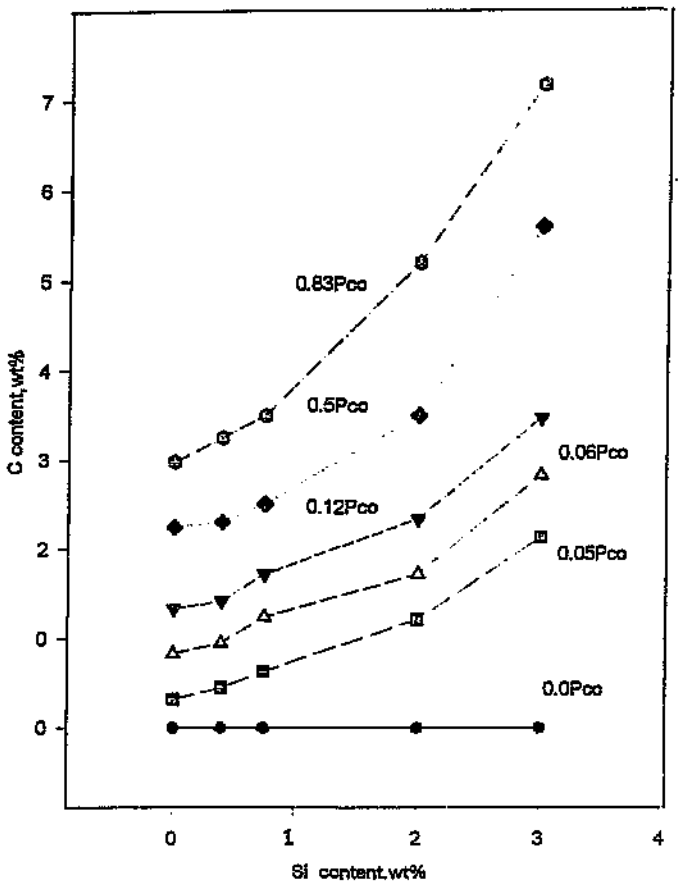


Figure 4.1.3. Relations of carbon and silicon and partial pressure of carbon monoxide for alloys of 61%Cr-Fe-Si-C by mass in CO/Ar gas at 1500°C.

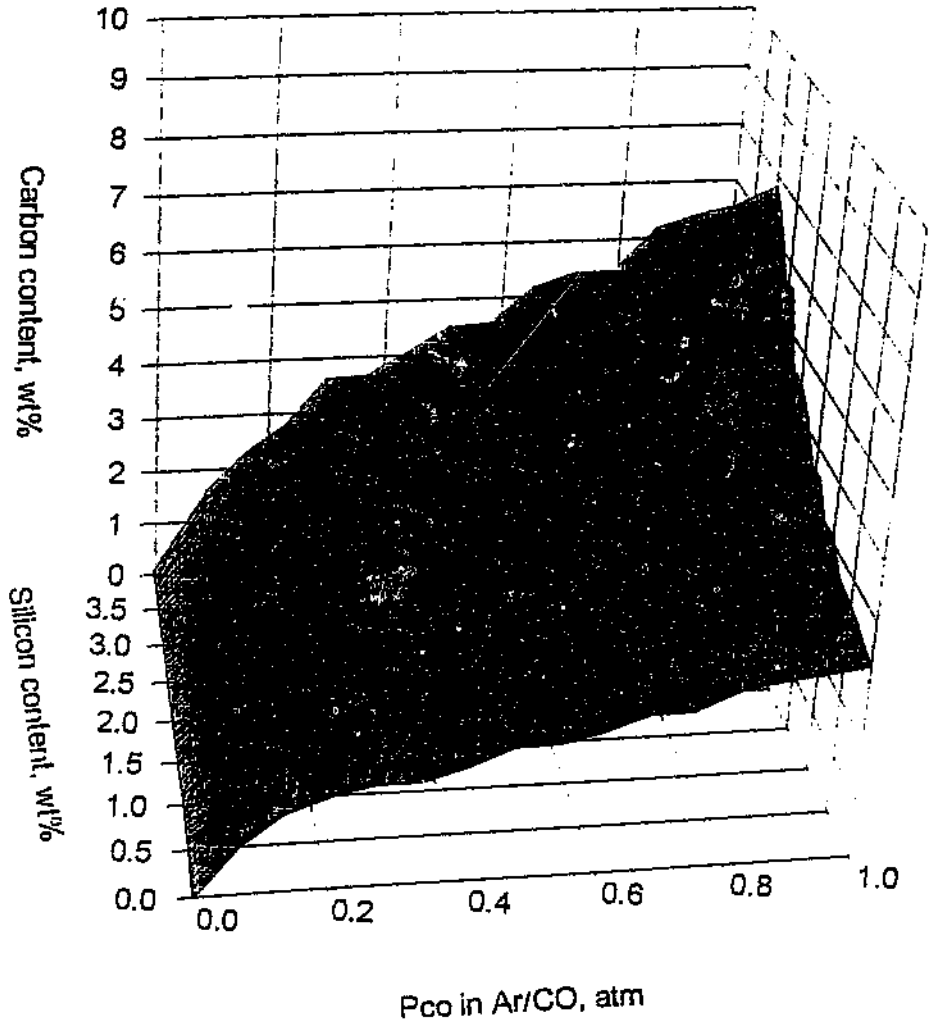


Figure 4.1.4. Relationship between carbon and silicon for alloys of 61%Cr-Fe-Si-C by mass in CO/Ar gas at 1500°C.

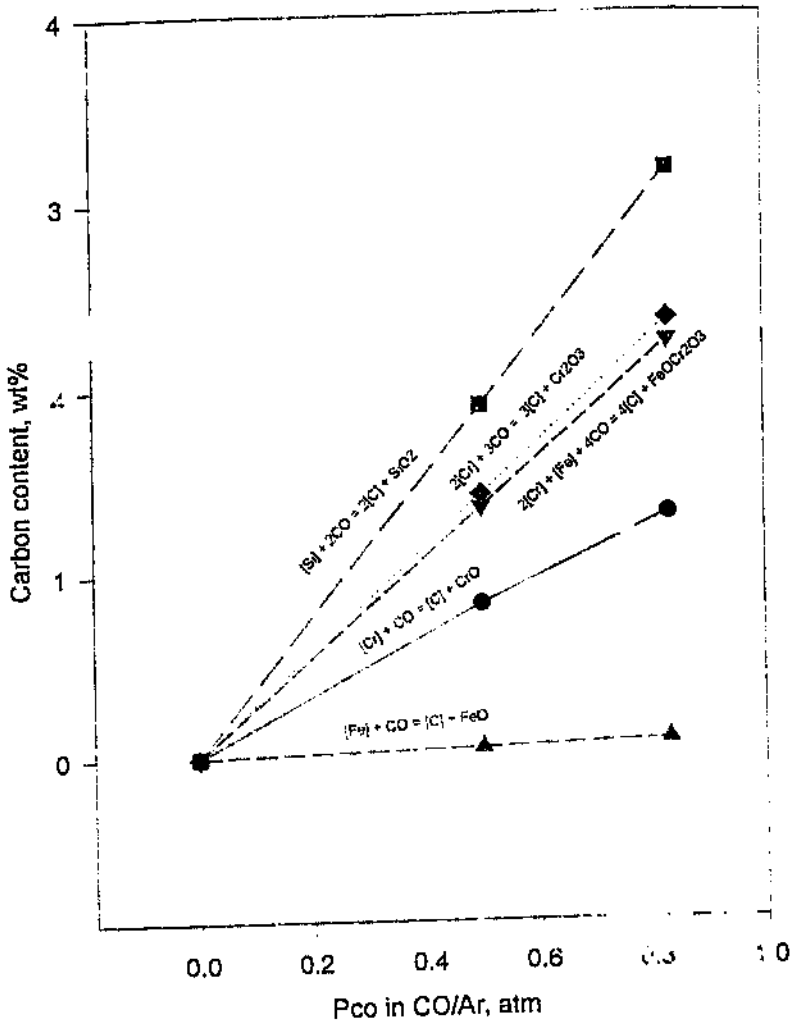


Figure 4.1.5. Calculation of carbon content picked up from CO gas at 1500°C, alloys of 63%Cr-34%Fe-3%Si-C by mass.

4.2. SILICON DISTRIBUTION BETWEEN SLAG AND METAL AT DIFFERENT PARTIAL PRESSURE OF CARBON MONOXIDE

The products tapped from a ferrochromium furnace, or from a refining furnace are an impure ferrochromium melt and a liquid slag. The ferrochromium alloy contains a high proportion of carbon and it is even saturated with carbon in most instances. The other solutes are silicon, phosphorus and sulphur in varying proportions. Silicon and phosphorus are reduced from the burden coming mainly from the ore gangue materials, while sulphur comes mainly from the coke. There is an equilibrium distribution of chromium, iron, silicon, sulphur and phosphorus between slag phase and metal phase. The concentrations of these elements in the metal phase, to some extent, are basically controlled by the furnace operation in terms of slag forming and slag controlling.

The phosphorus content of ferrochromium depends only on the phosphorus content of the ore charged. Virtually all the phosphorus charged into the furnace finds its way into the metal since under the operating conditions in the ferrochromium furnace, like in iron-making blast furnace. Slag is, in most operations, a solution of Al_2O_3, CaO, Cr-oxide, Fe-oxide, MgO and SiO_2 with small amount of P_2O_5 and sulphur.

In the present work, the relationships between the equilibrium partitions of silicon, sulphur and chromium have been investigated in silica and Cr-oxide crucibles at temperatures of 1500°C and 1580°C. The CO partial pressure of 0.034atm, 0.05atm and 0.83atm are used in the experiments. The results will be discussed in the following three sections in terms of the distributions of silicon, sulphur, and chromium.

A part of the SiO_2 in the burden is reduced to metal phase after it is dissolved in the slag by the overall reaction of SiO_2 reduction, expressed by equation (4.2.1):

$$(SiO_2) + 2[C] = [Si] + 2\,CO_{(g)} \qquad (4.2.1)$$

Where the round brackets refer to the slag phase and square brackets to the metal phase.

There are two major sources of SiO_2 in the production furnace: ore gangue and coke ash. SiO_2 content in ores varies considerably, but those in coke ash are roughly similar, about 50 per cent, although the ash content itself can vary substantially from coke to coke. The contribution of each is dependent on the kinds of coke and ore, as well as operational conditions.

The routes and mechanism of Si transfer from the burden to the metal have been a matter of concern. Two routes have been recognized: from molten slag to molten metal directly through the slag-metal reaction, and the indirect route where Si transfers from slag or coke ash to the gas phase as SiO and then into metal. It is natural to believe that the direct route is mainly responsible for SiO_2 reduction. Therefore silicon transfer through the slag-metal reaction has been extensively studied as one of the basic reactions of the processes for ferrochromium production.

Kinetic studies on slag-metal reactions have shown that the reduction of SiO_2 in slag phase by carbon in the metal phase is a first-order reaction with respect to the activity of SiO_2 and is very slow[101-104]. The observed activation energies varied with slag basicity and were fairly large in neutral and acidic slags, which means that the SiO_2 reduction rate under usual conditions of the operation has a large temperature dependence.

From thermodynamic point of view, the phase diagrams for the $CaO\text{-}SiO_2\text{-}Al_2O_3$ ternary system, as well as the quaternary system with MgO, and the activities involved both slag

phase and metal phase were systematically studied[92-96,105-107]. Those data have not lost their importance. They are extensively utilized presently with the equilibrium distribution of silicon, sulphur, chromium and the activities of silicon, sulphur and chromium. From the viewpoint of industrial application, the availability and the reliability of such data have become of greater importance because of the need for a higher rate for chromium recovery, a higher rate for sulphur elimination and a higher degree of control in present process technology.

4.2.1. Influence of Slag Composition on the Silicon Partition

The effect of chromium oxide in the slag phase expressed in terms of chromium content of the slag on the equilibrium partition of silicon between slag phase and metal phase in terms of the mole partition ratio of [Si]/(SiO_2) is illustrated in figure 4.2.1. As the chromium content of the slag phase increases, the ratio of [Si]/(SiO_2) decreases and it is more remarkable at lower Pco values. At 0.05atm of partial pressure of carbon monoxide, the silicon partition between slag and metal decreases from 0.025 to 0.011 with an increase of chromium in slags from 0.05 to 0.085 by mole fraction. A slow decrease in the silicon partition ratio is clarified from 0.01 to 0.009 with increasing chromium in slags from 0.1 to 0.2. Under pure carbon monoxide atmosphere (Pco 0.83 atm due to elevation of temperature), the equilibrium distribution of silicon declines quite fast from 0.026 to 0.017 when chromium content of the slags increases from 0.05 to 0.1. The silicon partition does not decrease further when chromium content in the slag phase is higher than 0.2 mole fraction.

The result also discloses that both silicon partition and the partial pressure of carbon monoxide play a great role to achieve a high rate of chromium recovery from slag phase to metal phase. A high silicon partition and a low partial pressure of carbon monoxide

favour a high chromium recovery. There is a threshold for certain partial pressure of carbon monoxide.

At 0.05atm of the partial pressure of carbon monoxide, the threshold content of chromium in the slags is 0.085 and the silicon partition ratio is about 0.011. Meanwhile, at 0.83atm of the partial pressure of carbon monoxide the threshold content of chromium in the slag is about 0.125 and the corresponding silicon partition ratio is about 0.015. When chromium is higher than the threshold content, chromium content in the slag phase decreases very fast with a very little increase of silicon ratio, and after the threshold a substantial increase of the silicon ratio can only reduce very little chromium from slag phase to metal phase. A lower partial pressure of carbon monoxide will help to lower the threshold content of chromium with a lower ratio of silicon.

In practice, the silicon content in the metal must be taken into account with the silicon oxide in the slag phase and the threshold with certain partial pressure of carbon monoxide, when silicon content in the metal phase is used to discuss and control the chromium content in the slag phase.

The effect of Al_2O_3 on the equilibrium partition of silicon is exhibited in figures 4.2.2 and 4.2.3. The results exhibit that the increase of alumina content in the slag phase increases the equilibrium distribution of silicon. Figure 4.2.2 is from the experiments where the metal phase contains 0.55 mole fraction chromium, using Cr-oxide crucibles and silica crucibles. Figure 4.2.3 displays the results from those experiments where silica crucibles were used with the metal phase containing 0.22 mole fraction chromium. With Cr-oxide crucibles, the increase of Al_2O_3 content and the partial pressure of carbon monoxide do not effect the silicon partition remarkably. The equilibrium partition of silicon increases from 0.02 to 0.14 with an increase of alumina content from about 0.07 to 0.14 with the metal phase containing about 0.55 mole fraction chromium. The equilibrium partition of silicon increase from 0.005 to 0.05 with an increase of alumina content from 0.075 to

0.15 with the metal phase containing only 0.22 mole fraction chromium.

The results are consistent with the study done by Fulton and Chipman[107], illustrated in figure 4.2.4. Their experiments were conducted under CO atmosphere at temperatures of 1425°C, 1500°C, 1600°C and 1700°C. They found that an increase in the Al_2O_3 content caused an increase in the silicon content of the metal at 1500°C, 1600°C and 1700°C. At 1425°C, on the other hand, this effect persists only in the more basic slags.

The influence of MgO on the partition ratio of silicon is elucidated in figure 4.2.5. In general, the increase of MgO in the slag decreases the partition ratio of silicon. The results from the experiments where Cr-oxide crucibles were used disclose very small effect of MgO and the partial pressure of carbon monoxide on the silicon distribution. However, the results from those experiments conducted in silica crucibles show a substantial decrease of silicon partition ratio from 0.14 to 0.04 with an increase of MgO molar fraction from about 0.1 to 0.17. While the result achieved in silica crucibles with the metal phase containing 0.22 mole fraction of chromium demonstrates an unremarkable effect of MgO on the silicon partition ratio, as seen in figure 4.2.6.

The effect of silica content of the slag phase on the equilibrium distribution of silicon is illustrated in figure 4.2.7 and figure 4.2.8. The partial pressure of carbon monoxide and the silica of the slag phase have little effect on the silicon partition ratio, except the result from the metals of 0.55 chromium in silica crucibles. The result is displayed in figure 4.2.7, which shows a remarkable increase of the silicon partition from 0.02 to about 0.13 with an increase of silica from 0.55 to 0.64. The results are in good agreement with the results from M. Akyuzlu and R. H. Eric[33] in their studies on slag-metal equilibrium in the smelting of high-carbon ferrochromium. Their results elucidated that the silicon content of the metal phase was directly proportional to the silica content of the slag phase with which it is in equilibrium. The increase of silicon content in the metals with increasing silica in the slags was more pronounced at 1580°C. This can be explained by

the increase in the value of the equilibrium constant of reaction (4.2.1), which increases with the increase of temperature due to the endothermic nature of reaction (4.21).

$$(SiO_2) + 2[C] = [Si] + 2\,CO_{(g)} \qquad (4.2.1)$$

4.2.2. Effects of Metal Composition on the Partition of Silicon

The influence of the chromium content of the metal phase on the silicon partition is illustrated in figures 4.2.9 and 4.2.10. In general, the increase of chromium in the metal phase results in a little increase of silicon partition when Cr-crucibles are used. On the other hand, the results from the experiments conducted in silica crucibles illustrate that the silicon partition ratio increases from 0.04 to 0.15 with an increase of chromium in the metal from 0.50 to 0.55 mole fraction.

The effect of silicon content on the silicon partition ratio is illustrated in figures 4.2.11 and 4.2.12. The results exhibit that the equilibrium distribution of silicon is proportional to the content of silicon in the metal phase. The results from the metals containing about 0.22 mole fraction of chromium demonstrate that the silicon partition increases quite quickly from 0.006 to 0.03 with the increase of silicon from 0.004 to 0.01 but thereafter the partition increases slowly from 0.03 to 0.05 with the increase of silicon from 0.014 to 0.03 by mole fraction.

The effect of carbon content on the distribution of silicon is illustrated in figures 4.2.13 and 4.2.14. Carbon content enhances the equilibrium distribution ratio of silicon. A higher silicon distribution ratio can be achieved at a lower partial pressure of carbon monoxide when the content of carbon in the metal phase exceeds 0.14 mole fraction.

With an increase of carbon content from 0.14 to 0.22, the silicon partition ratio increases from 0.01 to 0.018 and 0.026 at 0.83atm and 0.05atm of the partial pressure of carbon monoxide respectively, as seen in figure 4.2.13. The results from the experiments where the metal phase contains 0.22 mole fraction chromium, as seen in figure 4.2.14, show that the silicon partition ratio increases from 0.006 to 0.03 when carbon content increases from 0.02 to 0.08 by mole fraction. A further increase of carbon content in the metal phase does not effect the equilibrium partition ratio of silicon. The silicon partition ratios shown in figure 4.2.14 are higher than those displayed in figure 4.2.13 with the metal phase containing higher chromium content.

The reaction expressed in equation 4.2.1 plays a significant part in the relationships among the silicon partition, the partial pressure of carbon monoxide, and the carbon content.

$$(SiO_2) + 2[C] = [Si] + 2CO \qquad (4.2.1)$$

$$[Si]/(SiO_2) = K_{4.2.1}\{[a_C]^2(\gamma_{SiO2})\}/\{P^2_{CO}[\gamma_{Si}]\}$$

$$= K_{4.2.1}\{[X_C]^2/P^2_{CO}\}\{[\gamma_C]^2(\gamma_{SiO2})/[\gamma_{Si}]\} \qquad (4.2.2)$$

As displayed in equation 4.2.2, a decrease of the partial pressure of carbon monoxide will increase the silicon partition ratio. An increase of carbon content will also increase the silicon partition ratio because the increase of carbon content increases both the [Xc] value and the ratio of $[\gamma_C]^2/[\gamma_{Si}]$ due to the little change in the slag composition, which leads little change in the value of (γ_{SiO2}). The relations between carbon content and the $[\gamma_C]^2/[\gamma_{Si}]$ ratio is plotted by using the data from the works[105,106], as shown in figure 4.2.16. Due to the saturation of silica in the slags, the SiO_2 activity is unit in the slags when the silica crucibles being utilized, which will absolutely result in the increase of silicon partitions.

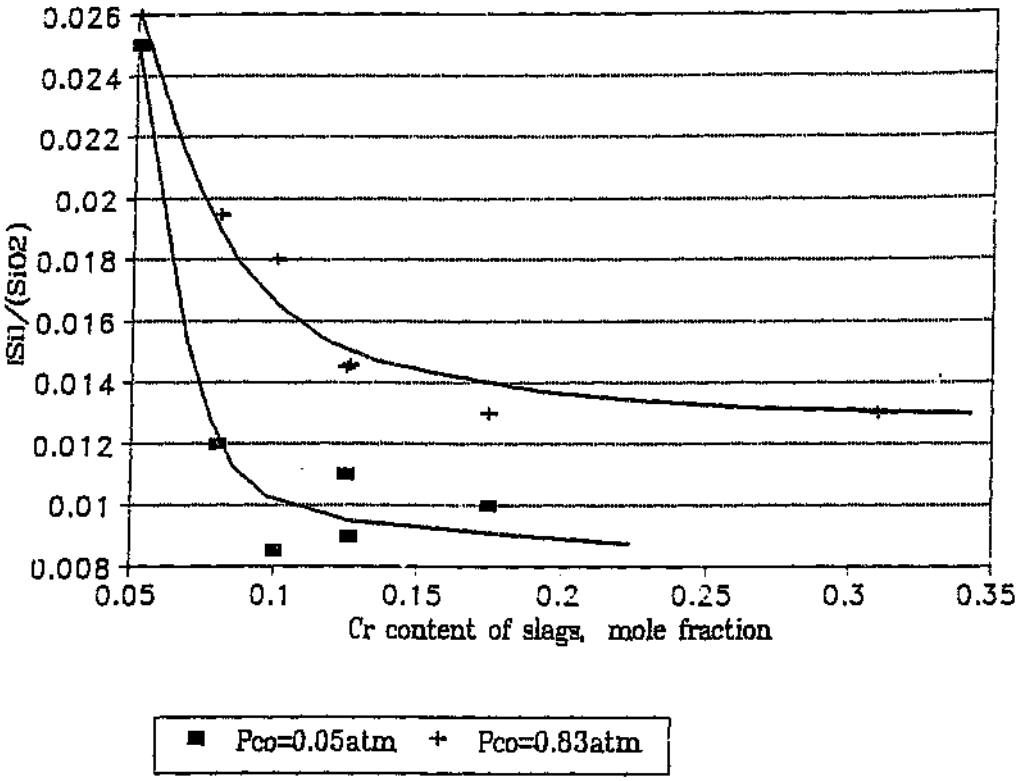


Figure 4.2.1. Effect of Cr content in slags on silicon partition with metals of 0.55Cr-Fe-C-S-0.04Si and slags of 0.01CaO-Fe_2O_3-MgO-Cr_2O_3-SiO_2-Al_2O_3 in mole fraction, Al_2O_3/MgO=1.7. in Cr-oxide crucibles at 1580°C.

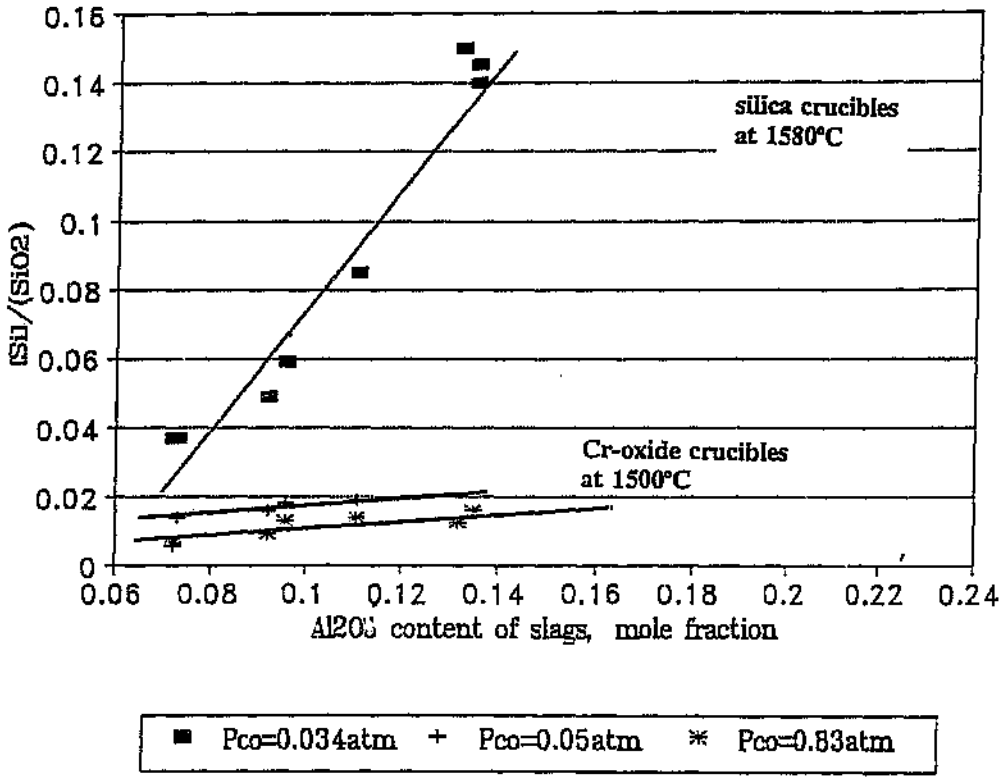


Figure 4.2.2. Effect of Al_2O_3 content in slags on silicon partition with metals of 0.55Cr-Fe-C-S-0.04Si and slags of 0.01CaO-Fe_2O_3-MgO-Cr_2O_3-SiO_2-Al_2O_3 in mole fraction, Al_2O_3/MgO=1.7, in Cr/Si-oxide crucibles at 1500°C/1580°C.

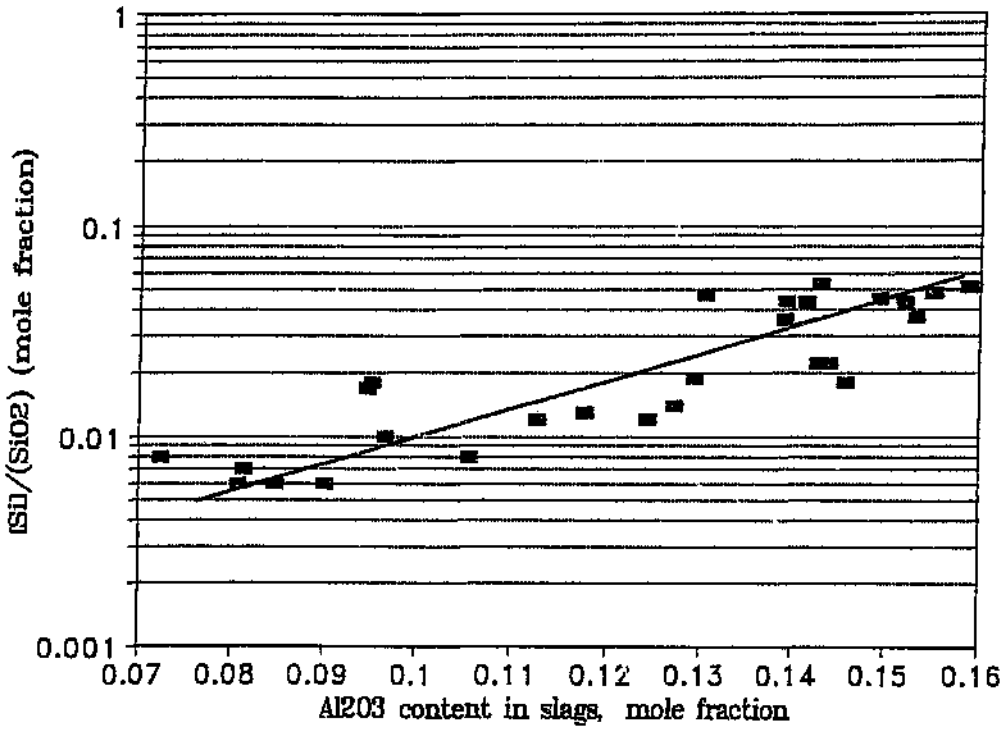


Figure 4.2.3. Effect of Al_2O_3 content in slags on silicon partition with metals of 0.22Cr-Fe-C-S-0.04Si and slags of 0.01CaO-Fe_2O_3-MgO-Cr_2O_3-SiO_2-Al_2O_3 in mole fraction, Al_2O_3/MgO=1.7, in Si-oxide crucibles at 1580°C at 0.034 Pco.

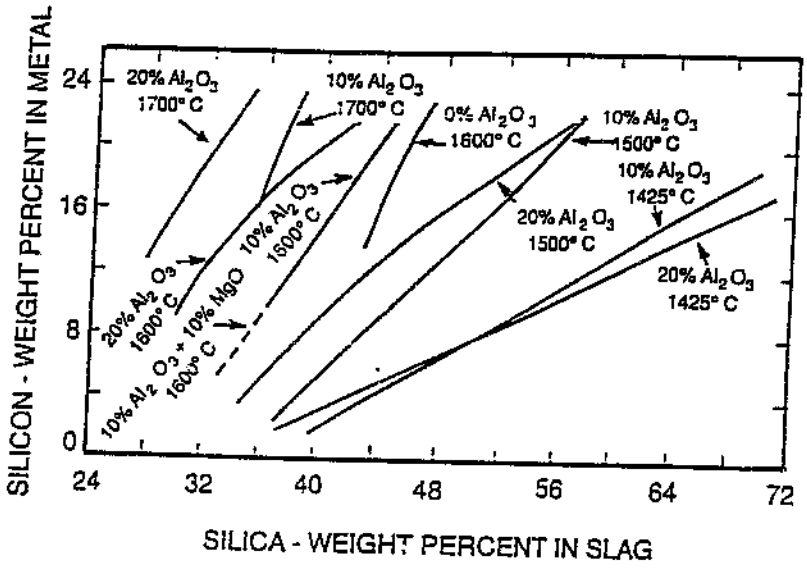


Figure 4.2.4. Summary of silicon-reduction equilibrium. After Fulton and Chipman [107].

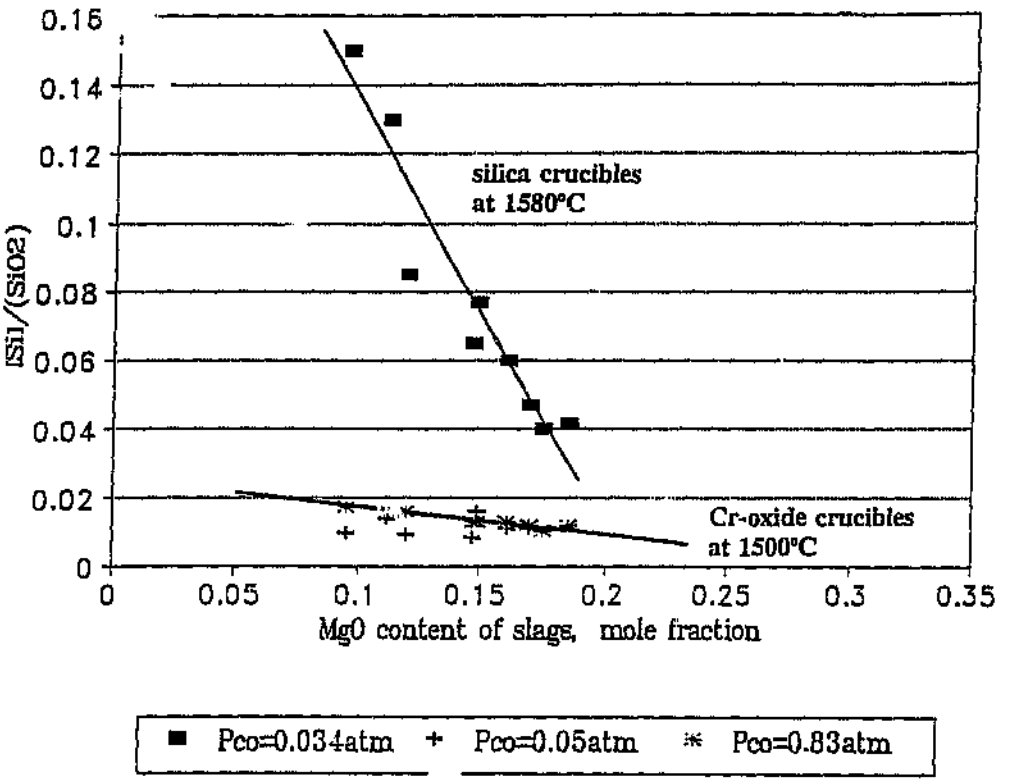


Figure 4.2.5. Effect of MgO content on silicon partition with metals of 0.55Cr-Fe-C-S-0.04Si and slags of 0.01CaO-Fe_2O_3-MgO-Cr_2O_3-SiO_2-Al_2O_3 in mole fraction, Al_2O_3/MgO=1.7, in Cr/Si-oxide crucibles at 1500°C/1580°C.

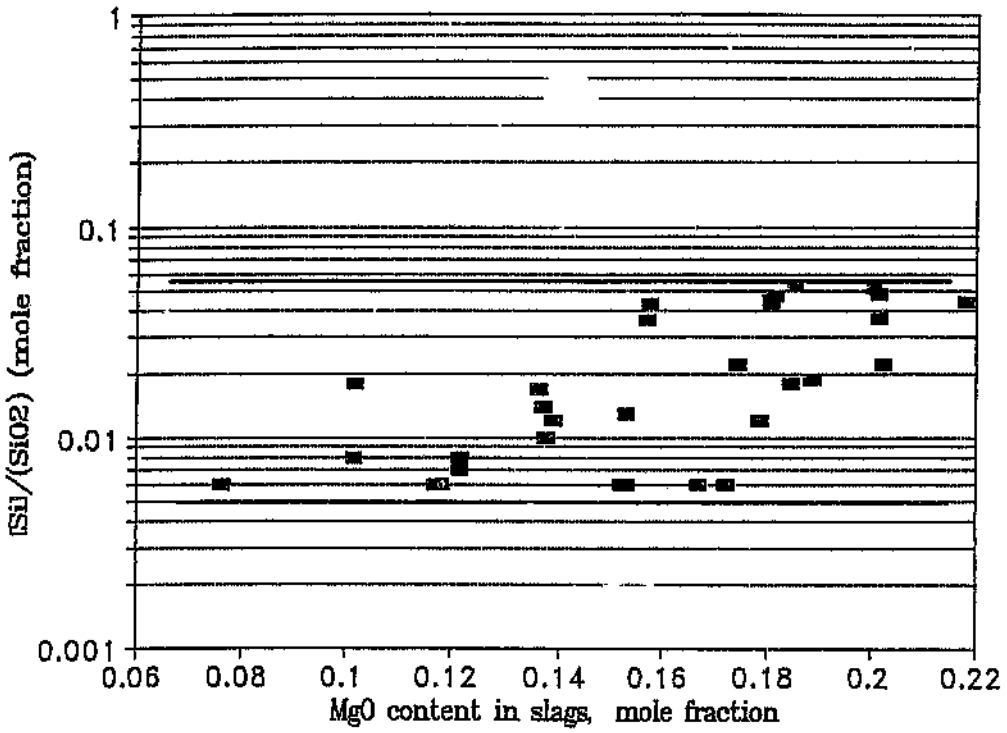


Figure 4.2.6. Effect of MgO content on silicon partition with metals of 0.22Cr-Fe-C-S-0.04Si and slags of 0.01CaO-Fe_2O_3-MgO-Cr_2O_3-SiO_2-Al_2O_3 in mole fraction, Al_2O_3/MgO=1.7, in silica crucibles at 1580°C at 0.034 Pco.

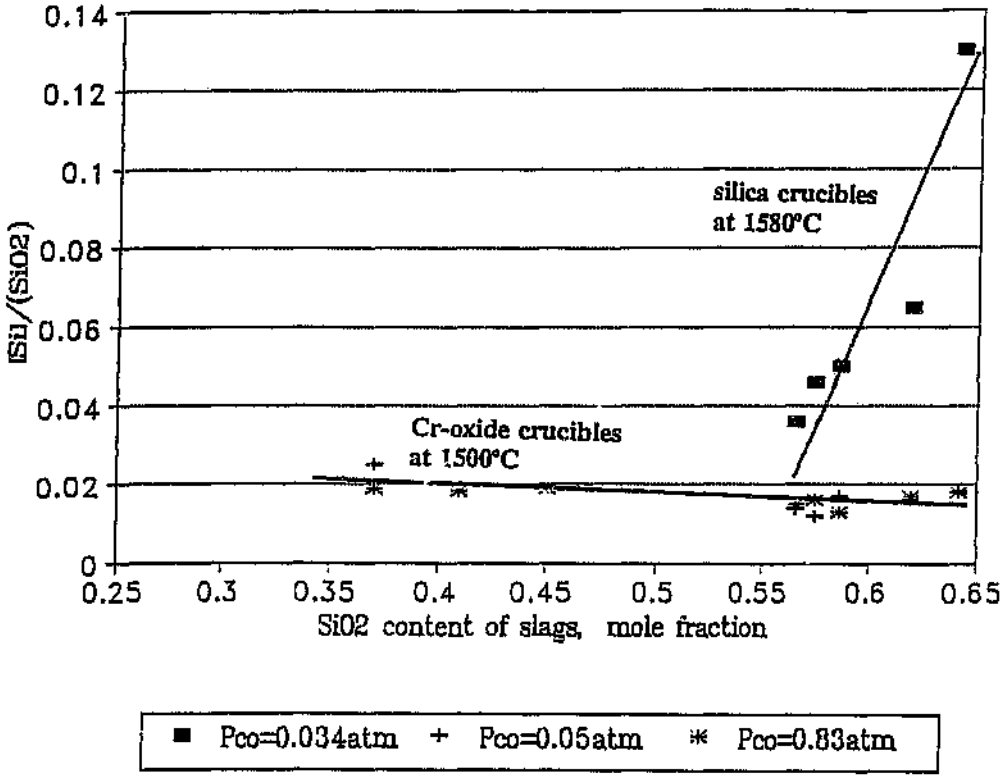


Figure 4.2.7. Effect of SiO_2 content on silicon partition with metals of 0.55Cr-Fe-C-S-Si and slags of 0.01CaO-0.005Fe_2O_3-MgO-Cr_2O_3-SiO_2-Al_2O_3 in mole fraction, Al_2O_3/MgO=1.7, in Cr/Si-oxide crucibles at 1500°C/1580°C.

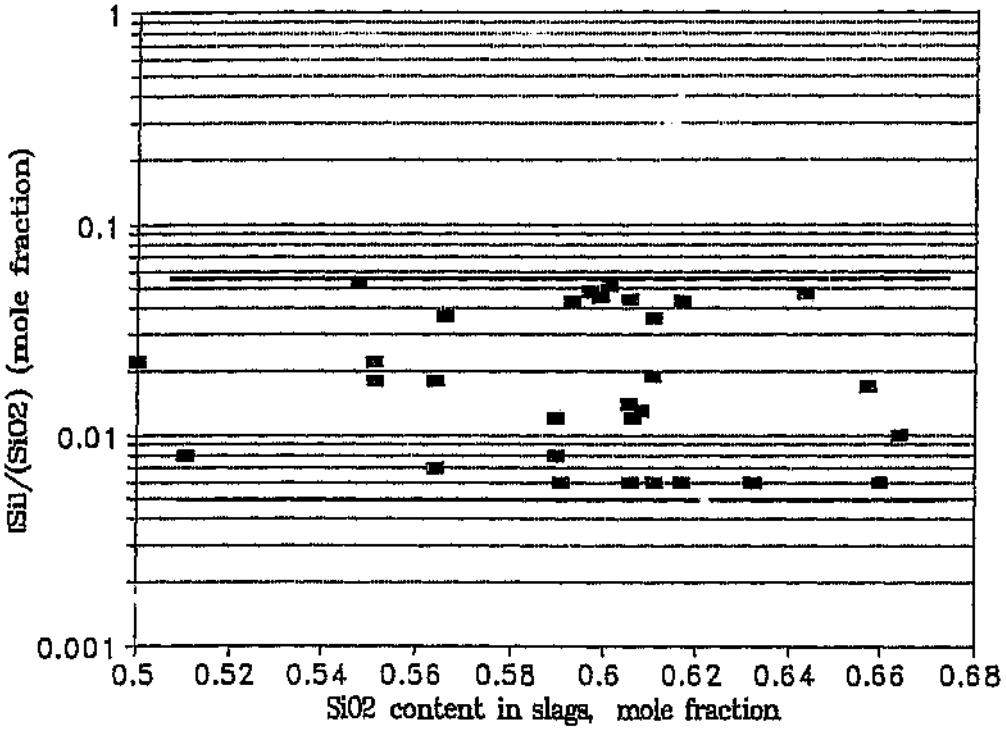


Figure 4.2.8. Effect of SiO_2 content on silicon partition with metals of 0.22Cr-Fe-C-S-Si and slags of 0.01CaO-0.005Fe_2O_3-MgO-Cr_2O_3-SiO_2-Al_2O_3 in mole fraction, Al_2O_3/MgO=1.7, in silica crucibles at 1580°C at 0.034 Pco.

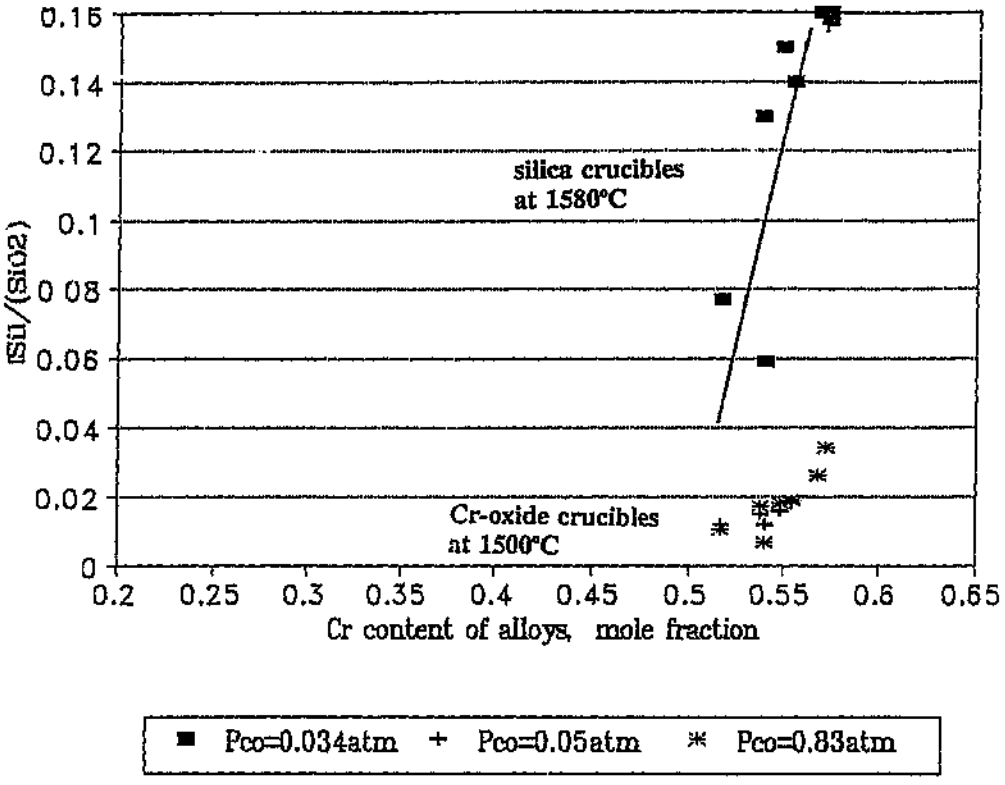


Figure 4.2.9. Effect of Cr content of metal on silicon partition with metals of Cr-Fe-C-S-0.04Si and slags of 0.01CaO-0.005Fe_2O_3-MgO-Cr_2O_3-SiO_2-Al_2O_3 in mole fraction, Al_2O_3/MgO=1.7, in Cr/Si-oxide crucibles at 1500°C/1580°C, relevant to FeCr Alloys.

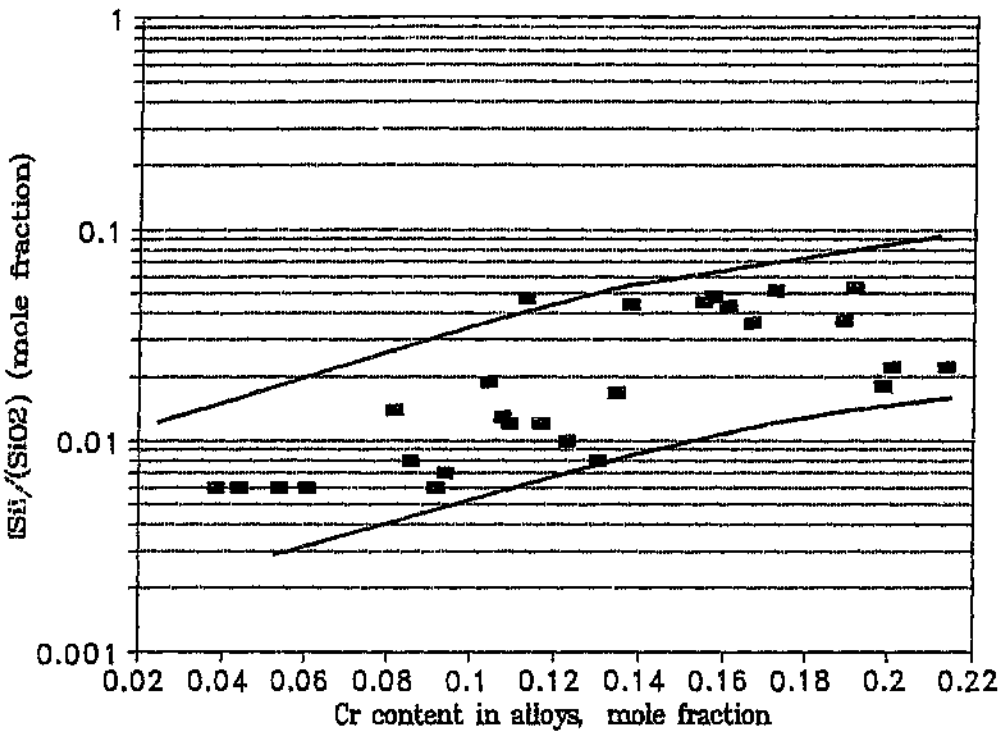


Figure 4.2.10. Effect of Cr content of metal on silicon partition with metals of Cr-Fe-C-S-0.04Si and slags of 0.01CaO-0.005Fe_2O_3-MgO-Cr_2O_3-SiO_2-Al_2O_3 in mole fraction, Al_2O_3/MgO=1.7, in silica crucibles at 1580°C at 0.034 Pco, relevant to stainless steel.

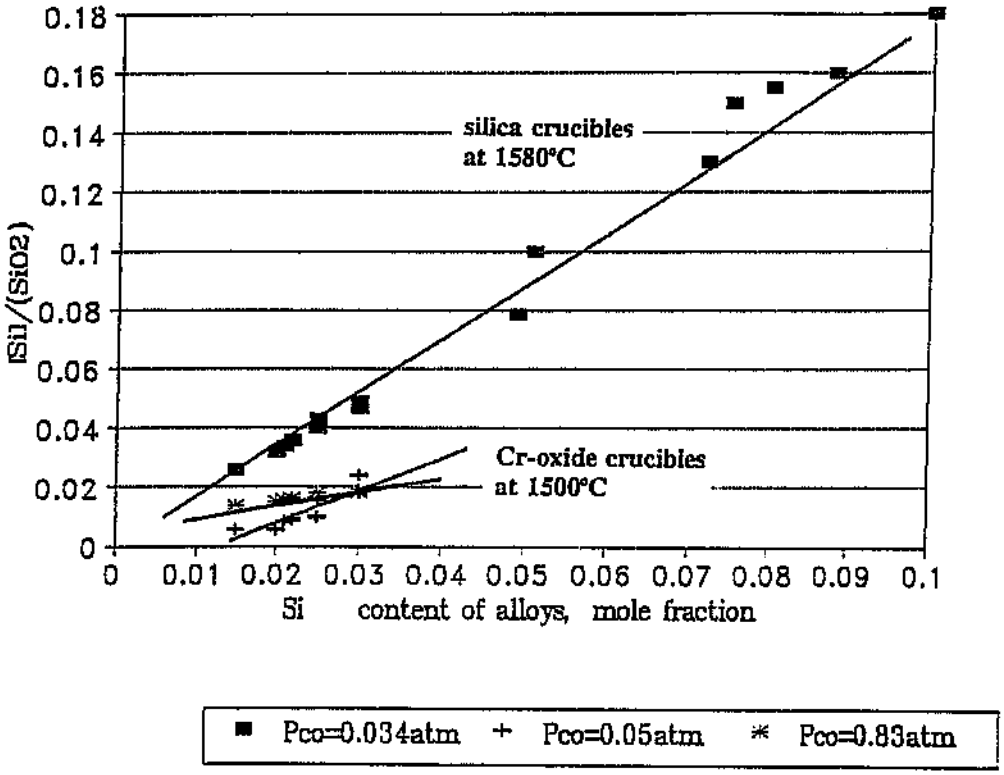


Figure 4.2.11. Effect of Si content of metal on silicon partition with metals of 0.55Cr-Fe-C-S-Si and slags of 0.01CaO-0.005Fe_2O_3-MgO-Cr_2O_3-SiO_2-Al_2O_3 in mole fraction, Al_2O_3/MgO=1.7, in Cr/Si-oxide crucibles at 1500°C/1580°C.

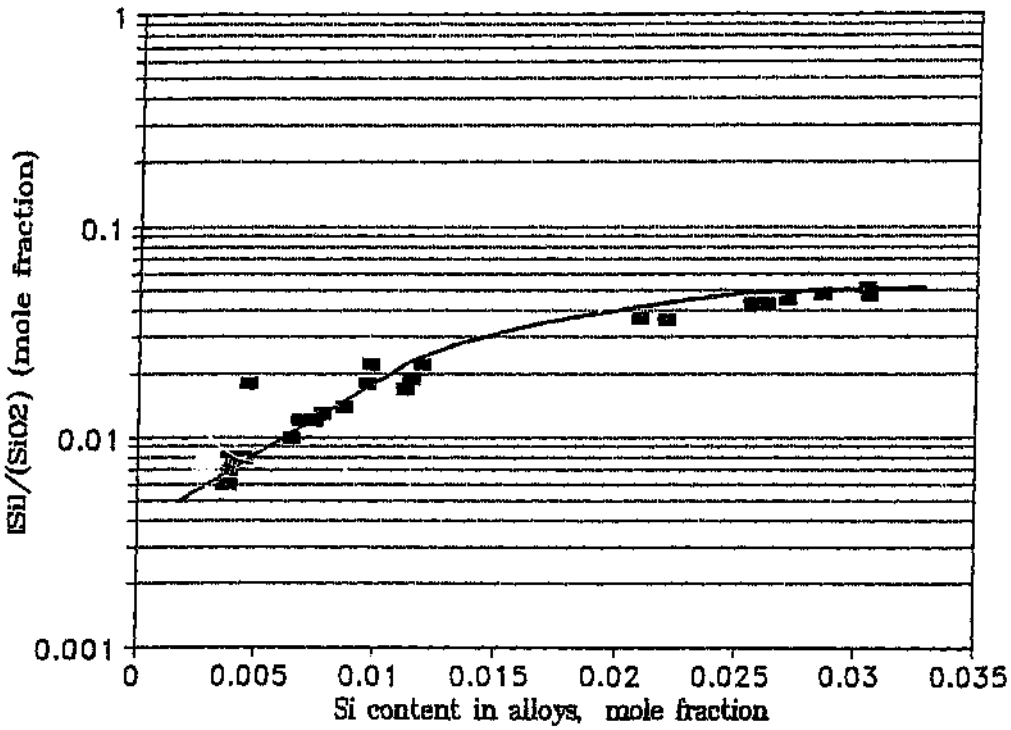


Figure 4.2.12. Effect of Si content of metal on silicon partition with metals of 0.22Cr-Fe-C-S-Si and slags of 0.01CaO-0.005Fe_2O_3-MgO-Cr_2O_3-SiO_2-Al_2O_3 in mole fraction, Al_2O_3/MgO=1.7, in silica crucibles at 1580°C at 0.034 Pco.

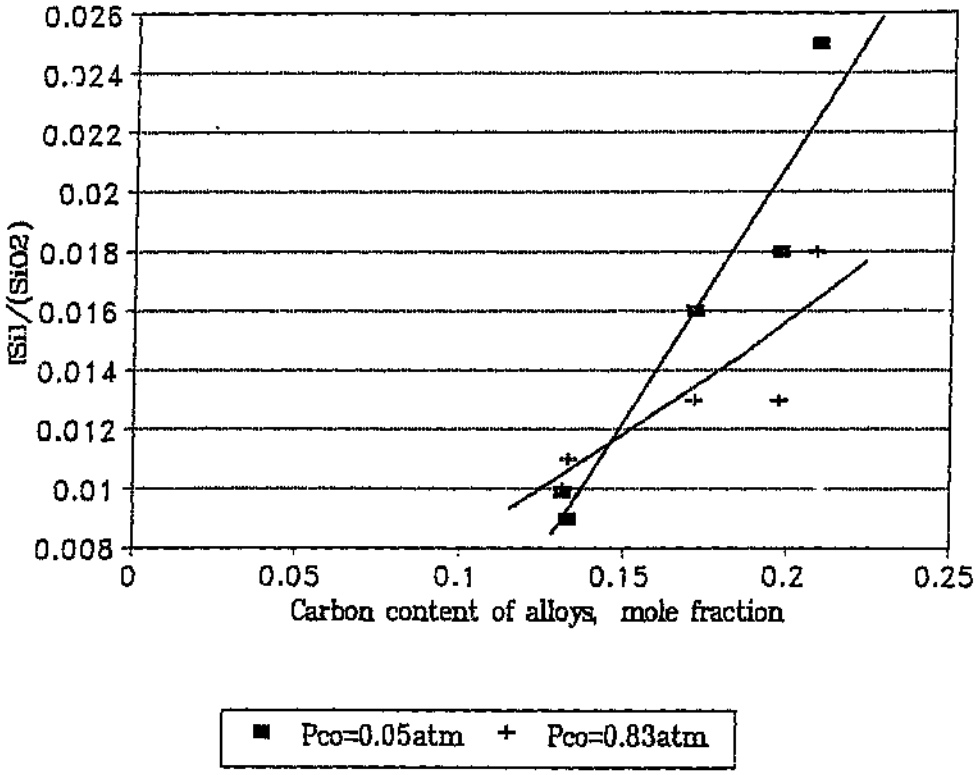


Figure 4.2.13. Effect of C content of metal on silicon partition with metals of 0.55Cr-Fe-C-S-Si and slags of 0.01CaO-0.005Fe_2O_3-MgO-Cr_2O_3-SiO_2-Al_2O_3 in mole fraction, Al_2O_3/MgO=1.7, in Cr-oxide crucibles at 1500°C.

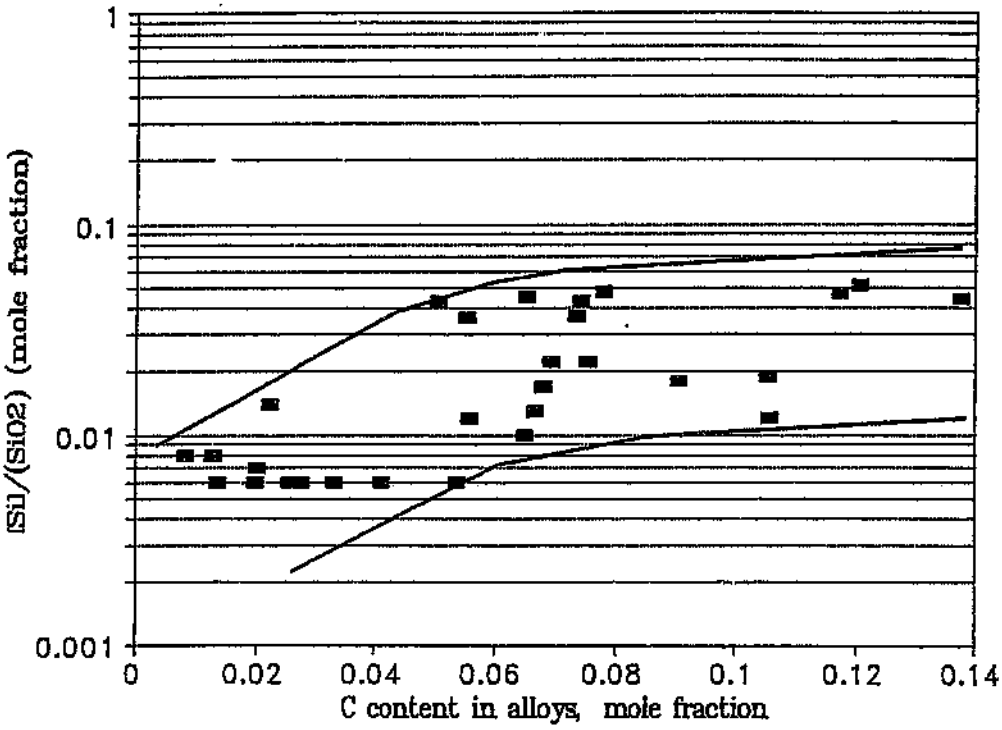


Figure 4.2.14. Effect of C content of metal on silicon partition with metals of 0.22Cr-Fe-C-S-Si and slags of 0.01CaO-0.005Fe_2O_3-MgO-Cr_2O_3-SiO_2-Al_2O_3 in mole fraction, Al_2O_3/MgO=1.7, in silica crucibles at 1580°C at 0.034 Pco.

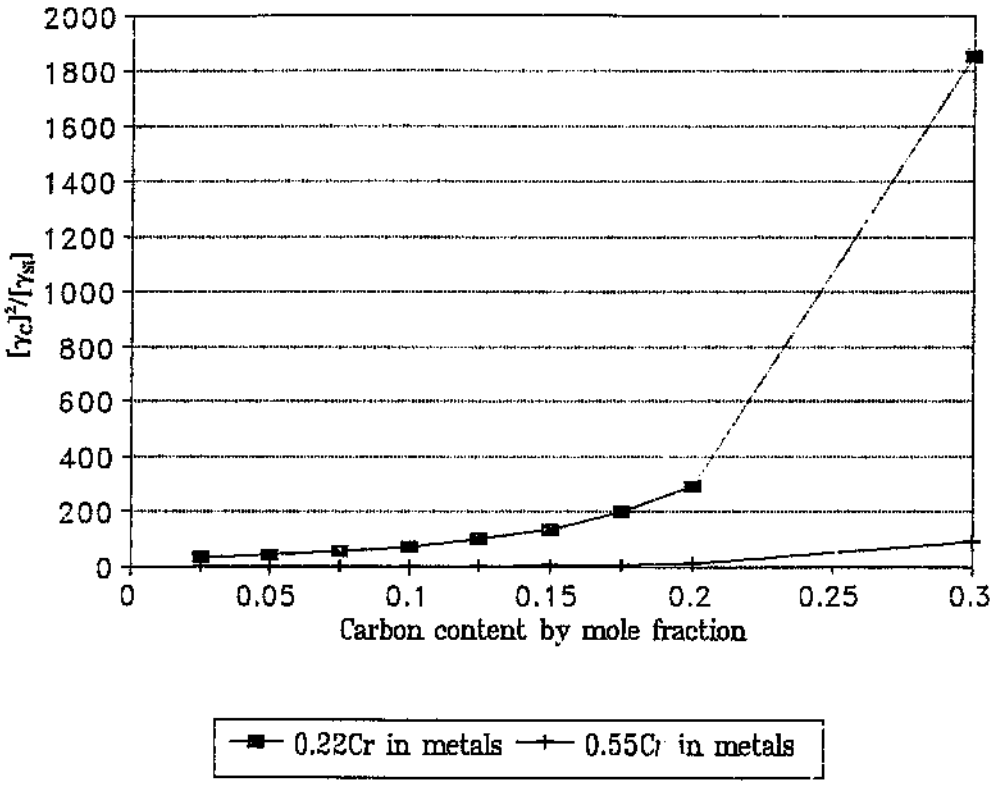


Figure 4.2.15. Effect of carbon content on the ratio of $[\gamma_C]^2/[\gamma_{Si}]$ with metals containing Cr-Fe-C-0.001S-0.005Si in mole fraction at 1550°C.

4.3. EQUILIBRIUM PARTITION OF SULPHUR BETWEEN SLAG AND METAL AT CONSTANT PARTIAL PRESSURE OF CARBON MONOXIDE

With the increasing demand for low-sulphur steels, the requirement on ferro-chromium of low sulphur content has been critical. As an important raw material of steel making like that of LC FeCr and Simplex-FeCr alloys, HC FeCr is standing in a leading position of the quality control. A great effort has been made to reduce the sulphur content in commercial production of HC FeCr alloy. Coke or coal used in smelting of HC FeCr is the greatest source of sulphur.

From the economic point of view, desulphurization in the smelting process is more important than choosing low-sulphur coke or coal to use, which are produced from quite limited reserves. It is known that there are certain relations among sulphur content and composition of both slag and alloy. The studies[108,109,110] demonstrated that when increasing silicon or/and carbon in the metal phase or increasing CaO content in the slags, sulphur content of the alloy decreases. Sulphur, however, fluctuates in most cases.

In the smelting of this grade alloy and in the refining of HC FeCr to reduce carbon and silicon, how to utilize other conditions to minimize sulphur content in the alloys is vital to produce both HC FeCr alloy and LC FeCr alloy with low sulphur content. When refining FeCr alloys by means of oxygen-blowing processes, the oxygen blown into the metal bath reacts with carbon and produces carbon monoxide extremely fast, due to the high temperature and the favourite conditions for mass transfer. The carbon monoxide produced in the reactions actually plays an important role in the gas-slag-metal equilibration relevant to both FeCr alloy smelting and refining processes.

In the practice, Ar/O2 ratio is one of the control parameters used in the refining process. The Ar/O2 ratio can be set up, if the equilibrium partial pressure of carbon monoxide in the Ar/O2 gas phase is known.

In this study, the influences of the partial pressure of carbon monoxide, metal and slag compositions on the sulphur behaviour have been investigated at 1500°C and 1580°C in Cr-oxide crucibles and silica crucibles.

A presentation based upon this part of the results was made at the 5th International Conference on Molten Slags, Fluxes and Salts '97 and a paper was published in the proceedings of the conference[111].

4.3.1. Influence of Slag and Metal Compositions on Equilibrium Distribution of Sulphur

The relationships were invested between the sulphur distribution and the contents of the most constituents in the slag and metal phases at different Pco and temperatures. The sulphur distribution is expressed by the (S)/[S] ratio by mole fraction, where round and square brackets indicate the slag and metal phase respectively. The slag contained 0 to 0.1 per cent of sulphur, 0 to 25 per cent of chromium, 10 to 60 per cent of SiO_2, 2 to 20 per cent of MgO, 10 to 30 per cent of Al_2O_3 and about 0.5 per cent of iron. The metal composition related to ferrochromium alloys was in the range of 45 to 65 per cent of chromium, 0 to 10 per cent of carbon, 0 to 5 per cent of silicon, 0 to 0.05 per cent of sulphur, and the balance iron. The metal composition relevant to stainless-steel making contained 10 to 20 per cent of chromium, 0.2 to 2.0 per cent of silicon, 0.04 to 0.4 per cent of sulphur, 0.18 to 3.5 per cent of carbon and the balance iron.

With the increase of MgO content in slags, shown in figure 4.3.1, the slags' capability of desulphurization increases. The experiments in both Cr-oxide crucible at 1500°C and silica crucible at 1580°C illustrate the same trend. The sulphur distribution ratio resulted from using Cr-oxide crucible is higher than that from the experiments conducted in silica crucibles at higher temperature. The results from experiments in Cr-oxide crucibles indicate that the distribution ratio of sulphur increases when the partial pressure of carbon monoxide is reduced from 0.83atm to 0.05atm in the MgO range of 0.17 to 0.35 by mole fraction. Figure 4.3.2 manifests the results, acquired from the experiments with alloys containing about 0.22 mole fraction of chromium at 0.034atm of partial pressure of carbon monoxide at 1580°C in silica crucibles. The results show a similar influence of MgO on the sulphur distribution ratio and have a higher distribution ratio, compared with the result illustrated in figure 4.3.1 at 0.034atm of partial pressure of carbon monoxide in silica crucibles.

The slag-metal equilibrium in terms of sulphur and oxygen species can be written as:

$$[S] + (O^{2-}) = (S^{2-}) + [O] \qquad (4.3.1)$$

where square and round brackets indicate the metal and slag phases respectively. MgO in the slag will dissociate according to:

$$(MgO) = (Mg^{2+}) + (O^{2-}) \qquad (4.3.2)$$

An increase in MgO content of the slag will increase free O^{2-} anions in the slag resulting in an increase of the activity of O^{2-} anions, which will help to shift reaction(4.3.1) to the right direction and assist sulphur remove from the metal phase.

The effect of MgO can also be explained in terms of slag basicity (B) and the sulphide

capacity (Cs).The thermodynamics of sulphur dissolved as a sulphide ion in slags may be expressed in terms of sulphide capacity of the slag, sulphur activity of the metal [a_s] and oxygen activity a_o at the slag-metal interface, according to Sharma and Richardson[92]:

$$(\%S) = Cs[a_s]/a_o \qquad (4.3.3)$$

Cs was defined from reaction (4.3.4) and was represented by equation (4.3.5):

$$1/2S_2(g) + (O^{2-}) = (S^{2-}) + 1/2O_2(g) \qquad (4.3.4)$$

$$Cs = (wt\%S)(Po_2/Ps_2)^{1/2} \qquad (4.3.5)$$

Cs is a function of several variables, such as temperature, slag composition, but mainly temperature and basicity of the slag.

By the work[83,84,85,88], the following equation was obtained:

$$\log Cs = B/A + 2.28 - 13300/T \qquad (4.3.6)$$

where:

$$B = 5.623\%CaO + 4.15\%MgO - 1.152\%SiO_2 + 1.457\%Al_2O_3$$

$$A = \%CaO + 1.391\%MgO + 1.867\%SiO_2 + 1.65\%Al_2O_3$$

An increase in MgO content of the slag will increases the B/A and thus the sulphide capacity Cs will increase as well. The relation between Cs, B/A and %MgO is annotated in figure 4.3.3 , for a slag containing 5%CaO, 20%Al_2O_3, 45%SiO_2, 0.5%Fe_2O_3, 5-25%

MgO and balance Cr_2O_3.

The impacts of slag basicity on the removal of sulphur from metal phase to slag phase have been utilized in the production of ferrochromium alloys by addition of lime or lime stone. In the report[110], sulphur content in HC FeCr alloy is reduced from 0.045 percent to 0.018 percent by adding CaO in the charge of a HC FeCr furnace from 1 percent to 10 percent by mass. However, according to the study[3], chromium content in slags will increase when CaO content increases, which is one of the reasons that the addition of lime or lime stone is limited in the production of ferrochromium alloys. That is one of the reasons that CaO content of the slag is not chosen to be experimental parameter is fixed at a low level of 1 to 2 percent by mass.

The effect of chromium oxide in the slags on sulphur distribution ratio is shown in figure 4.3.4. In general, when chromium content decreases, sulphur transfer from metal to slag declines.

This indicates that when chromium-oxide content increases in the slags, the portion of Cr_2O_3 in the slag increases, which increases the network former and consumes more free oxygen (O^{2-}) of the slag, according to the reaction:

$$(Cr_2O_3) + (MO) = (MOCr_2O_3) \qquad (4.3.7)$$

Same results have been reported recently by Xiao and Holappa's work[62,63]. In the silicate slags containing chromium oxides, The higher the chromium oxide in the slags, the lower the divalent chromium fraction and the higher trivalent chromium in the slags.

In addition, the results from the experiments conducted in Cr-oxide crucible at 1500°C illustrates higher sulphur content in the slags than that in silica crucible at 1580°C, which

even has more favourable condition for desulphurization according to the effect of temperature on sulphide capacity expressed in equation (4.3.6). The sulphur partition ratio, furthermore, is increased by decreasing the partial pressure of carbon monoxide.

The result achieved in the experiments with the alloys of 0.22 mole fraction of chromium shown in figure 4.3.5 demonstrates that the sulphur partition between slag and metal decreases from about 1.0 to 0.15 when the mole fraction of chromium increases from 0.025 to 0.075 in the slag. The sulphur distribution ratio only decreases slightly with the increase of chromium from 0.08 to 0.25. The sulphur distribution ratio of the alloys of 0.22 mole fraction has a higher values than that of the alloys containing higher chromium shown in figure 4.3.4.

The effect of the Al_2O_3 in slag on the partition ratio of sulphur is shown in figure 4.3.6. The (S)/[S] ratio decreases slightly with increasing Al_2O_3 content in the slags. It appears that part of the alumina in the slags acts as network former and reacts with oxygen ions in reaction (4.3.8), which reduces the free oxygen in the slag.

$$(Al_2O_3) + (O^{2-}) = 2(AlO_2^-) \qquad (4.3.8)$$

The results obtained by using Cr-oxide crucibles have more sulphur in the slags than those obtained by using silica crucibles. Changing the partial pressure of carbon monoxide has little effect. A similar influence of slag's alumina on the sulphur distribution has been obtained in the experiments conducted in silica crucibles with the metals of 0.22 mole fraction of chromium at 0.034atm of partial pressure of carbon monoxide, as shown in figure 4.3.7. The sulphur distribution ratio is inversely proportional to the mole fraction of alumina in the slag phase. A decrease of the sulphur partition from 0.15 to 0.045 takes place when the mole fraction of alumina increases

from about 0.07 to 0.16.

The effect of silica content of the slags on the thermodynamic partition of sulphur is shown in figure 4.3.8. The results from those experiments at 0.83atm of the partial pressure of carbon monoxide show a nearly constant ratio of sulphur when SiO_2 content changes from 0.3 to 0.45 and an increase with increasing silica in the range of 0.45 to 0.6.

Moreover, results from the experiments at lower partial pressure of carbon monoxide in both Cr-crucible and silica crucible illustrate a remarkable decline with the increase of silica content in slags. In addition, the effect of silica on the sulphur partition, illustrated in figure 4.3.9, seems very little in the range of 0.54 to 0.66 of silica in the slags by mole fraction.

From the view-point of basicity, the equilibrium distribution of sulphur between slag and metal , expressed by equation (4.3.9) from reaction (4.3.1), increases with increasing activity of free oxygen ions O^{2-} in the slags, or with decreasing activity of oxygen dissolved in the metals.

$$[S] + (O^{2-}) = (S^{2-}) + [O] \qquad (4.3.1)$$

$$(X_S)/[X_S] = K_{4.3.1}\{(a_{O^{2-}})/[a_O]\}*\{[\gamma_S]/(\gamma_S)\} \qquad (4.3.9)$$

Increasing SiO_2 content of the slag results in decreasing oxygen ions by the reactions like the one expressed in equation (4.3.10). More and more free oxygen ions will be consumed by adding silica into the slags when the slags contain lower SiO_2(about 0.45 by mole fraction).

$$(SiO_2) + 2(O^{2-}) = 2(SiO_4^{4-}) \qquad (4.3.10)$$

When the slags possess more than 0.45 mole fraction of SiO_2, the free oxygen ion in the slag may reach a so low level that they do not change a lot with the increase of SiO_2 in the slags. Meanwhile, the silicon content and the oxygen content of the metals increase with increasing SiO_2 in the slags according to reaction (4.3.11).

$$1/2[Si] + [O] = 1/2(SiO_2) \qquad (4.3.11)$$

Increasing silicon content of the metal will increase the activity coefficient of sulphur in metal phase(more details will be discussed in the next section) and will increase the sulphur partition ratio. On the other hand, increasing dissolved oxygen in the metal phase will help reduce the ratio of sulphur according to reaction (4.3.1).

4.3.2. Influence of Metal Composition on Equilibrium Partition of Sulphur

The effects of the metal composition, namely C, Cr, Si, on the equilibrium partition of sulphur are illustrated in figure 4.3.10, 4.3.11, 4 3.12 respectively. In general the (S)/[S] ratio decreases with increasing chromium of metal phase. A lower partial pressure of carbon monoxide helps to move sulphur from metal phase to slag phase.

Carbon is the only element that enhances the equilibrium distribution of sulphur with the increase of its content in the metal phase, seen in figure 4.3.10. At high carbon content (say higher than 0.15), the effect of carbon can be strengthened greatly by lowering the partial pressure of carbon monoxide from 0.83atm to 0.05atm. When slag phase contains more silica due to the use of silica crucibles, the effects of carbon and partial pressure of carbon monoxide on the sulphur partition dwindles. While at a low level of carbon where carbon content is less than 0.15, the effect of partial pressure of carbon monoxide on the sulphur partition diminishes.

Figure 4.3.11 demonstrates that the sulphur partition decreases with the increase of chromium content in the slag phase, specifically when chromium content of the slag is less than 0.45 mole fraction. A lower partial pressure of carbon monoxide increases the sulphur ration. Figure 4.3.12 shows the relationship between silicon and sulphur partition ratio. In the range of less 0.02 molar fraction of silicon, the sulphur distribution decreases when silicon content increases. A lower partial pressure of carbon monoxide also increases the sulphur distribution ration.

Figure 4.3.13, 4.3.14 show the influences of carbon and silicon of the metal phase on the partition ratio of sulphur from those experiments, carried out in silica crucibles at 1580°C at 0.034atm of partial pressure of carbon monoxide with the metals containing 0.15 mole fraction of chromium. The results are quietly similar to those results illustrated in figure

4.3.10 and 4.3.12.

According to the sulphur distribution between slag and metal, expressed in reaction (4.3.1) and equation (4.3.9), the factors, which decrease the activity or the concentration of oxygen and increase the activity coefficient of sulphur in the metal, promote the partition ratio of sulphur between slag and metal. The content of carbon, chromium and silicon are typical those factors for ferro-chromium alloys:

$$(O^{2-}) + [S] = (S^{2-}) + [O] \qquad (4.3.1)$$

$$(X_S)/[X_S] = K_{4.3.1}\{(a_{O2-})/[a_O]\}^*\{[\gamma_s]/(\gamma_s)\} \qquad (4.3.9)$$

According to the equation of activity coefficient of sulphur and oxygen in terms of the interaction coefficients $E_i^{j\ [105,106]}$, as expressed in equations (4.3.12) and (4.3.13), the increase of carbon and silicon in the metals can lower the activity coefficient of oxygen of the metals and can increase the activity coefficient of sulphur of the metals and in contrary the contents of chromium and sulphur in the metal phase will reduce the activity coefficient of sulphur.

$$\ln \gamma_s = 6.45(X_C) + 7.76(X_{Si}) - 3.3(X_S) - 2.23(X_{Cr}) \qquad (4.3.12)$$

$$\ln \gamma_o = -22(X_C) - 8.5(X_{Cr}) - 17(X_S) - 15(X_{Si}) \qquad (4.3.13)$$

From reaction (4.3.1) and equation (4.3.9) and reaction (4.3.11), the following expression could be drawn:

$$(S^{2-})/[S] = \{K_{4.3.1}K_{4.3.11}\}\{[\gamma_s]/(\gamma_s)\}\{[\gamma_{Si}]/(\gamma_{SiO2})\}^{1/2}\{[X_{Si}]/(X_{SiO2})\}^{1/2}\{a_{(O2-)}\} \qquad (4.3.14)$$

When silicon content of metals (X_{Si}) increases, the activity coefficients of both silicon and sulphur of metal phase increase, which results in an enlargement of the values of $([\gamma si]^{1/2}[Xsi]^{1/2}\gamma s)$, as shown in figure 4.3.15 and 4.3.16. But the value of $([\gamma si]^{1/2}[Xsi]^{1/2}\gamma s)$ increases extremely slow when silica content is less than 0.02 in mole fraction, which means that the enhancement of silicon does not effectively increase sulphur distribution at low silicon level.

On another hand, when silicon of the metal phase rises, the silica content of the slag phase in equilibrium with the silicon will increase as well, as shown in the work done by Fulton and Chipman[107] in figure 4.2.4. The increase of silica will decrease the free oxygen (O^{2-}) in the slag dramatically, especially when silicon and silica are at a low levels. For instance, when one mole of silicon enters into slags in the form of (SiO_2), two moles of free oxygen in terms of O^{2-} will be consumed by the following reaction at low silica slags:

$$(SiO_2) + 2(O^{2-}) = (SiO_4^{4-}) \qquad (4.3.15)$$

The free oxygen in slag phase decreases tremendously fast with the increase of silicon ions. It may reach a minimum level, on which the content of the free oxygen does not change remarkably. More and more silicon ions reduce the number of oxygen they have and share the fixed oxygen each other in the silicon network in the slags.

Therefore, the comprehensive effects of slags and metals on the sulphur partition may make the partition decline with the increase of silicon at low content level. On one hand, the effects of slags, caused by increasing silicon content, on the sulphur distribution will become smaller at higher silica content, which may result in a promotion of the sulphur distribution due to the contribution of silicon to increasing the term of $([\gamma si]^{1/2}[Xsi]^{1/2}\gamma s)$ in the metal phase.

On the other hand, the sulphur partition between slag phase and metal phase could escalate extremely fast with the increase of silicon content in the metal phase at high level of silicon content, as a result of the increased value of $([\gamma si]^{1/2}[Xsi]^{1/2}\gamma s)$ and insensitively changing the activity of free oxygen in the slag phase. It has been recognised and utilised widely in the production of ferrochromium alloys that more effective removal of sulphur from ferrochromium alloys could be materialized to the metals with a higher carbon content or/and a higher silicon content[110].

By the combination of reaction (4.3.1) and (4.3.16), the sulphur partition between slag and metal is determined by the activity of free oxygen, activity of carbon and partial pressure of carbon monoxide, as expressed by equation (4.3.17):

$$(O^{2-}) + [S] = (S^{2-}) + [O] \qquad (4.3.1)$$

$$[C] + [O] = CO \qquad (4.3.16)$$

$$(Xs)/[Xs] = \{K_{4.3.1}(a_{O2-})\} * \{[\gamma_s]/(\gamma_s)\} * \{K_{4.3.15}[ac]/Pco\} \qquad (4.3.17)$$

The effect of carbon content on the equilibrium partition ratio of sulphur can be undertaken mainly by remarkably varying the activity of carbon and the activity coefficient of sulphur in the metal phase. The activity coefficients of carbon and sulphur, expressed in equation 4.3.18 and 4.3.12 in terms of interaction coefficients E_i^j [105,106], can be increased by the increase of carbon content in the metal phase.

$$\ln\gamma_c = -0.562 + 7.8(X_C) + 9.72(X_{Si}) + 6.45(X_S) - 5.1(X_{Cr}) + 11.18(X_C)^2 - 0.115(X_{Cr})^2 + (X_{Si})^2 + 3.06(X_C X_{Cr}) + (X_C X_{Si}) \qquad (4.3.18)$$

Despite the inadequate information about (γ_s) and the activity of free oxygen ion in slags, an increase of sulphur removal from metals to slags can be achieved by enhancing the

contents of carbon, combined with lowering the partial pressure of carbon monoxide in the gas phase at certain temperature. In addition, the slag with a high free-oxygen activity, and the metal with a high carbon activity and high activity coefficient of sulphur, can enhance the desulphurisation of metals. The activity of free oxygen ion and the activity coefficient of sulphur in slag phase are related to the composition of slags, largely dependent upon the basicity of slags determined commonly by a ratio of network-breaker oxides to network-former oxides.

Higher content of carbon in the metal phase enhances the activity coefficients of carbon and sulphur, leading to a higher sulphur partition. Higher chromium content reduces activity coefficients of carbon and sulphur, resulting in a lower value of sulphur distribution ratio.

4.3.3. Influence of Partial Pressure of Carbon monoxide Phase

All the experimental results discussed above illustrate that an increase of the equilibrium partition ratio of sulphur can be achieved by means of reducing the partial pressure of carbon monoxide in gas phase. The effect of partial pressure of carbon monoxide will be more effective when combined with a higher content of carbon and a higher basicity of slags.

The effect of partial pressure of carbon monoxide on sulphur distribution ratio is similar to the treatment of vacuum. As far as the desulphurisation is concerned, under vacuum or in a gas phase where the partial pressure of sulphur is very low, sulphur will transfer from metal phase to the gas, according to Sievert's law expressed by reaction (4.3.19) and equation (4.3.20). The solubility of sulphur gas in metal varies with temperature, and metal composition.

$$[S] = 1/2\ S_2(gas) \qquad (4.3.19)$$

$$[Xs] = (P_{S_2})^{1/2}/\{K_{14}\,[\gamma_s]\} \qquad (4.3.20)$$

When reducing the partial pressure of carbon monoxide, the concentration of elements in both metal phase and slag phase changes, particularly oxygen and carbon, silicon, and chromium, through the following reactions:

$$[C] + [O] = CO \qquad (4.3.16)$$

$$2[C] + (SiO_2) = [Si] + 2CO \qquad (4.3.21)$$

$$[C] + (Cr_2O_3) = 2(CrO) + CO \qquad (4.3.22)$$

$$[C] + (CrO) = [Cr] + CO \qquad (4.3.23)$$

$$[Si] + 2(CrO) = 2[Cr] + (SiO_2) \qquad (4.3.24)$$

The effect of the partial pressure of carbon monoxide on the equilibrium partition of sulphur, as discussed above, is through by changing the compositions of both the metal and the slag phase, which effect the activities of the free oxygen ion in slags and the dissolved oxygen in metals, as expressed by reaction (4.3.1) and equation (4.3.9). In the system involved with reaction (4.3.16), a decrease of partial pressure of carbon monoxide will decrease the dissolved oxygen [O] content in the metal phase and in turn it will increase the sulphur distribution ratio.

In general those factors, which reduce the content and activity coefficient of dissolved oxygen of the metals and reduce the activity coefficient of sulphur in the slags, and those conditions, which help increase the content and activity coefficient of free oxygen ion in the slags and increase the activity coefficient of sulphur in the metal phase, will result in a promotion of the distribution ratio of sulphur between slags and metals.

It can be shown that, by combining reaction (4.3.1), and (4.3.16), the (S)/[S] ratio is proportional to the factor of ($[\gamma_s][\gamma_c][X_C]/P_{CO}$) at a given temperature with same slag:

$$(X_S)/[X_S] = K'_{4.3.25} * \{[\gamma_s][\gamma_c][X_C]/P_{CO}\} \qquad (4.3.25)$$

Where $K'_{4.3.25}$ is a constant, determined by temperatures and slag composition. Those factors, which can increase the term of ($[\gamma_s][\gamma_c]$), will increase the equilibrium partition ratio of sulphur, leading to an increase of sulphur removal from metal phase to slag phase. The effects of chromium, carbon and silicon on the activity coefficients of carbon and sulphur in terms of ($[\gamma_s]$), ($[\gamma_c]$) and ($[\gamma_s][\gamma_c]$) are shown in figure 4.3.17, 4.3.18 and 4.3.19.

It is known that chromium in slags, like any of the transition metal ions, can change its valency in accordance with the oxidation conditions and the compositions of slags. In current study it is found that a higher percentage of CrO exists in the slags when a lower partial pressure of carbon monoxide is imposed in figure 4.4.4 (the details can be seen in Section 4.4.1 entitled Chromium in the Slag Phase). The reaction at the slag/metal interface can be expressed as the following:

$$(CrO_{1.5}) = (CrO) + \tfrac{1}{2}[O] \qquad (4.3.26)$$

$$K_{4.3.26} = \{[a_o](a_{CrO})/(a_{CrO1.5})\} \qquad (4.3.27)$$

A higher portion of CrO in the slag due to a lower pe.tial pressure of carbon monoxide means a lower oxygen activity in the metal phase, which means in turn a higher sulphur distribution ratio between slag and metal according to the reaction (4.3.1) and equation (4.3.2). The change in the activity coefficients of chromium in the slag for the above reaction could be very small because no change in the slag composition takes place except the ratio of CrO to $CrO_{1.5}$.

As far as the practical desulphuration is concerned in the production processes, those treatments combined with lower partial pressure of carbon monoxide, such as VOD and AOD, are favourable to remove sulphur from metal phase to slag phase. It can be more efficient with the slags of higher basicity at the beginning period of ferrochromium refining by using the advantages of higher carbon content and higher silicon content. The attention lays on the forming of high-basicity slags as soon as possible in the initial period of ferrochromium refining.

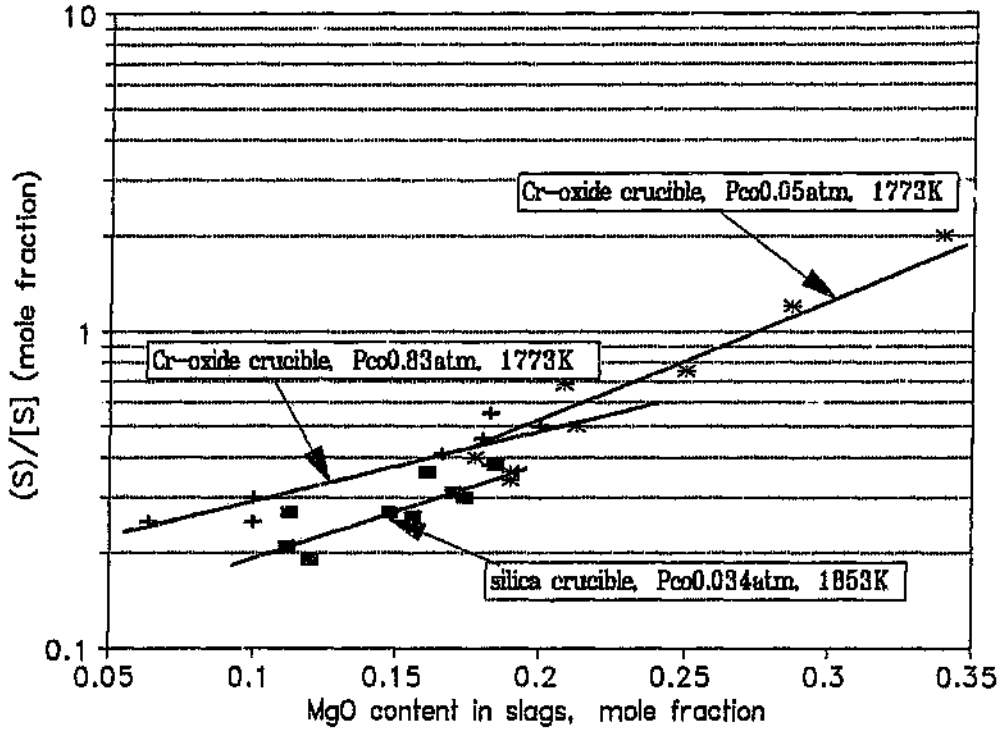


Figure 4.3.1. Effect of MgO on the distributions of sulphur with metals of 0.55Cr-C-Fe-S-Si and slags of 0.01CaO-Fe_2O_3-MgO-Cr_2O_3-SiO_2-Al_2O_3, Al_2O_3/MgO=1.7, 0.03-0.05/0.02-0.1 Si in Cr/Si oxide crucibles at 1500°C/1580°C.

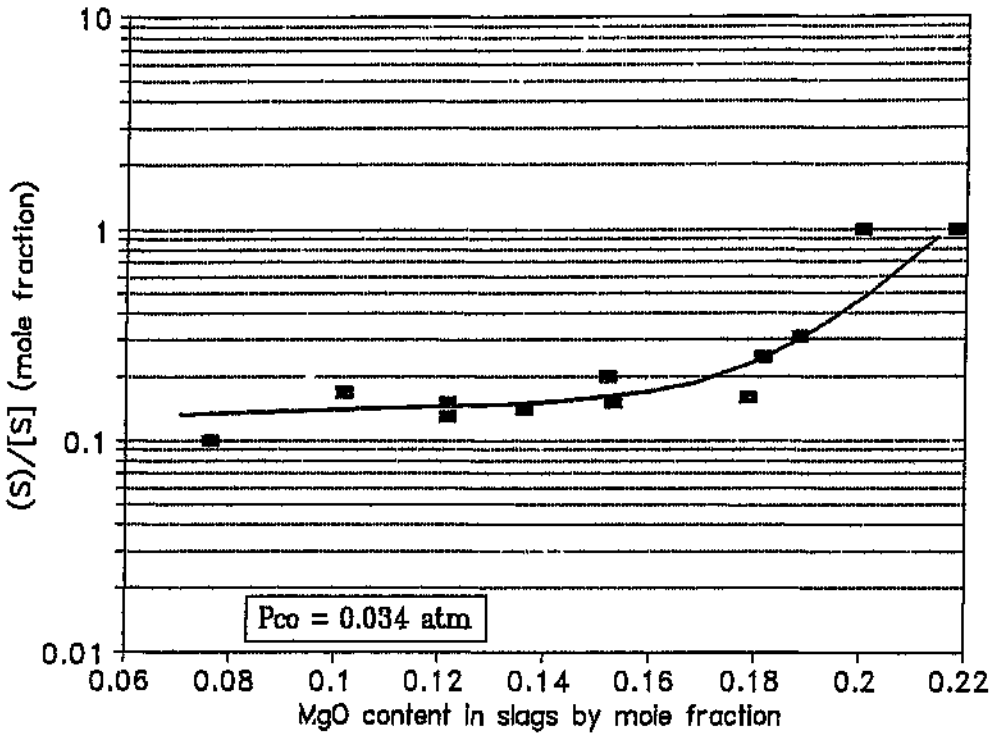


Figure 4.3.2. Effect of MgO on the distributions of sulphur with metals of 0.22Cr-C-Fe-S-Si and slags of 0.01CaO-Fe_2O_3-MgO-Cr_2O_3-SiO_2-Al_2O_3, Al_2O_3/MgO=1.7, 0.02-0.1 Si in metals, in SiO_2 crucibles at 1580°C at 0.034 Pco.

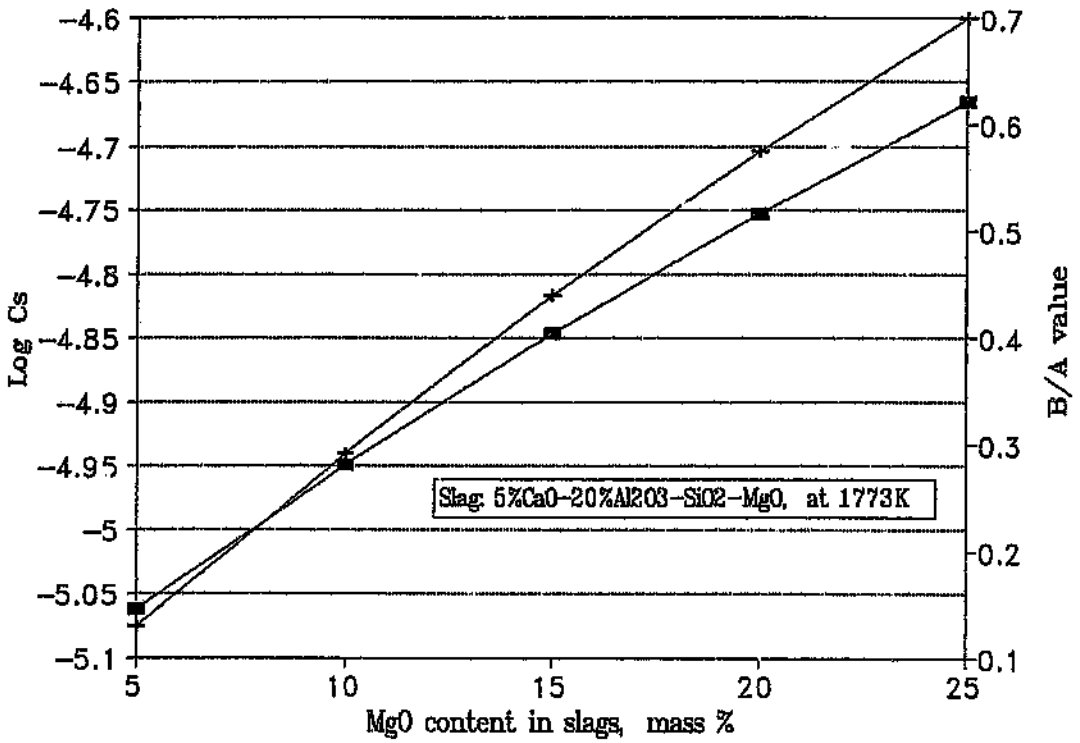


Figure 4.3.3. Relationships between MgO and sulphide capacity Cs at 1500°C with slag containing 5%CaO, 20%Al_2O_3, 45%SiO_2, 0.5%Fe_2O_3, MgO and Cr_2O_3

■ --- B/A value
\+ --- Log Cs

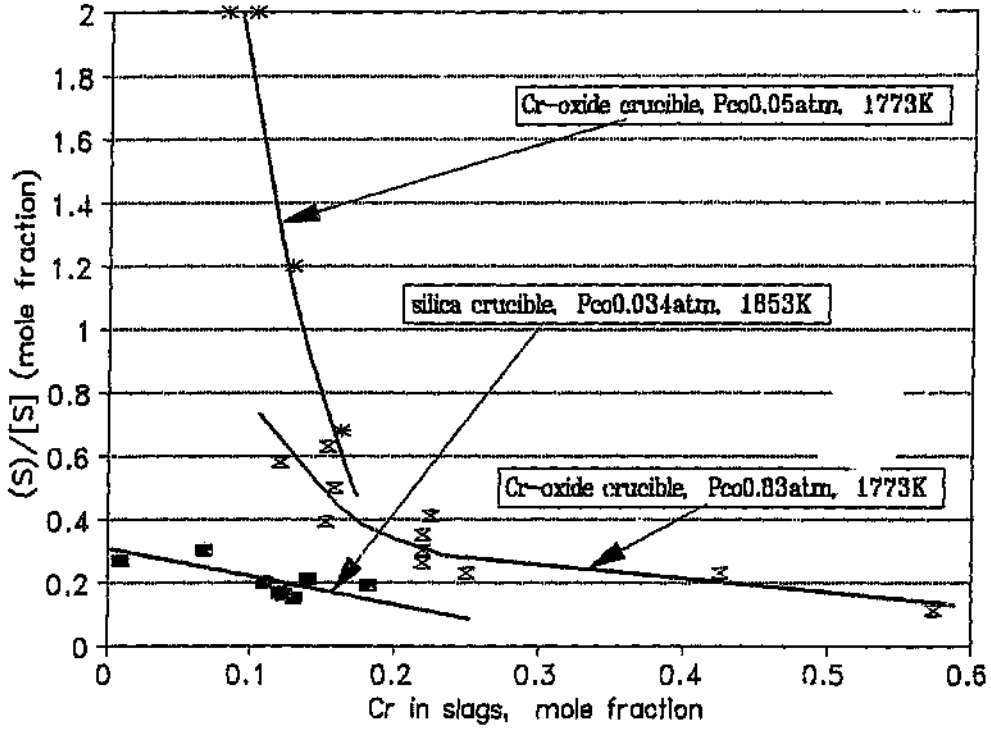


Figure 4.3.4. Effect of Cr of slags on the distributions of sulphur with metals of 0.55Cr-C-Fe-S-Si and slags of 0.01CaO-Fe_2O_3-MgO-Cr_2O_3-SiO_2-Al_2O_3, Al_2O_3/MgO=1.7, 0.03-0.05/0.02-0.1 Si in Cr/Si oxide crucibles at 1500°C/1580°.

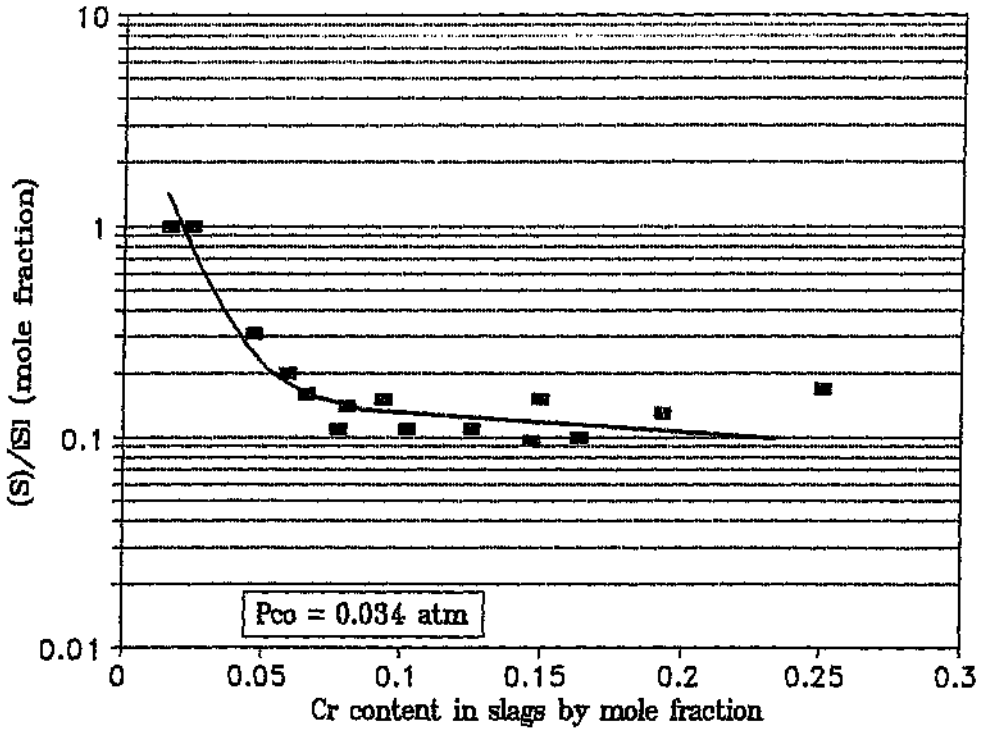


Figure 4.3.5. Effect of Cr of slags on the distributions of sulphur with metals of 0.22Cr-C-Fe-S-Si and slags of 0.01CaO-Fe_2O_3-MgO-Cr_2O_3-SiO_2-Al_2O_3, Al_2O_3/MgO=1.7, 0.02-0.1 Si in Si-oxide crucibles at 1580°C at 0.034 Pco.

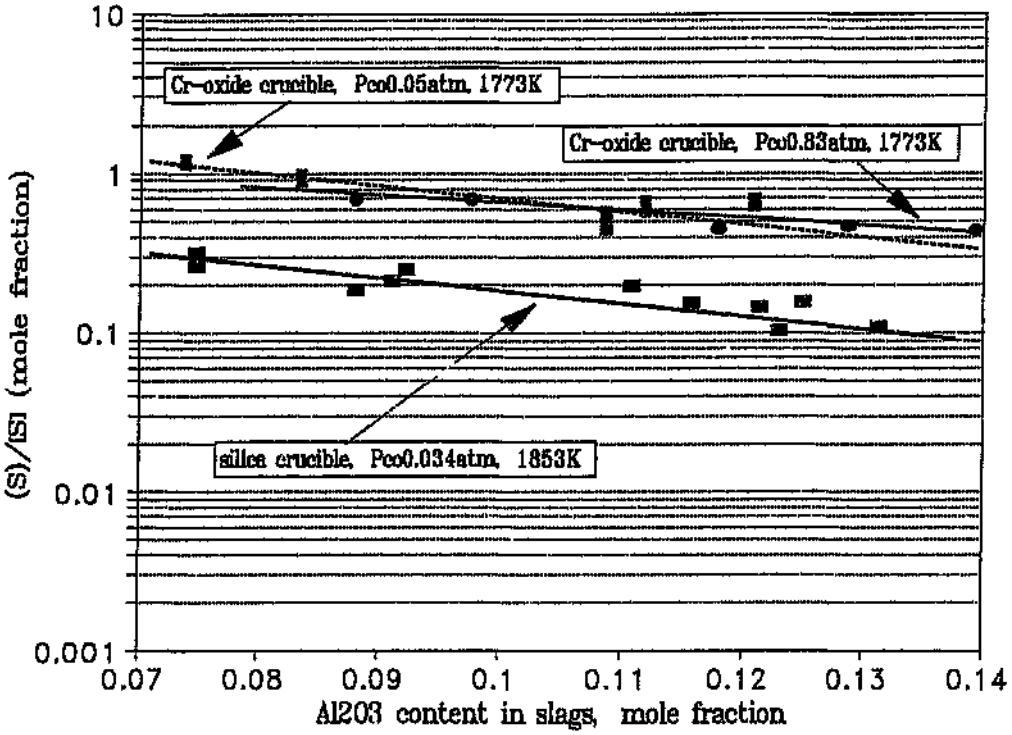


Figure 4.3.6. Effect of Al2O3 on partition of sulphur with metals of 0.55Cr-Fe-C-S-Si and slags of 0.01CaO-Fe2O3-MgO-Cr2O3-SiO2-Al2O3, Al2O3/MgO=1.7, 0.03-0.05/0.02-0.1 Si in Cr/Si oxide crucibles at 1500°C/1580°C.

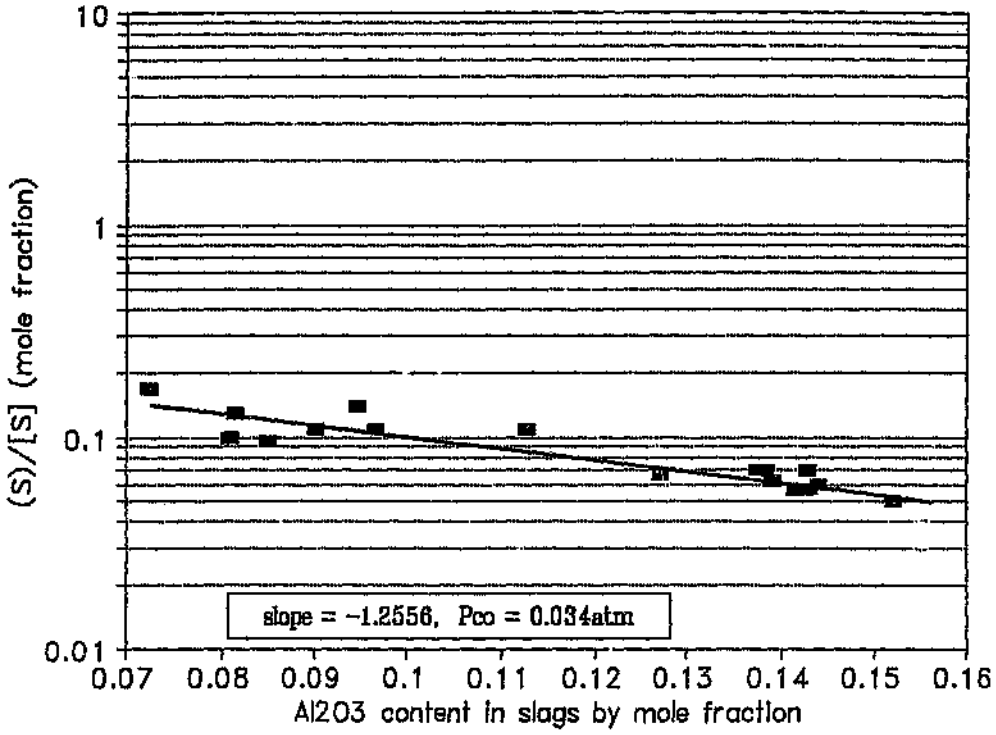


Figure 4.3.7. Effect of Al_2O_3 on partition of sulphur with metals of 0.22Cr-Fe-C-S-Si and slags of 0.01CaO-Fe_2O_3-MgO-Cr_2O_3-SiO_2-Al_2O_3, Al_2O_3/MgO=1.7, 0.02-0.1 Si in Si-oxide crucibles at 1580°C at 0.034 Pco.

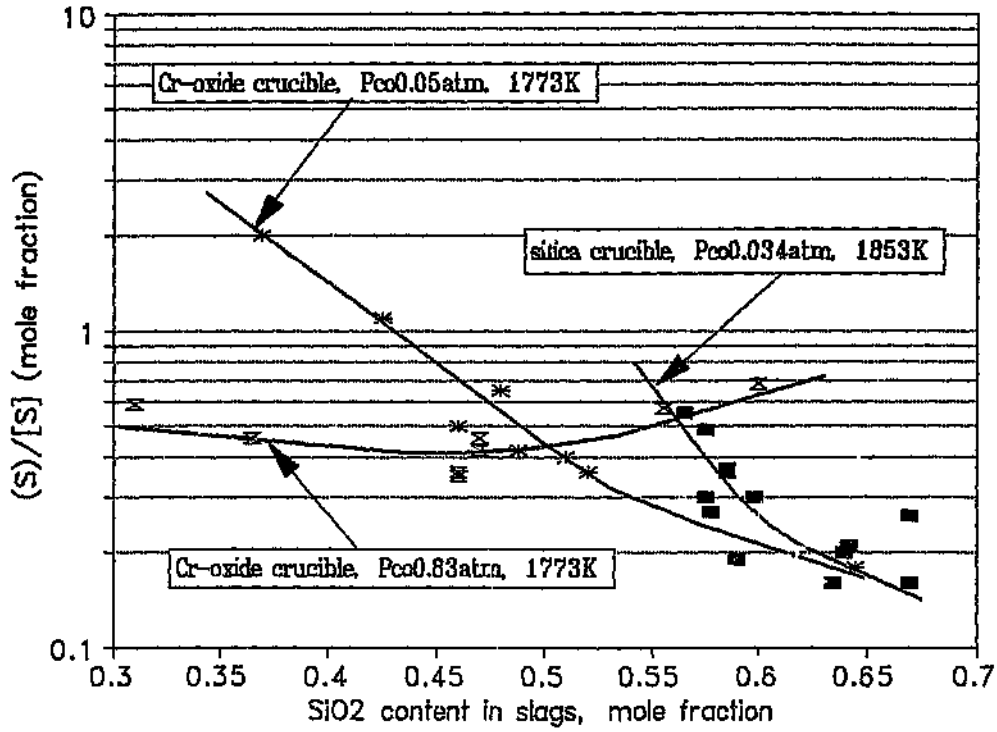


Figure 4.3.8. Effect of SiO_2 on the distribution of sulphur with metals of 0.55Cr-Fe-C-S-Si and slags of 0.01CaO-Fe_2O_3-MgO-Cr_2O_3-SiO_2-Al_2O_3, Al_2O_3/MgO=1.7, 0.03-0.05/0.02-0.1 Si in Cr/Si oxide crucibles at 1500°C/1580°C.

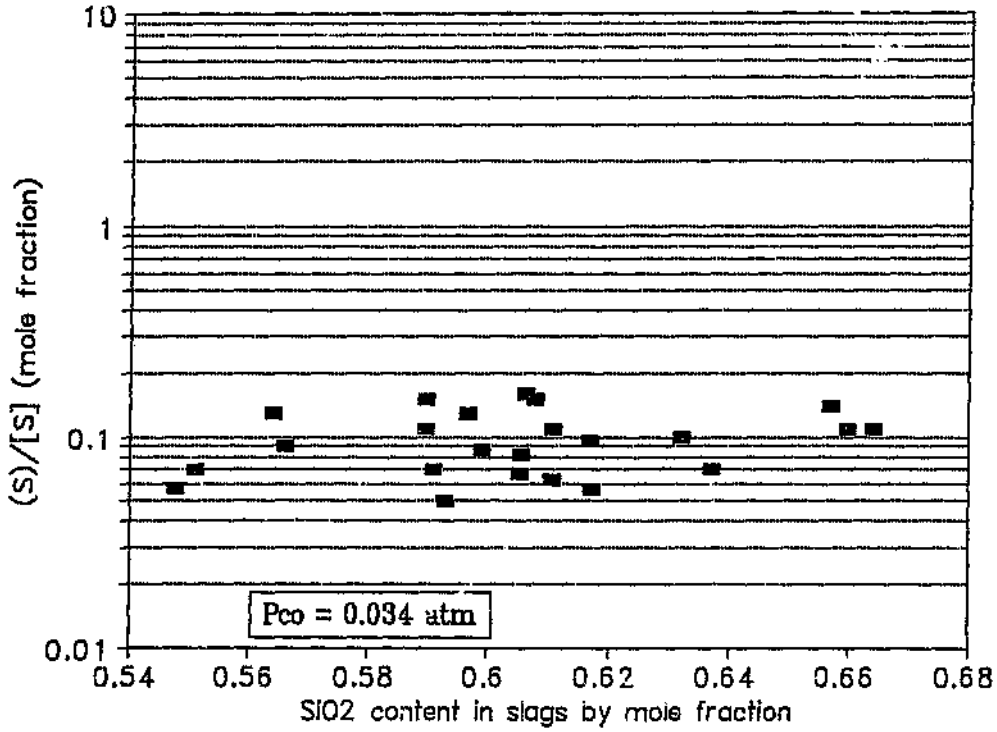


Figure 4.3.9. Effect of SiO_2 on the distribution of sulphur with metals of 0.22Cr-Fe-C-S-Si and slags of 0.01CaO-Fe_2O_3-MgO-Cr_2O_3-SiO_2-Al_2O_3, Al_2O_3/MgO=1.7, 0.02-0.1 Si in Si-oxide crucibles at 1580°C at 0.034 Pco.

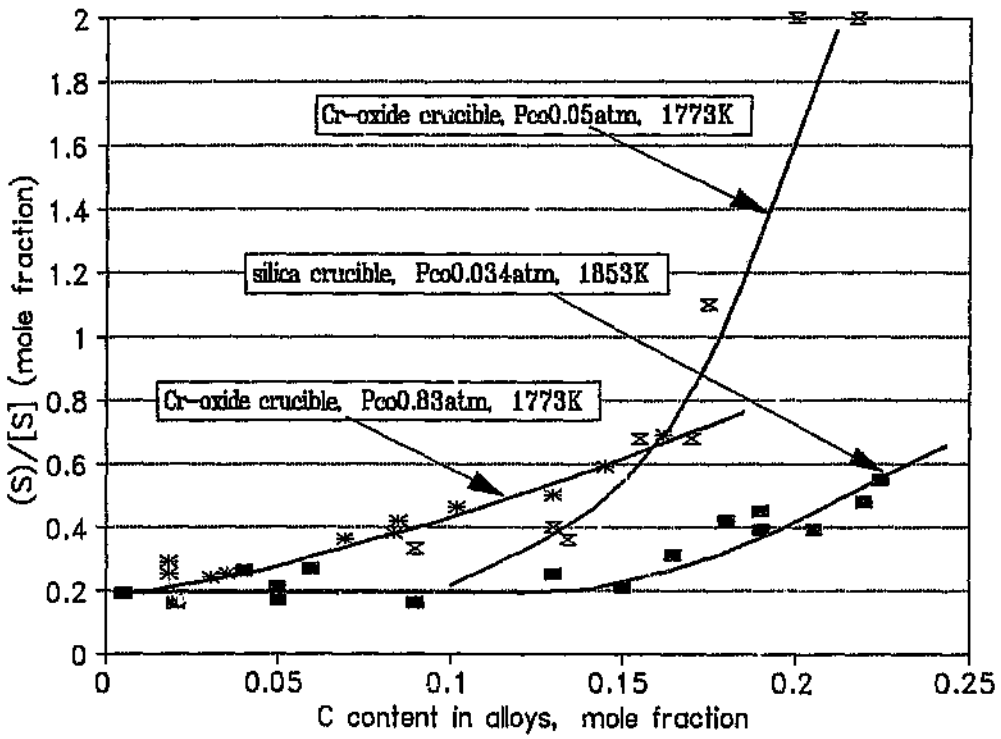


Figure 4.3.10. Effect of [C] on the distribution of sulphur with metals of 0.55Cr-Fe-C-S-Si and slags of 0.01CaO-Fe_2O_3-MgO-Cr_2O_3-SiO_2-Al_2O_3, Al_2O_3/MgO=1.7, 0.03-0.05/0.02-0.1 Si in Cr/Si oxide crucibles.

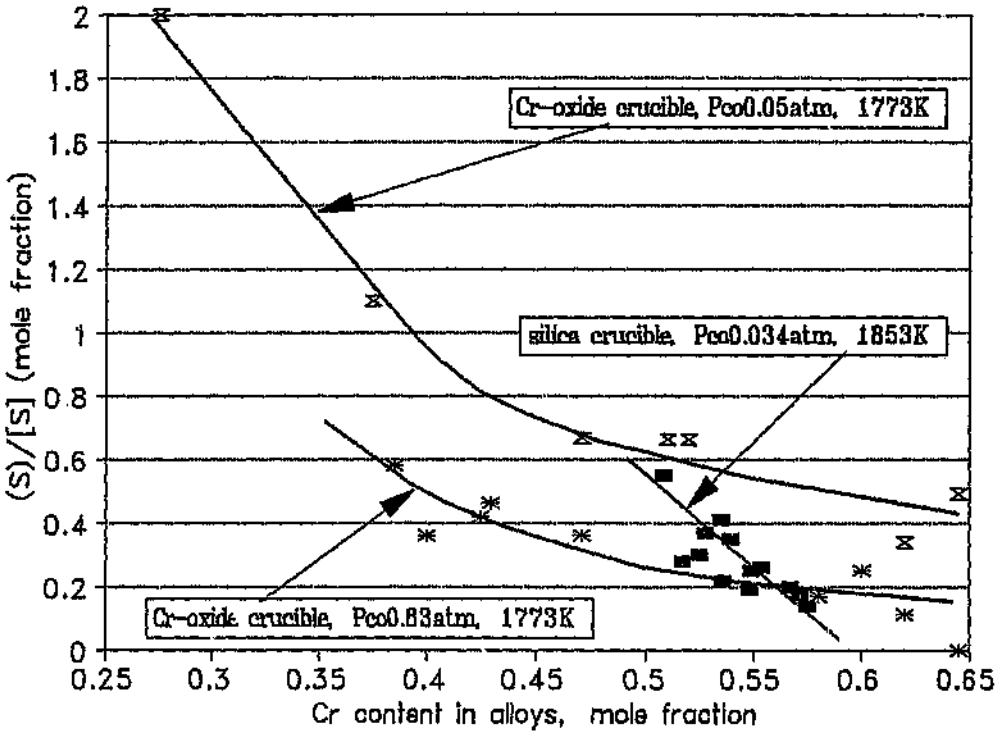


Figure 4.3.11. Effect of [Cr] on the distribution of sulphur with metals of Cr-Fe-C-S-Si and slags of 0.01CaO-Fe_2O_3-MgO-Cr_2O_3-SiO_2-Al_2O_3, Al_2O_3/MgO=1.7, 0.03-0.05/0.02-0.1 Si in Cr/Si oxide crucibles at 1500°C/1580°C.

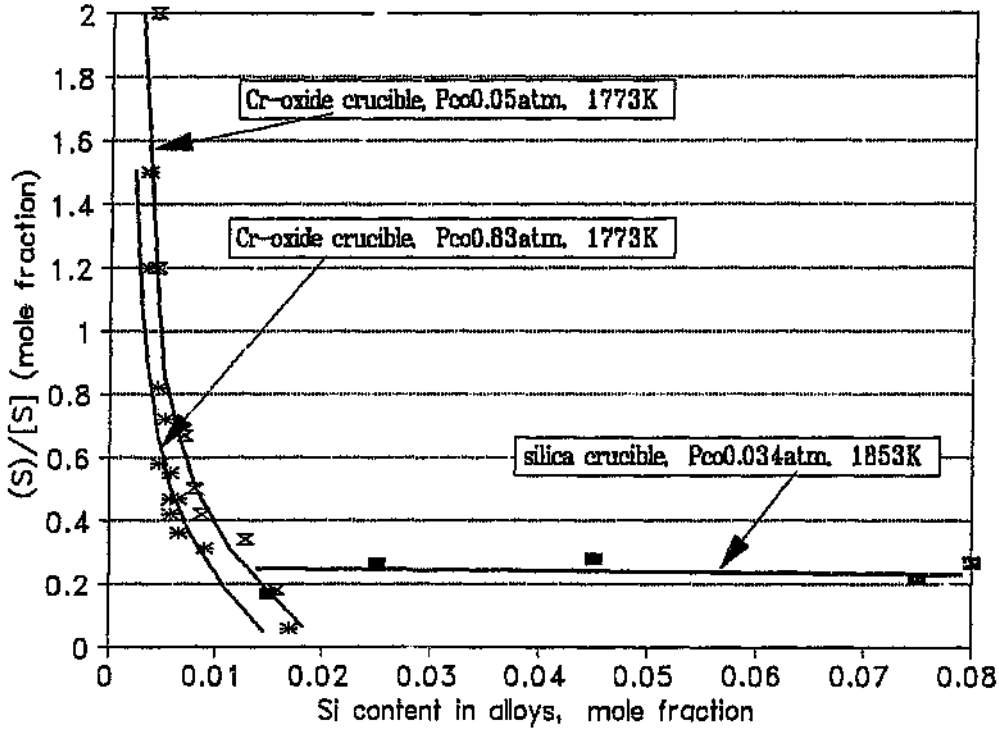


Figure 4.3.12. Effect of [Si] on the distribution of sulphur with metal of 0.55Cr-Fe-C-S-Si and slags of 0.01CaO-0.007Fe_2O_3-MgO-Cr_2O_3-SiO_2-Al_2O_3, Al_2O_3/MgO=1.7.

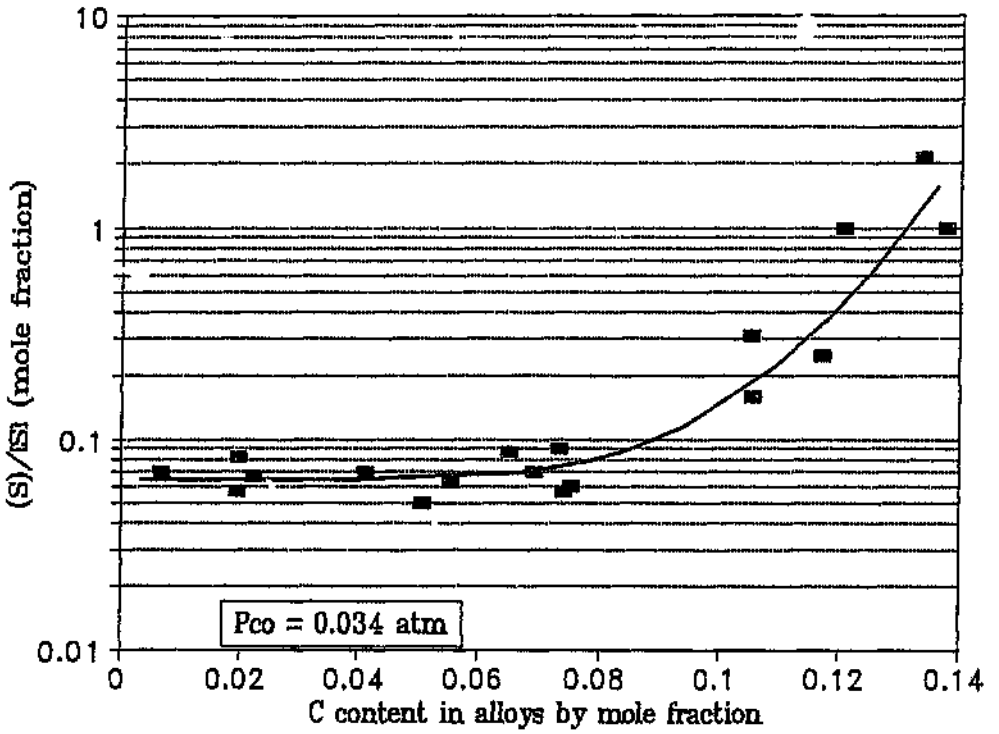


Figure 4.3.13. Effect of [C] on the distribution of sulphur with metals of 0.22Cr-Fe-C-S-Si and slags of 0.01CaO-Fe_2O_3-MgO-Cr_2O_3-SiO_2-Al_2O_3, Al_2O_3/MgO=1.7, 0.02-0.1 Si in Si-oxide crucibles at 1580°C at 0.034 Pco.

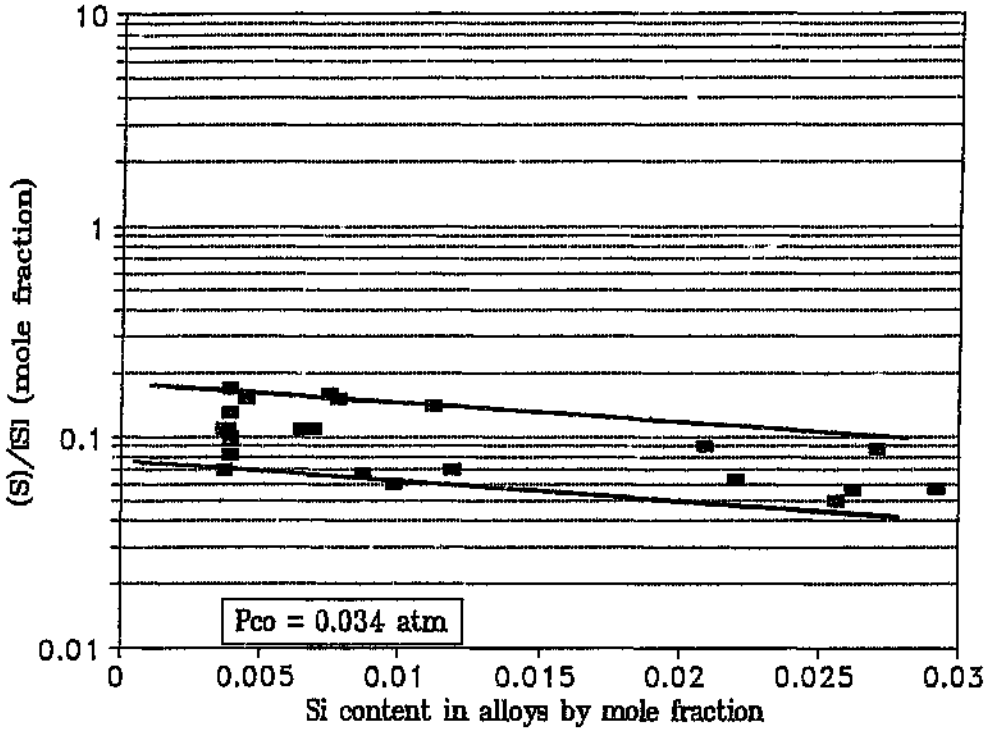


Figure 4.3.14. Effect of [Si] on the distribution of sulphur with metals of 0.22Cr-Fe-C-S-Si and slags of 0.01CaO-0.007Fe_2O_3-Mg-Cr_2O_3-SiO_2-Al_2O_3, Al_2O_3/MgO=1.7, in Si-oxide crucibles at 1580°C at 0.034 Pco.

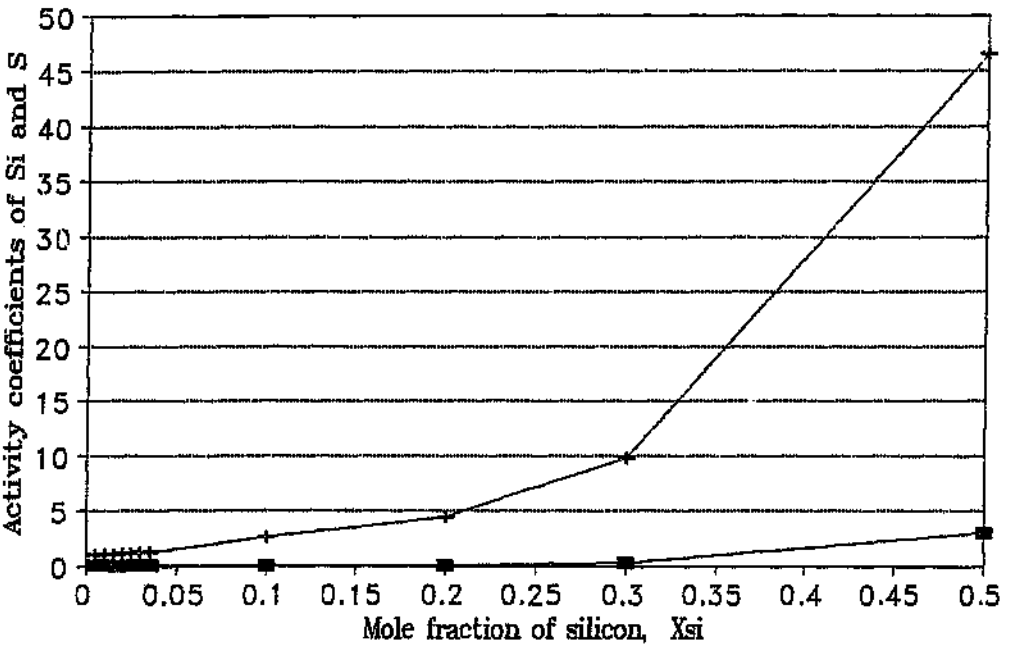


Figure 4.3.15. Relations of activity coefficients of silicon and sulphur with silicon content in the alloys of 0.15C-0.45Cr-0.001S-Si-Fe by mole fraction at 1550°C.

--- [γsi], + --- [γs]

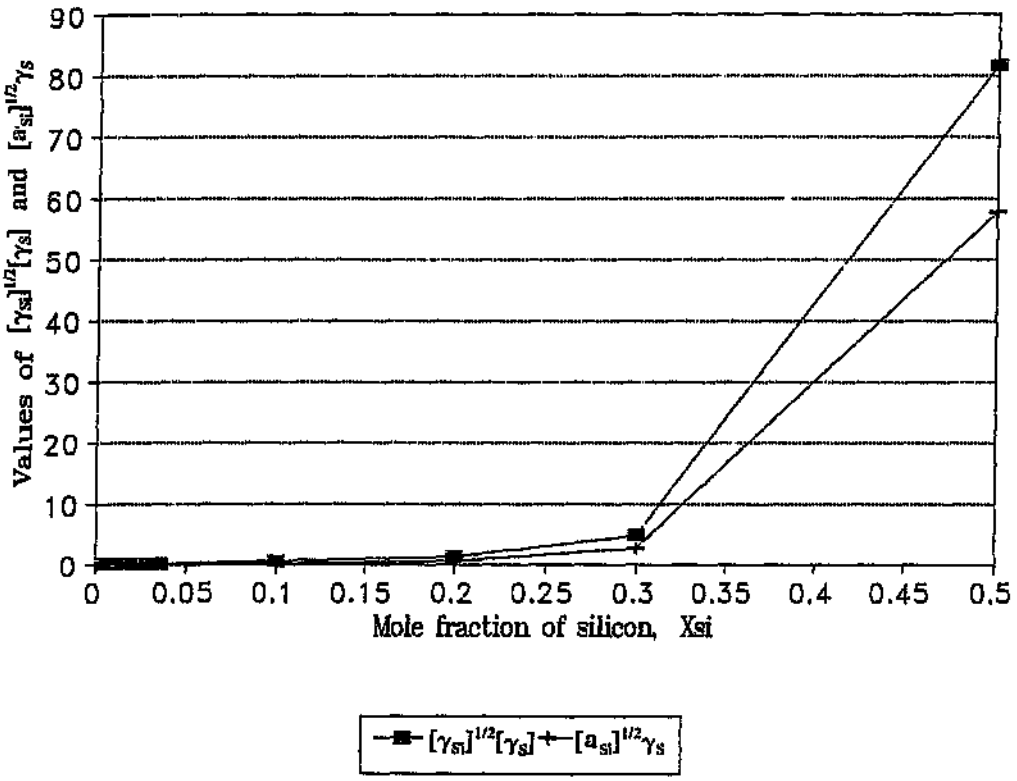


Figure 4.3.16. Effects of silicon content on $[\gamma si]^{1/2}/[\gamma s]$ and $[a_{Si}]^{1/2}/[\gamma s]$ at 1550°C, with metals containing 0.15C-0.45Cr-0.001S-Si-Fe by mole fraction.

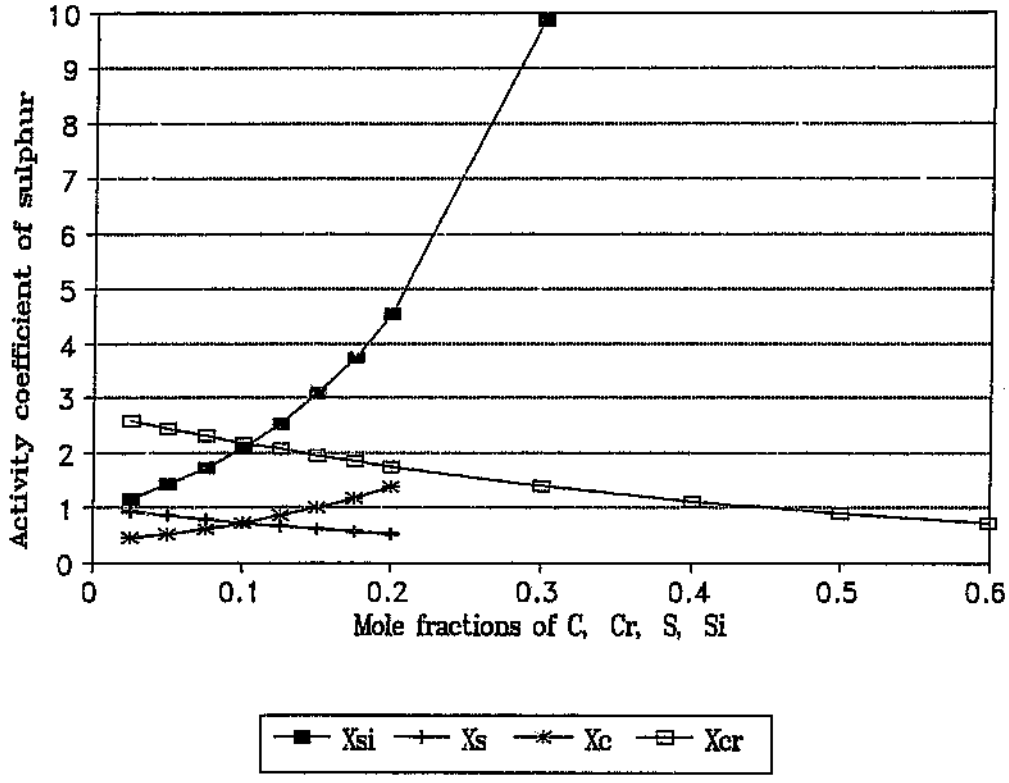


Figure 4.3.17. Effect of silicon, carbon, chromium and sulphur on the activity coefficient of sulphur ($[\gamma_S]$) at 1550 °C with base alloys of 0.15C-0.45Cr-0.001S-0.01Si-Fe.

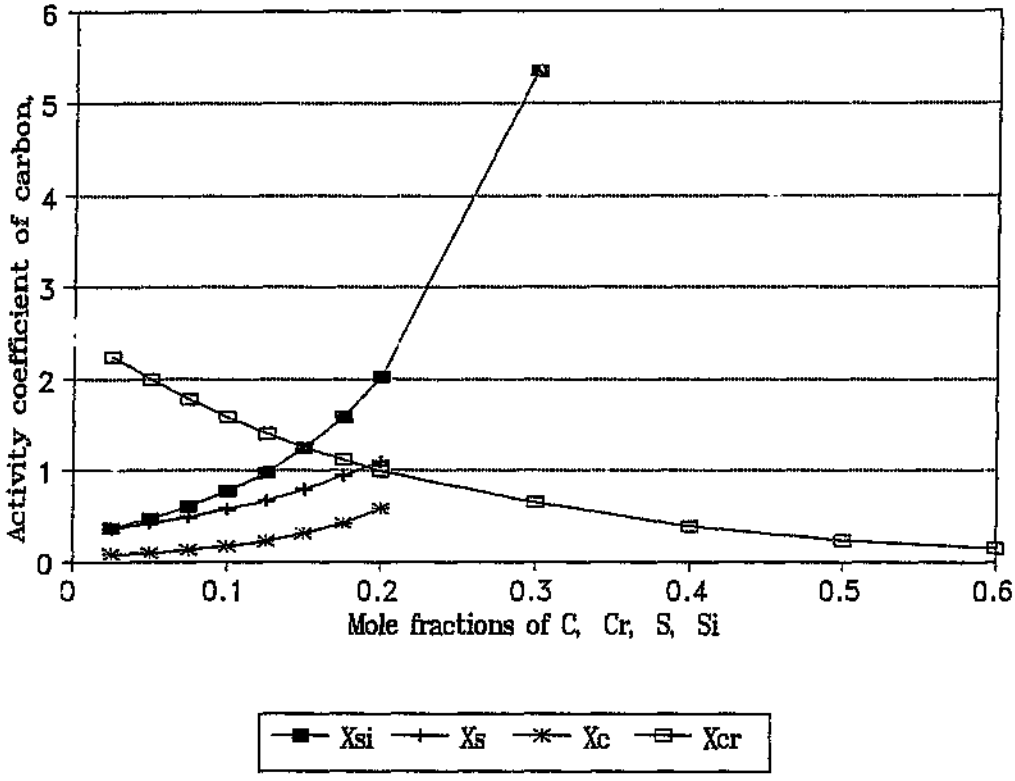


Figure 4.3.18. Effect of silicon, carbon, chromium and sulphur on the activity coefficient of carbon ($[\gamma_c]$) at 1550 °C with the alloys of 0.15C-0.45Cr-0.001S-0.01Si-Fe.

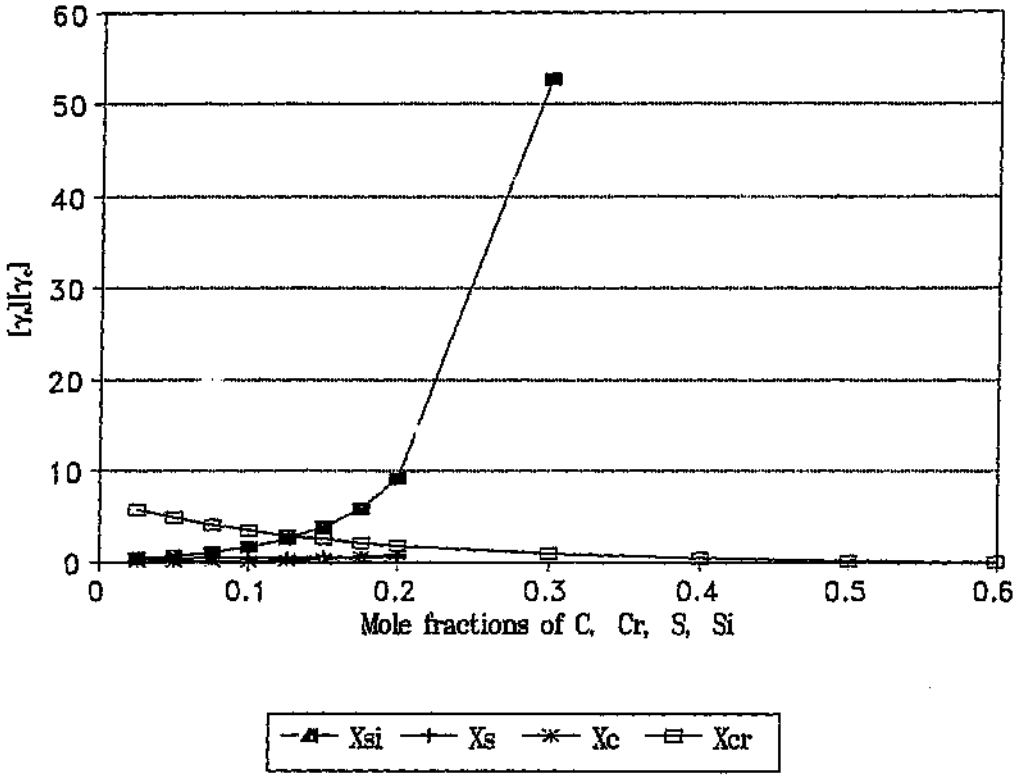


Figure 4.3.19. Effect of silicon, carbon, chromium and sulphur on the term of ($[\gamma_s][\gamma_e]$) at 1550°C with base alloys of 0.15C-0.45Cr-0.001S-0 01Si-Fe.

4.4. CHROMIUM DISTRIBUTION BETWEEN SLAG AND METAL AT DIFFERENT PARTIAL PRESSURE OF CARBON MONOXIDE

Chromium is a commodity of critical and strategic importance, imparting unique qualities to the materials to which it has been added. The change in the technology of stainless-steel production considerably affected the consumption pattern of chromium alloys in the past decades because about 79 per cent of the world's chromium products are utilized to produce the steel and other special alloys mostly in the forms of high-carbon ferrochromium and low-carbon ferrochromium. Low-carbon ferrochromium was used to a large extent in the past. But high-carbon ferrochromium becomes dominant owing to the replacement of conventional processes of electric arc furnace by oxygen-blowing processes, such as argon-oxygen decarbonization (AOD), and vacuum-oxygen decarbonization (VOD), which permit decarbonization without significant loss of chromium from metal phase to slag phase by oxidization.

High-carbon ferrochromium is produced by the smelting of chromium ore in a submerged arc furnace with a carbonaceous reducing agent in excess of that required to reduce the chromium and iron. The non-reducible oxides in the ore form slag and, although a self-fluxing charge is sometimes possible, fluxes must usually be added to make a slag with the desired characteristics.

One of the critical problems encountered in the processes of ferrochromium refining is that the slags contain very high chromium, about 10 to 25 per cent of the slag in the form of oxides, which must be re-treated before being discarded. Increasing chromium recovery in both the production of high-carbon ferrochromium and the refining of ferrochromium is a challenge to the producers.

4.4.1. Chromium in Slag Phase

Chromium in slags, like any of the transition metal ions, can respond to the changes in the oxidation conditions and in the compositions of slags and metals by changing their valency. They may also change their structure role, for example by acting as a network modifier under reducing conditions, but as a network former when the slag is oxidised.

Spectroscopic analysis can provide data about the electronic and physical configuration, and hence can supply the structural role of transition metal ions in slags. Such studies can also provide information about the slag matrix. An investigation of Cr(II), Cr(III), and Cr(VI) in silicate slags has been made recently by H. Marston and B. B. Argent[36]. They used spectroscopic and chemical analyses to investigate the behaviour of chromium in four vitreous lime-silicate slags produced under reducing and oxidising conditions. The slags' composition is in the range of CaO 30% to 37%, MgO 0% to 7%, Al_2O_3 0% to 16%, SiO_2 40% to 60%, Cr_2O_3 0.05% to 3% by mass at temperature between 1580 to 1600 °C.

In the slags equilibrated at $Po_2 = 1.6*10^{-9}$ atmosphere, 71 per cent of chromium is present as Cr(II), reducing to an average figure of 14 per cent at $Po_2 = 1.1*10^{-5}$ atmosphere. At $Po_2 = 0.1$ atmosphere, 14 per cent is Cr(VI). In each case, the balance is Cr(III). Spectroscopy provided evidence of Cr(III) in all slags. The varying quantities of Cr(II) and Cr(VI) were detected, but not simultaneously in the same samples. Within the compositional range studied, no consistent effect of the chromium level, the slag basicity or the presence of MgO or Al_2O_3 on either the chromium distribution or the molar absorptivity could be discerned. Under the circumstances of our present investigation, the partial pressure of oxygen can be calculated by the following reaction and its free-energy change:

$$[C] + 1/2O_2 = CO \qquad (4.4.1)$$

$$\Delta G^\circ = -52,125.55 - 16.97T \qquad (4.4.2)$$

$$P_{O_2} = \{P_{CO}/([a_C]_{4.4.1})\}^2 \qquad (4.4.3)$$

Under the particulars of present experiments and the calculated carbon activity, The value of P_{O_2} is about 8.4308×10^{-4} to 7.8775×10^{-5}. Therefore, the chromium oxides must exist only in the forms of CrO and $CrO_{1.5}$ according to the study above done by H. M[illegible]on and B. B. Argent[36]. The activity of carbon used in the calculation is in the range of 0.025 to 0.1172, calculated with the metals containing 0.025-0.2C, 0.55Cr, 0.001S, 0.005Si and Fe in balance by using the formula expressed in equation (4..3.18):

$$\ln\gamma_C = -0.562 + 7.8(X_C) + 9.72(X_{Si}) + 6.45(X_S) - 5.1($$

$$+ 11.18(X_C)^2 - 0.115(X_{Cr})^2 + (X_{Si})^2$$

$$+ 3.06(X_C X_{Cr}) + (X_C X_{Si}) \qquad (4.3.18)$$

The nature and behaviour of CrO and $CrO_{1.5}$ in the slag [illegible]SiO_2-Al_2O_3-FeO-CrO_x in equilibrium with Fe-Cr-Si-C alloys at certain partial pressure of carbon monoxide can be determined by means of thermodynamic analysis of the experimental data. A slag-metal reaction can be written between carbon and chromium oxides:

$$(CrO_x) + x[C] = [Cr] + x(CO) \qquad (4.4.5)$$

$$K_{4.4.5} = \{(P_{CO})^x[a_{Cr}]\}/\{(a_{CrO_x})[a_C]^x\} \qquad (4.4.6)$$

By taking logarithm, equation (4.4.6) can be rearranged in terms of activity coefficient multiplied by concentration for each activity:

$$\ln \{[\%Cr]/(\%Cr)\} = x\ln\{[\%C]/Pco\}$$

$$+ \ln\{K_{4.4.5}C'(\gamma_{Cr})[\gamma_C]^x/[\gamma_{Cr}]\} \qquad (4.4.7)$$

Where C' is a constant representing all constants for converting mole fractions to mass percentages. If the partition ratio is defined as L_{Cr} = [%Cr in metal]/(%Cr in slag), and $K'_{4.4.5} = \ln\{K_{4.4.5}C'(\gamma_{Cr})[\gamma_C]^x/[\gamma_{Cr}]\}$, equation (4.4.7) can be re-arranged for the sake of simplicity:

$$\ln L_{Cr} = x\ln\{[\%C]/Pco\} + K'_{4.4.5} \qquad (4.4.8)$$

Equation (4.4.8) is linear with slope 'x' and intercept $K'_{4.4.5}$. Graphs were plotted for all three series of experiments, which were conducted at 1500°C in Cr-oxide crucibles at 0.83atm and 0.05atm of partial pressure of carbon monoxide, at 1580°C in silica crucibles at 0.034atm of partial pressure of carbon monoxide. The results are shown in figure 4.4.1, 4.4.2, 4.4.3. The data are scattered due to the huge influences of metal composition and slag composition on the intercept $K'_{4.4.5}$ in terms of $\{(\gamma_{Cr})[\gamma_C]^x/[\gamma_{Cr}]\}$.

The slopes are 1.125, 1.10 and 1.07, which represent that CrO in the slag phase is 75 per cent of chromium oxides under the atmosphere of carbon monoxide in Cr-oxide crucible at 1500°C, 80 per cent at 0.05atm of partial pressure of carbon monoxide in Cr-oxide crucible at 1500°C and 86 per cent at 0.034atm of partial pressure of carbon monoxide in silica crucible at 1580°C respectively. The balance is $CrO_{1.5}$. The results are illustrated in figure 4.4.4.

A higher percentage of CrO exists in the slags when a lower partial pressure of carbon

monoxide is imposed. The percentage of CrO in slags increases in silica crucible, compared with that in Cr-oxide crucible, which is consistent with the results from the study on thermodynamics of slags containing chromium oxides made by Y. Xiao and L. Holappa[63]: the divalent chromium fraction decreases and the trivalent chromium increases with the decrease of silica in the slags of SiO_2-CrO-$CrO_{1.5}$. The higher the slag's basicity, the lower the divalent chromium fraction and the higher the activities of chromium oxides.

When the reaction (4.4.8) is considered:

$$(CrO_{1.5}) + 1/2[C] = (CrO) + 1/2CO \qquad (4.4.8)$$

$$\Delta G^{\circ} = 36{,}722.22 - 22.79T \ (J/mol) \qquad (4.4.9)$$

$$K_{4.4.8} = \{(a_{CrO})/(a_{CrO1.5})\}\{(P_{CO})/[ac]\}^{1/2} \qquad (4.4.10)$$

The equation can be re-written into:

$$(X_{CrO})/(X_{CrO1.5}) = K_{4.4.8}\{(\gamma_{CrO1.5})/(\gamma_{CrO})\}\{[ac]/P_{CO}\}^{1/2} \qquad (4.4.11)$$

It is known that the partition ratio of CrO to $CrO_{1.5}$ by molar fraction is correlated with reaction temperatures in terms of $K_{4.4.8}$, partial pressure of carbon monoxide, metal's composition in forms of activity of carbon and slag's composition in regards to activity coefficients of divalent and trivalent oxides of chromium in the slags.

As far as the activity of carbon is concerned by means of metal's composition, as described in equation(4.3.18), the contents of carbon, chromium and silicon are those major factors, which change the activity of carbon significantly. The influences of metal's

composition on the ratio of CrO to $CrO_{1.5}$ are plotted in figures 4.4.5, 4.4.6, and 4.4.7 at 0.83atm, 0.05atm and 0.034atm of the partial pressure of carbon monoxide respectively.

In general, the increase of silicon, sulphur and carbon in the metal phase increases the value of the activity ratio $(a_{CrO})/(a_{CrO_{1.5}})$. The activity ratio decreases when the chromium content of the metal phase increases. The decrease of the partial pressure of carbon monoxide increases the activity ratio.

Similar treatment and results were reported by Rankin and Biswas[37] in their study on the slags of SiO_2-CaO-Al_2O_3-FeO-CrO_x in equilibrium with Fe-Cr-Si alloys. The experiments were conducted at 1600°C in alumina and silica crucibles. The data were analyzed in terms of the equilibria:

$$(CrO_x) + x[Fe] = [Cr] + x(FeO) \qquad (2.3)$$

$$K_{2.3} = \{(a_{FeO})^x[a_{Cr}]\}/\{(a_{CrO_x})[a_{Fe}]^x\} \qquad (2.4)$$

and

$$2(CrO_x) + x[Si] = 2[Cr] + x(SiO_2) \qquad (2.5)$$

$$K_{2.5} = \{[a_{Cr}]^2(a_{SiO2})^x\}/\{[a_{Si}]^x(a_{CrO_x})^2\} \qquad (2.6)$$

These constants were defined as

$$K'_{2.3} = \{(\%Fe)^x[\%Cr]\}/\{(\%Cr)[\%Fe]^x\} \qquad (2.7)$$

$$k'_{2.5} = [\%Cr]^2/\{(\%Cr)^2[a_{Si}]^x\} \qquad (2.8)$$

In $K'_{2.5}$ the silica term was omitted, since it was approximately constant for each group of runs (silica saturation).

These expressions may be rewritten in terms of activity coefficient multiplied by concentration for each activity. Finally, by taking logarithms and rearranging, the following equations were obtained:

$$\log\{(\%Cr)/[\%Cr]\} = x\log\{(\%Fe)/[\%Fe]\}$$

$$+\log\{(\gamma_{FeO})[\gamma_{Cr}]C_1\}/\{[\gamma_{Fe}](\gamma_{CrO})K'_{2.5}\} \qquad (2.9)$$

$$\log\{(\%Cr)/[\%Cr]\} = -(x/2)\log(a_{Si})$$

$$+\log\{(\gamma_{FeO})[\gamma_{Cr}]C_2\}/\{[\gamma_{Fe}](\gamma_{CrO})K'_{2.5}\} \qquad (2.10)$$

where C_1 and C_2 are the constants representing all constants for converting mole fractions to mass percentages. For the first series of experiments in alumina crucibles in the study, Rankin and Biswas found the average value of the x to be 1.07. This meant that 86 per cent of chromium present in the slag was in the form of Cr^{2+} ions and the balance was Cr^{3+}. For the second series of experiments under silica saturation(silica crucibles), the average value of x for all groups was found to be 1.04. This corresponds to a value of 92 per cent of Cr^{2+} ion in the slag, the balance being Cr^{3+}. The present results are fairly consistent with their study.

In their study on slag-metal equilibrium in the smelting of high-carbon ferrochromium, M. Akyuzlu and R. H. Eric[33] utilized the same thermodynamic treatment and found the slope is 0.86 at 1500°C under an argon atmosphere, 0.62 at 1500°C, 0.73 at 1600°C both under carbon monoxide. Normally the slope should be between 1 and 1.5, which means that CrO is the only chromium oxide in the slags if the slope is unity and $CrO_{1.5}$ is



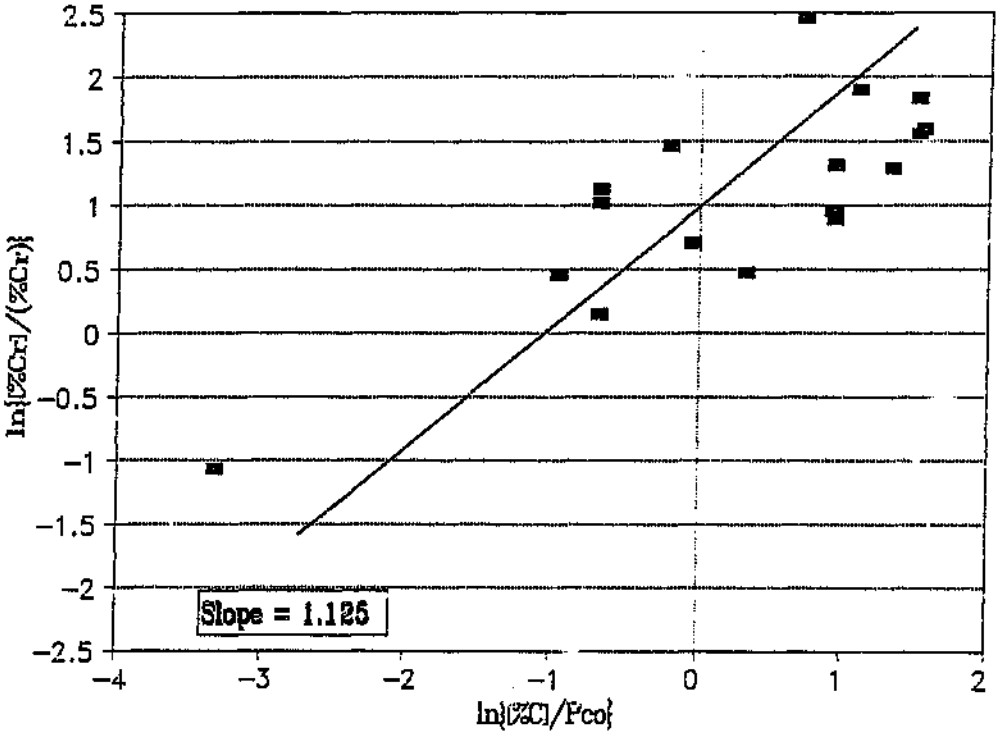


Figure 4.4.1. Variation in the ln(partition ratio of chromium) with the ln (partition ratio of carbon to 0.83atm Pco) at 1500°C in Cr-oxide crucible.

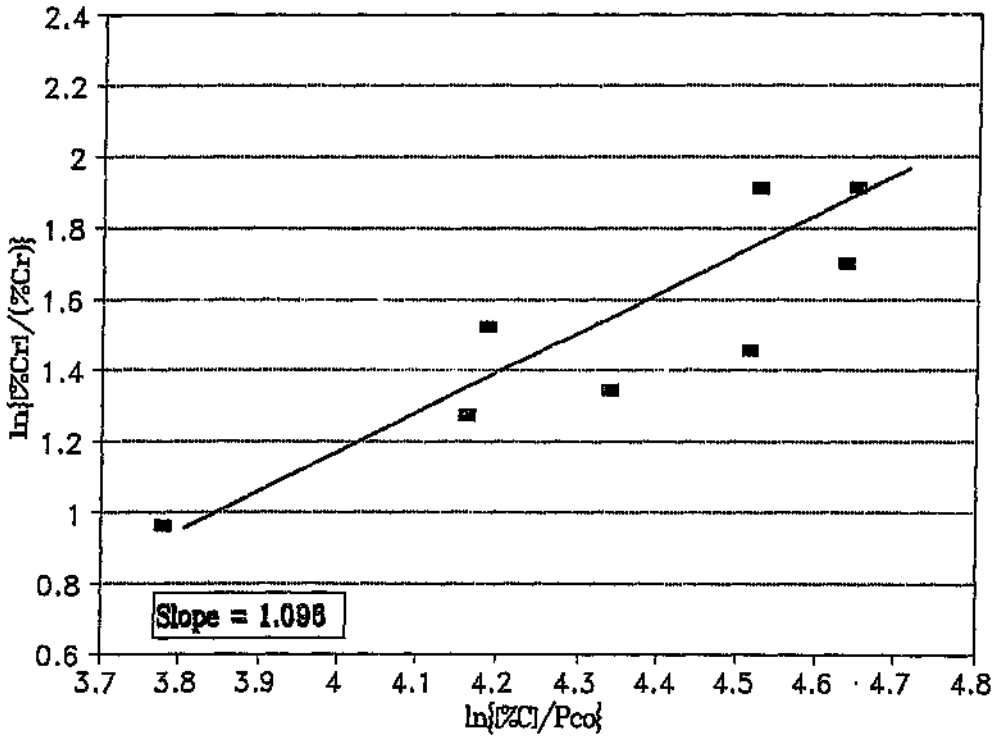


Figure 4.4.2. Variation in the ln (partition ratio of chromium) with the ln (partition ratio of carbon to 0.05atm Pco) at 1500°C in Cr-oxide crucible.

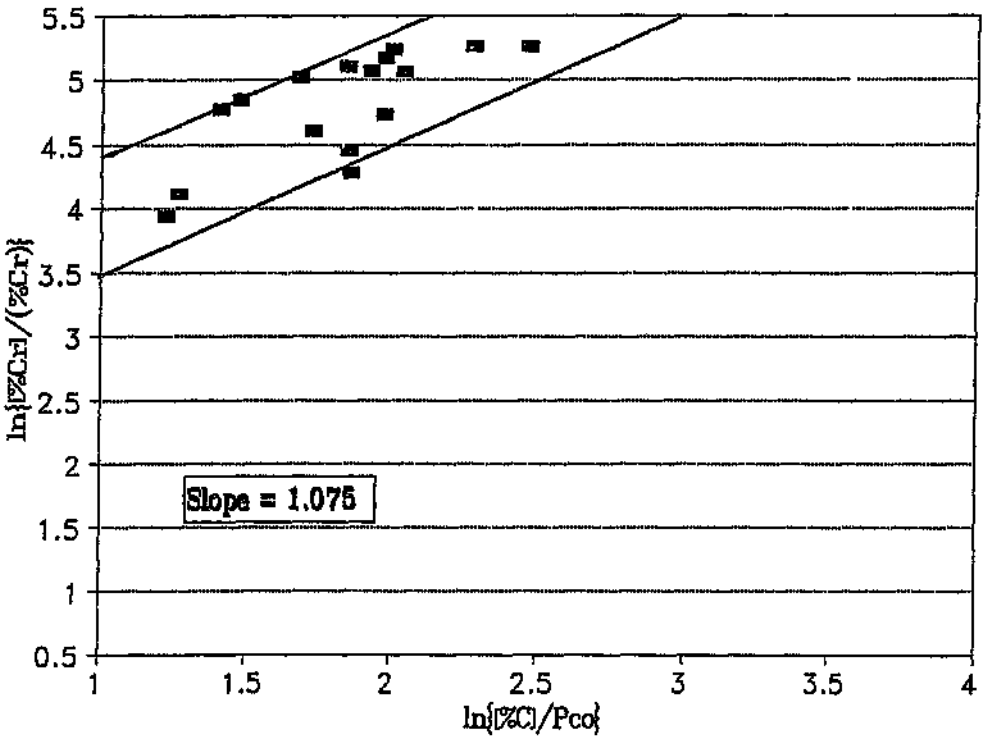


Figure 4.4.3. Variation in the ln (partition ratio of chromium) with the ln (partition ratio of carbon to 0.034atm Pco) at 1580°C in silica crucible.

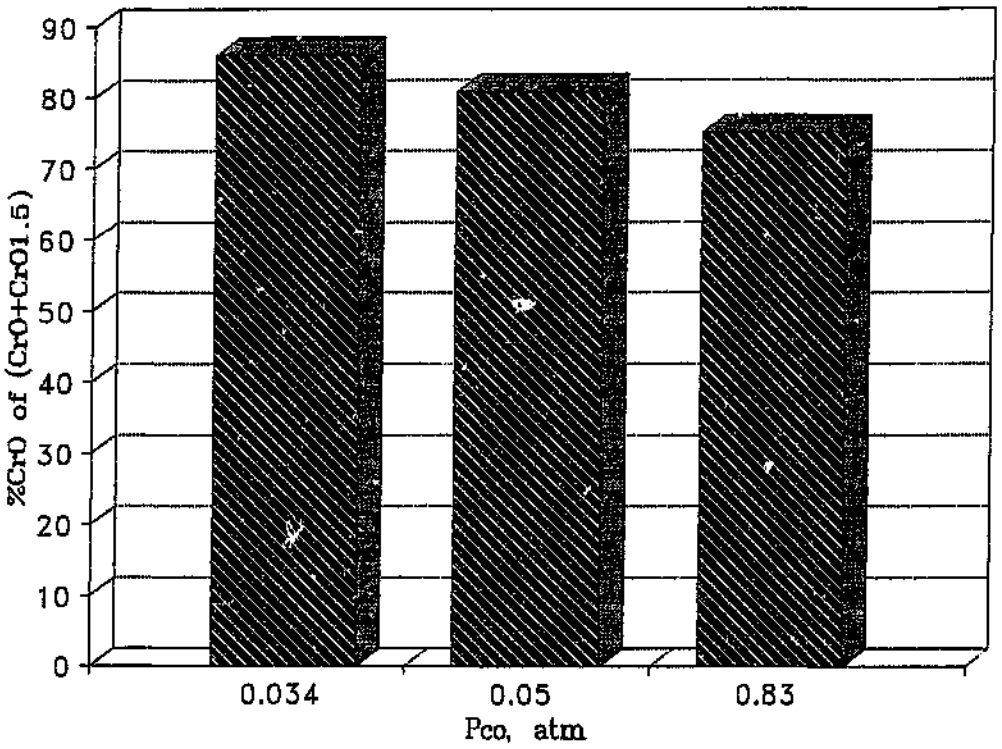


Figure 4.4.4. Formalisation of chromium in slags with partial pressure of carbon monoxide. Case 1 at 0.034atm Pco in silica crucible at 1580°C; case 2 at 0.83 and 0.05atm of Pco in Cr-oxide crucible at 1500°C.

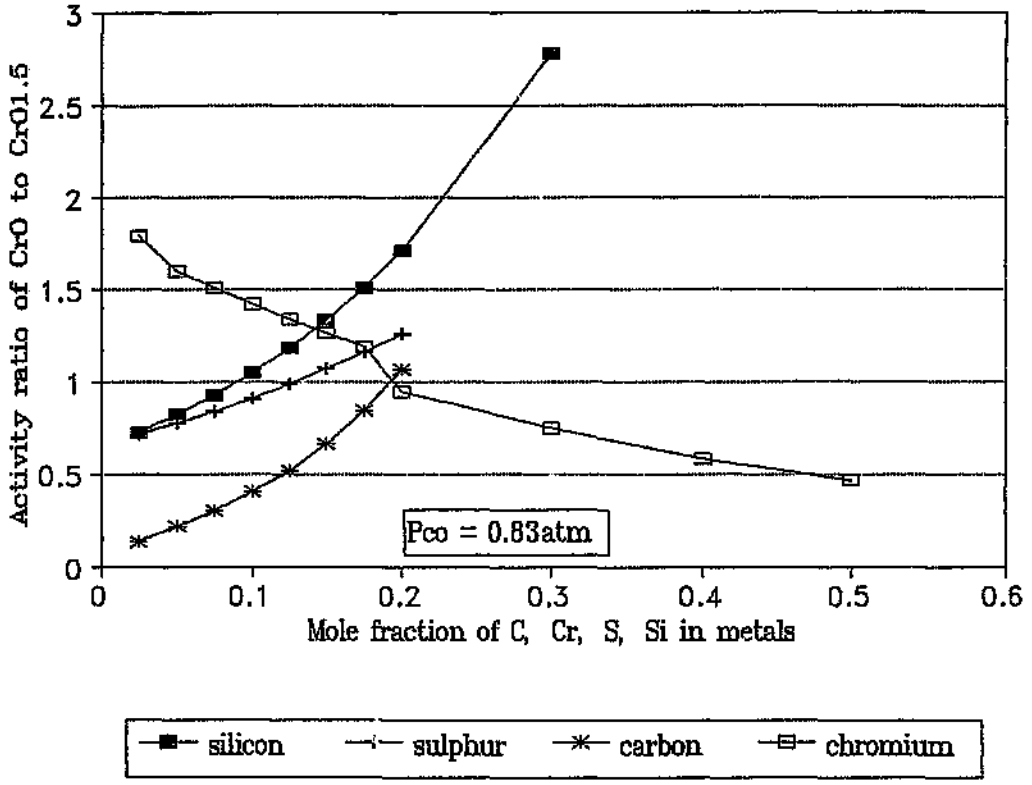


Figure 4.4.5. Influence of C, Cr, S and Si on $(a_{CrO})/(a_{Cr_2O_3})$ ratio with base metals of 0.15C-0.55Cr-0.001S-0.005Si-Fe by mole fraction at 0.83atm Pco and 1500°C.

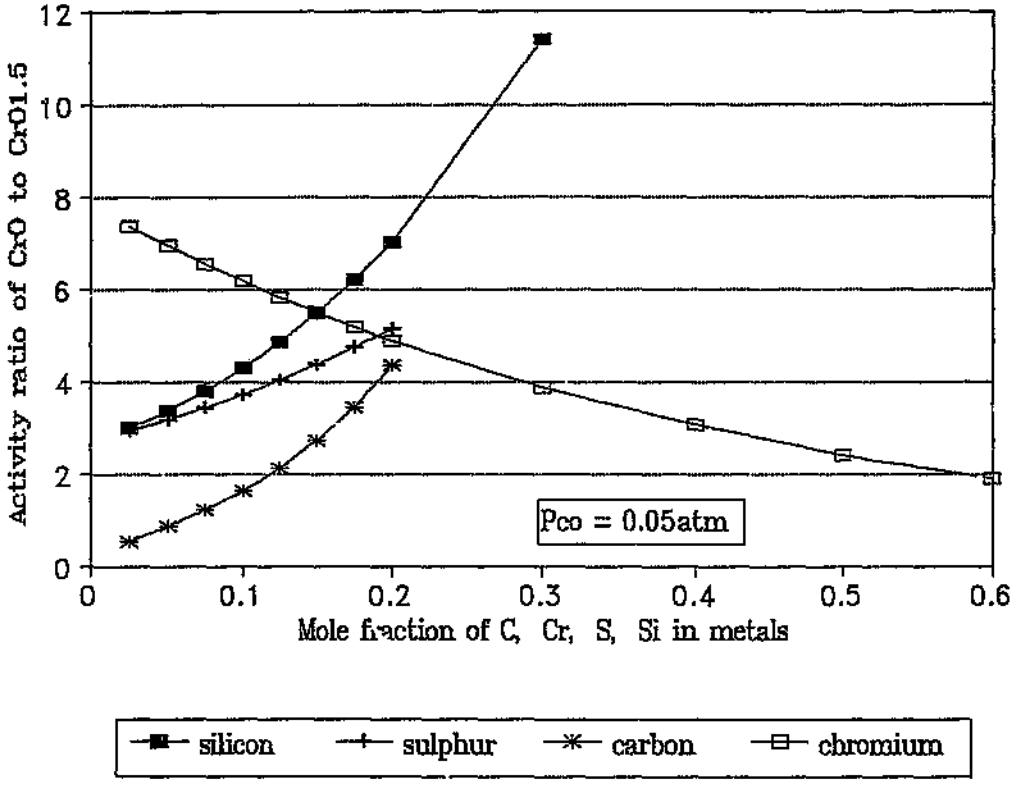


Figure 4.4.6. Influence of C, Cr, S and Si on the $(a_{CrO})/(a_{CrO1.5})$ ratio with base metals of 0.15C-0.55Cr-0.001S-0.005Si-Fe by mole fraction at 0.05atm Pco and 1500°C.

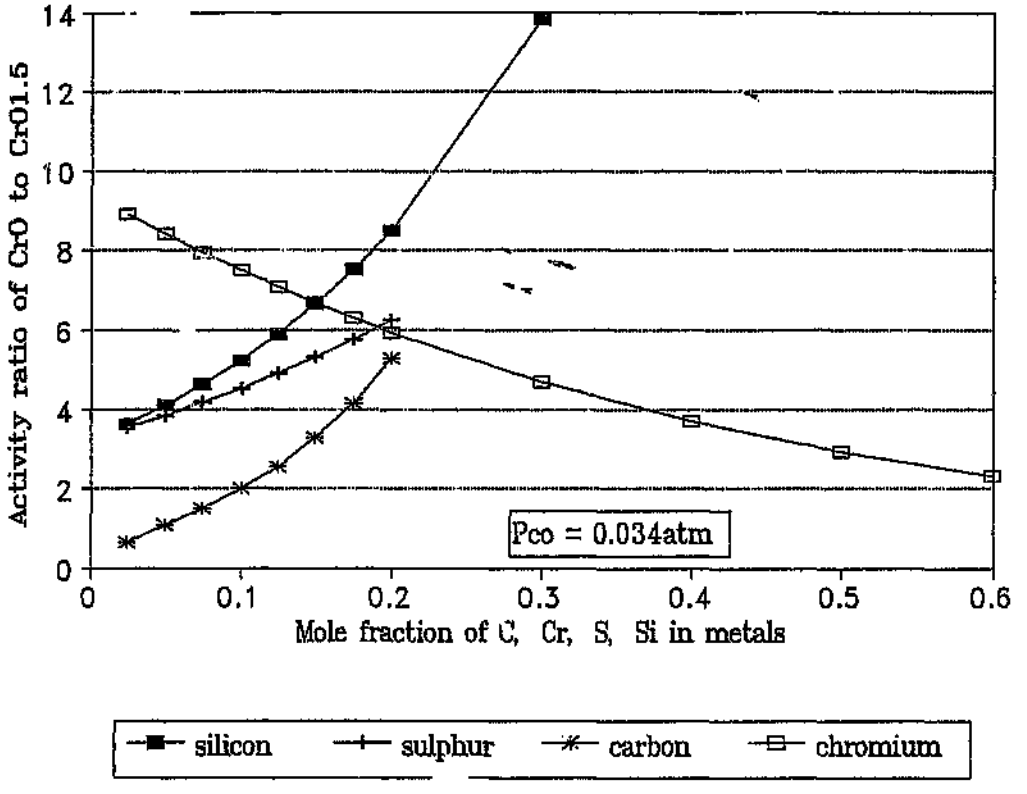


Figure 4.4.7. Influence of C, Cr, S and Si on the (a_{CrO})/($a_{CrO1.5}$) ratio with base metals of 0.15C-0.45Cr-0.001S-0.005Si-Fe by mole fraction at 0.034atm Pco and 1580°C.

4.4.2. Variation of Chromium Content in slags

As discussed above, the chromium in slag phase changes its valency, responding to the oxidation conditions, slag composition, metal cc. .)sition and partial pressure of carbon monoxide. Because no reliable and affordable method is available to be used to analyse the contents of different chromium oxides in the slags, the chromium content of the slag phase is expressed by means of chromium in the current study, instead of chromium oxides.

The influence of chromium content of metals on the content of chromium in slag phase is shown in figure 4.4.8. The content of chromium in the slags increases with increasing chromium of the metal phase. At a lower partial pressure of carbon monoxide (0.05atm), the chromium content in slags is about 1 per cent lower than the results acquiring in Cr-oxide crucibles at 0.83atm of partial pressure of carbon monoxide. Figure 4.4.9 demonstrates the relations between chromium of slag phase and the chromium in alloys from the experiments carried out in silica crucibles with metals containing 0.06 to 0.22 mole fraction of chromium relevant to the situations of stainless-steel making. The chromium in slags increases from 0.03 to 0.15 with the increase of chromium content in the metal phase from 0.06 to about 0.22. The chromium content in the slag phase is less than that with the metals of a higher chromium content, compared with the results in figure 4.4.3.

The relations between chromium content of slags and carbon content of metals are elucidated in figure 4.4.10. Chromium of slags is quite low, shown from the results in silica crucibles and the decreasing of chromium smoothly from 0.17 to about 0.1 when carbon content of metals increases from 0.005 to 0.225 by mole fraction. The results carried out in Cr-oxide crucibles clarify a sharp decline of chromium in slags, from about 0.55 to about 0.1 when carbon content increases from 0.05 to 0.225 by mole fraction. A lower chromium content in the slags is procured by utilizing lower partial pressure of

carbon monoxide. The difference of chromium content between 0.05atm and 0.83atm of the partial pressure of carbon monoxide is about 0.05 mole fraction in the slags. Figure 4.4.11 illustrates the results from the experiments conducted in silica crucibles with the metals of about 15 per cent of chromium by mass at 1580°C and at 0.034atm of the partial pressure of carbon monoxide. The chromium content in slag phase is inversely proportional to the carbon content of the metal phase. The chromium content in the slags decreases from 0.25 to 0.016 when carbon content of the metals increases from 0.01 to 0.14.

The reasons why the reduction of chromium in slags can be promoted by increasing carbon content, decreasing chromium of metals and lowering the partial pressure of carbon monoxide in the gas phase, could be explained by introducing the reaction between carbon dissolved in the metal phase and CrO of the slags.

$$[C] + (CrO) = CO + [Cr] \qquad (4.4.10)$$

$$\Delta G^{\circ} = 47754.45 - 32.22T \quad (Kcal/mole) \qquad (4.4.11)$$

$$(X_{CrO}) = \{[a_{Cr}]P_{CO}\}/\{[a_C](\gamma_{CrO})K_{4.4.10}\}$$

$$= \{[\gamma_{Cr}][X_{Cr}]P_{CO}\}/\{[a_C](\gamma_{CrO})K_{4.4.10}\} \qquad (4.4.12)$$

Chromium content in slags is influenced by the factors expressed in equation (4.4.12), such as activities of chromium and carbon in metal, activity coefficient of chromium in slag, partial pressure of carbon monoxide in the gas phase and reaction temperature. The declination of chromium in slags could be promoted by reducing chromium activity in metal, lowering the partial pressure of carbon monoxide in the gas phase, increasing activity coefficient of chromium oxide CrO, enhancing activity of carbon, and elevating the reaction temperature, which causes an enlarging value of the equilibrium constant $K_{4.4.10}$.

As far as the activity coefficients of chromium and carbon in the metal phase are concerned, the major influence comes from the concentration of chromium, carbon and silicon, even sulphur[105,106].

$$\ln\gamma_C = -0.562 + 7.8(X_C) + 9.72(X_{Si}) + 6.45(X_S) - 5.1(X_{Cr}) + 11.18(X_C)^2 - 0.115(X_{Cr})^2 + (X_{Si})^2 + 3.06(X_CX_{Cr}) + (X_CX_{Si}) \quad (4.3.18)$$

$$\ln\gamma_{Cr} = -0.305 - 5.17(X_C) + 0.42(X_{Cr}) - 1.6(X_{Si}) - 0.115(X_{Cr})^2 - 4.94(X_C)^2 + 5.18(X_CX_{Cr}) - 2.23(X_S) \quad (4.4.13)$$

Carbon is one of the most powerful elements, which decreases the content of chromium in the slags by decreasing the activity coefficient of chromium of metal phase and increasing the activity coefficient of itself. The influences of carbon on the activity coefficients of carbon and chromium, and the value of $[a_{Cr}]/[a_C]$ ratio are illustrated in figure 4.4.12. The effect of the chromium of the metal phase on the chromium content of the slag phase can be analysed by means of activity of chromium, activity coefficients of carbon in the metal phase and activity of chromium oxide in slag phase. The increase of chromium concentration in metal decreases the activity coefficient of carbon and proliferates the activity of itself by increasing both content and activity coefficient. The influences of chromium content of the metal phase on the activity coefficients of chromium and carbon, and on the value of $[a_{Cr}]/[a_C]$ ratio are calculated and exhibited in figure 4.4.13.

The activity coefficient of chromium oxide in slag phase also is one of the factors, which

influence the content of chromium in slags, as clarified in equation (4.4.12). From the study done by Y. Xiao and L. Holappa [63], the activities of CrO and $CrO_{1.5}$ in the slags of CrO-$CrO_{1.5}$-SiO_2 in equilibrium with chromium metal increase with increasing chromium oxides and increasing CaO in the slags. It also shows that increasing CaO content of the slag phase can reduce chromium oxides in the slags. Their conclusions are in good agreement with the results of the present investigation, in which the content of chromium in the slags decreases with increasing MgO content, considering that MgO and CaO behave quietly similarly as basic oxides, as shown in figure 4.4.14 and figure 4.4.15. The results are also consistent with the study made by Morita and Sano[64].

The relation between chromium content and aluminum oxide content of the slag phase is illustrated in figure 4.4.16. At 0.83atm of partial pressure of carbon monoxide with Cr-oxide crucibles, the chromium content of slags expressed by mole fraction increases from 0.35 to 0.58 with an increase of alumina from 0.085 to 0.22. When alumina content declines from 0.08 to 0.04, the chromium concentration in the slag phase has no significant change. The experimental result at lower partial pressure of carbon monoxide (0.05atm and 0.034atm) demonstrates a similar trend. Chromium content of the slag decreases at low alumina concentration in the slag and then rises when alumina is higher than 0.17, with increasing alumina in the slag. The influence of alumina on the chromium of the slag phase may be analysed by means of activity coefficient of chromium oxide in the slag phase; γ_{CrO}, as expressed in equation (4.4.14). The results elucidated in figure 4.4.17 demonstrate that chromium of the slag phase decreases from 0.25 to 0.04 when alumina content increases from about 0.07 to 0.16 by mole fraction.

Morita and Sano[64] investigated the solubility of $MgO.Cr_2O_3$ in MgO-Al_2O_3-SiO_2-CaO melts at 1600°C. In air the solubility of $MgO.Cr_2O_3$ was found to be 1.1 to 4.5 per cent of Cr_2O_3 for MgO-SiO_2 melts. When Al_2O_3 was added to the melts, the solubility decreased to less than 1 per cent of Cr_2O_3, and the Cr in the coexisting $MgO.Cr_2O_3$ was replaced by Al in proportion to Al_2O_3 content in the slag. For MgO-CaO melts the solubility substantially rose to as much as 40 to 55 per cent of CrO_y, although more than

50 per cent of chromium was in the form of Cr^{6+} in an air atmosphere. For $MgO-Al_2O_3-SiO_2-CaO$ melts, which are typical for smelting reduction of chromium ore, the solubility decreased with increasing MgO and Al_2O_3 contents. The effect of CaO/SiO_2 ratio on the solubility in the melts was found to be unexpectedly small as long as CaO was added. When 22.1 per cent of BaO was added to $20\%MgO-20\%Al_2O_3-30\%SiO_2-30\%CaO$ melts, an increase in the solubility from 1.1 per cent to 4.4 per cent Cr_2O_3 was observed in air. Under reducing conditions, for $MgO-SiO_2$ melts saturated with SiO_2 however, the CaO addition had no effect on the solubility of $MgO.Cr_2O_3$ at $P_{O_2} = 2.37\times10^{-11}$ atm. For $20\%MgO-Al_2O_3-SiO_2-CaO$ (CaO/SiO_2 = 1) melts, the solubility decreased with increasing Al_2O_3 content at $P_{O_2} = 2.73\times10^{-10}$ atm. This trend is consistent with that in air, though the solubility was twice as much as that in air. They thought in the conclusion that careful adjustment of slag composition, mainly by lowering MgO and Al_2O_3 contents, is recommended to enhance the dissolution of $MgO.Cr_2O_3$ for promotion the reduction of chromium ore, and that the strongly reducing condition on smelting reduction also functions favourably for the dissolution of chromium ore into molten slags through the appearance of CrO.

The relation between chromium and silica content of slag is shown in figures 4.4.18 and 4.4.19. The chromium in slag decreases with increasing SiO_2 and the lower the partial pressure of carbon monoxide, the lower chromium content in the slags. The influence of partial pressure of carbon monoxide can be explained by the discussions mentioned above. The effect of silica content on the chromium content in the slag phase is quite small for the alloys containing 0.22 mole fraction chromium, comparing with the result shown in figure 4.4.18.

It is known from the study by Y. Xiao and L. Holappa [63] that the activities of both CrO and $CrO_{1.5}$ decrease with an increase of Silica in the slags of SiO_2-CrO_x and $CaO-SiO_2-CrO_x$ and that the CrO percentage of $(CrO+CrO_{1.5})$ of the slags can be enhanced by increasing the silica content in the slags. By a careful analysis of the results provided by Y. Xiao and L. Holappa [63], it is found that the chromium content of the SiO_2-CrO_x slag

also decreases with the increase of SiO_2 content in the slags. By studying the following reaction:

$$[C] + (CrO) = CO + [Cr] \qquad (4.4.14)$$

$$(X_{CrO}) = P_{CO}\{[a_{Cr}]/[ac]\}/\{(\gamma_{CrO})K_{4.37}\} \qquad (4.4.15)$$

$$(SiO_2) = [Si] + 2[O] \qquad (4.4.16)$$

When silica increases in slags, the equilibrium silicon content also increases in metal phase. The increase of silicon in the metal, illustrated in figure 4.4.20, from 0.025 to 0.2 decreases the activity coefficient of chromium in the metal very little from 0.5 to 0.35 and enhances the activity coefficient of carbon from about 0.4 to 2.0 and causes the $[a_{Cr}]/[ac]$ ratio decline dramatically from 4.0 to about 0.5, which is one of the reasons why an increase of the silica concentration in the slag reduces the chromium content of the slags. As clarified in figure 4.4.21, chromium content in the slag decreases from 0.58 to 0.15, with an increase of the silicon in the metal from 0.005 to 0.01 in Cr-oxide crucibles. The chromium content of slags is quite low and stable in silica crucibles , which decreases from 0.2 to only 0.13 by mole fraction.

In the same consideration, the increase of silicon in the metals will decrease the activity of CrO. The influence of silicon on the activity of CrO can be calculated by using the equations (4.4.15), (4.4.4) and (4.4.13) and is illustrated in figure 4.4.22. A consistent result has been achieved in the system with the metal containing 0.22 mole fraction chromium in silica crucibles at 0.034 atm of the partial pressure of carbon monoxide at 1580°C, as escalated in figure 4.4.23.

4.4.3. Expressions of Contents of C and Cr in ternary diagrams of Slag's Composition

The data from the experiments are the compositions of the slag phase and metal phase in terms of Al_2O_3, Cr_2O_3, Fe_2O_3, SiO_2, CaO, MgO, S in slag and Cr, Fe, C, Si, S in metal, with 12 variables in compositions. It is impossible to understand the relationships among those all variables. A two-dimensional plot can only express the relationship between two variables in a system with only one freedom. A three-dimensional graph can be used to illustrate the relationship among three variables in a system with only two freedoms. To meet the requirement of the number of expressive variables and the number of freedom in the system, systematic treatments are necessary both in the experimental design and in the data treatment.

The phase rule is a very useful tool to analyse the multi-phase equilibria[10,30,31]. The Gibbs Phase Rule is expressed as follows:

$$F + P = C + 2 - R$$

Where F is the number of degrees of freedom, P the number of phases, C the number of components and R the number of independent restrictions.

The system is comprised of the following:

phases: slag, metal, gas, Cr-oxide crucible/ or silica crucible;
slag: Al_2O_3, Cr_2O_3, Fe_2O_3, SiO_2, CaO, MgO and S;
metal: Cr, Fe, C, Si, S;
gas: CO

When C is 9 and P is 4,

$$F = 9 + 2 - 4 - R$$
$$= 7 - R$$

In order to express all relations among the compositions of both slag and metal in a ternary diagram, F has to be 2. Another three independent restrictions must be introduced to the system except Pco=0.83 atm and T=1500°C. For instance, a control of silicon content of 0.25% by mass in the metal phase; the ratio of Al_2O_3 to MgO 1.6 and CaO=1.4 in slag could be taken into consideration.

Because Fe_2O_3 changes very little compared with Cr_2O_3, only from 0.4% to 1.0% by mass, it is taken into account together with Cr_2O_3 in terms of (Cr_2O_3+Fe_2O_3). The ratio of Al_2O_3 to MgO and CaO content of the slag can be controlled by the composition of the slag, due to their inertia and stability in the system.

The same considerations are used in the current study for the all expressions of the experimental results. Most of the experimental results in this section was represented at the 7th International Ferro-alloys Congress (INFACON 7), Trondheim, Norway, 1995[10].

The results achieved in Cr-crucibles at 1500°C and 0.83atm of the partial pressure of carbon monoxide, are expressed in SiO_2-(Al_2O_3+CaO+MgO)-(Cr_2O_3+Fe_2O_3) ternary diagrams by means of iso-concentration lines for carbon and chromium in figures 4.4.24 and 4.4.25. Si in metal is 0.21% to 0.29% (0.25% average), S 0.03% to 0.4% and Fe the balance by mass.

The activity coefficients of carbon, chromium and the activities of carbon and chromium can be calculated based upon the measuring compositions of alloys in equilibrium with the slag phase. Therefore the activity coefficients and the activities for carbon and

chromium in the metal phase are computed and plotted in the SiO_2-(Al_2O_3+CaO+MgO)-(Cr_2O_3+Fe_2O_3) ternary diagrams by means of iso-activity coefficient lines for carbon and chromium and iso-activity lines for carbon and chromium in figure 4.4.26, 4.4.27, 4.4.28 and 4.4.29 respectively.

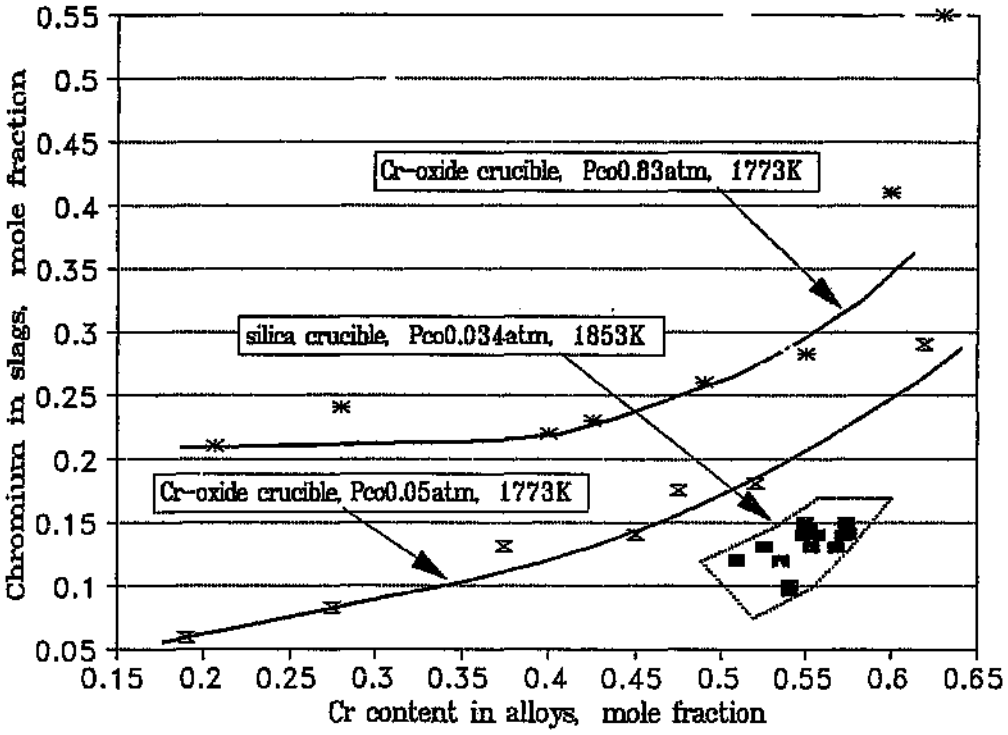


Figure 4.4.8. Effect of [Cr] on chromium of slags with metals of Cr-Fe-C-S- Si and slags of 0.01CaO-0.007Fe_2O_3-MgO-Cr_2O_3-SiO_2-Al_2O_3, Al_2O_3/MgO=1.7, 0.03-0.05/0.02-0.1 Si in Cr/Si oxide crucibles.

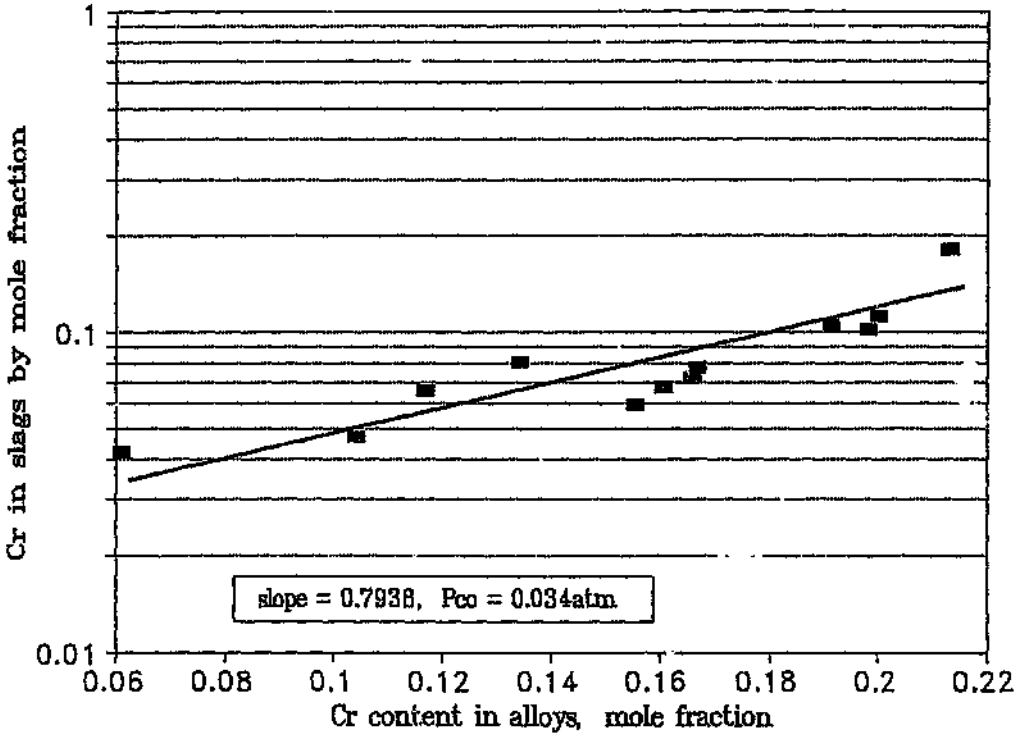


Figure 4.4.9. Effect of [Cr] on chromium of slags with metals of Cr-Fe-C-S-Si and slags of 0.01CaO-0.007Fe_2O_3-MgO-Cr_2O_3-SiO_2-Al_2O_3, Al_2O_3/MgO=1.7, 0.02-0.1 Si in Si-oxide crucibles at 1580°C.

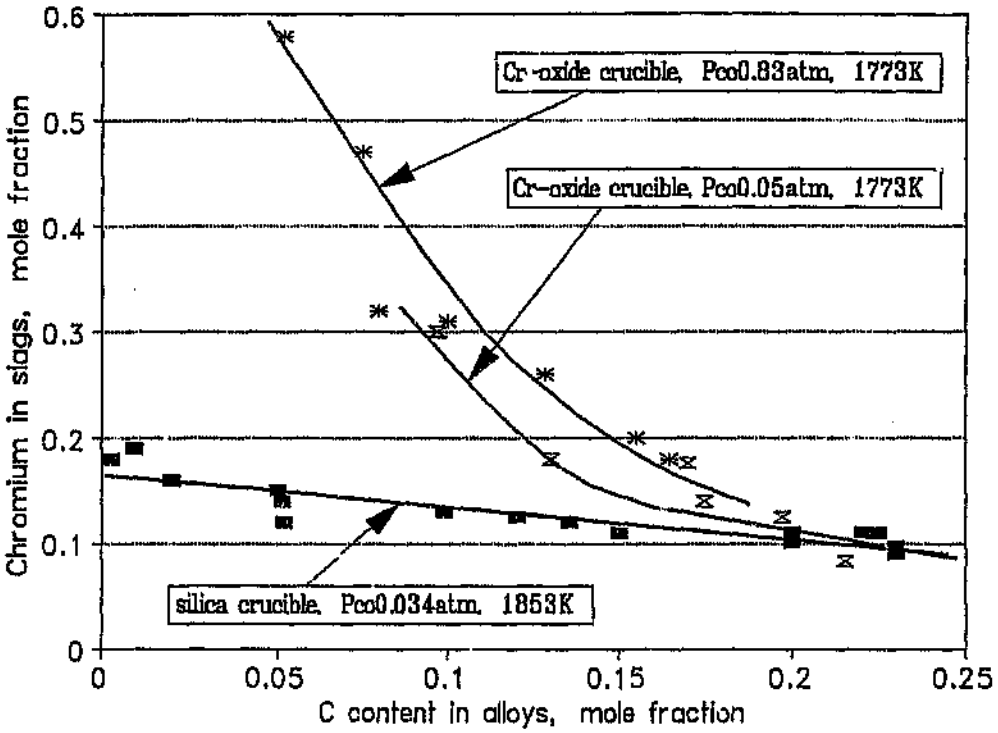


Figure 4.4.10. Effect of [C] on chromium of slags with metals of 0.55Cr-Fe-C-S-Si and slags of 0.01CaO-Fe_2O_3-MgO-Cr_2O_3-SiO_2-Al_2O_3, Al_2O_3/MgO=1.7, 0.03-0.05/0.03-0.1 Si in Cr/Si oxide crucibles.

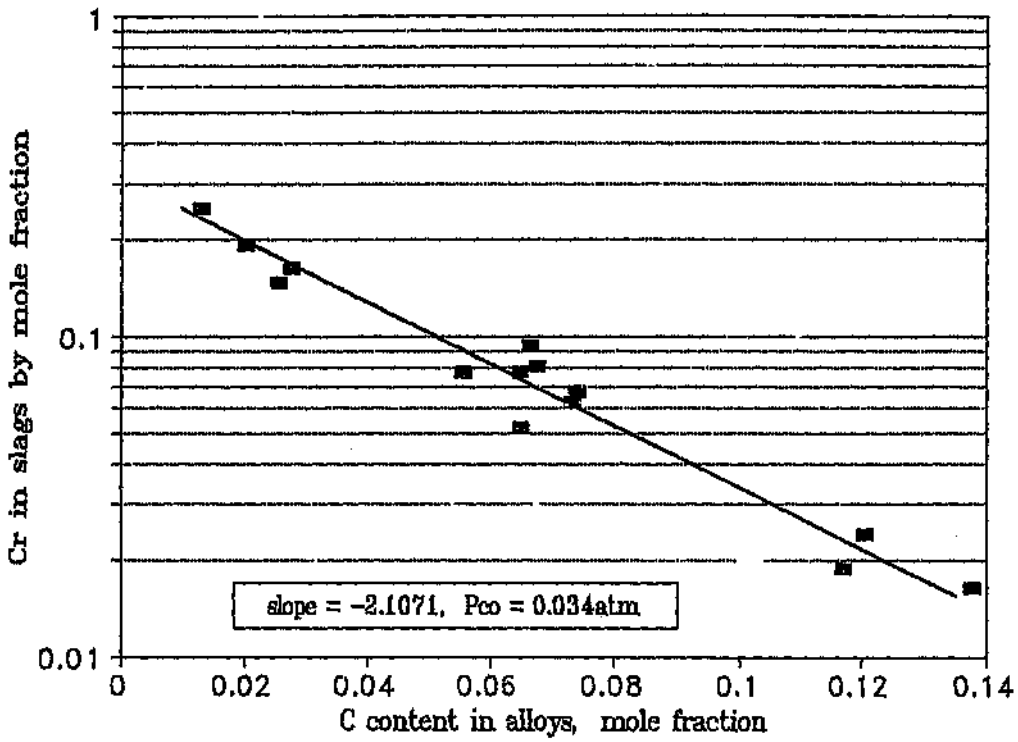


Figure 4.4.11. Effect of [C] on chromium of slags with metals of 0.22Cr-Fe-C-S-Si and slags of 0.01CaO-Fe_2O_3-MgO-Cr_2O_3-SiO_2-Al_2O_3, Al_2O_3/MgO=1.7, 0.02-0.1 Si in Si-oxide crucibles at 1580°C at 0.034 Pco.

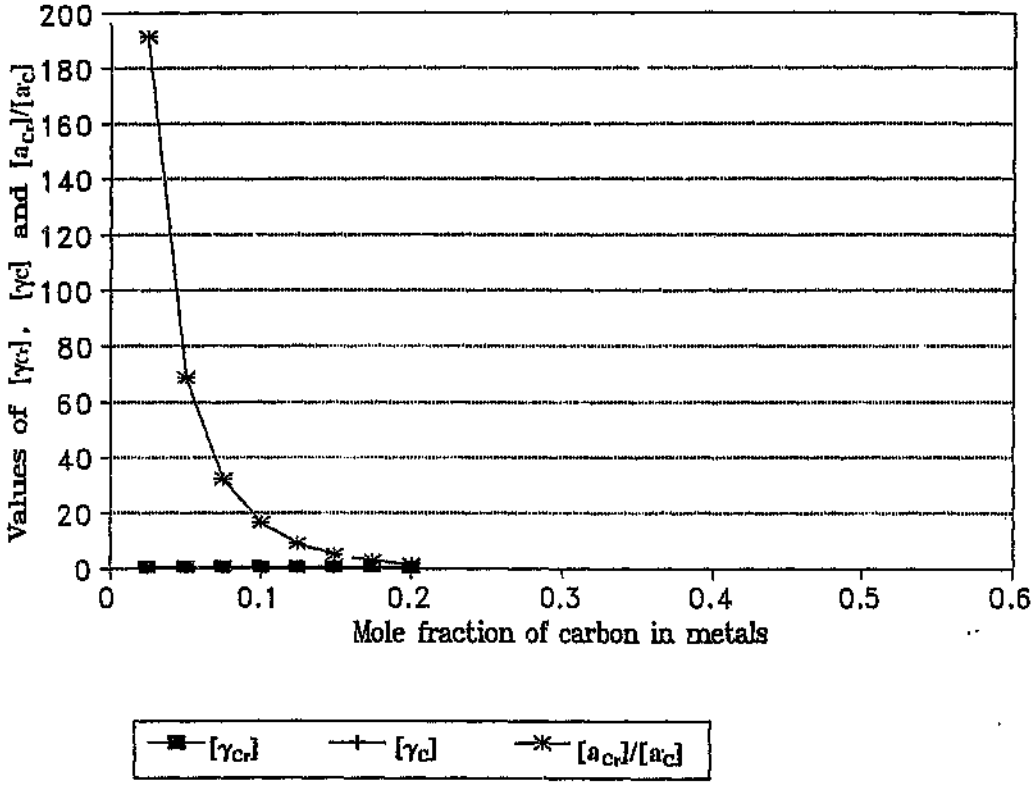


Figure 4.4.12. Relations between carbon and [γ_C], [γ_{Cr}] and [a_{Cr}]/[a_C] with base metals of C-0.45Cr-0.001S-0.005Si-Fe by mole fraction at 1500°C.

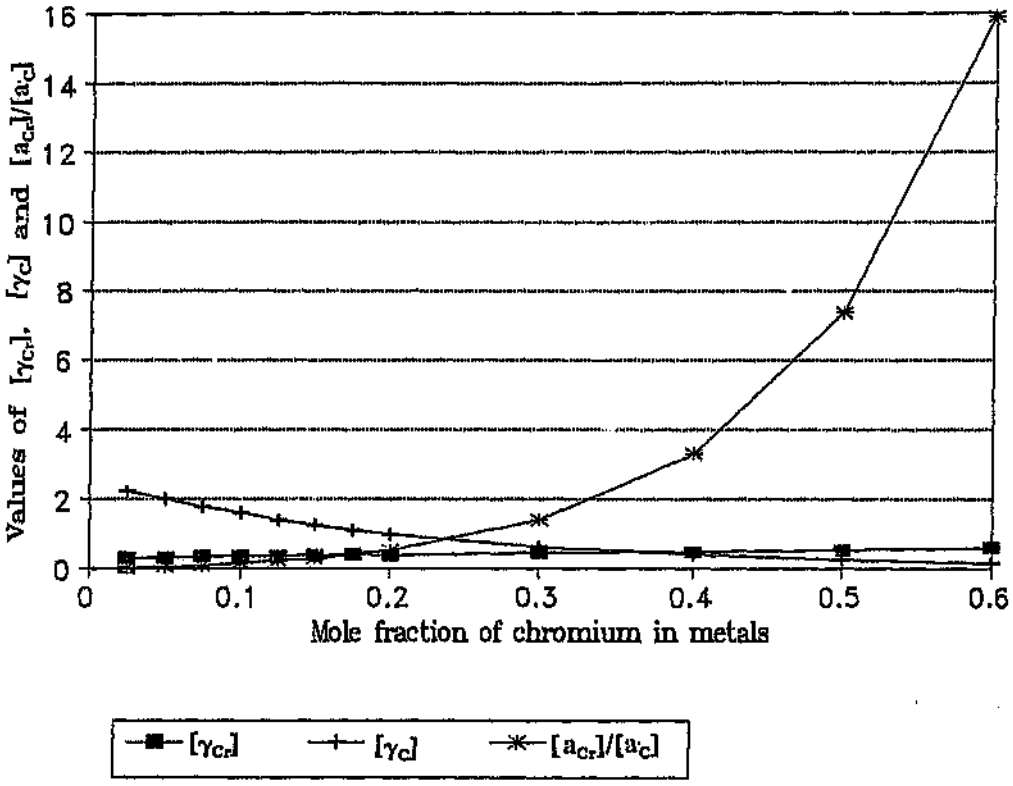


Figure 4.4.13. Relations between chromium and [γc],[γcr] and [acr]/[ac] with metals containing C-0.45Cr-0.001S-0.005Si-Fe by mole fraction at 1500°C.

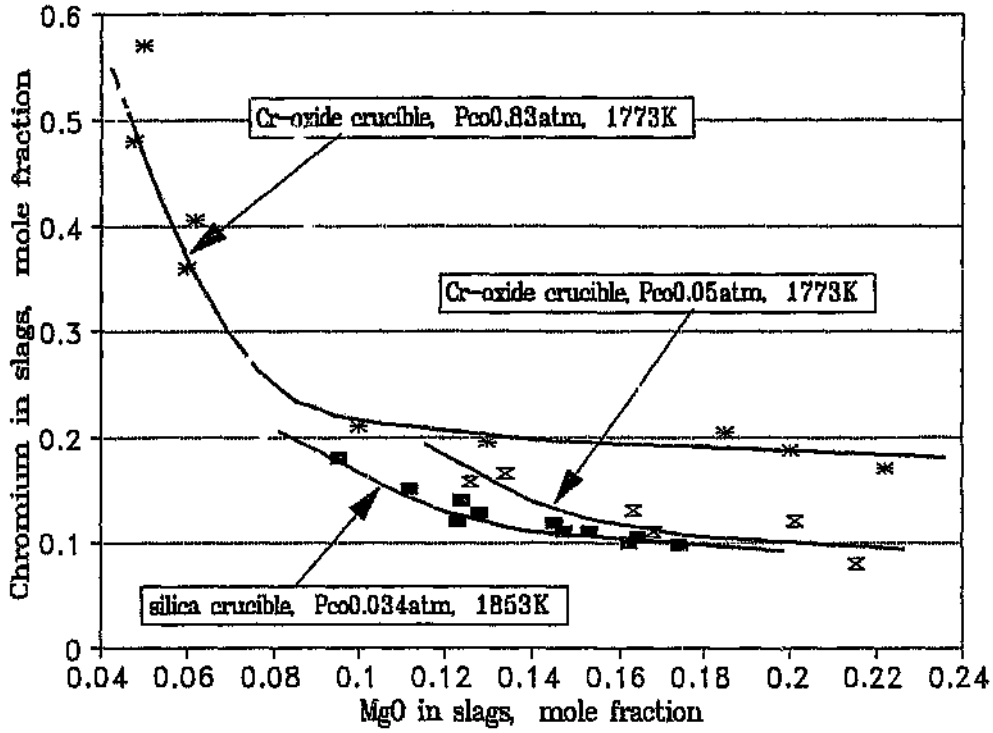


Figure 4.4.14. Effect of MgO on chromium of slags with metals of 0.55Cr-Fe-C-S-Si and slags of 0.01CaO-Fe_2O_3-MgO-Cr_2O_3-SiO_2-Al_2O_3, Al_2O_3/MgO=1.7, 0.03-0.05/0.02-0.1 Si in Cr/Si oxide crucibles.

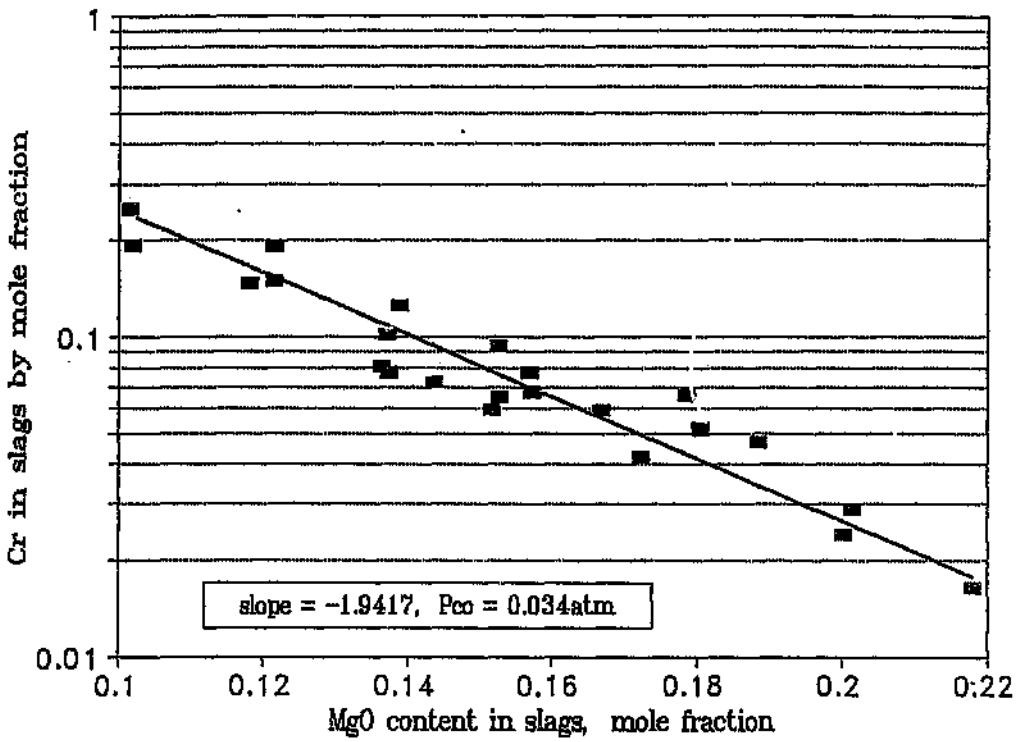


Figure 4.4.15. Effect of MgO on chromium of slags with metals of 0.22Cr-Fe-C-S-Si and slags of 0.01CaO-Fe_2O_3-MgO-Cr_2O_3-SiO_2-Al_2O_3, Al_2O_3/MgO=1.7, 0.02-0.1 Si in Si-oxide crucibles at 1580°C at 0.034 Pco.

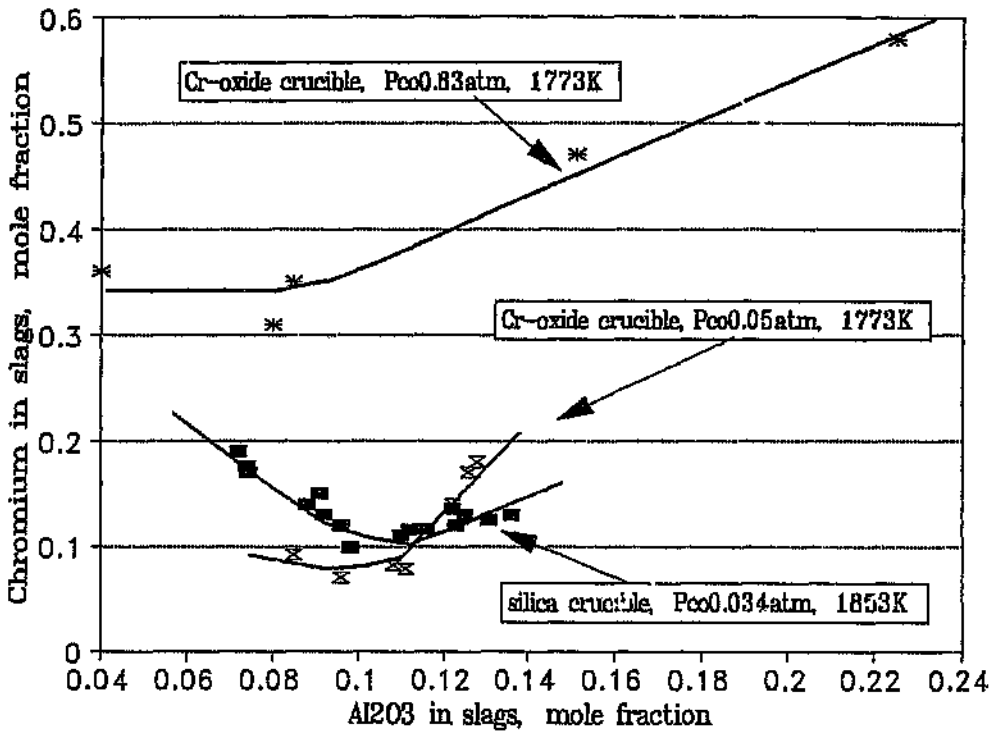


Figure 4.4.16. Effect of Al_2O_3 on chromium of slags with metals of 0.55Cr-Fe-C-S-Si and slags of 0.01CaO-Fe_2O_3-MgO-Cr_2O_3-SiO_2-Al_2O_3, Al_2O_3/MgO=1.7, 0.03-0.05/0.02-0.1 Si in Cr/Si oxide crucibles.

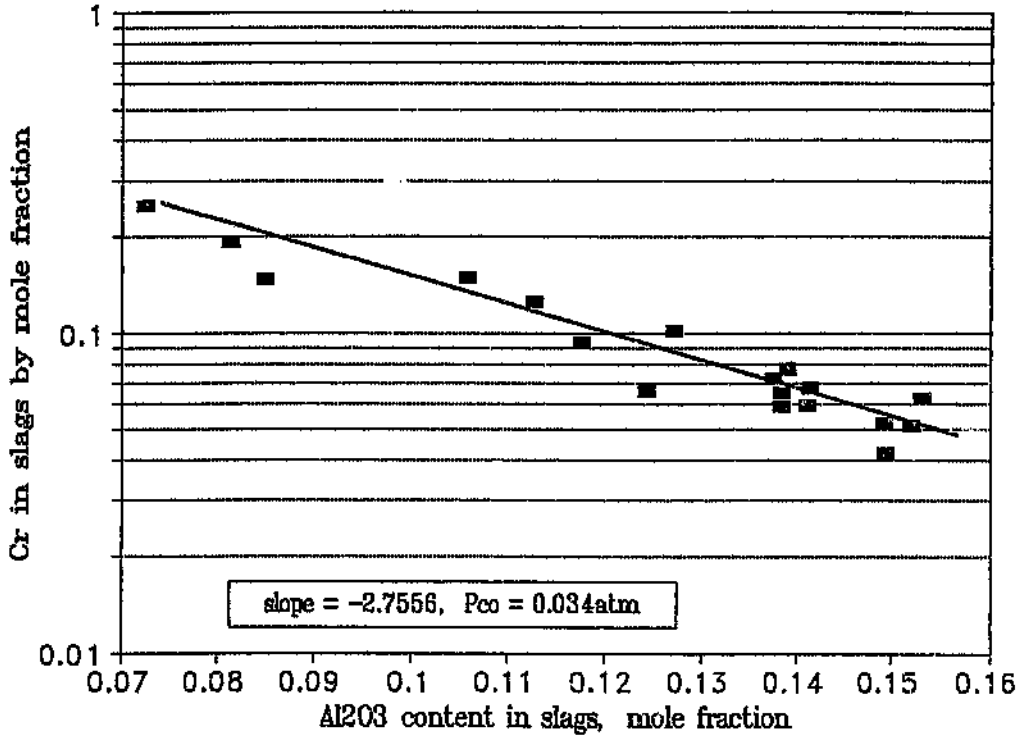


Figure 4.4.17. Effect of Al_2O_3 on chromium of slags with metals of 0.22Cr-Fe-C-S-Si and slags of 0.01CaO-Fe_2O_3-MgO-Cr_2O_3-SiO_2-Al_2O_3, Al_2O_3/MgO=1.7, 0.02-0.1 Si in Si-oxide crucibles at 1580°C at 0.034 P_{CO}.

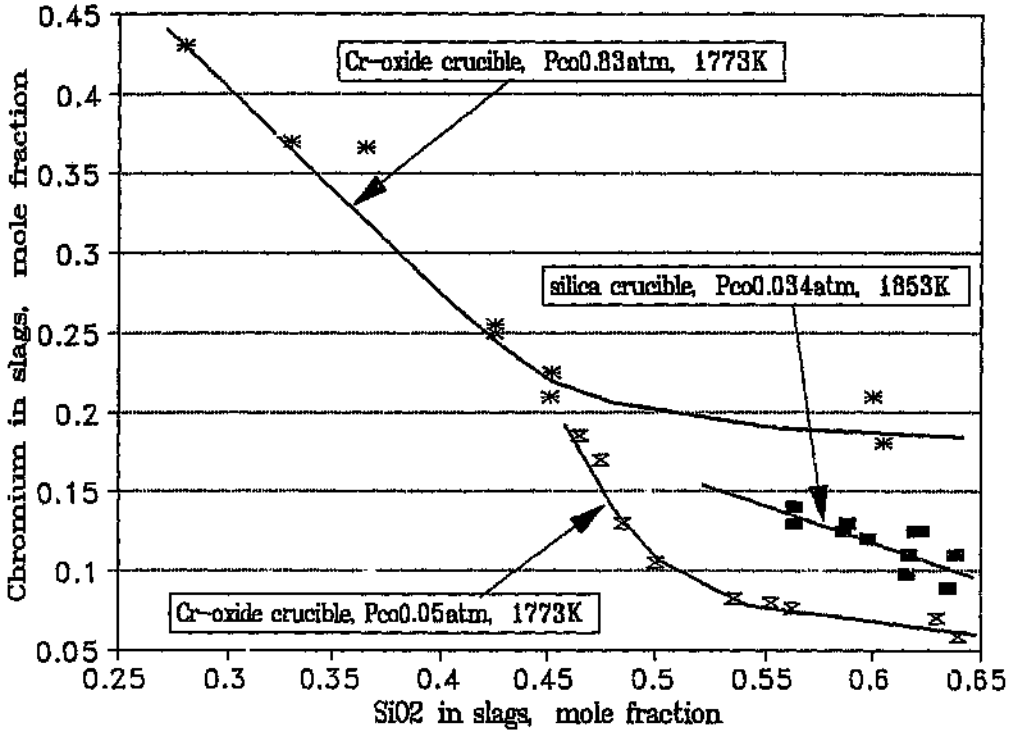


Figure 4.4.18. Effect of SiO_2 on chromium of slags with metals of 0.55Cr-Fe-C-S-Si and slags of 0.01CaO-Fe_2O_3-MgO-Cr_2O_3-SiO_2-Al_2O_3, Al_2O_3/MgO=1.7, 0.03-0.05/0.02-0.1 Si in Cr/Si oxide crucibles.

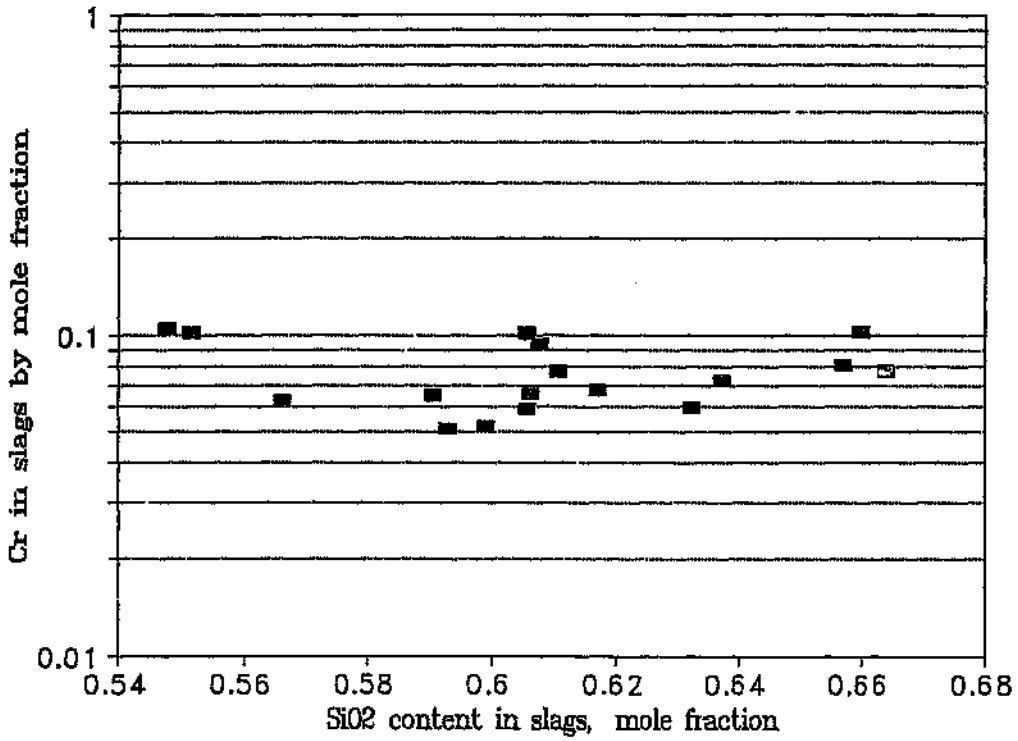


Figure 4.4.19. Effect of SiO_2 on chromium of slags with metals of 0.22Cr-Fe-C-S-Si and slags of 0.01CaO-Fe_2O_3-MgO-Cr_2O_3-SiO_2-Al_2O_3, Al_2O_3/MgO=1.7, 0.02-0.1 Si in Si-oxide crucibles at 1580°C at 0.034 Pco.

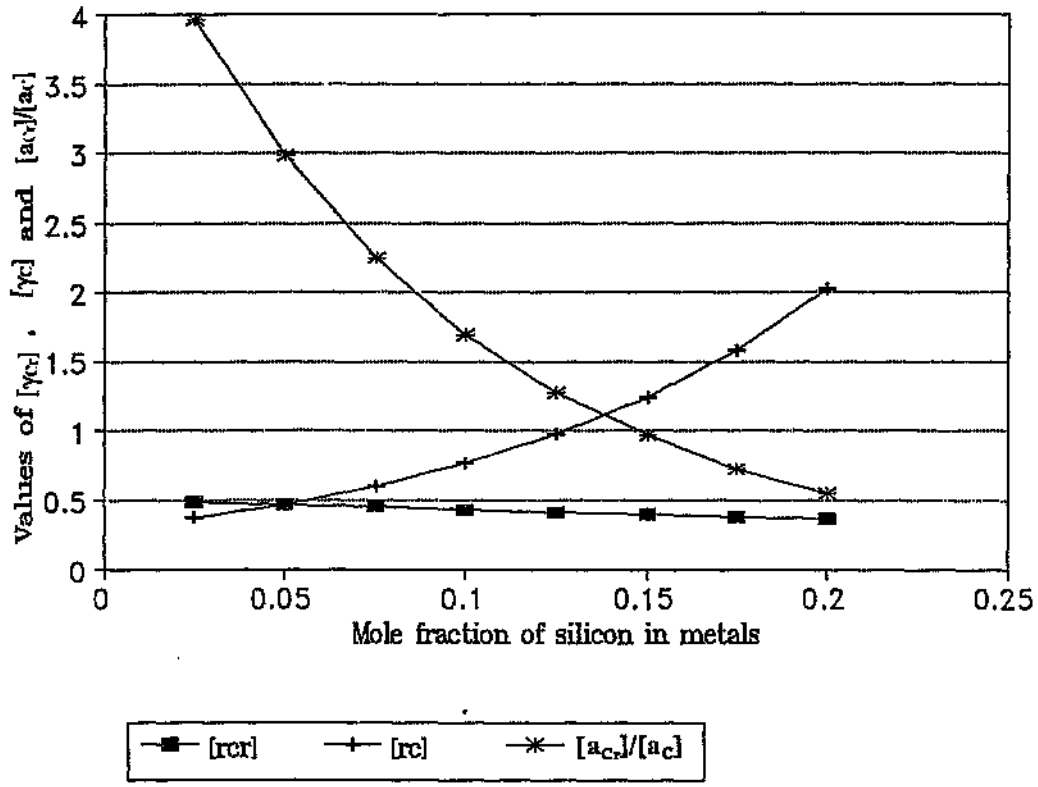


Figure 4.4.20. Relations between silicon and $[\gamma_{Cr}]$, $[\gamma_C]$ and $[a_{Cr}]/[a_C]$ with metals containing C-0.45Cr-0.001S-0.005Si by mole fraction at 1500°C.

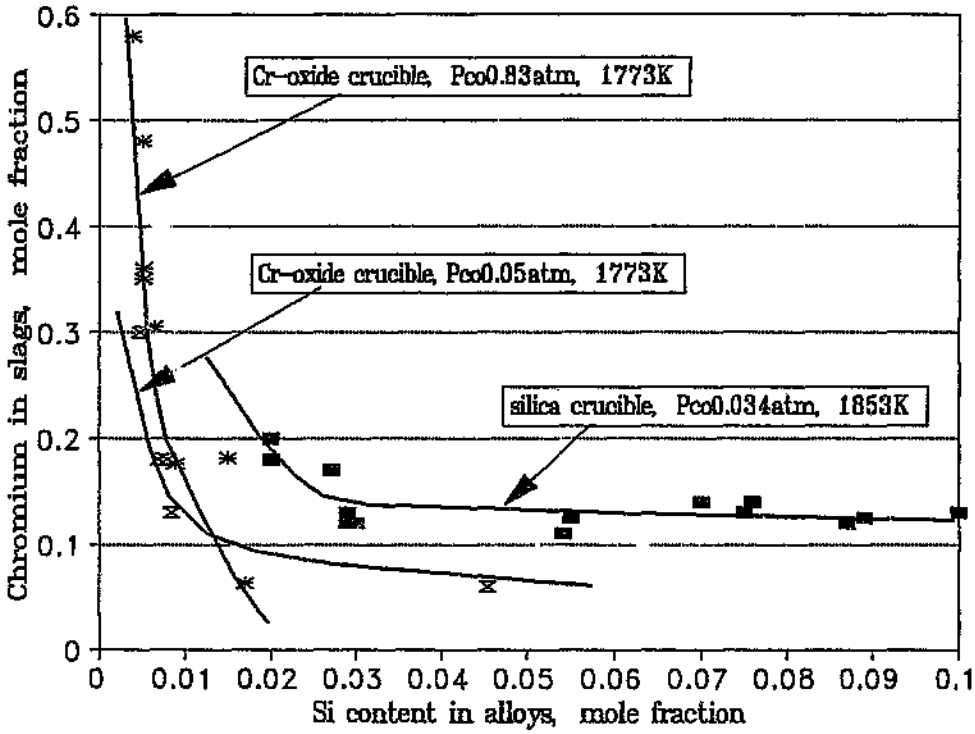


Figure 4.4.21. Effect of Si on chromium of slags with metals of 0.55Cr-Fe-C-S-Si and slags of 0.01CaO-Fe_2O_3-MgO-Cr_2O_3-SiO_2-Al_2O_3, Al_2O_3/MgO=1.7, 0.03-0.05/0.02-0.1 Si in Cr/Si oxide crucibles.

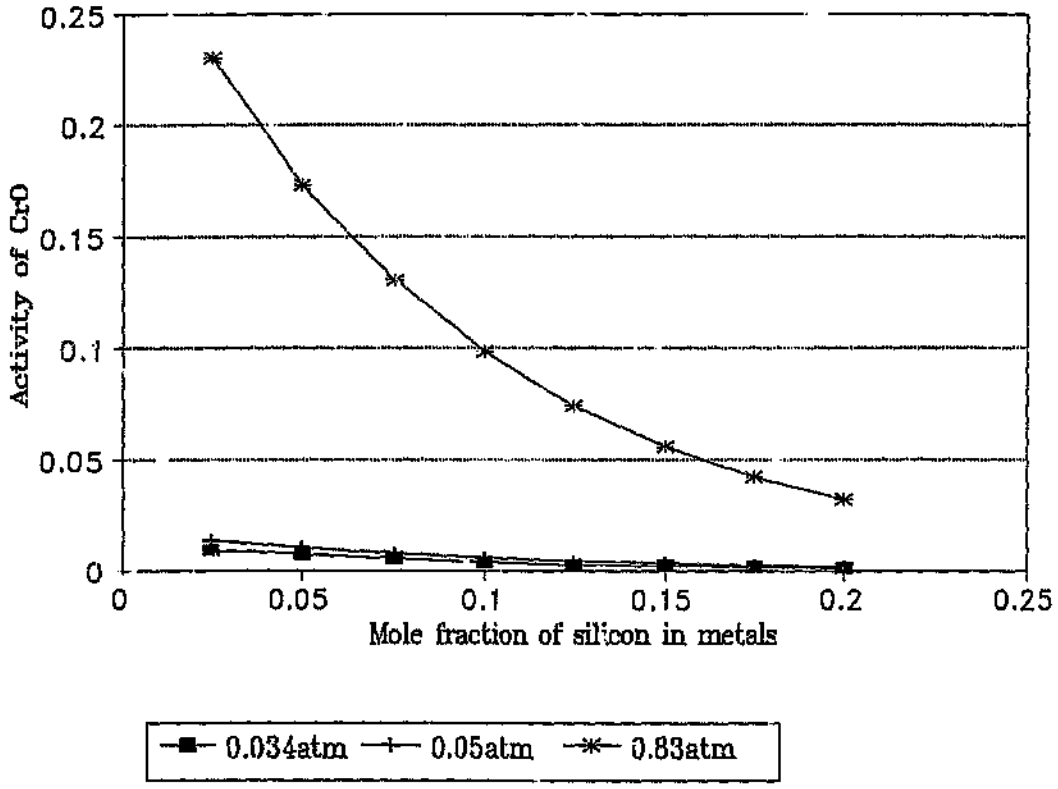


Figure 4.4.22. Relations between silicon concentration in metal and activity of CrO (a_{CrO}) in slag, metal containing C-0.45Cr-0.001S-0.005Si-Fe by mole fraction at 1500°C.

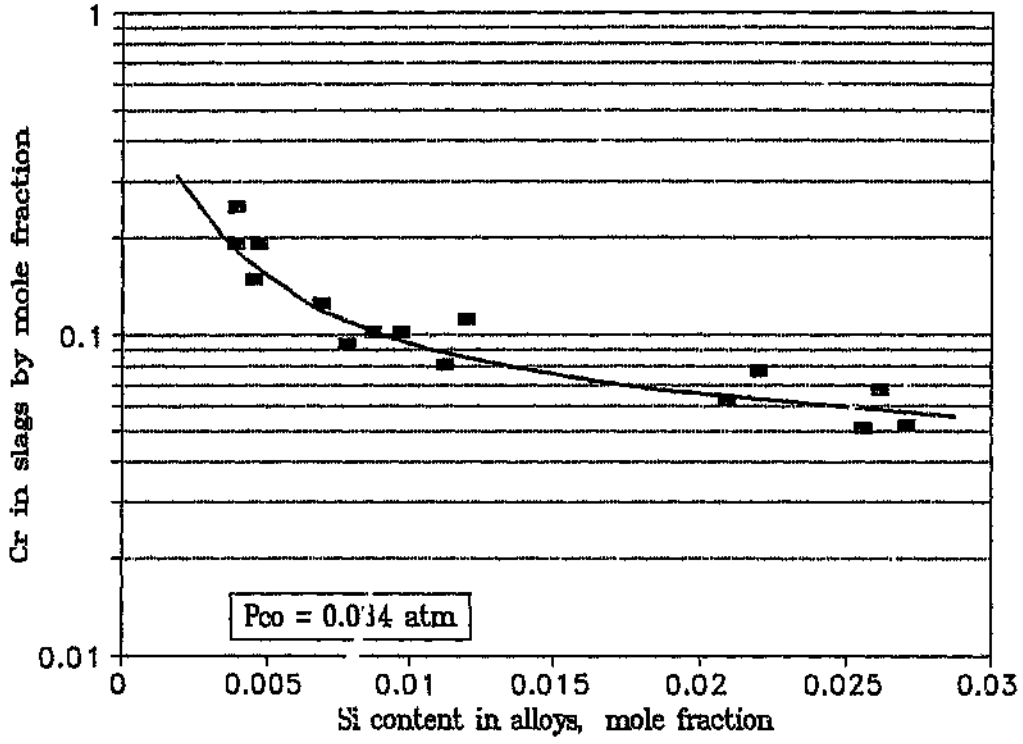


Figure 4.4.23. Effect of [Si] on chromium of slags with metals of 0.22Cr-Fe-C-S-Si and slags of 0.01CaO-0.007Fe_2O_3-MgO-Cr_2O_3-SiO_2-Al_2O_3. Al_2O_3/MgO=1.7, in Si-oxide crucibles at 1580°C at 0.034 Pco.

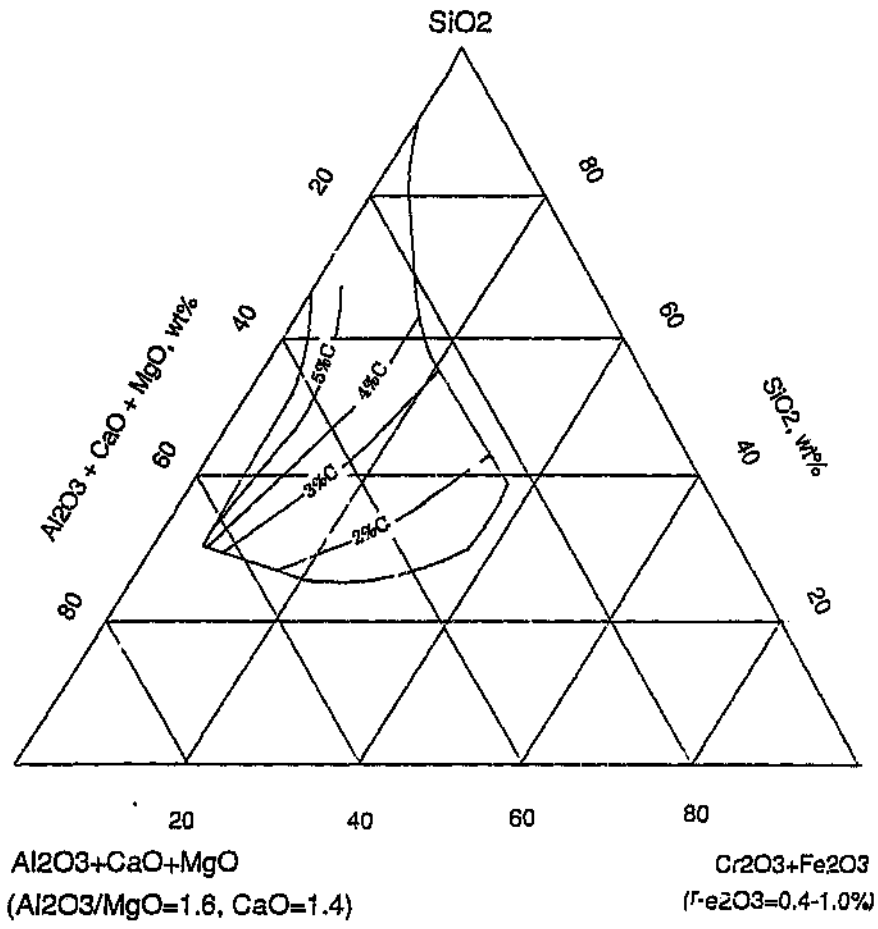


Figure 4.4.24. Carbon iso-concentration line of metals containing Cr-Fe-C-0.25%Si-(0.03-0.4)%S at 1500°C under CO atmosphere.

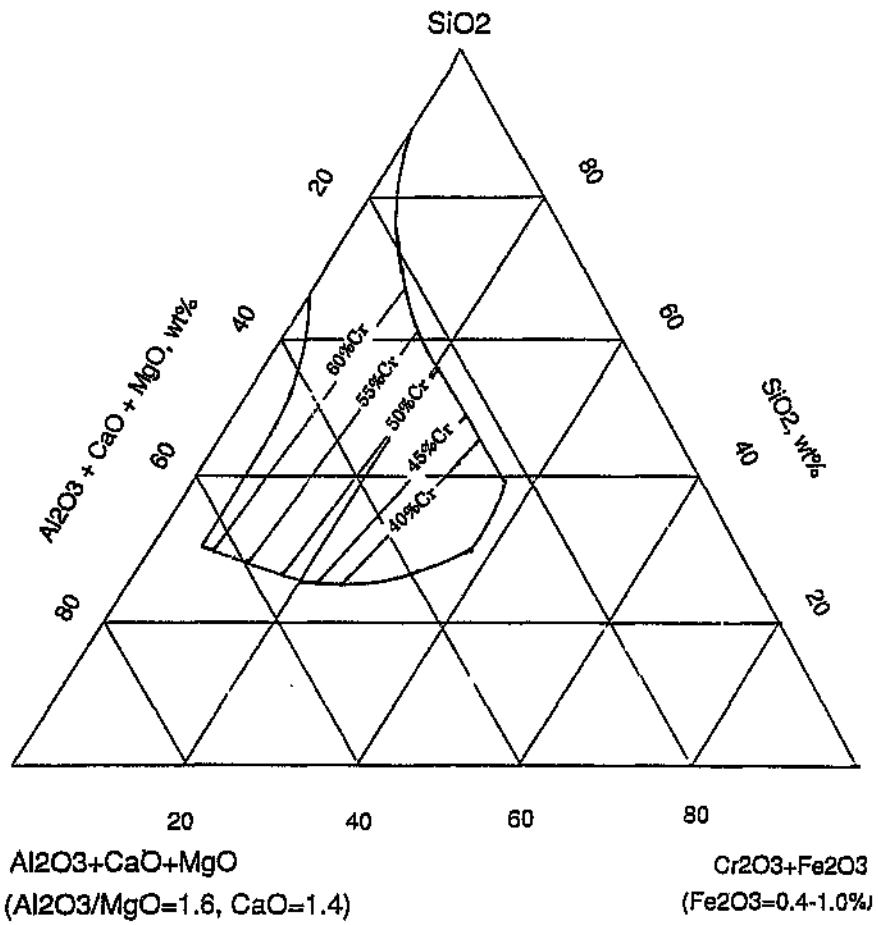


Figure 4.4.25. Chromium iso-concentration line of metals containing Cr-Fe-C-0.25%Si-(0.03-0.4)%S at 1500°C under CO atmosphere.

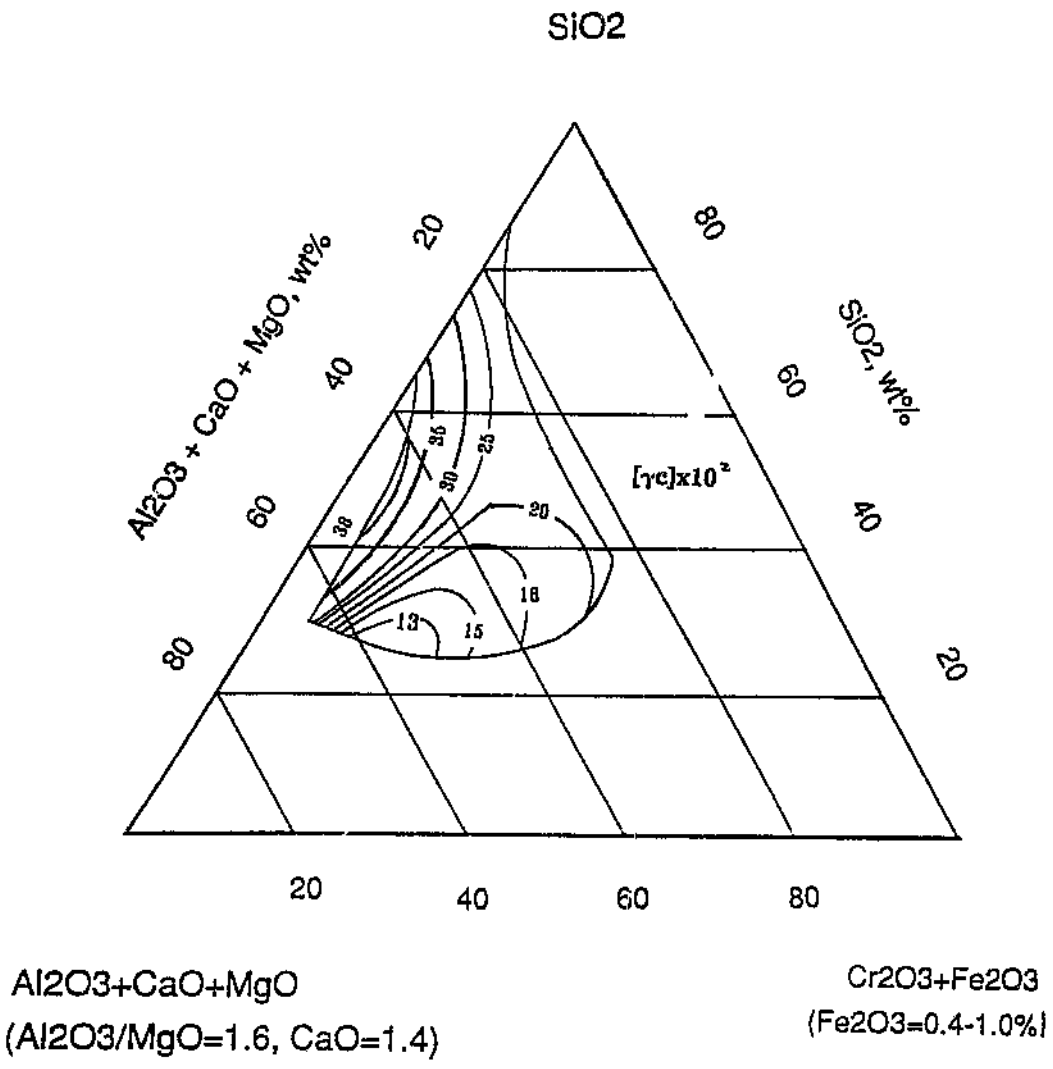


Figure 4.4.26. Iso-activity coefficient line for carbon in SiO_2-(Al_2O_3+CaO+MgO)-(Cr_2O_3+Fe_2O_3) ternary diagram with metals containing Cr-Fe-C-0.25%Si-(0.03-0.4)%S at 1500°C under CO atmosphere.

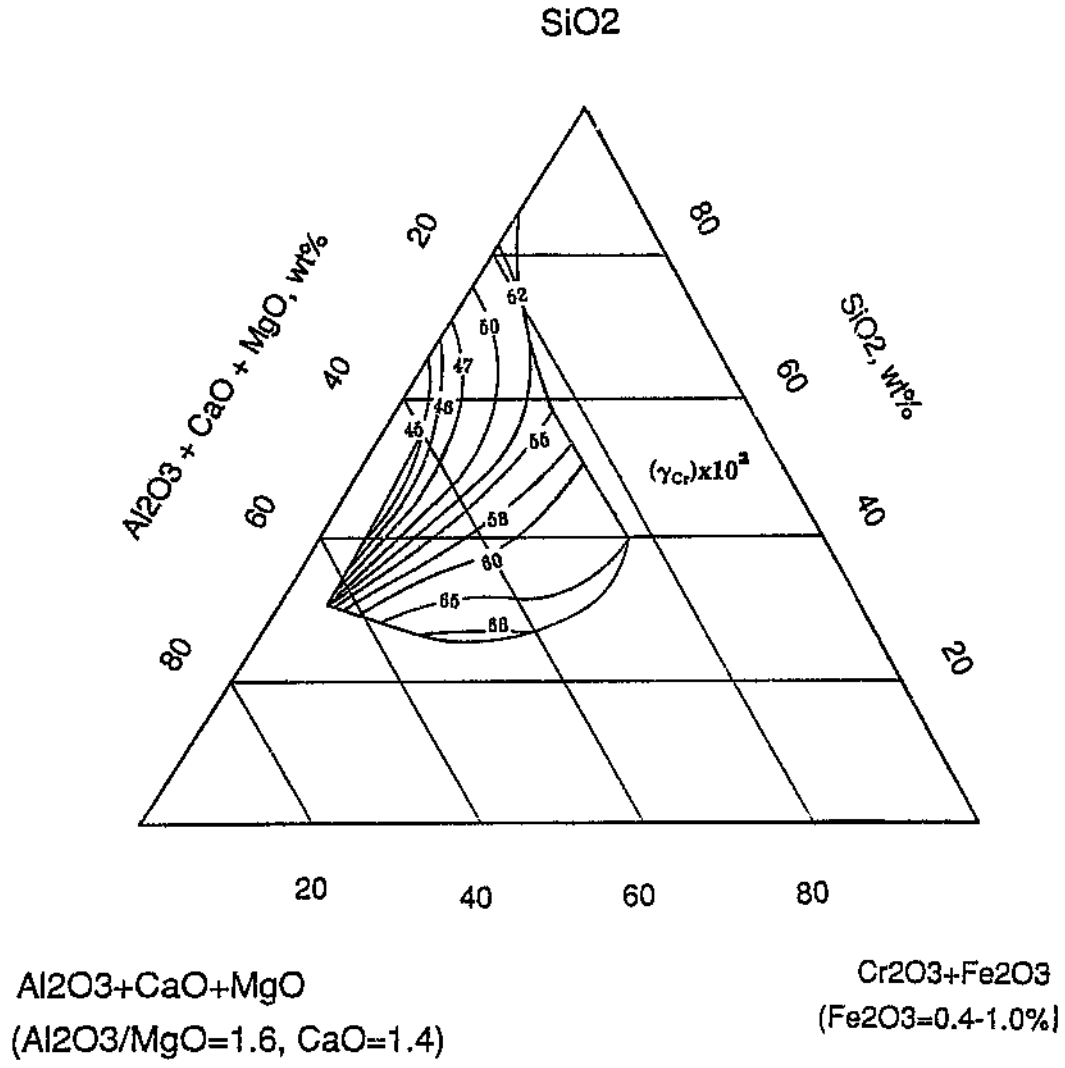


Figure 4.4.27. Iso-activity coefficient line for chromium in SiO_2-(Al_2O_3+CaO+MgO)-(Cr_2O_3+Fe_2O_3) ternary diagram with metals containing Cr-Fe-C-0.25%Si-(0.03-0.4)%S at 1500°C under CO atmosphere.

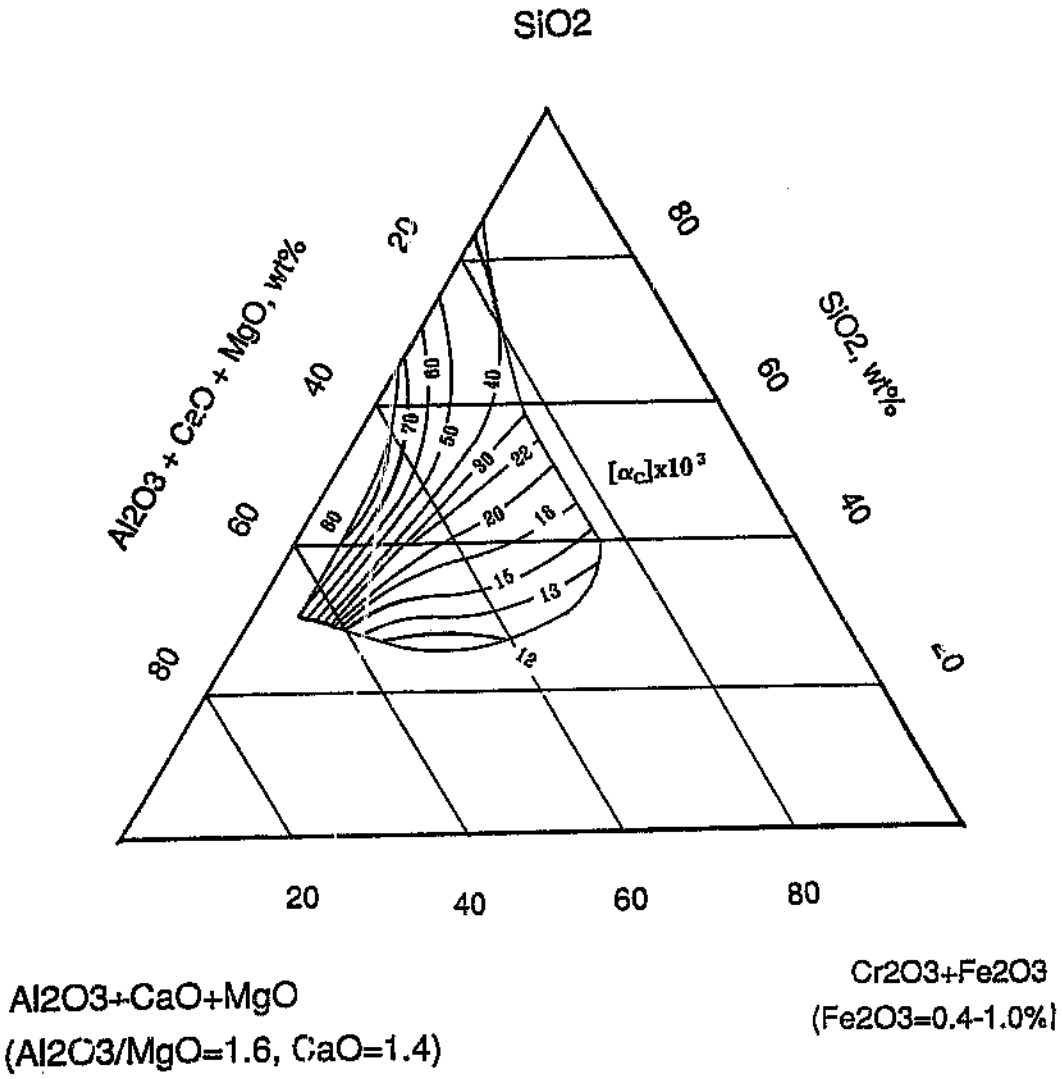


Figure 4.4.28. Iso-activity line for carbon in SiO_2-(Al_2O_3+CaO+MgO)-(Cr_2O_3+Fe_2O_3) ternary diagram with metals containing Cr-Fe-C-0.25%Si-(0.03-0.4)%S at 1500°C under CO atmosphere.

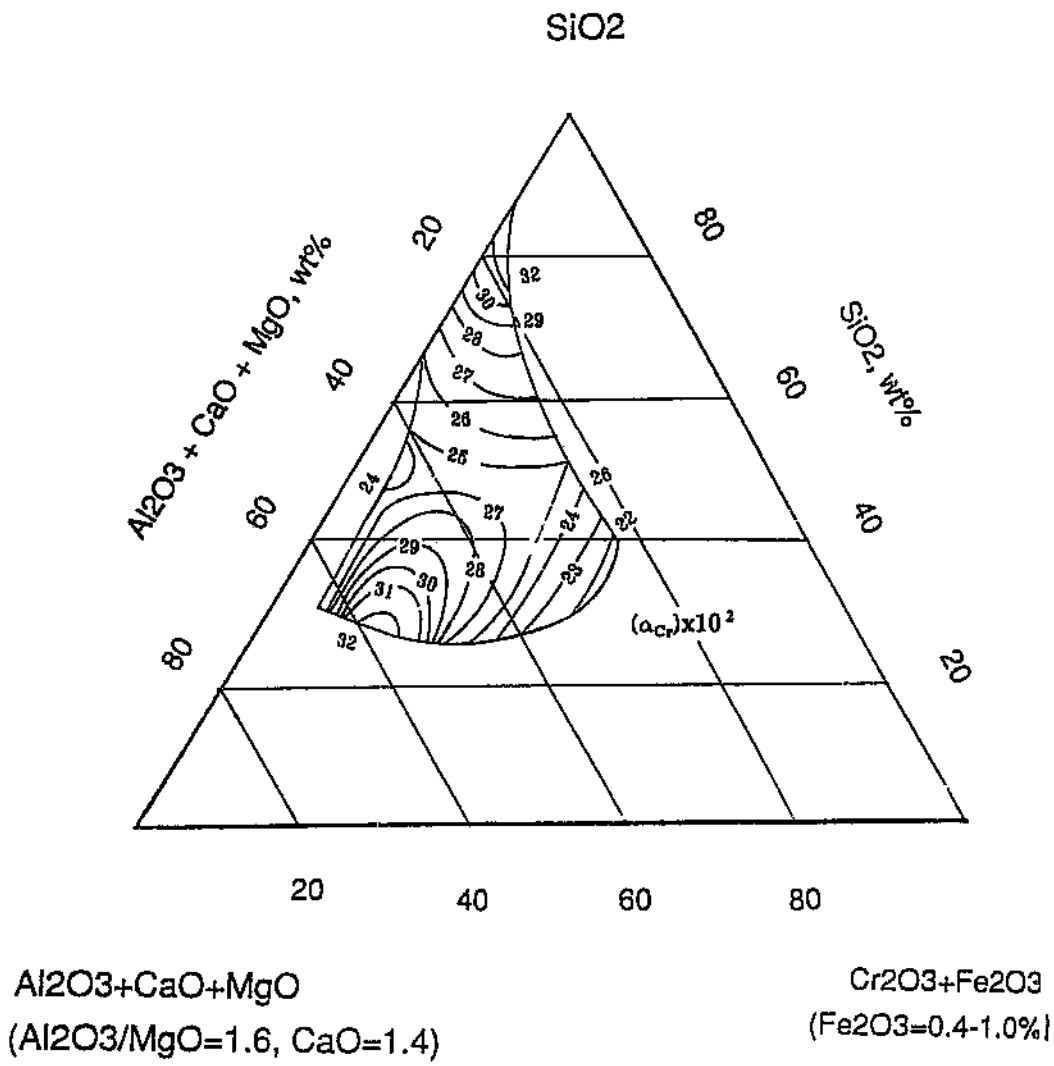


Figure 4.4.29. Iso-activity line for chromium in SiO_2-(Al_2O_3+CaO+MgO)-(Cr_2O_3+Fe_2O_3) ternary diagram with metals containing Cr-Fe-C-0.25%Si-(0.03-0.4)%S at 1500°C under CO atmosphere.

5. CONCLUSIONS

In the present investigation, 168 successful experiments were conducted. The samples were chemically analyzed at MINTEK. Among them 51 samples were from the experiments of gas-metal equilibrium and 234 slag and metal samples were from 117 successful gas-slag-metal experiments. The experimental results related to the alloys for both ferrochromium alloys containing about 45 to 65 per cent of chromium and stainless steel containing 15 to 25 per cent of chromium by mass.

The relation among carbon content, silicon content and the partial pressure of carbon monoxide has been studied in terms of gas-metal equilibrium in alumina crucible. The equilibrium distribution of sulphur, silicon and chromium between slag and metal phases has been investigated at 0.034atm, 0.05atm and 0.83atm of partial pressure of carbon monoxide in Cr-oxide crucibles at 1500°C and in silica crucibles at 1580°C.

Chromite crucibles and chromium oxide crucibles have been manufactured and used for the experimental work. The experimental results have been achieved by using chromium-oxide crucible, silica crucible for gas-slag-metal equilibrium study and alumina crucible for gas-metal equilibrium study.

Some of the problems and difficulties occurred in the experimental work and the methods used to overcome them were mentioned, such as the choice of crucible materials, the cracking of the chromium-oxide crucibles and the breaking down of the experimental furnace. The study on the behaviour of chromium-oxide crucible done by using SEM-EDAX, X-ray diffraction and chemical analysis is used to interpret the reasons why the chromium-oxide crucibles can be successfully utilised for the investigation.

The results and the relevant discussions are elucidated by 73 figures in the two

subsections of gas-metal equilibria and gas-slag-metal equilibria in forms of silicon distribution, sulphur partition and chromium distribution. The results expressed in two-dimensional graphs and ternary diagrams are treated and scrutinised in accordance with the Gibbs Phase Rule.

5.1. Gas-Metal Equilibrium

The relations among carbon content, silicon content and the partial pressure of carbon monoxide have been conducted in terms of gas-metal equilibrium. The results show that carbon content increases in the alloys with the increase of silicon content and the partial pressure of carbon monoxide.

Up to 0.15 atm of the partial pressure of carbon monoxide, the carbon content increases very quickly. Silicon in the metal phase promotes the increase of carbon in the alloy, when CO exists in the gas phase.

5.2. Silicon Distribution between Slag and Metal

The effects of slag composition, metal composition and tne partial pressure of carbon monoxide on the equilibrium partition of silicon between slag phase and metal phase have been scrutinised. In general, when the chromium concentration in the slag phase increases or when the partial pressure of carbon monoxide increases, the ratio of $[Si]/(SiO_2)$ decreases. The silicon partition does not decrease since the chromium content in the slag phase is higher than 0.2 mole fraction. The equilibrium distribution ratio of silicon increases with an increase of alumina content in the slag phase; or with a

decrease of MgO concentration in the slag phase. A high chromium concentration in the metal promotes a high effect of both MgO and alumina.

The metal containing higher chromium concentration shows a greater effect of MgO on the silicon ratio, compared with the result from the metal containing only 0.22 mole fraction chromium, which demonstrates an unremarkable effect of MgO on the silicon partition. The silica content in the slag phase and the partial pressure of carbon monoxide have little effect on the silicon ratio, except the result with the metal of 0.55 chromium at 0.034 atm Pco.

The silicon partition ratio increases with an increase of chromium concentration in the metal containing high chromium at a low partial pressure of carbon monoxide. The increase of carbon content in the metal phase increases the silicon distribution ratio. A higher silicon distribution can be acquired at a lower partial pressure of carbon monoxide when the content of carbon in the metal phase excesses 0.14 mole fraction. The effect of carbon concentration on the silicon partition ratio is scrutinised and discussed by using the term of the $[\gamma_C]^2/[\gamma_{Si}]$ ratio.

5.3. Sulphur Distribution between Slag and Metal

The sulphur transfer from metal phase to slag phase increases with lowering partial pressure of carbon monoxide, increasing MgO content of the slag phase, decreasing SiO_2 content of slag, dwindling Al_2O_3 content of slag , and declining chromium oxides in the slag phase. When SiO_2 content is in the range of 0.35 to 0.5 of molar fraction, the sulphur distribution ratio increases tremendously with reducing partial pressure of carbon monoxide from 0.83atm to 0.05atm. When SiO_2 raises from 0.5 to 0.65, a lower partial pressure of carbon monoxide favours a lower sulphur partition ratio. With a low

partial pressure of carbon monoxide, sulphur transfer from metal phase to slag phase increases by decreasing chromium concentration in the slag phase.

The sulphur transfer from metal phase to slag phase increases by the factors like increasing carbon content in the metal; decreasing chromium content of the metal phase; declining sulphur content in the metal; dwindling silicon content of the metal phase in the range of 0.005 to 0.02 molar fraction; and particularly lowering the partial pressure of carbon.

The partial pressure of carbon monoxide has no pronounced effects on the sulphur partition when carbon content of the metal is less than 0.15 in molar fraction. The impacts of partial pressure of carbon monoxide, combined with carbon content of metal phase are influenced greatly by the silica content in the slag phase.

The relations between MgO and sulphur capacity, the effects of silicon on the terms of $[\gamma_{Si}]^{1/2}/[\gamma_S]$ and $[a_{Si}]^{1/2}/[\gamma_S]$, and the influences of silicon, carbon, chromium and sulphur on the activity coefficients of sulphur and carbon and on the term of $[\gamma_S][\gamma_C]$ have been examined and used to interpret the experimental results. 22 figures are elucidated in this section.

5.4. Chromium Distribution in Gas-Slag-Metal Equilibria

By contemplating the formula of " $\ln L_{Cr} = x\ln\{[\%C]/Pco\} + K'_{4.4.5}$ ", The slopes of 1.125, 1.10 are acquired from the two series of experiments, conducted at 1500°C in Cr-oxide crucibles at 0.83atm; and 0.05atm of partial pressure of carbon monoxide respectively. A slope of 1.07 is achieved by the experiments conducted at 1580°C in silica crucibles at 0.034atm of partial pressure of carbon monoxide.

The results represent that CrO is 75 per cent of the total chromium oxides in the slag under the atmosphere of carbon monoxide in Cr-oxide crucible at 1500°C, 80 per cent at 0.05atm of partial pressure of carbon monoxide in Cr-oxide crucible at 1500°C and 86 per cent at 0.034atm of partial pressure of carbon monoxide in silica crucible at 1580°C respectively. A higher percentage of CrO exists in the slag when a lower partial pressure of carbon monoxide is imposed. The percentage of CrO in slag increases with the increase of silica concentration in the slag.

The chromium concentration in the slag decreases with the factors such as increase of carbon content in the metal; increase of silicon concentration of the metal phase; and decrease of the partial pressure of carbon monoxide. The effect of carbon on the chromium concentration in the slag is higher when the metal contains lower chromium.

The chromium concentration in the slag decreases when MgO content increases in the slag. When the metal contains high chromium, the chromium content of slag decreases with an increase of alumina when alumina concentration is lower than 0.1 mole fraction in the slag, and a further increase of alumina increases the chromium content in the slag. Meanwhile the chromium in the slag only decreases with the increase of alumina when the metal contains low chromium. The chromium concentration in slag decreases with increasing SiO_2 content in the slag when the metal contains high chromium.

The results achieved in Cr-crucibles at 1500°C and 0.83atm of the partial pressure of carbon monoxide, are expressed in the SiO_2-(Al_2O_3+CaO+MgO)-(Cr_2O_3+Fe_2O_3) ternary diagrams by means of iso-concentration lines for carbon and chromium. Based upon the measuring compositions of alloys in equilibrium with the slag phase, the activity coefficients and the activities for carbon and chromium in the metal phase are computed and plotted in the SiO_2-(Al_2O_3+CaO+MgO)-(Cr_2O_3+Fe_2O_3) ternary diagrams by means of iso-activity coefficient lines and iso-activity lines for carbon and chromium.

6. REFERENCE

1. D. Slatter, The chromium resources of Zimbabwe, International Economic Resources Conference on Zimbabwe held in Salisbury, Zimbabwe, 1st-5th Sep., 1980, pp27-36.
2. A. H. Sully and E. A. Brandes, Chromium, second edition, London, 1967, pp1-17.
3. P. E. Streicher, Metal Bulletin's, the Second International Ferro-Alloys Conference, 1979, Copenhagen, pp20-25.
4. D. D. Howat, Chromium in South Africa, J. SAIMM, March 1994, pp335-240.
5. D. Slatter, The physical properties of Rhodesian chromium ores and their significance in ferro-chromium production, Report (No.28) to Institute of Mining Research, University of Rhodesia, 1978.
6. P. Brethier, Ann. Chim. Phys. 17 (1821), pp55.
7. E. C. R. Fremy, Acad. Sci., Paris 44 (1857), pp632.
8. E. G. Odelstjerna, Fernkontor. Ann. 70 (1887), pp297.
9. H. C. R. Moissan, Acad. Sci., Paris 116 (1893), pp349.
10. X. W. Pan and R. H. Eric, Proceedings of INFACON 7, Trondheim, Norway, June 1995, pp383-390.
11. D. Slatter, Proceedings of INFACON 7, Trondheim, Norway, June,1995, pp249-262.
12. C.P. Heanley and P. M. Cowx, 40th Elec. Furn. Conf. Iron & Steel Soc. of AIME, Kansas City, 1982, pp257.
13. A. B. Wikander, H. G. Herlitz and S. O. Santen, Elec. Furn. Proc. 1987, pp225-231.
14. H. R. Larson, J. F. Elliott and B. R. Perking, Proceedings of INFACON 6, Cape Town, April 1992, pp93-97.
15. M. Ford, J. F. Oosthuien, Proceedings of INFACON 7, Trondheim,

Norway, June 1995, pp263-272.

16. H. J. Kammeyer, K. U. Maske and G. Puggh, Proceedings of the Fifth International Ferro Alloys Congress, INFACON 89, 1989, Vol. 1, pp95.
17. T. Hamada, et al, Fifth Iron and Steel Congress, Washington DC, April 1986, pp19-25.
18. P. R. Thomas and E. H. Boyle, J., U.S. Bureau of Mines, I.C.8977, 1984.
19. G. Rath and G. Rottmann, Elec. Furn. Conf. Proc., AIME, 1980, 38 pp1228.
20. G. Volkert and K. D. Frank, Metallurgie de Ferrolegierungen, 2nd ed. 1972, Berlin, Springer, pp341-344.
21. W.Dresler, I&SM, January 1988, pp43-50.
22. W.Dresler. Proc. of 6th international I&S Cong. 1990, Nagoya, ISIJ, pp194-199.
23. P.A. Sakharuk, G.D.Dmityovskayaa and O.V. Geev, Stal, 1961, pp31-33.
24. H.Franke and G.Duderstadt, INFACON 74, 1974, Johannesburg, pp58-65.
25. Taizoh Senga, et al. INFACON 89, New Orleans, Vol.1, pp69-76.
26. M.Sciarone. I&SM, April, 1987, pp28-29.
27. H.Franke and G.Duerstadt. Metal Bulletins Second International Ferro-Alloys Conference, Copenhagen, 1979,pp81-84.
28. W.Krieger, J.Nakesch, et al. I&SM,March, 1988, pp19-24.
29. F.J.Hahn, H.P.Hastert, et al. I&SM, March,1990, pp43-47.
30. W.Ding and S.E. Olsen, Elec. Fur. Conf. Procc., 1991, pp259-264.
31. J.K.S.Tuset. INFACON 6, Vol.1, 1992, pp193-199.
32. M. Maeda, Ph.D. thesis, University of Tokyo, 1981.
33. M. Akyuzlu and R. H. Eric, J. of SAIMM, Vol.92, No. 4, April 1992, pp101-110.
34. J. D. Gilchrist, Extraction Metallurgy, 2nd edition, Pergamon Press, 1980.
35. E. T. Turkdogan, Physicochemical properties of molten slags and glasses, London, the Metal Society, 1983.
36. W. J. Rankin A. K. Biswas, The behaviour of chromium in reduced slag-

metal systems, Arch. Eisenhuttenwes, 50, (1), 7-11, ISSN:0003-8962, Jan. 1972.

37. H. F. Marston and B. B. Argent, Spectroscopic investigation of Cr(II), Cr(III), and Cr(VI) in silicate slags, Proceedings of the Sixth International Iron and Steel Congress, 1990, Nagoya, ISIJ, pp175-180.
38. V. N. Boronenkov et al, Steel USSR, Vol.1, No. 12, 1971 pp959-961.
39. R. C. Urquhart, Report No. 1482, National Institute for Metallurgy, Johannesburg, South Africa 1975.
40. R. B. Bird, et al. Transport phenomena, New York, Wiley & Sons, 1960 pp558.
41. O. Demir and R. H. Eric, Kinetics of chromite dissolution in liquid slags, Proceeding of INFACON 7, Trondheim, June 1995, pp339-350..
42. C. W. McCoy and W. O. Philbrook, The behaviour of chromium in slag-metal systems under reducing conditions, Trans. AIME, 1958, Vol. 212, PP226-235.
43. H. Cengizler, The thermodynamic activity of MnO in manganese slags and slag-metal equilibrium, Ph.D. thesis, University of the Witwatersrand, 1993, Johannesburg.
44. G. W. Healy et al, The thermodynamics of chromite ore smelting, Trans. ISS, 1987, No.12, pp51-59.
45. D. Neuschutz, P. Janben, et al, effect of flux additions on the kinetics of chromite ore reduction with carbon, INFACON 7, Trondheim, June 1995, pp371-381.
46. P. Weber, The reduction behaviour of Bushveld Complex chromites, Ph.D. thesis, University of the Witwatersrand, 1991, Johannesburg.
47. M. Fujita, et al, Influence of slag composition on smelting reaction mechanism, Tetsu-to-Hagane, Vol.70, pp117.
48. Xu, W. Dai, The melting behaviour of chromite ores and the formation of slag in the production of high carbon ferro-chromium, INFACON 6, Cape town, Johannesburg, 1992, pp87-92.

49. Shin-ya Kitamura, Takashi Arai, Michitaka Matsuo and Kazuo Okohira, Influence of various factors on the transfer rate of oxide Cr in molten slag phase, Proceedings of the Sixth International Iron and Steel Congress, 1990, Nagoya, ISIJ, pp139-146.

50. N. R. Griffing, W. D. Forgeng, G. W. Healy, C-Cr-Fe liquidus surface, Trans. AIME, Vol. 224, Feb. 1962, pp148-159.

51. J. C. M. Wethmar, D. D. Howat, P. R. Jochens, Phase equilibrium in the Cr-Fe-Si-C system in the composition range representative of high carbon ferro-chromium alloys produced in South Africa, Journal metal. Sci., Journal announcement 7511, 9, (6), June, 1975, pp291-296.

52. J. C. M. Wethmar, Phase quilibria in the system Cr-Fe-Si-C, Msc. thesis, Univ. of the Witwatersrand, JHB, 1975.

53. O. Lucas, H. Wentrup, Solubility of carbon in Fe-Cr-Si alloys, Z. Anorg. Allg. Chem., Vol. 220, 1934, pp3229-339.

54. M. S. Petrushevski, and P. V. Gel'd, Solubility of carbon in liquid ferrosilicochromium, Zhurnal Prikladnoi Khimi, Vol.35, No. 6, June 1962, pp1227-1236.

55. M. S. Petrushevski, and P. V. Gel'd, Calculation of the solubility of carbon in liquid ferrosilicochromium and ferrosilicomanganese in the quasi-chemical approximation, Zhurnal Prikladnoi Khimi, Vol. 40, No. 11, 1967, pp2399-2405.

56. M. S. Petrushevski, and P. V. Gel'd, Influence of the ferrosilicomanganese and ferrosilicochromium on the activity coefficient of carbon, Zhurnal Prikladnoi Khimi, Vol.40, No. 11, Nov. 1965, pp2568-2571.

57. K. L. Kossyrev and S. E. Olsen, Silicon and carbon in chromium alloys, INFACON 7, Trondheim, June 1995, pp229-338.

58. G. W. Healy, activities in the liquid Cr-Fe-C system above 1600°C, Iternational symposium on innovative technology on reactor design, Colorado, 1986, pp667-679.

59. W. Dresler, Activities of silicon and carbon in liquid iron-silicon-carbon

alloys, I&SM, March 1990, pp95-100.

60. W. Dresler, Thermodynamic aspects of oxygen refining and carbothermic reduction processes for the syste.. Fe-Cr-Ni-C-Si-Cr_2O_3, Proceedings of the sixth international iron and steel congress, 1990, Nagoya, ISIJ, pp198-200.
61. I. A. Pavars, B. A. Baum and P. V. Gel'd, Kinematic viscosity and electrical resistance of molten iron-chromium alloys, Russian Journal of physical chemistry, 43(11), 1969, pp1542-1545.
62. Y. Xiao and L. Holappa, Determination of activities in slags containing chromium oxides, ISIJ Int., 1993, Vol. 33, pp66.
63. Y. Xiao and L. Holappa, Thermodynamics of slags containing chromium oxides, INFACON 7, Trondheim, June 1995, pp319-328.
64. M. Maeda, N. Sano, Thermodynamics of chromium oxide in molten CaO-MgO- Al_2O_3-SiO_2 slags coexisting with solid carbon, Fac. of Eng., The Univ. of Tokyo, 7-3-1 Hongo Bunkyo-ku 113, June 16, 1981.
65. G. H. Johnston, P. R. Jochens and D. D. Howat, Physicochemical properties of slags in system MgO-Al_2O_3-SiO_2 and their application to the technology of ferro-alloy smelting, Proc. INFACON 74, 1974, Johannesburg, pp217-225.
66. H. Flood, K. Grjotheim, thermodynamic calculation of slag equilibria, J of the Iron and Steel Institute. Vol. 171, May 1952, pp64-70.
67. J. F. Elliot, D. C. Lynch and T. B. Braun, A criticism of the flood-Grjotherm ionic treatment of slag-equilibria, Metallurgical Transactions of AIME, Vol. 6b, Dec. 1975, pp495-501.
68. K. Grjotheim, M. K. Brun, Application of the Flood-Grjotheim thermodynamic treatment to the slag-metal equilibria, Canadian Metallurgical Quarterly, Vol. 16,1977, pp161-165.
69. G. W. Toop and C. S. Samis, Activities of ionic in silicate melts, Transactions of Metallurgical Society of AIME, Vol. 224, Oct. 1962, pp878-887.

70. C. R. Masson, Ionic equilibria in liquid slags, Journal of American Ceramics Society, Vol. 51, No.3, May 1967, pp134-143.
71. C. R. Masson, An approach to the problem of ionic distribution in liquid slags, Halifax, Report of the National Research Council, 1965, pp201-221.
72. C. R. Masson, Thermodynamics and constitution of silicate slags, Journal of the Iron and Steel Institute, Vol. 210, No. 2, 1972, pp89-96.
73. S. G. Whiteway, I. B. Smith and C. R. Masson, Activities and ionic distributions in liquid silicates: application of polymer theory, Canadian Journal of Chemistry, Vol.48, 1970, pp1456-1464.
74. C. R. Masson, I. D. Sommerville, and D. J. Sosinsky, Extension of polymer theory to ternary silicate melts, Proceedings of the 3rd Interactional Conference on Molten Slags and Fluxes, Institute of metals, Glasgow, 1988, pp241.
75. T. Yokokawa, K. Niwa, Free energy of solution in binary silicate melts, Transactions of the Japan Institute of Metals, Vol.10, 1969, pp3-7.
76. M. L. Kapoor, M. G. Frohberg, Theoretical treatment of activities in silicate melts, Proceedings of the International Symposium on Metallurgical Chemistry- applications of Ferrous Metallurgy, Sheffield, 1971.
77. D. R. Gaskell, Thermodynamic models of liquid silicates, Canadian Metallurgical Quarterly, Vol. 20, No. 1, pp3-19.
78. P. L. Lin, A. D. Pelton, A structural model for binary silicate system, Metallurgical Transactions of AIME, Vol. 10B, No. 4, 1979, pp667-675
79. J. Q. Chen, The thermodynamic data for metallurgist, CSM press, 1985, pp217-235
80. J. Lumsden, Physical Chemistry of Process Metallurgy; Part 1, edt. G. R. St Pierre, AIME, New York, 1961, p165.
81. L. S. Darken, Thermodynamics of binary metallic solutions. Trans. Metall. Soc. AIME, 1967, Vol. 239, pp80.
82. M. Fujita, S. Maruhashi, Equilibrium between FeO-MnO-SiO_2 slags and molten iron. Tetsu-to-Hagane, 1970, Vol.51, pp830.

83. R. A. Sharma and F. D. Richardson, Activities of manganese oxide sulphide capacities and activity coefficients in aluminate melts. Transactions of the metallurgical Society of AIME, Vol. 233, Aug.1965, pp1586-1592.

84. R. Altman and H. H. Kellogg, Thermodynamics of FeO-MnO-TiO_2 melts saturated with iron at 1475°C, Trans. IMM, Sect. c, 1972, Vol. 81, pp163

85. E. Martin, I. Abdelkarim, I. D. Sommerville and H. B. Bell, Metal-slag–gas reactions and processes, Electrochem. Soc., Toronto, 1975, pp1-7.

86. S. Ban-Ya, A. Chiba and A. Hikosaka, Thermodynamics of Fe_tO-M_xO_y (M_xO_y-CaO, SiO_2, TiO_2 and Al_2O_3) binary melts saturated with solid iron, Australia-Japan Extractive Metallurgy Symposium, Austr. IMM, Sydney, July, 1980, pp457.

87. R. M. Grant, The derivation of thermodynamic properties of slags from slag fuming plant data, ibid., pp75.

88. J. Shim and S. Ban-ya, The solubility of magnesia and ferric-ferrous equilibrium in liquid Fe_tO-SiO_2-CaO-MgO slags. Tetsu-to-Hagane, 1981, Vol. 67, pp1735.

89. S. Ban-ya and M. Hino, Calculation of activities of the constituents in Fe_tO-(CaO+MgO)-(SiO_2+P_2O_5) slags by regular solution model, Tetsu-to-Hagane, 1987, Vol. 73, pp476.

90. R. Nagabayashi, M. Hino and S. Ban-ya, Mathematical expression of phosphorus distribution in steelmaking process by quadratic formalism, ISIJ Int.,1989, Vol.29 pp140.

91. S. Ban-ya, Y. Iguchi and H. Honda, Proceedings of International Symposium on the Physical Chemistry of Iron and Steelmaking, Can IMM, Toronto, 1982, pp39.

92. R. A. Sharma and F. D. Richardson, The solubility of calcium sulphide and activities in lime-silica melts, J. of the Iron and Steel Inst., 1962, vol.200, pp373

93. J. D. Baird and J. Taylor, Reaction between silica and carbon and the activity of silica in slag solution, Trans. of the Faraday Soc., 1958, Vol. 54,

pp526.

94. D. A. R. Kay and J. Taylor, Activities of silica in the lime+alumina+silica system, Trans. Faraday Soc., 1960, Vol.56, pp1372.

95. R. H. Rein and J. Chipman, The distribution of silicon between Fe-Si-C alloys and SiO_2-CaO-MgO-Al_2O_3 slags. Trans. AIME, Vol.227, 1963, pp1193-1203.

96. H. R. Richard and J. Chipman, Activities in the liquid solution Sio_2-CaO-MgO-Al_2O_3 at 1600°C, Trans. of the metallurgical Society of AIME, Vol.233, 1965, pp415-425.

97. K.Morita, N. Sano, Solubility of MgO-Cr_2O_3 in MgO-Al_2O_3-SiO_2-CaO melts, ibid., pp43-45.

98. J. Chipman and R. Baschwitz, The activity of silicon in liquid Fe-Si-C alloys, Trans.AIME.,Vol277, April 1963, pp473-478.

99. Handbook of tri-flat variable-area flowmeters, Fischer & porter GMBH

100. T. R. Curr, Dissolution of Transvaal chromite in liquid silicate slag under a inert atmosphere at 1550, 1650°C, 1990, Msc thesis, University of the Witwatersrand, Johannesburg.

101. K. Sano and T. Miyazaki, Tetsu-to-Hagane, 66(1980), S36.

102. S. Taguchi, H. Katayama, N. Tsuchiya, K. Okabe, K. Tanaka and K. Okumura, Stahl u. Eisen, 101(1981), pp1173.

103. T. Uchida and S. Komatsu (eds), Kasshiki no Jidai, Tsusho Sangyo Chosakai, (1980), pp49.

104. K. Okumura, T. Kawai, etal, Tetsu-to-Hagane, 66(1980), pp1956.

105. J. F. Elliott, M. Gleiser and V. Ramakrishna, Thermochemistry for steelmaking, Vol. 2, Addison-Wesley(1963).

106. J. Chen, Thermodynamic Data for Steelmaking, CCM Press, pp511-519 .

107. J. C. Fulton and J. Chipman, Slag-metal graphite reactions and the activity of silica in lime-alumina-silica slags, Transactions of the Metallurgical Society of AIME, Vol. 200, 1954, pp1136-1146.

108. L. Hu, A study in sulphur control in HC FeCr process, Ferroalloys, Vol.4,

1980, pp14.

109.C. Pickles, A review of behaviour of impurities in HC FeCr production, Iron & Steelmaker, 1986, No.12, pp37-48.

110.W. Dai and L. Shu, On sulphur control in HC FeCr production, INFACON 7, Trondheim, June 1995, pp288-296.

111.X. Pan and R.H. Eric, Sulphur behaviour under different partial pressure of CO for refining of FeCr alloy, Proceedings of the 5th International Conference on molten slags, fluxes and salts 97, Jan. 5-8, 1997, Sydney, Australia, pp191-199.

7. APPENDIX

Table 7.1. Gas-metal equilibrium data at 1500°C by mole fraction.

No.	Cr	Fe	Si	S	C	Pco atm
39-1	0.5478	0.3396	0.0040	0.0030	0.1056	0.83
39-2	0.5705	0.3521	0.0093	0.0016	0.0666	0.50
39-3	0.6018	0.3187	0.0131	0.0016	0.0649	0.10
39-4	0.5984	0.3301	0.0123	0.0016	0.0577	0.10
39-5	0.6198	0.3079	0.0146	0.0016	0.0561	0.05
39-6	0.5886	0.3558	0.0196	0.0016	0.0343	0.01
39-7	0.6011	0.3473	0.0178	0.0016	0.0322	0.01
39-8	0.6507	0.3029	0.0160	0.0016	0.0288	0.01
39-9	0.6594	0.3202	0.0188	0.0016	0.0000	0.00
42-1	0.6356	0.3183	0.0190	0.0002	0.0270	0.01
42-2	0.6470	0.3149	0.0178	0.0002	0.0202	0.01
42-3	0.6527	0.3095	0.0183	0.0002	0.0192	0.01
42-4	0.6749	0.2920	0.0170	0.0002	0.0159	0.01
42-5	0.6238	0.3427	0.0167	0.0002	0.0166	0.01
42-6	0.6293	0.3454	0.0162	0.0002	0.0134	0.01
42-7	0.5563	0.4372	0.0017	0.0002	0.0045	0.01
42-8	0.7237	0.2450	0.0151	0.0002	0.0161	0.01
42-9	0.9411	0.0254	0.0242	0.0002	0.0011	0.01
42-10	0.4260	0.5586	0.0093	0.0002	0.0059	0.01
42-11	0.4157	0.5393	0.0074	0.0002	0.0374	0.01
42-12	0.6174	0.3272	0.0053	0.0002	0.0500	0.83
42-13	0.5835	0.3104	0.0067	0.0002	0.0992	0.10
42-14	0.6140	0.3244	0.0055	0.0002	0.0560	0.01
42-15	0.6670	0.2930	0.0066	0.0002	0.0333	0.05

Table 7.1. Gas-metal equilibrium data at 1500°C by mole fraction (continue).

No.	Cr	Fe	Si	S	C	Pco atm
42-16	0.6352	0.3160	0.0069	0.0002	0.0417	0.05
42-17	0.6333	0.3184	0.0071	0.0002	0.0410	0.10
42-18	0.6826	0.3012	0.0068	0.0002	0.0092	0.10
42-19	0.5635	0.2868	0.0075	0.0001	0.1420	0.83
42-20	0.6213	0.0981	0.0430	0.0001	0.2375	0.83
42-21	0.6553	0.0470	0.0479	0.0001	0.2497	0.50
42-22	0.6978	0.0516	0.0520	0.0001	0.1985	0.50
42-23	0.7821	0.0590	0.0512	0.0001	0.1075	0.02
42-24	0.8336	0.0416	0.0446	0.0001	0.0800	0.01
43-1	0.5472	0.3071	0.0085	0.0001	0.1370	0.83
43-2	0.5855	0.3448	0.0168	0.0002	0.0523	0.10
43-3	0.5864	0.3455	0.0163	0.0002	0.0516	0.10
43-4	0.3058	0.6540	0.0128	0.0002	0.0272	0.10
43-5	0.7048	0.1201	0.0129	0.0001	0.1620	0.10
43-6	0.6734	0.1339	0.0103	0.0001	0.1822	0.10
43-7	0.6204	0.2600	0.0156	0.0002	0.1038	0.10
43-10	0.6311	0.3215	0.0144	0.0002	0.0328	0.10
43-12	0.6371	0.3172	0.0144	0.0002	0.0311	0.83
43-13	0.6294	0.3139	0.0164	0.0002	0.0401	0.83
43-14	0.6056	0.3243	0.0209	0.0002	0.0489	0.01
43-15	0.6133	0.2885	0.0612	0.0002	0.0368	0.01
43-16	0.6026	0.2693	0.0758	0.0002	0.0522	0.01
43-17	0.6115	0.2704	0.0743	0.0002	0.0436	0.01
43-18	0.4430	0.5043	0.0071	0.0002	0.0454	0.50
43-19	0.4518	0.4853	0.0160	0.0002	0.0467	0.50

Table 7.2. Metal composition in mole fraction from gas-slag-metal equilibrium data at 1500°C under CO atmosphere in Cr-oxide crucibles

Number	Cr	Fe	Si	S	C
48-1	0.4981	0.3661	0.0058	0.0004	0.1296
48-2	0.4959	0.3669	0.0054	0.0004	0.1304
48-3	0.4715	0.4290	0.0090	0.0028	0.0877
48-4	0.4029	0.5188	0.0066	0.0017	0.070[illegible]
48-5	0.2852	0.6773	0.0052	0.0017	0.0306
48-11	0.5305	0.3128	0.0057	0.0035	0.1475
48-12	0.2096	0.623[illegible]	0.0169	0.0035	0.1470
48-13	0.4295	0.4574	0.0065	0.0037	0.1029
49-1	0.4257	0.4778	0.0057	0.0021	0.0886
49-2	0.4676	0.4427	0.0044	0.0023	0.0829
49-3	0.5532	0.3499	0.0037	0.0016	0.0915
49-4	0.2102	0.7625	0.0039	0.0039	0.0194
49-5	0.4726	0.5040	0.0053	0.0026	0.0154
49-6	0.5526	0.3523	0.0037	0.0011	0.0903
49-11	0.5934	0.2411	0.[illegible]038	0.0043	0.1574
49-12	0.6066	0.330[illegible]	[illegible]040	0.0049	0.0539
49-13	0.6004	0.3553	0.[illegible]	0.0041	0.0362
49-14	0.3893	0.5246	0.0047	0.0047	0.0767
49-15	0.5519	0.2705	0.0106	0.0025	0.1645
49-16	0.6240	0.3430	0.0050	0.0050	0.0230
49-17	0.5740	0.4000	0.0040	0.0040	0.0180

Table 7.3. Metal composition in mole fraction from the gas-slag-metal equilibrium data at 1500°C at 0.05atm of Pco in Cr-oxide crucibles.

Number	Cr	Fe	Si	S	C
52-1	0.5215	0.3000	0.0070	0.0006	0.1708
52-2	0.6452	0.2386	0.0080	0.0008	0.1073
52-3	0.6192	0.2689	0.0128	0.0018	0.0973
52-4	0.5058	0.2897	0.0042	0.0001	0.2000
52-5	0.4734	0.3185	0.0049	0.0020	0.1311
52-6	0.4579	0.3330	0.0087	0.0019	0.1984
52-9	0.5142	0.3252	0.0035	0.0006	0.1564
52-11	0.4726	0.3368	0.0036	0.0009	0.1871
52-12	0.1946	0.5801	0.0156	0.0013	0.2084
52-13	0.4590	0.4040	0.0049	0.0006	0.1322
52-14	0.2800	0.4980	0.0045	0.0005	0.2170
52-15	0.4544	0.4066	0.0047	0.0006	0.1337
52-17	0.3390	0.4400	0.0045	0.0006	0.1767

Table 7.4. Metal composition in mole fraction from the gas-slag-metal equilibrium data at 0.034atm of Pco and 1580°C in silica crucibles.

Number	Cr	Fe	Si	S	C
53-8	0.4544	0.4066	0.0047	0.0006	0.1337
57-1	0.5718	0.3365	0.0867	0.0023	0.0027
57-2	0.5725	0.2880	0.0696	0.0051	0.0647
57-3	0.5485	0.1985	0.0164	0.0013	0.2352
57-4	0.5528	0.1992	0.0284	0.0013	0.2183
57-5	0.5354	0.2253	0.0387	0.0014	0.1992
57-6	0.5544	0.3087	0.0922	0.0047	0.0400
57-11	0.5260	0.2148	0.0243	0.0013	0.2336
57-12	0.5686	0.2230	0.0546	0.0041	0.1497
57-13	0.5524	0.3211	0.1000	0.0055	0.0210
57-14	0.5397	0.2296	0.0294	0.0028	0.1985
57-15	0.5717	0.2518	0.0757	0.0038	0.0970
57-16	0.5780	0.2660	0.0580	0.0037	0.1141
57-17	0.5683	0.2723	0.0869	0.0039	0.0686
57-18	0.5750	0.2750	0.0899	0.0051	0.0550

Table 7.4. Metal composition in mole fraction from the gas-slag-metal equilibrium data at 0.034atm of Pco and 1580°C in silica crucibles. (continue)

Number	Cr	Fe	Si	S	C
57-21	0.5047	0.2213	0.0358	0.0018	0.2364
57-22	0.5282	0.2367	0.0249	0.0032	0.2069
57-23	0.5492	0.2827	0.0296	0.0032	0.1354
57-24	0.5379	0.3308	0.0765	0.0047	0.0502
57-25	0.5485	0.3570	0.0830	0.0043	0.0072
57-26	0.5500	0.2319	0.2537	0.0028	0.1935
57-31	0.5536	0.2470	0.0269	0.0044	0.1681
57-32	0.5085	0.2445	0.0204	0.0022	0.2245
57-33	0.5088	0.2438	0.0205	0.0022	0.2246
57-34	0.5455	0.2728	0.0208	0.0025	0.1584
57-35	0.5172	0.3494	0.0447	0.0023	0.0864

Table 7.5. Metal composition in mole fraction from the gas-slag-metal equilibrium data relevant to stainless steel at 0.034atm of Pco and 1580°C in silica crucibles.

Number	Cr	Fe	Si	S	C
48-2	0.0880	0.9013	0.0073	0.0020	[illegible]
48-6	0.0270	0.9554	0.0054	0.0042	[illegible]
53-1	0.1377	0.6973	0.0268	0.0004	[illegible]
53-2	0.1132	0.7378	0.0305	0.0012	[illegible]
53-3	0.1041	0.7781	0.0115	0.0013	0.1051
53-4	0.1170	0.7669	0.0075	0.0031	0.1055
53-5	0.1076	0.8149	0.0078	0.0033	0.0665
53-6	0.1093	0.8227	0.0069	0.0055	0.0557
53-7	0.0857	0.8954	0.0045	0.0060	0.0083
53-11	0.1344	0.7825	0.0112	0.0042	0.0678
53-12	0.1231	0.8017	0.0065	0.0038	0.0649
53-13	0.0917	0.8737	0.0039	0.0052	0.0256
53-14	0.0540	0.9074	0.0039	0.0070	0.0277
53-15	0.1303	0.8459	0.0039	0.0070	0.0128
53-16	0.0939	0.8769	0.0039	0.0052	0.0201
53-17	0.0919	0.8670	0.0038	0.0045	0.0333
53-19	0.0440	0.9261	0.0039	0.0061	0.0199
53-21	0.0610	0.8770	0.0037	0.0046	0.0537

Table 7.5. Metal composition in mole fraction from the gas-slag-metal equilibrium data relevant to stainless steel at 0.034atm of P_{CO} and 1580°C in silica crucibles,(continue).

Number	Cr	Fe	Si	S	C
56-1	0.1606	0.7355	0.0262	0.0036	0.0741
56-2	0.1550	0.7506	0.0271	0.0023	0.0650
56-3	0.1914	0.7530	0.0292	0.0070	0.0195
56-4	0.1668	0.7496	0.0220	0.0063	0.0554
56-5	0.0816	0.8814	0.0087	0.0060	0.0223
56-6	0.1575	0.7331	0.0286	0.0031	0.0777
56-13	0.1777	0.8061	0.0066	0.0002	0.0094
56-14	0.1704	0.7978	0.0169	0.0014	0.0135
56-15	0.1769	0.7976	0.0079	0.0012	0.0163
56-16	0.1713	0.7047	0.0319	0.0016	0.0905
56-21	0.1556	0.8250	0.0038	0.0020	0.0136
56-22	0.1609	0.7585	0.0256	0.0044	0.0507
56-23	0.1724	0.6762	0.0304	0.0006	0.1205
56-24	0.1888	0.7126	0.0209	0.0044	0.0733
56-25	0.1660	0.7328	0.2018	0.0061	0.0069
56-26	0.1983	0.6494	0.0097	0.0071	0.0905
56-27	0.0385	0.9080	0.0037	0.0086	0.0412
56-28	0.2003	0.7130	0.0119	0.0057	0.0692
56-29	0.2135	0.6948	0.0098	0.0067	0.0751

Table 7.6. Slag composition from gas-slag-metal equilibrium data at 1500°C under CO atmosphere in Cr-oxide crucibles in mole fraction.

Number	Al_2O_3	CaO	MgO	SiO_2	Cr	Fe	S
48-1	0.1222	0.0193	0.1993	0.4694	0.1864	0.0032	0.0002
8-2	0.1129	0.0159	0.1846	0.4320	0.2530	0.0030	0.0005
48-3	0.1272	0.0191	0.2226	0.4578	0.1653	0.0070	0.0010
48-4	0.1219	0.0192	0.1860	0.4554	0.2117	0.0052	0.0006
48-5	0.1191	0.0132	0.1852	0.4300	0.2448	0.0073	0.0004
48-11	0.1212	0.0191	0.1851	0.5552	0.1149	0.0025	0.0020
48-12	0.0997	0.0125	0.1745	0.6420	0.0623	0.0087	0.0002
48-13	0.1130	0.0133	0.1795	0.3656	0.3124	0.0146	0.0017
49-1	0.1139	0.0148	0.1678	0.4664	0.2289	0.0073	0.0009
49-2	0.0824	0.0089	0.1166	0.4708	0.3135	0.0059	0.0019
49-3	0.0760	0.0089	0.1209	0.5138	0.2737	0.0051	0.0017
49-4	0.0700	0.0075	0.1009	0.5983	0.2137	0.0983	0.0012
49-5	0.0424	0.0038	0.0615	0.5233	0.3499	0.0171	0.0019
49-6	0.0760	0.0009	0.1208	0.5137	0.2737	0.0054	0.0017
49-11	0.3395	0.0095	0.1308	0.3127	0.1960	0.0108	0.0007
49-12	0.2236	0.0045	0.0495	0.1207	0.5723	0.0289	0.0005
49-13	0.2443	0.0047	0.0646	0.2811	0.4232	0.0111	0.0010
49-14	0.1577	0.0043	0.0472	0.3107	0.4678	0.0095	0.0027
49-15	0.0658	0.0095	0.1198	0.6036	0.1700	0.0296	0.0017
49-16	0.0910	0.0080	0.1310	0.3320	0.3460	0.0900	0.0006
49-17	0.0700	0.0070	0.1010	0.5990	0.2140	0.0090	0.0010

Table 7.7. Slag composition from gas-slag-metal equilibrium da : at 1500°C at 0.05atm of Pco in Cr-oxide crucibles in mole fraction.

Number	Al_2O_3	CaO	MgO	SiO_2	Cr	Fe	S
52-1	0.2165	0.0107	0.2087	0.4806	0.1638	0.0030	0.0004
52-2	0.1276	0.0168	0.2120	0.4610	0.1789	0.0032	0.0004
52-3	0.1161	0.0141	0.1910	0.3763	0.2959	0.0061	0.0006
52-4	0.1348	0.0201	0.2385	0.5041	0.1030	0.0057	0.0002
52-5	0.1179	0.0188	0.1782	0.5059	0.1745	0.0038	0.0008
52-6	0.1329	0.0196	0.2333	0.4884	0.1152	0.0035	0.0008
52-9	0.0964	0.0163	0.1632	0.6354	0.0706	0.0177	0.0004
52-11	0.0852	0.0120	0.1504	0.6543	0.0917	0.0059	0.0006
52-12	0.1006	0.0152	0.1744	0.6424	0.0585	0.0087	0.0002
52-13	0.1115	0.0140	0.1829	0.3705	0.3051	0.0145	0.0017
52-14	0.1350	0.0220	0.3390	0.4080	0.0830	0.0100	0.0017
52-15	0.1225	0.0210	0.1911	0.5198	0.1337	0.0115	0.0003
52-16	0.1940	0.0240	0.4270	0.6360	0.1900	0.0160	0.0013

Table 7.8. Slag composition from gas-slag-metal equilibrium data at 1580°C at 0.034atm of Pco in silica-oxide crucibles in mole fraction.

Number	Al_2O_3	CaO	MgO	SiO_2	Cr	Fe	S
53-8	0.0759	0.0128	0.1020	0.5643	0.1931	0.0307	0.0013
57-1	0.1314	0.0104	0.0954	0.6129	0.1730	0.0056	0.0013
57-2	0.0888	0.0088	0.0790	0.5631	0.1314	0.1222	0.0068
57-3	0.1158	0.0127	0.1443	0.6352	0.0867	0.0052	0.0002
57-4	0.1136	0.0138	0.1538	0.5984	0.1142	0.0055	0.0006
57-5	0.1159	0.0134	0.1478	0.6018	0.1159	0.0046	0.0006
57-6	0.1353	0.0090	0.1140	0.7213	0.0099	0.0094	0.0012
57-11	0.1439	0.0109	0.1751	0.5983	0.0677	0.0042	0.0004
57-12	0.1108	0.0120	0.1200	0.6397	0.1121	0.0045	0.0008
57-13	0.1214	0.0109	0.1246	0.6048	0.1338	0.0037	0.0008
57-14	0.1346	0.0101	0.1613	0.5867	0.1028	0.0034	0.0010
57-15	0.1358	0.0094	0.1644	0.5632	0.1228	0.0039	0.0006
57-16	0.1314	0.0089	0.1464	0.5877	0.1216	0.0037	0.0004
57-17	0.1231	0.0084	0.1231	0.6235	0.1166	0.0049	0.0004
57-18	0.1250	0.0090	0.1283	0.6080	0.1250	0.0039	0.0008
57-21	0.0975	0.0085	0.1739	0.6167	0.0974	0.0051	0.0010
57-22	0.9620	0.0086	0.1855	0.5860	0.1182	0.0044	0.0012
57-23	0.0923	0.0082	0.1576	0.6080	0.1289	0.0050	0.0008
57-24	0.0911	0.0070	0.1122	0.6425	0.1417	0.0045	0.0010
57-25	0.0880	0.0067	0.1285	0.5892	0.1825	0.0042	0.0008
57-26	0.0754	0.0032	0.1601	0.6138	0.1421	0.0050	0.0012
57-31	0.0748	0.0031	0.1696	0.5762	0.1696	0.0053	0.0014
57-32	0.0717	0.0029	0.1549	0.5662	0.1961	0.0069	0.0012
57-33	0.0918	0.0077	0.1654	0.6177	0.1107	0.0054	0.0012
57-34	0.0732	0.0033	0.1634	0.5759	0.1772	0.0058	0.0012
57-35	0.0748	0.0032	0.1489	0.5783	0.1885	0.0058	0.0006

Table 7.9. Slag composition from gas-slag-metal equilibrium data at 1580°C at 0.034atm of Pco in silica-oxide crucibles relevant to stainless-steel in mass per cent (%).

Number	Al_2O_3	CaO	MgO	SiO_2	Cr	Fe	S
53-1	0.1393	0.0171	0.2181	0.6054	0.0165	0.0034	0.0004
53-2	0.1303	0.0147	0.1812	0.6432	0.0189	0.0055	0.0003
53-3	0.1294	0.0159	0.1886	0.6105	0.0470	0.0083	0.0004
53-4	0.1243	0.0144	0.1785	0.6063	0.0661	0.0099	0.0005
53-5	0.1176	0.0132	0.1528	0.6078	0.0937	0.0145	0.0005
53-6	0.1127	0.0122	0.1388	0.5896	0.1254	0.0207	0.0006
53-7	0.1056	0.0116	0.1217	0.5897	0.1493	0.0213	0.0009
53-11	0.0945	0.0112	0.1363	0.6570	0.0804	0.0201	0.0006
53-12	0.0966	0.0112	0.1375	0.6640	0.0772	0.0131	0.0004
53-13	0.0848	0.0098	0.1182	0.6169	0.1465	0.0233	0.0005
53-14	0.0807	0.0077	0.0761	0.6319	0.1634	0.0394	0.0007
53-15	0.0725	0.0086	0.1016	0.5104	0.2506	0.0551	0.0012
53-16	0.0813	0.0096	0.1217	0.5641	0.1926	0.0299	0.0007
53-17	0.0901	0.0100	0.1172	0.6598	0.1023	0.0201	0.0005
53-19	0.1383	0.0076	0.1668	0.6057	0.0588	0.0222	0.0005
53-21	0.1495	0.0082	0.1722	0.6109	0.0420	0.0166	0.0005
56-1	0.1415	0.0089	0.1574	0.6170	0.0677	0.0073	0.0002
56-2	0.1493	0.0095	0.1804	0.5191	0.0523	0.0093	0.0002
56-3	0.1429	0.0110	0.1848	0.5477	0.1050	0.0086	0.0004
56-4	0.1390	0.0087	0.1570	0.6107	0.0775	0.0067	0.0004
56-5	0.1272	0.0079	0.1[illegible]	0.6055	0.1014	0.0205	0.0004

Table 7.9. Slag composition from gas-slag-metal equilibrium data at 1580°C at 0.034atm of Pco in silica-oxide crucibles relevant to stainless-steel by mass per cent (continue).

Number	Al_2O_3	CaO	MgO	SiO_2	Cr	Fe	S
56-6	0.1551	0.0107	0.2014	0.5968	0.0289	0.0067	0.0004
56-13	0.0842	0.0030	0.0092	0.6627	0.2207	0.0198	0.0004
56-14	0.0791	0.0028	0.0018	0.7182	0.1801	0.0177	0.0004
56-15	0.0839	0.0028	0.0017	0.7156	0.1768	0.0187	0.0004
56-16	0.0831	0.0027	0.0017	0.6630	0.2299	0.0189	0.0006
56-21	0.1411	0.0091	0.1518	0.6324	0.0592	0.0060	0.0004
56-22	0.1520	0.0099	0.1805	0.5930	0.0509	0.0135	0.0002
56-23	0.1589	0.0105	0.2003	0.6009	0.0243	0.0044	0.0006
56-24	0.1532	0.0105	0.2015	0.5661	0.0621	0.0062	0.0004
56-25	0.1375	0.0087	0.1436	0.6370	0.0721	0.0007	0.0004
56-26	0.1452	0.0106	0.1843	0.5515	0.1014	0.0068	0.0002
56-27	0.1384	0.0093	0.1530	0.5908	0.0649	0.0430	0.0006
56-28	0.1428	0.0107	0.1742	0.5512	0.1121	0.0087	0.0004
56-29	0.1438	0.0108	0.2025	0.4549	0.1802	0.0074	0.0004

Table 7.10. Relations between X_C and $[\gamma_{Cr}]$, $[\gamma_C]$, $[a_{Cr}]/[a_C]$ and $(a_{Cr\text{-}O})$ with metals of C-0.45Cr-Fe-0.001S-0.005Si in mole fraction at 1550°C.

X_C	$[\gamma_{Cr}]$	$[\gamma_C]$	$[a_{Cr}]/[a_C]$	$(a_{Cr\text{-}O})$ 0.034Pco	$(a_{Cr\text{-}O})$ 0.05Pco
0.025	0.7997	0.0752	191.42	0.4552	0.6694
0.050	0.7380	0.0976	68.69	0.1633	0.2402
0.075	0.6769	0.1261	32.31	0.0766	0.1126
0.100	0.6171	0.1667	16.66	0.0396	0.0583
0.125	0.5590	0.2235	9.01	0.0214	0.0314
0.150	0.5033	0.3039	4.97	0.0118	0.0173
0.175	0.4504	0.4190	2.76	0.0066	0.0097
0.200	0.4006	0.5859	1.53	0.0036	0.0054

Table 7.11. Relations between X_{Cr} and $[\gamma_{Cr}]$, $[\gamma_C]$, $[a_{Cr}]/[a_C]$ and $(a_{Cr\text{-}O})$ with metals of 0.15C-Cr-Fe-0.001S-0.005Si in mole fraction at 1550°C.

X_{Cr}	$[\gamma_{Cr}]$	$[\gamma_C]$	$[a_{Cr}]/[a_C]$	$(a_{Cr\text{-}O})$ 0.034Pco	$(a_{Cr\text{-}O})$ 0.05Pco	$(a_{Cr\text{-}O})$ 0.83Pco
0.025	0.3097	2.2356	0.0231	2.5E-5	8.1E-5	1.3E-3
0.050	0.3091	1.9902	0.0534	1.3E-4	1.9E-4	3.1E-3
0.075	0.3287	1.7716	0.0928	2.2E-4	3.2E-4	5.4E-3
0.100	0.3286	1.5767	0.1389	3.3E-4	4.9E-4	8.1E-3
0.125	0.3485	1.4031	0.2070	4.9E-4	7.2E-4	12E-3
0.150	0.3588	1.2484	0.2874	6.8E-4	1.1E-3	16.8E-3
0.175	0.3694	1.1106	0.3880	9.2E-4	1.4E-3	22.5E-3
0.200	0.3809	0.9879	0.5141	1.2E-3	1.8E-3	29.8E-3
0.300	0.4261	0.6175	1.3801	3.3E-3	4.8E-3	80.2E-3
0.400	0.4764	0.3851	3.2989	7.8E-3	1.2E-2	0.1910
0.500	0.5315	0.2396	7.3943	1.76E-2	2.6E-2	0.4290
0.600	0.5915	0.1488	15.9005	3.78E-2	5.6E-2	0.9230

Table 7.13. Relations between $(a_{CrO})/(a_{Cr_2O_{1.5}})$ and mole fraction of C, Cr, S, Si at 0.034atm of Pco at 1550°C. The metals contain 0.15C-0.45Cr-0.001S-0.005Si-Fe.

X	$(a_{CrO})/(a_{Cr_2O_{1.5}})$ X = C	$(a_{CrO})/(a_{Cr_2O_{1.5}})$ X = Cr	$(a_{CrO})/(a_{Cr_2O_{1.5}})$ X = S	$(a_{CrO})/(a_{Cr_2O_{1.5}})$ X = Si
0.025	0.6692	8.9374	3.5604	3.6315
0.050	1.0732	8.4326	3.8590	4.1005
0.075	1.5009	7.9650	4.1833	4.6305
0.100	1.9927	7.5056	4.5346	5.2284
0.125	2.5796	7.0804	4.9153	5.9040
0.150	3.2952	6.6787	5.3279	6.6666
0.175	4.1792	6.2993	5.7752	7.5280
0.200	5.2832	5.9411	6.2600	8.5005
0.300		4.6971		13.8200
0.400		3.7094		
0.500		2.9259		
0.600		2.3058		

Table 7.14. Relations between $(a_{CrO})/(a_{CrO1.5})$ and mole fraction of C, Cr, S, Si at 0.05atm of Pco at 1550°C. The metals contain 0.15C-0.45Cr-0.001S-0.005Si-Fe.

X	$(a_{CrO})/(a_{CrO1.5})$ X = C	$(a_{CrO})/(a_{CrO1.5})$ X = Cr	$(a_{CrO})/(a_{CrO1.5})$ X = S	$(a_{CrO})/(a_{CrO1.5})$ X = Si
0.025	0.5516	7.3699	2.9360	2.9946
0.050	0.8849	6.9537	3.1822	3.3814
0.075	1.2377	6.5607	3.4496	3.8184
0.100	1.6433	6.1893	3.7393 2	4.3115
0.125	2.1272	5.8386	4.0532	4.8686
0.150	2.7273	5.5073	4.3935	5.4974
0.175	3.4462	5.1945	4.7624	6.2077
0.200	4.3566	4.8992	5.1621	7.0097
0.300		3.8733		11.3962
0.400		3.0588		
0.500		2.4127		
0.600		1.9014		

Table 7.15. Relations between $(a_{CrO})/(a_{CrO1.5})$ and mole fraction of C, Cr, S, Si under CO atmosphere at 1550°C. The metals contain 0.15C-0.45Cr-0.001S-0.005Si-Fe.

X	$(a_{CrO})/(a_{CrO1.5})$ X = C	$(a_{CrO})/(a_{CrO1.5})$ X = Cr	$(a_{CrO})/(a_{CrO1.5})$ X = S	$(a_{CrO})/(a_{CrO1.5})$ X = Si
0.025	0.1345	1.7969	0.7159	0.7230
0.050	0.2172	1.6954	0.7759	0.8244
0.075	0.3038	1.5996	0.8411	0.9310
0.100	0.4033	1.5091	0.9117	1.0542
0.125	0.5221	1.4236	0.9883	1.1870
0.150	0.6669	1.3428	1.0712	1.3404
0.175	0.8459	1.2665	1.1611	1.5136
0.200	1.0693	1.1945	1.2586	1.7091
0.300		0.9444		2.7786
0.400		0.7458		
0.500		0.5883		
0.600		0.4636		

Author: Pan X
Name of thesis: Gas-slag-metal equilibria without carbon-saturation for ferrochromium refining and stainless-steel making. (2)

PUBLISHER:
University of the Witwatersrand, Johannesburg
©2015

LEGALNOTICES:

Copyright Notice: All materials on the University of the Witwatersrand, Johannesburg Library website are protected by South African copyright law and may not be distributed, transmitted, displayed or otherwise published in any format, without the prior written permission of the copyright owner.

Disclaimer and Terms of Use: Provided that you maintain all copyright and other notices contained therein, you may download material (one machine readable copy and one print copy per page)for your personal and/or educational non-commercial use only.

The University of the Witwatersrand, Johannesburg, is not responsible for any errors or omissions and excludes any and all liability for any errors in or omissions from the information on the Library website.